Phase Domain Transmission Line Modelling for EMTP-Type Studies with Application to Real-Time Digital Simulation

by

John A. Parle

A Thesis submitted to the
Department of Electronics & Electrical Engineering of
The University of Glasgow
for the degree of Doctor of Philosophy

January 2000

ABSTRACT

Digital computer based simulation packages such as EMTP and EMTDC are extensively used for analysing the transient waveforms that arise as a result of abrupt changes in the otherwise steady-state operating conditions of the power network. In principal, the conclusions drawn from such analysis can be utilized to achieve effective system protection and insulation co-ordination to prevent equipment failures and unnecessary transmission line outages during these transient conditions.

However, one of the most significant disadvantages of software based simulators such as these, arises as a consequence of their non-real-world time operation, i.e. the solution is obtained at a faster or slower rate than the dynamics of the phenomena under analysis dictate. The interfacing of external equipment to the simulator in these cases is therefore precluded. Since the control inputs necessary for the testing of physical control and protection equipment are dynamic in nature, meaningful testing of these devices requires the simulated waveforms to be input into the device in real-time. Simulation packages such as EMTP and EMTDC have therefore been of little use in these areas. Alternatively, analogue HVDC simulators and AC Transient Network Analyzers (TNAs) have been used in the past in this respect. However, due to their size, cost and time cycle required for a specific analysis, they are no longer in widespread use.

Manufacturers, large utilities and research organisations have in the last decade adopted a new, more cost effective and flexible technology to replace the previous generation of analogue network analysers, namely real-time digital power system simulators with hardware-in-the-loop (HIL) capabilities.

This research project is primarily concerned with the development of a new generation of power transmission lines for both non-real-time and real-time electromagnetic transient studies. The method proposed is entirely formulated in phase co-ordinates, avoiding the use of modal transformation matrices at every stage in the analysis. In comparison, the phase domain models presented thus far in the open literature have all incorporated the concept of modal decomposition in the initial frequency domain formulation of the problem. Only the time domain analysis is conducted in the phase domain. These models can therefore be regarded as a hybrid between the phase and modal methodologies.

Algorithms are presented which allow accurate and efficient determination of the characteristic admittance matrix, $\mathbf{Y}_c(\omega)$, and wave propagation matrix, $\mathbf{H}(\omega)$, directly in phase co-ordinates. A Padé iteration scheme is used for evaluating the characteristic admittance matrix, derived by exploiting a relationship between the matrix sign function and the matrix square root. Padé techniques have also been used to approximate the matrix exponential in order to evaluate the wave propagation function. By evaluating $\mathbf{Y}_c(\omega)$ and $\mathbf{H}(\omega)$ directly in phase co-ordinates, any imbalances naturally present in the line will intrinsically be taken into account in these functions. Both methods have been extensively tested using line configurations of different size and complexity and both algorithms are shown to be very robust, accurate and efficient in all cases.

One of the main difficulties in formulating the analysis entirely in phase co-ordinates for multiconductor systems concerns the unwinding of the wave propagation matrix. This is addressed in this research by evaluating a matrix phase shift function in phase co-ordinates. Since the method inherently takes into account the coupled time delays of

the line, the elements of $\mathbf{H}(\omega)$ can be successfully unwound, irrespective of the configuration of the line, e.g. single-circuit, multi-circuit or asymmetrical.

The frequency-dependence of $\mathbf{Y}_c(\omega)$ and $\mathbf{H}(\omega)$, due to the presence of a resistive ground, are accurately taken into account by introducing numerical convolutions in the time domain between these impulse responses and the line end quantities. To increase the computational efficiency of the time domain simulation, $\mathbf{Y}_c(\omega)$ and $\mathbf{H}(\omega)$ are approximated with rational functions using the method of Vector Fitting, thereby allowing a recursive formulation of the convolution integrals to be constructed.

The phase domain model can be represented by a time-dependent vector of current sources in parallel with a constant admittance in the time domain, making it compatible with general electromagnetic transient programs. Time domain simulations are performed on a real-life transmission circuit and the results compared with actual field measurements to assess the accuracy of the proposed methodology.

Finally, a real-time simulation environment for conducting electromagnetic studies has been developed on a commercially available simulator. The phase domain transmission line model has been successfully incorporated within this environment in addition to frequency-independent and frequency-dependent line models that utilise modal decomposition techniques. This represents the first time the phase domain methodology has been applied in the context of real-time digital simulation.

Acknowledgments

I wish to express my deep sense of gratitude to my supervisor Dr. Enrique Acha for his technical support, encouragement and valued friendship during the past three years of this research.

I would also like to thank my ex-colleague, Dr Claudio Fuerte-Esquivel for his knowledge and encouragement during the first year of the research project it was a great help. Also I wish to express my many thanks to Dr Hugo Ambriz-Perez for his encouragement and friendship.

Many thanks to Professor Adam Semlyen and Dr. Bjørn Gustavsen for making available the Vector Fitting algorithm, it has been of invaluable assistance. My thanks also go to Jim Robertson at ADI for his technical assistance regarding the real-time station.

I gratefully acknowledge the financial assistance given to me by the Engineering and Physical Sciences Research Council (EPSRC), UK during my doctoral studies.

Many thanks to my colleagues at Glasgow University for assistance over the last three years, in particular to Stephen Gallagher for helping out with all things computer related.

Finally, to my friends & family - Cheers, you knew it made sense.....

Contents

List of Figures

List of Tables

ABBREVIATIONS

EMTP	ElectroMagnetic Transients Program
EMTDC	Electromagnetic transient direct current
TNA	Transient Network Analyser
HVDC	High voltage direct current
HIL	Hardware-in-the-loop
S/C	Short-circuit
O/C	Open-circuit
AC	Alternating current
DC	Direct Current
RTS	Real-time station
COP	Communications Processor
VIM	VMEbus interact manager
SP	Simulation Processor
CE	Compute Engine
AIM	Analogue interface module
DIM	Digital interface module
AFT	Actual frame time
CPU	Central processing unit
IDE	Integrated development environment
ms	milliseconds
μs	microseconds
V	Volts
pu	per unit

In this thesis, unless otherwise stated, bold face type represents matrix quantities, e.g. **H**
Upper case letters represent frequency domain quantities, e.g. $V(\omega)$
Lower case letters represent time domain quantities, e.g. $h(t)$

CHAPTER 1

INTRODUCTION

1.1 Foreword

Power system networks are subjected to many forms of transient phenomena that arise as a result of abrupt changes to the otherwise steady-state operational condition of the network. Sudden changes in the voltage and current may arise as a result of a variety of disturbances, ranging from the deliberate operation of circuit-breakers for connecting and disconnecting various system components, to unforeseen events such as lightening discharges or the malfunctioning of system equipment [1-4].

The waveforms generated after a transient process can attain peak magnitudes after a very short time period, depending on the parameters of the system and the nature of the disturbance. The transient conditions arising from lightening discharges on or near a phase conductor typically have a duration of a few microseconds, while those associated with switching overvoltages, following line energization through circuit-breakers, typically have time periods of a few hundred microseconds [3,4]. The transient waveforms associated with these phenomena can produce damaging stresses on the system equipment, and they must therefore be limited to safe levels.

In order to protect the power system equipment during abnormal operating conditions, devices such as surge arresters and protective relays are usually employed within the network to limit the duration of the transients associated with these conditions. As power systems become more complex and sophisticated, it is essential that the location and settings of these devices are well co-ordinated to provide effective system protection, while in no way interfering with the normal operation of the power system, e.g. during necessary switching operations.

As transmission system voltage levels have increased, the limiting factor in insulation co-ordination is determined by system generated overvoltages [1,4]. Overvoltages arising from such events are directly proportional to the system voltage and their magnitudes increase as the system voltage increases. In particular, the overvoltages caused by the energization of transmission lines are particularly significant since, given the necessary conditions, overvoltage levels of over three times the phase to neutral voltage are possible [1-4]. In contrast, the power system voltage does not significantly affect the magnitude of lightening surges on power transmission lines [1].

The system insulation level must be sufficiently high in order not to endanger the reliability of the system, however, at the same time there are strong economic pressures for keeping it as low as possible. Thus, in order to optimise the system insulation levels and reduce the severity of system generated overvoltages, it is increasingly important to be able to predict system overvoltages at the planning stage [1-4].

In order to adequately study the performance of protective strategies in moderating transient conditions and the ability of the equipment to sustain the remaining transients, detailed representation of the power system components are required to accurately describe and predict the behaviour of the system during these periods. Transient

simulations are therefore performed in order to examine these disturbed conditions and to evaluate what effects they will have on the system being studied.

1.2 Power Transmission Line Modelling for Electromagnetic Transient Studies

AC power transmission lines and underground cables constitute one of the most important components for the transmission and distribution of electrical energy in a power system. The accurate modelling of these power system components has been an area of constant interest ever since the first general program for calculating electromagnetic transients was introduced by Dommel [5,7] over thirty years ago. The detail with which the line is represented has increased considerably, from the initial lossless, frequency-independent transmission line [7] described by Dommel, to the sophisticated phase domain representations that have recently been presented [28-40].

The most widely used industrial computer programs available today for the calculation of transients in power systems, such as the EMTP [5] and EMTDC [6], are based on Dommel's algorithm. In these programs, the trapezoidal rule of integration is used to discretize the ordinary differential equations that describe the dynamic behaviour of lumped parameter elements. A complete network solution is then formulated from both the transmission line and the lumped parameter equations, with both sets of equations represented by simple equivalent impedance networks consisting of a current source in parallel with a constant admittance, i.e. a Norton equivalent [5,7,10]. The set of nodal equations can then be solved to obtain a solution vector of nodal voltages throughout the network, at every time step of the simulation.

The principal properties influencing electromagnetic transients on power transmission lines are those of the wave transit time, wave attenuation, and characteristic impedance. These quantities can be determined from the four parameters that characterize a given line, namely the resistance, inductance, capacitance and conductance (which is usually negligible) [2,17,31]. For transmission systems with ground return, as is the general case, these basic properties may be very sensitive to variations in frequency [11-13]. The solution of the partial differential equations that describe the behaviour of the voltage and current along the line is therefore easier to construct when the variables are expressed as a function of frequency.

However, despite the advantages of modelling transmission lines in the frequency domain, the solution for a complete power system, in which a large variety of components and conditions may be simulated, is more conveniently formulated directly in the time domain. For example, the incorporation of time dependent current and voltage sources, the opening and closing of circuit-breakers at specific times, as well as the effect of non-linearities due to surge arresters, magnetic saturation, corona and circuit-breaker arc, are more conveniently modelled in the time domain [1,3,17]. Furthermore, power electronics based devices, i.e. Flexible AC Transmission Systems (FACTS) and Custom Power technologies, which are increasingly being utilised in power networks, contain many time-dependent switching devices, e.g. Thyristors, IGBTs etc. that can be more efficiently analysed in the time domain [63]. Finally, if one considers performing real-time, hardware-in-the-loop dynamic simulations, then the power system model must obviously be constructed in the time domain.

It follows therefore, that a recurring aspect in the development of electromagnetic transient modelling of power transmission lines has been that of accurately and efficiently incorporating the frequency-dependent characteristics of the line in a general time domain transient program [8,9,14-20,25-40].

The original transmission line model developed in the EMTP assumed the transmission line to be lossless with the line parameters evaluated at a constant frequency (usually the power frequency) [7]. The transmission line in this case is characterized by a time delay and a characteristic impedance. The losses can be approximated by adding lumped resistances in the middle, and at both ends of the line [7].

In the general case, the transmission system cannot be assumed lossless if accurate results are required since the waves become distorted as they propagate along the line. The most widely applied methodology to take into account the distorting effects of the losses on the propagating characteristics of the line is through the use of impulse response functions, defined as the wave propagation function and the characteristic admittance, or alternatively the characteristic impedance. The transmission line model in these cases is then imbedded in the power network by means of convolutions between the impulse responses and the voltage and current quantities at each line end. The formulation of these models in general electromagnetic transient programs, such as the EMTP [5], occurs in much the same way as for lossless lines, in the sense that they are interfaced to the power network by means of Norton equivalent representations.

The main drawback of this approach concerns the practical evaluation of the convolution integrals. These integrals must be calculated at each time step of the simulation and as a consequence the resulting method is computational inefficient. This problem is compounded for power networks in which many lines are present. However, the computational efficiency of the travelling wave method can be greatly increased if the impulse responses of the line are approximated using rational functions in the frequency domain [16-17,25-28,30-31,39], *z*-domain [34-36], or piecewise linear functions in the time domain [19,29,37]. With the impulse responses approximated in this way, a recursive formulation of the convolution integrals can be constructed and significant savings in computational efficiency are thus obtained [18,19].

When the modelling of transmission lines is extended to multiconductor systems, the problem becomes significantly more complex due to the magnetic coupling that exists between the phase conductors. For an n conductor system, the equations governing the propagation of the voltage and current waves along the line form a coupled system involving complex matrix and vector quantities.

The established approach for solving these coupled wave equations was proposed nearly forty years ago by Wedepohl [21] and Hedman [22]. Independently from each other they proposed using elegant numerical linear algebra techniques to transform the set of coupled partial differential wave equations into a set of uncoupled modal equations. At each frequency point of interest, the wave equation is diagonalized, using eigenvector analysis, into a set of n independent modes, where n is the number of phase conductors. The transformation matrix is, in general, frequency-dependent and therefore the diagonalization process must be conducted at each frequency point of interest to ensure the system is accurately diagonalized. The solution for the voltage and current for each independent mode can then be obtained with relative ease, in a manner similar to that for a single-phase system. The modal solution is then constructed in the phase domain using the transformation matrix of eigenvectors and its inverse [21].

Such was the impact of this methodology, that subsequent to it, almost every multiconductor transmission line model presented in the open literature for electromagnetic transient studies have incorporated some aspect of this technique in the modelling process [8,9,15-20,25-39].

While the complex transformation matrix is, in general, frequency-dependent, it is commonly assumed to be independent of frequency for many practical lines of interest.

This assumption has been justified on the grounds that the variation of the elements of the transformation matrix with frequency can be very small [16]. It has been judged to be sufficient in these cases to evaluate the transformation matrix at a single frequency, specified by the user. Neglecting the complex component, this transformation matrix is then used to decouple the system of equations over the frequency interval of interest (typically 10^{-2}-10^{6}Hz for electromagnetic transient analysis). At frequency values other than the user specified frequency, the off-diagonal elements will not be zero, but are in general small compared to the diagonal and can be neglected [39]

However, although the assumption of a real and constant transformation matrix can give acceptable results in the case of single-circuit overhead lines with a plane of symmetry, for multi-circuit or asymmetrical line configurations and cables, this assumption may result in significant inaccuracies [25,27,28]. The reason being that the transformation matrix is in general strongly dependent on frequency such that the contribution from the off-diagonal elements can no longer be assumed negligible in these cases.

Furthermore, if significant geometric imbalances are present in the transmission system, i.e. unequal spacing between conductors, then the mutual coupling that exists between the phase conductors will not be well represented in these models. Since mutual coupling between phase conductors can impinge on the magnitude of overvoltages caused by transmission line energization [1], the geometric imbalances naturally present in the system must be accurately taken into account to reproduce these phenomena.

In principle, the frequency-dependence of the transformation matrices can be taken into account in the time domain simulation through convolutions between the transformation matrices and the line end quantities. This approach has been applied in [25-26] for cable systems, in which the transformation matrices depend heavily on frequency. In a similar approach to that of [16,17], the transformation matrix is approximated with rational functions in the frequency domain so that a recursive formulation of the convolution integrals can be established. However, it has been observed that the eigenvectors of the transformation matrix can sometimes interchange between columns of the matrix when the diagonalization process is recalculated at a new frequency. The elements of the transformation matrix may therefore display a somewhat erratic behaviour, as functions of frequency. It is then very difficult to approximate these functions accurately with rational functions in the frequency domain [25-26]. Special diagonalization or 'tracking' routines are therefore necessary to avoid the problem of eigenvector switchovers [34-35]. Also, while this methodology has been successfully applied to cable systems, in the case of overhead lines, it has been found that it may not always be possible to fit the elements of the transformation matrix using stable poles only [27,28,40].

A further problem that could arise in all methods employing modal decomposition at some stage in the analysis concerns the actual diagonalization process itself. It is tacitly assumed that the coupled equations governing the propagation of waves along the conductor can always be reduced to an uncoupled system. However, it was shown in [23,24] that in some instances this assumption does not hold, in which case the conventional modal theory breaks down. Since in reality this may only occur at a single frequency point (as noted in the discussion of [23]), the main difficulty may arise when the transformation is nearly singular for frequencies leading up to, and beyond the non-diagonalization frequency point. However, in such situations, a more generalized modal domain methodology may be employed involving a Jordan decomposition of the argument matrix [23,24].

An alternative approach that has seen considerable interest in recent years [28-40] is to represent the transmission line directly in the phase domain, essentially the natural co-

ordinates of the system. Since the rest of the network is formulated in the phase domain, this completely avoids the problem of using frequency-dependent transformation matrices in the solution process. The additional time domain convolutions required to incorporate the transformation matrices in the solution process are avoided making the phase domain approach slightly more computationally efficient [27,34]. Furthermore, any problems relating to the modal decomposition technique itself, such as non-diagonalization situations, are avoided, preserving the generality of the method. Also, since the analysis is conducted in the natural frame of reference of the system, any geometric imbalances present in the line will intrinsically be taken into account in the solution process.

However, despite the interest that this methodology has received in recent times, the phase domain analysis of power transmission lines remains unsatisfactorily resolved. In all of the methods presented in the open literature thus far [28-40], the initial formulation of the problem in the frequency domain is still undertaken using the established method of modal decomposition to evaluate the transmission line response functions. The phase domain analysis refers only to the solution of the equations in the time domain (see discussion in [28]). In essence these models can be considered as a hybrid of the modal and phase domain methods.

Thus, a complete phase domain transmission line model remains to be realized, and the development and application of such a model provides the focus of this research project.

1.3 Real-Time Digital Power System Simulation

Digital computer based simulation packages such as EMTP [5] and EMTDC [6] are widely used for analysing the overvoltages and overcurrents that arise as a result of abrupt changes in the otherwise steady-state operating conditions of the network, e.g. from switching operations or lightening discharges. In principle, the information obtained from such analysis can be utilized to achieve effective system protection and insulation co-ordination so that equipment failures and unnecessary transmission line outages are prevented during transient conditions.

However, one of the most significant disadvantages of these software based simulators concerns the computational efficiency with which they operate. A transient disturbance in the network, which may only last for a period of milliseconds, may take the simulator many seconds or even minutes to perform the necessary computations and produce a solution for the given disturbance [48,49]. Since the simulator in this case does not operate in real-world time (i.e. the solution output is determined at either a slower or faster rate) external equipment cannot be interfaced directly to the simulator. Since the control inputs necessary for the testing of physical control and protection equipment are dynamic in nature, meaningful testing of these devices requires the simulated waveforms to be input into the device in real-time . Simulation packages such as EMTP [5] and EMTDC [6] have therefore been of little use in these areas [48,49].

In order to fulfill this aspect of dynamic simulation, the testing of physical control and protection equipment has instead been undertaken using special playback devices, or analogue simulators [48,49,53,58,59]. For the playback device, the results from an off-line electromagnetic transient simulation, or actual data obtained from Digital Fault Recorders (DFRs), are fed, in real-time, to the device under test. However, these devices are restricted to open-loop testing – there can be no dynamic interaction between the device under test and the simulator [48]. In addition, storage requirements can limit the length of the simulation that can be played back for a particular test [53].

In order to conduct closed-loop testing of physical control and protection equipment, analogue HVDC simulators and AC Transient Network Analyzers (TNAs) have been widely used throughout the power system industry [48,49,53,58,59]. These simulators are essentially made up of scaled down power system components, with each component physically connected to the next in a similar manner to that of the real system. However, traditional analogue simulators can be very expensive to maintain and operate, and general accessibility is low since the time cycle for a particular study may occupy the analogue simulator for many weeks [48,49].

In the last decade, there has been a growing trend by manufacturers, large utilities and research organizations to adopt a new, more cost effective and flexible technology to replace the previous generation of analogue network analyzers - real-time digital power system simulators with hardware-in-the-loop (HIL) capabilities [43-52,54-62].

The term "real-time" as it relates in this context, requires that the digital computer simulation of the modelled power system is executed in real-world time (i.e. not faster or slower). Thus, these simulators can represent dynamic phenomena in the power system as they occur. This permits actual hardware to be mixed with computer models to replicate the total power network under investigation. In addition, the time cycle for performing such tests is reduced from weeks (for the case of analogue simulators) to days [48]. Furthermore, simulation results can be conveniently analysed as tabulated data or waveforms that can be displayed, printed, or saved for later analysis.

The closed-loop operation of these simulators provides a very powerful tool for extensively evaluating and accurately testing new and existing equipment under normal and abnormal operating conditions to verify the equipment's performance and settings. This also enables the response of the power system to the operation, or miss-operation of the device under test to be analysed. With the increasing complexity of modern power systems, the effects and interactions of the various power system components on each other is increasingly important and real-time technology provides a convenient tool to analyze such problems [48,49,59].

1.4 Motivation Behind This Research

This research is primarily concerned with the phase domain modelling of power transmission lines for both non-real-time and real-time electromagnetic transient studies. The modelling of transmission lines in the phase domain using conventional digital computers, i.e. non-real-time, has been an area of great interest in recent years [28-40]. Despite this however, there is to date no phase domain model available in the open literature in which the complete analysis is undertaken in phase co-ordinates.

Thus far, the initial formulation of the problem in the frequency domain has involved evaluating impulse responses using the method of modal decomposition [28-40], a method presented over forty years ago [21,22]. As stated earlier, current phase domain models can therefore be regarded as a hybrid between the phase and modal methodologies.

The very important aspect of unwinding the wave propagation matrix in the phase domain is still to be satisfactorily resolved. For asymmetrical and multi-circuit transmission line configurations, attempting to unwind the elements of the phase domain wave propagation matrix using modal domain type methods, as in current phase domain models, has not proved universally successful [28,30-33].

However, performing the analysis in the phase domain, which may be regarded as the natural frame of reference for the system, should provide inherent advantages over conventional modal domain approaches: -

1. Any geometric imbalances associated with the transmission line design, such as the spacing and configuration of the phase conductors, are intrinsically taken into account when the analysis is formulated in phase co-ordinates.
2. Since the rest of the network is represented in the phase domain, performing the analysis in this frame of reference completely avoids the problem of having to include frequency-dependent transformation matrices in the time domain solution to exchange information between the modal and phase domains, and vice-versa. The number of time domain convolutions is therefore reduced for phase domain models making the methodology slightly more computational efficient.
3. Since modal transformations are not required at any point in the formulation of the problem, any difficulties that might arise concerning the non-diagonalization of the governing coupled wave equations (which would necessitate a more generalized modal approach using Jordan decompositions) can never arise, preserving the generality of the proposed method.
4. With the use of modal transformations, a mathematical description of the transmission line is created which may prove difficult to relate to the actual electromagnetic transient phenomena. In contrast, conducting a similar analysis, but in the frame of reference of the phases should provide a closer resemblance to the actual electromagnetic transient phenomena under study.

This research is therefore dedicated to developing a new overhead transmission line model for conducting electromagnetic transient simulations in which not only the frequency-dependent effects are accurately included, but also the transmission line imbalances.

Concerning real-time applications, the cost effective, compact and flexible qualities associated with real-time digital power system simulators, as compared to traditional analogue simulators, will no doubt continue to see their adoption into manufacturing, utility and research organizations. The computational power of these simulators is increasingly expanding allowing more complex power networks and simulation scenarios to be investigated. Coupled with this, more accurate representations of the individual power system components can be realized. However, in order to make use of these expanded capabilities, the system models must be continually upgraded and improved upon.

As a part of this drive for new and improved component models, this research project has focussed on the development of a new generation of transmission line models for performing general electromagnetic transient simulations. Unlike all previous line representations proposed for real-time digital simulation thus far, based on a modal domain methodology [43,44,46,47], the model presented in this thesis is formulated directly in the phase domain.

It is proposed therefore to develop a real-time simulation environment in which the improved accuracy and generality afforded with the new phase domain representation of the line can be utilized, so as to provide a standard model for analysing electromagnetic transients in power transmission lines in real-time.

1.5 Objectives and Purposes of the Present Work

The objectives of the research carried in this thesis were as follows:

- To construct both frequency-independent and frequency-dependent transmission line models, based on well-established methodologies, whose use has been widespread for performing electromagnetic transient studies, and to integrate these

models into a digital computer program. These models provide a comparable capability to what is available in existing industrial computer programs and provide a benchmark for assessing the accuracy of newly developed methods.

- To develop a new transmission line model in which both the frequency and time domain analysis is undertaken entirely in phase co-ordinates, and which accurately takes into account all the frequency-dependent effects given in the available frequency domain data as well as any geometric imbalances naturally present in the transmission line. The development of such a model should provide improved levels of accuracy and generality over existing methods for performing electromagnetic transient simulations.

- To develop accurate and efficient methods for evaluating the phase domain characteristic admittance and wave propagation functions in the frequency domain, completely avoiding the use of eigenvector transformation matrices in the process. The algorithms must be generally applicable and not restricted to certain transmission line topologies or number of phase conductors. As already stated, by evaluating these functions directly in the phase domain, any geometric imbalances naturally present in the line are intrinsically taken into account. This ensures a very high level of accuracy is achieved when evaluating these functions.

- To develop a process whereby the phase domain wave propagation matrix, $\mathbf{H}(\omega)$, can be 'unwinded', directly in phase co-ordinates, in such a way that accurate, rational function approximations can be made without requiring an excessive number of poles in the fitting process. By unwinding this function directly in the phase domain, the coupled travel times of the system are intrinsically taken into account in the process, ensuring the elements of $\mathbf{H}(\omega)$ are obtained as smooth functions of frequency. The method of Vector Fitting [41] is to be applied to obtain the low-order rational function approximations in the phase domain so that each element of a column of $\mathbf{H}(\omega)$ can be fitted with the same set of poles thereby increasing the efficiency of the final time domain algorithm by 2-fold [38] over element-by-element fitting.

- The phase domain transmission line model should be constructed in such a way that in can be interfaced directly into a general-purpose electromagnetic transient program. A digital program should then be developed to perform time domain electromagnetic transient studies, incorporating the new transmission line representation.

- To assess the accuracy of the newly developed model by performing various electromagnetic transient simulations and comparing the results against those obtained using conventional transmission line representations utilizing modal domain decompositions and available field measurements to ensure model fidelity.

- To develop an environment for performing accurate and reliable real-time electromagnetic transient simulations of practical transmission systems, incorporating the transmission line models implemented in this research. The efficiency and practical application of each line model for conducting real-time simulations should also be investigated. This will provide a means for accurately testing and developing new and existing power system components in an efficient manner.

1.6 Publications

The following publications were generated during the course of the present research:

1.6.1 Transaction-graded Papers

- J. A. Parle and E. Acha: 'Phase Domain Evaluation of Transmission Line Responses for Electromagnetic Transient Analysis Using Padé Approximation', Submitted to IEEE Transactions on Power Delivery, 2000.
- J. A. Parle and E. Acha: 'A Phase Domain Transmission Line Model for Real-Time Electromagnetic Transient Studies', Submitted to IEEE Transactions on Power Delivery, 2000.

1.6.2 Conference Papers

- J. A. Parle, E. Acha and C. R. Fuerte-Esquivel: 'Real-Time Digital Simulation of Electromagnetic Transient Phenomena in Power Transmission Lines', Proceedings of the International Conference on Advances in Power System Control, Operation and Management 1997 (APSCOM 99), Vol. 2, Hong Kong, November 11-14, 1997, pp. 563-568.
- J. A. Parle, E. Acha and C. R. Fuerte-Esquivel: 'Real-Time Implementation of Transmission Line Models for Electromagnetic Transient Studies', Proceedings of the International Conference on Digital Power System Simulators 1999 (ICDS 99), Västerås, Sweden, May 25-28, 1999.
- J. A. Parle, E. Acha and C. R. Fuerte-Esquivel: 'Real-Time Simulation of Transmission Line Transients Using Vector Fitting', Proceedings of the Power Systems Computation Conference 1999 (PSCC 99), Vol. 2, Trondheim, Norway, June 28-July 2, 1999, pp. 1033-1039.

1.7 Contributions

The main contributions of the research work are summarized below:

- Algorithms are presented which allow accurate and efficient determination of both the characteristic admittance and wave propagation matrices directly in the phase domain using Padé approximation techniques. By conducting the analysis in this frame of reference, all the frequency-dependent effects associated with these functions, as well as any geometric imbalances in the line are intrinsically taken into account. The algorithms can be applied to single circuit, multi-circuit and asymmetrical line configurations, with no restriction on the number of phase conductors included. The algorithm for evaluating the characteristic admittance matrix is derived by exploiting a relationship between the matrix sign function and the matrix square root. The wave propagation matrix is evaluated directly in phase co-ordinates by applying a Padé approximation technique to the matrix exponential function. Computation of eigenvector transformation matrices is completely avoided in these methods.
- The difficulty of 'unwinding' the elements of the wave propagation matrix in the phase domain is overcome by applying a matrix phase shift function. Since the problem is formulated in phase co-ordinates, the coupled time delays of the system are intrinsically taken into account in the unwinding process. The elements of the phase domain wave propagation function can then be approximated with rational functions, with a relatively small number of poles used in the fitting process. The phase shift function is approximated in the time domain with scalar impulse functions.

- The equivalent circuit representation of the new phase domain transmission line model is compatible with general purpose electromagnetic transient programs and can be interfaced in a similar manner to existing models.
- A digital computer program has been written to perform time domain electromagnetic transient simulations. The new phase domain model is incorporated within this program and test cases have been performed. The accuracy of the proposed method is further assessed by comparing the time domain results with actual field measurements [42].
- A real-time simulation environment has been developed for performing real-time electromagnetic transient studies, using a commercially available real-time digital simulator. Conventional frequency-independent [7] and frequency-dependent [16,17] models utilizing modal decomposition have been incorporated within this simulation environment. The new phase domain model has been developed within the real-time simulation environment and the accuracy and efficiency of this approach is compared with both the frequency-independent and frequency-dependent line representations.

1.8 Outline of the Thesis

The thesis is organised into seven chapters as described below:

- Chapter 2 deals with the general formulation of two modal domain based transmission line models, which have been widely used for analysing electromagnetic transient problems. The models differ significantly in the degree of accuracy to which the line is represented. The first model assumes the parameters of the line are frequency-independent [7], while the second model takes into account the frequency-dependent characteristics of the parameters by approximating them with rational functions [16] using the method of Vector Fitting [41]. Time domain simulations are presented with the results compared against actual field measurements [42] and EMTP simulation results [5].
- Chapter 3 presents the frequency domain formulation of a new transmission line model in which all the analysis is performed in the phase domain. Algorithms are presented which allow accurate and efficient determination of the characteristic admittance and wave propagation matrices directly in phase co-ordinates. There is no requirement to exchange information between the phase and modal domains when calculating these functions, since the latter is not used. A Padé iteration scheme is used for evaluating the characteristic admittance matrix, derived by exploiting a relationship between the matrix sign function and the matrix square root. Padé approximation techniques have also been used to approximate the matrix exponential in order to evaluate the wave propagation function. Both methods have been extensively tested using line configurations of different size and complexity.
- Chapter 4 describes the time domain formulation of the new phase domain transmission line model. The unwinding of the wave propagation matrix using a matrix phase shift function is discussed. The equivalent circuit representation in the time domain is compatible with general purpose electromagnetic transient programs, such as EMTP and EMTDC.
- Chapter 5 presents the time domain simulations using the newly developed phase domain transmission line model. The accuracy and efficiency of the model is compared to the previous two transmission lines. The results obtained with this new model are compared against available field measurements [42] to assess the accuracy of the proposed methodology.

- Chapter 6 outlines the development of a real-time simulation environment for conducting electromagnetic transient simulations on a commercially available real-time simulator. The transmission line models presented in this thesis are implemented within this simulation environment and their suitability for performing real-time simulations is assessed. The results of a sequential energization of a real-life transmission circuit are presented and for the case of the phase domain transmission line model, compared against actual field measurements [42].
- Chapter 7 presents the conclusions and discusses areas that require further investigation and research effort.

1.9 References

[1] Bickford, J. P., Mullineux, N. and Reed, J. R.: 'Computation of power-system transients', IEE Monograph Series 18, 1980, ISBN 0-906048-35-4.

[2] Gönen, T.: 'Electric Power Transmission System Engineering: Analysis and Design', Wiley, 1988, ISBN 0-471-53313-0.

[3] Humpage, W. D.: 'Z-transform Electromagnetic Transient Analysis in High-Voltage Networks', IEE Power Engineering Series 3, 1982, ISBN 0-906048-79-6

[4] Glover, J. D. and Sarma, M.: 'Power Systems Analysis and Design', PWS-Kent, 1989, ISBN 0-534-07860-5

[5] Dommel, H. W.: 'Electromagnetic Transients Program (EMTP) Rule Book', EPRI EL6421-1, Vol. 1, June 1989.

[6] Manitoba HVDC Research Centre: 'EMTDC Reference – Theory Manual', 1988.

[7] Dommel, H. W.: 'Digital Computer Solution of Electromagnetic Transients in Single-and Multiphase Networks', IEEE Transactions on Power Apparatus and Systems, Vol. PAS-88, No. 4, April 1969, pp. 388-399.

[8] Budner, A.: 'Introduction of Frequency-Dependent Line Parameters into an Electromagnetic Transients Program', IEEE Transactions on Power Apparatus and Systems, Vol. PAS-89, No. 1, January 1970, pp. 88-97.

[9] Snelson, J. K.: 'Propagation of Travelling Waves on Transmission Lines – Frequency Dependent Parameters', IEEE Transactions on Power Apparatus and Systems, Vol. PAS-91, January/February 1972, pp. 85-91.

[10] Dommel, H. W. and Meyer, W. S.: 'Computation of Electromagnetic Transients', Proceedings of the IEEE, Vol. 62, No. 7, July 1974, pp. 983-993.

[11] Carson, J. R.: 'Wave Propagation in Overhead Wires with Ground Return', Bell System Technical Journal, Vol. 5, 1926, pp. 539-554.

[12] Deri, A., Tevan, G., Semlyen, A. and Castanheria, A.: 'The Complex Ground Return Plane, a Simplified Model for Homogeneous and Multi-Layer Earth Return', IEEE Transactions on Power Apparatus and Systems, Vol. 100, 1981, pp. 3686-3693.

[13] Semlyen, A. and Deri, A.: 'Time Domain Modelling of Frequency Dependent Three Phase Transmission Line Impedance', IEEE Transactions on Power Apparatus and Systems, Vol. 94, 1985, pp. 1549-1555.

[14] Meyer, W. S. and Dommel, H. W.: 'Numerical Modelling of Frequency-Dependent Transmission-Line Parameters in an Electromagnetic Transients Program', IEEE

Transactions on Power Apparatus and Systems, Vol. PAS-93, September/October 1974, pp. 1401-1409.

[15] Carroll, D. P. and Nozari, F.: 'An Efficient Computer Method for Simulating Transients on Transmission Lines with Frequency Dependent Parameters', IEEE Transactions on Power Apparatus and Systems, Vol. PAS-94, No. 4, July/August 1975, pp. 1167-1176.

[16] Marti, J.: 'Accurate Modelling of Frequency-Dependent Transmission Lines in Electromagnetic Transient Simulations', IEEE Transactions on Power Apparatus and Systems, Vol. PAS-101, No. 1, January 1982, pp. 147-157.

[17] Marti, J.: 'The Problem of Frequency Dependence in Transmission Line Modelling', PhD Thesis, The University of British Columbia, Canada, April 1981.

[18] Semlyen, A. and Dabuleanu, A.: 'Fast and Accurate Switching Transient Calculations on Transmission Lines with Ground Return Using Recursive Convolutions', IEEE Transactions on Power Apparatus and Systems, Vol. PAS-94, No. 2, March/April 1975, pp. 561-571.

[19] Ametani, A.: 'A Highly Efficient Method for Calculating Transmission Line Transients', IEEE Transactions on Power Apparatus and Systems, Vol. PAS-95, No. 5, September/October 1976, pp. 1545-1551.

[20] Naidu, S. R. and de Lima, F. N.: 'A Frequency-Dependent Transmission Line Model for Electromagnetic Transient Studies', IEE Proceedings, Vol. 132, Pt. C, No. 6, November 1985, pp. 294-297.

[21] Wedepohl, L. M.: 'Application of Matrix Methods to the Solution of Travelling-Wave Phenomena in Polyphase Systems', Proceedings of the IEE, Vol. 100, No. 12, 1963, pp. 2200-2212.

[22] Hedman, D. E.: 'Propagation on Overhead Transmission Lines I-Theory of Modal Analysis', IEEE Transactions on Power Apparatus and Systems, Vol. PAS-84, March 1965, pp. 200-205.

[23] Brandão, J. A. and Borges da Silva, J. F.: 'Wave Propagation in Polyphase Transmission Lines a General Solution to Include Cases Where Ordinary Modal Theory Fails', IEEE Transactions on Power Delivery, Vol. PWRD-1, No. 2, April 1986, pp. 182-189.

[24] Brandão, J. A.: 'Overhead Three-Phase Transmission Lines – Non-Diagonalizable Situations', IEEE Transactions on Power Delivery, Vol. 3, No. 4, October 1988, pp. 1348-1355.

[25] Marti, L.: 'Simulation of Electromagnetic Transients in Underground Cables with Frequency-Dependent Modal Transformation Matrices', PhD Thesis, The University of British Columbia, Canada, November 1986.

[26] Marti, L.: 'Simulation of Transients in Underground Cables with Frequency-Dependent Modal Transformation Matrices', IEEE Transactions on Power Delivery, Vol. 3, No. 3, July 1988, pp. 1099-1110.

[27] Gustavsen, B. and Semlyen, A.: 'Simulation of Transmission Line Transients Using Vector Fitting and Modal Decomposition', IEEE Transactions on Power Delivery, Vol. 13, No. 2, pp. 605-614.

[28] Gustavsen, B. and Semlyen, A.: 'Combined Phase and Modal Calculation of Transmission Line Transients Based on Vector Fitting', IEEE Transactions on Power Delivery, Vol. 13, No. 2, April 1998, pp. 596-604.

[29] Gustavsen, B., Sletbak, J., and Henriksen, T.: 'Calculation of Electromagnetic Transients in Transmission Line Cables and Lines Taking Frequency Dependent Effects Accurately Into Account', IEEE Transactions on Power Delivery, Vol. 10, No. 2, April 1995, pp. 1076-1084.

[30] Nguyen, H. V., Dommel, H. W. and Marti, J. R.: 'Direct Phase Domain Modelling of Frequency-Dependent Overhead Transmission Lines', IEEE Transactions on Power Delivery, Vol. 12, No. 3, July 1997, pp. 1335-1342.

[31] Nguyen, H.: 'Simulation of Lightning Surges on Transmission Lines', PhD Thesis, The University of British Columbia, Canada, February 1996.

[32] Castellanos, F. and Marti, J. R.: 'Phase-Domain Multiphase Transmission Line Models', International Conference on Power System Transients, Lisbon, 3-7 September 1995.

[33] Castellanos, F., Marti, J. R. and Marcano, F.: 'Phase-Domain Multiphase Transmission Line Models', Electrical Power & Energy Systems, Vol. 19, No. 4, 1997, pp. 241-248.

[34] Noda, T., Nagaoka, N. and Ametani, A.: 'Phase Domain Modeling of Frequency-Dependent Transmission Lines by Means of an ARMA Model', IEEE Transactions on Power Delivery, Vol. 11, No. 1, January 1996, pp. 401-411.

[35] Noda, T., Nagaoka, N. and Ametani, A.: 'Further Improvements to a Phase-Domain ARMA Line Model in Terms of Convolution, Steady-State Initialization, and Stability', IEEE Transactions on Power Delivery, Vol. 12, No. 3, July 1997, pp. 1327-1334.

[36] Angelidis, G. and Semlyen, A.: 'Direct Phase-Domain Calculation of Transmission Line Transients Using Two-Sided Recursions', IEEE Transactions on Power Delivery, Vol. 10, No. 2, April 1995, pp. 941-949.

[37] Gustavsen, B: 'A Study of Overvoltages in High Voltage Cables With Emphasis on Sheath Overvoltages', Dr. Ing. Thesis, The Norwegian Institute of Technology, Trondheim, Norway, 1993.

[38] Morched, A., Gustavsen, B. and Tartibi, M.: 'A Universal Model for Accurate Calculation of Electromagnetic Transients on Overhead Lines and Underground Cables', IEEE Transactions on Power Delivery, Vol. 14, No. 3, July 1999, pp. 1032-1038.

[39] Soysal, A. O. and Semlyen, A.: 'State Equation Approximation of Transfer Matrices and its Applications to the Phase Domain Calculation of Electromagnetic Transients', IEEE Transactions on Power Systems, Vol. 9, No. 1, February 1994, pp. 420-428.

[40] Castellanos, F. and Marti, J. R.: 'Full Frequency-Dependent Phase-Domain Transmission Line Model', IEEE Transactions on Power Systems, Vol. 12, No. 3, August 1997, pp. 1331-1339.

[41] Gustavsen, B. and Smelyen, A.: 'Rational Approximation of Frequency Domain Responses by Vector Fitting', IEEE Transactions on Power Delivery, Vol. 14, No. 3, July 1999, pp. 1052-1061.

[42] Dommel, H. W., Yan, A., Ortiz de Marcano, R. J. and Miliani, A. B.: 'Case Studies for Electromagnetic Transients', Internal Report, The Department of Electrical Engineering, The University of British Columbia, Canada, May 1983.

[43] Mather, R. M. and Wang, X.: 'Real-Time Digital Simulator of the Electromagnetic Transients of Power Transmission Lines', IEEE Transactions on Power Delivery, Vol. 4, No. 2, April 1989, pp. 1275-1280.

[44] Wang, X. and Mather, R. M.: 'Real-Time Digital Simulator of the Electromagnetic Transients of Transmission Lines with Frequency Dependence', IEEE Transactions on Power Delivery, Vol. 4, No. 4, October 1989, pp. 2249-2255.

[45] Devaux, O., Levacher, L. and Huet, O.: 'An Advanced and Powerful Real-Time Digital Transient Network Analyser', IEEE Transactions on Power Delivery, Vol. 13, No. 2, April 1998, pp. 421-426.

[46] Dufour, C., Le-Huy, H., Soumagne, J. and El Hakimi, A.: 'Real-Time Simulation of Power Transmission Lines Using Marti Model with Optimal Fitting on Dual-DSP Card', IEEE Transactions on Power Delivery, Vol. 11, No. 1, January 1996, pp. 412-419.

[47] Wang, X., Woodford, D. A., Kuffel, R. and Wierckx, R.:'A Real-Time Transmission Line Model for a Digital TNA', IEEE Transactions on Power Delivery, Vol. 11, No. 2, April 1996, pp. 1092-1097.

[48] Wierckx, R. P.: 'Fully Digital Real-Time Electromagnetic Transients Simulator', IERE International Electric Research Exchange, Workshop on New Issues in Power System Computation, Caen, France, March 1992.

[49] Kuffel, R., Giesbrecht, J., Maguire, T., Wierckx, R. P. and McLaren, P.: 'RTDS – A Fully Digital Power System Simulator Operating in Real Time', 1st International Conference on Digital Power System Simulators, ICDS '95, College Station, USA, April 1995.

[50] McLaren, P., Kuffel, R., Wierckx, R., Giesbrecht, J. and Arendt, L.: 'A Real-Time Digital Simulator for Testing Relays', IEEE Transactions on Power Delivery, Vol. 7, No. 1, January 1992, pp. 207-213.

[51] Kuffel, R., McLaren, P., Yalla, M. and Wang, X.: 'Testing of the Beckwith Electric M-0430 Multifunction Protection Relay Using a Real-Time Digital Simulator (RTDS), 1st International Conference on Digital Power System Simulators, ICDS '95, College Station, USA, April 1995.

[52] McLaren, P. C., Dirks, E. N., Jayasinghe, R. P., Swift, G. W. and Zhang, Z.: 'Using a Real-Time Digital Simulator to Develop an Accurate Model of a Digital Relay', 1st International Conference on Digital Power System Simulators, ICDS '95, College Station, USA, April 1995.

[53] Kezunović, M. *et al.*: 'Digital Simulator Performance Requirements for Relay Testing', IEEE Transactions on Power Delivery, Vol. 13, No. 1, January 1998, pp. 78-84.

[54] Lerch, E., Ruhle, O., Winter, W., Kulicke, B. and Pannhorst, H. –D.: 'Real-Time Simulator ARTEMAC for Enhanced Automated Interactive Testing of Digital Relays', International Conference on Power System Transients, IPST '99, Budapest, Hungary, June 1999.

[55] Kaiser, S., Lerch, E., Ruhle, O., Winter, W. and Kulicke, B.: 'New Approach for PC-Based Interactive Real-Time Testing of Digital Relays and Controller

Structures', 3rd International Conference on Digital Power System Simulators, ICDS '99, Västerås, Sweden, May 1999.

[56] Wierckx, R. P., Giesbrecht, W. J., Kuffel, R., Wang, X., Mazur, G. B., Weekes, M. A. and Gole, A. M.: 'Validation of a Fully Digital Real-Time Electromagnetic Transient Simulator for HVDC System & Control Studies', Athens Power Tech., Athens, Greece, September 1993.

[57] Wang, X., Giesbrecht, J., Woodford, D., Arendt, L., Wierckx, R. and Kuffel, R.: 'Enhanced Performance of a Conventional HVDC Analogue Simulator with a Real-Time Digital Simulator', 11th Power Systems Computation Conference, PSCC '93, Avignon, France, August 1993.

[58] Duchen, H., Lagerkvist M., Kuffel, R. and Wierckx, R. P.: 'HVDC Simulation and Control System Testing Using a Real-Time Digital Simulator (RTDS)', 1st International Conference on Digital Power System Simulators, ICDS '95, College Station, USA, April 1995.

[59] Kuffel, R., Wierckx, R. P., Duchén, H., Lagerkvist, M. and Wang, X.: 'Expanding an Analogue HVDC Simulator's Modelling Capability Using a Real-Time Digital Simulator (RTDS), 1st International Conference on Digital Power System Simulators, ICDS '95, College Station, USA, April 1995.

[60] Do, Van-Qué, Soumagne, J. C., Sybille, G., Turmel, G., Giroux, P., Cloutier, G. and Poulin, S.: 'Hypersim, an Integrated Real-Time Simulator for Power Networks and Control Systems', 3rd International Conference on Digital Power System Simulators, ICDS '99, Västerås, Sweden, May 1999.

[61] Fujimoto, Y., Bin, Y., Taoka, H., Tezuka, H., Sumimoto, S. and Ishikawa, Y.: 'Real-Time Power System Simulator on a PC Cluster', International Conference on Power Systems Transients, IPST '99, Budapest, Hungary, June 1999.

[62] Snider, L., Ggnon, C. and Cloutier, G.: 'Real-Time Power System Simulators: Contributing to the Successful Development of Complex Power Systems', 4th International Conference on Advances in Power System Control, Operation & Management, APSCOM'97, Hong Kong, Nov. 11-14 1997.

[63] Song, Y. H. & Johns, A. T.: 'Flexible AC Transmission Systems (FACTS)', IEE Power and Energy Series 30, 1999.

CHAPTER 2

MODAL DOMAIN POWER TRANSMISSION LINE MODELLING

The accurate and efficient modelling of multiphase power transmission lines has been the subject of much interest in the development of electromagnetic transient programs, such as the EMTP for many decades. This chapter therefore provides a summary of the techniques proposed in the open literature for EMTP-type studies. A frequency-independent transmission line model is presented that represents the line as a pure delay and a characteristic impedance. A second, more detailed line model is also presented that takes into account the frequency domain variation of the line parameters by fitting them with low-order rational functions using the method of Vector Fitting. This enables a recursive formulation of the convolution integrals to be obtained, increasing the computational efficiency of the model. A sequential energization of a 345kV transmission system is performed to assess the relative accuracy of the frequency-independent and frequency-dependent models. Results are compared to those obtained using the EMTP and with available field measurements to assess the accuracy of the line models.

2.1 Introduction

The accurate and efficient representation of multiconductor power transmission lines has been the subject of much effort, even before the Electromagnetic Transients Program (EMTP) was introduced by Dommel in the 1960s [1,3]. The method of characteristics and the trapezoidal rule of integration are combined in this method to accurately simulate transients arising in power networks involving distributed as well as lumped parameter elements. The equations of both methods are represented by simple equivalent impedance networks comprising of a current source in parallel with a constant admittance, i.e. a Norton equivalent representation. This leads to the solution of a system of linear (nodal) equations at each time step of the simulation [1,3,4].

The initial line model presented in [3] represented the line as lossless, with the travelling waves propagating with velocities characteristic to the media in which they are travelling. The parameters of the line, namely the resistance, inductance, capacitance and conductance (which is usually negligible) [10] are assumed constant and evaluated at a user defined frequency. The line model is then represented as a time delay and a characteristic impedance. However, due to the presence of the ground, these line parameters may vary significantly with frequency and therefore this variation must be taken into account if accurate results are sought [5-13]. A comment to this end was made in Dommel's original paper [3].

General electromagnetic transient programs such as EMTP [1] and EMTDC [2] obtain the network solution in the time domain, since most aspects of transient operation in power systems are more conveniently formulated when the variables are expressed as functions of time, e.g. the operation of circuit-breakers [10], as stated in the introduction. However, the modelling of power transmission lines is usually made initially in the frequency domain in order to reflect the frequency-dependent

characteristics of the line. These transmission line responses are then incorporated in the time domain through numerical convolutions [5-10].

A direct evaluation of the numerical convolutions can be performed at each time step of the simulation, but the resulting computational efficiency of the method is poor [9-11]. However, if the line responses are approximated in the frequency domain with rational function approximations, or in the time domain with piecewise linear functions [12], then a recursive formulation of the convolution integrals can be constructed, significantly increasing the overall efficiency of the analysis [11].

For multiconductor transmission lines, the magnetic coupling that exists between phase conductors results in a system of coupled partial differential equations in time and space. In conventional EMTP [24] studies, this system of coupled equations is reduced to a set of uncoupled single-phase like equations using the method of modal decomposition [14-15]. Calculations related to travelling waves are performed for the decoupled modes and phase domain variables are obtained by inverse transformation.

Although the transformation matrix is in general frequency-dependent, for improved efficiency it is common practice to use real and constant transformation matrices for performing the modal decomposition [9,18-20]. While a constant transformation matrix can obviously not provide perfect diagonalization over a wide frequency range, for single-circuit transmission line configurations the frequency-dependence of the transformation matrix is not significant [9]. The off-diagonal elements of the transformed transmission line responses may therefore be neglected, so that these matrices can essentially be assumed decoupled [39].

This chapter provides a summary of the main steps involved in power transmission line modelling for electromagnetic transient analysis. Both frequency-independent and frequency-dependent multiconductor transmission line models, based on well-established methodologies [3,9], are presented. In these models, the coupled equations that govern the behaviour of voltage and current waveforms along the line are decoupled into a set of independent modes using the method of modal decomposition [14,15]. The accuracy of both line models is assessed by performing a sequential energization of a real-life transmission system. The results are compared with those obtained using the EMTP and against available field measurements to assess modal accuracy [34].

2.2 Basic Transmission Line Theory

The electromagnetic behaviour of a system of n parallel conductors in the frequency domain can be described by the following two matrix equations relating phase voltages, $\mathbf{V}(x,\omega)$, to phase currents, $\mathbf{I}(x,\omega)$, at a distance x along the line [1,6,9-10,18,22,24-26,31]

$$-\frac{\partial \mathbf{V}(x,\omega)}{\partial x} = \mathbf{Z}(\omega)\mathbf{I}(x,\omega) \tag{2.1}$$

$$-\frac{\partial \mathbf{I}(x,\omega)}{\partial x} = \mathbf{Y}(\omega)\mathbf{V}(x,\omega) \tag{2.2}$$

where $\mathbf{Z}(\omega)$ and $\mathbf{Y}(\omega)$ are the per unit length series impedance and shunt admittance matrices, respectively, which can be expressed as,

$$\mathbf{Z}(\omega) = \mathbf{R}(\omega) + j\omega\mathbf{L}(\omega) \tag{2.3}$$

$$\mathbf{Y}(\omega) = \mathbf{G}(\omega) + j\omega\mathbf{C}(\omega) \tag{2.4}$$

where the n x n matrices $\mathbf{R}(\omega)$, $\mathbf{L}(\omega)$, $\mathbf{G}(\omega)$ and $\mathbf{C}(\omega)$ are defined as the resistance,

inductance, conductance and capacitance, respectively. Both $\mathbf{Z}(\omega)$ and $\mathbf{Y}(\omega)$ are complex n x n matrices. The vectors of voltage, $\mathbf{V}(x,\omega)$, and currents, $\mathbf{I}(x,\omega)$, are complex quantities of dimension n. Differentiating both (2.1) and (2.2), with respect to x, and combining, yields the well known wave propagation equations in the frequency domain,

$$\frac{\partial^2 \mathbf{V}(x,\omega)}{\partial x^2} = [\mathbf{Z}(\omega)\mathbf{Y}(\omega)]\mathbf{V}(x,\omega) = \gamma^2(\omega)\mathbf{V}(x,\omega) \tag{2.5}$$

$$\frac{\partial^2 \mathbf{I}(x,\omega)}{\partial x^2} = [\mathbf{Y}(\omega)\mathbf{Z}(\omega)]\mathbf{I}(x,\omega) = \gamma^2(\omega)\mathbf{I}(x,\omega) \tag{2.6}$$

2.2.1 Modal Decomposition

The above system of equations represents the system in terms of coupled (matrix) phase quantities, due to the magnetic coupling that exists between the travelling waves propagating along the conductors of the transmission lines [10,31]. Therefore, while the general solution to (2.5) and (2.6) can be obtained with relative ease, the practical calculation of the solution for the voltage and current profiles along the line is very difficult, since matrix computations of the form,

$$\boldsymbol{\gamma}(\omega) = [\mathbf{Z}(\omega)\mathbf{Y}(\omega)]^{1/2} \tag{2.7}$$

and

$$e^{-\boldsymbol{\gamma}(\omega)l} \tag{2.8}$$

are required (the product $\mathbf{Z}(\omega)\mathbf{Y}(\omega)$ being a full, complex n x n matrix). The accurate and efficient evaluation of (2.7) and (2.8) for calculating the phase domain characteristic admittance matrix, $\mathbf{Y}_c(\omega)$, and wave propagation matrix, $\mathbf{H}(\omega)$, for phase domain transmission line modelling is the subject of the next chapter.

The established approach to the problem of solving the coupled wave equations of (2.5) and (2.6) for multicondutor lines was proposed over forty years ago. Wedepohl [14] and Hedman [15] introduced elegant matrix algebra techniques to transfer the analysis from the coupled phase domain to the uncoupled modal domain. The resulting n independent single phase-like lines can then be solved directly in terms of modal parameters, in a similar manner to that of a single-phase system. The independent modal solutions are then recombined in the phase domain and the network solution is obtained in phase co-ordinates.

A new, alternative approach has been developed in this thesis which does not require the use of matrix eigenvector/eigenvalue decompositions. The coupled wave equations describing the propagation of the voltage and current along the line are evaluated directly in the phase domain. The new method is developed in the proceeding chapters.

The salient points of the method of modal decomposition are now described below:

At each frequency point of interest, it is assumed that there exists a non-singular matrix of eigenvectors, $\mathbf{T}_V(\omega)$, that diagonalizes the matrix product $\boldsymbol{\gamma}^2(\omega)$ in (2.5), as follows [14,15],

$$\mathbf{T}_V^{-1}(\omega)\boldsymbol{\gamma}^2(\omega)\mathbf{T}_V(\omega) = \boldsymbol{\gamma}^{m^2}(\omega) \tag{2.9}$$

where $\boldsymbol{\gamma}^{m^2}(\omega)$ is a diagonal matrix containing the eigenvalues of $\mathbf{Z}(\omega)\mathbf{Y}(\omega)$ (i.e. the squared modal propagation constants) along the diagonal. Since the matrices $\mathbf{Z}(\omega)$ and

$\mathbf{Y}(\omega)$ are both symmetric [14,15], the transformation matrix required to diagonalize the matrix product $\mathbf{Y}(\omega)\mathbf{Z}(\omega)$ in (2.6) follows immediately, being given by,

$$\mathbf{T}_I^{-1}(\omega)\mathbf{Y}(\omega)\mathbf{Z}(\omega)\mathbf{T}_I(\omega) = \gamma^{m^2}(\omega) \tag{2.10}$$

and the following relationship holds,

$$\mathbf{T}_V(\omega)\mathbf{T}_I'(\omega) = \mathbf{U} \tag{2.11}$$

where $\mathbf{U}$ is defined as the n x n identity matrix. A new set of quantities can now be defined using the transformation matrices $\mathbf{T}_V(\omega)$ and $\mathbf{T}_I(\omega)$ as follows,

$$\mathbf{V}^m(\omega) = \mathbf{T}_V^{-1}(\omega)\mathbf{V}(\omega) \tag{2.12}$$

$$\mathbf{I}^m(\omega) = \mathbf{T}_I^{-1}(\omega)\mathbf{I}(\omega) \tag{2.13}$$

Thus, by applying the transformation matrices $\mathbf{T}_V(\omega)$ and $\mathbf{T}_I(\omega)$, the reference system of the line is changed from phase co-ordinates to modal quantities (denoted by superscript m), with the advantage that all the travelling voltage and current waves are now uncoupled. Each mode has a distinctive pattern of propagation given by the modal propagation constant,

$$\gamma^m(\omega) = \alpha^m(\omega) + j\beta^m(\omega) \tag{2.14}$$

where $\alpha^m(\omega)$ is the modal attenuation factor and $\beta^m(\omega)$ defines the phase velocity of each mode. Substituting (2.12) and (2.13) into the coupled wave equations of (2.5) and (2.6) respectively yields the following modal wave propagation equations,

$$\frac{\partial^2\mathbf{V}^m(x,\omega)}{\partial x^2} = \left[\mathbf{T}_V^{-1}(\omega)\mathbf{Z}(\omega)\mathbf{Y}(\omega)\mathbf{T}_V(\omega)\right]\mathbf{V}^m(x,\omega) = \gamma^{m^2}(\omega)\mathbf{V}^m(x,\omega) \tag{2.15}$$

$$\frac{\partial^2\mathbf{I}^m(x,\omega)}{\partial x^2} = \left[\mathbf{T}_I^{-1}(\omega)\mathbf{Y}(\omega)\mathbf{Z}(\omega)\mathbf{T}_I(\omega)\right]\mathbf{I}^m(x,\omega) = \gamma^{m^2}(\omega)\mathbf{I}^m(x,\omega) \tag{2.16}$$

Thus, to summarise, the original coupled system of equations, as defined by (2.5) and (2.6) have been reduced to a decoupled system, (2.15) and (2.16), using modal transformation matrices. Each independent mode can be solved in a similar manner to that for a single-phase system. The modal voltages and currents are then transformed back and forth from the modal domain to the phase domain, at each time step of the simulation, by making use of the relationships defined in (2.12) and (2.13). The network solution is subsequently obtained directly in phase co-ordinates.

2.2.2 Frequency-Dependent Characteristics of $\mathbf{T}(\omega)$

As stated previously, the eigenvalue/eigenvector problem of (2.9) and (2.10) is solved at each discrete frequency point of interest [14,15]. In general, the modal transformation matrices will have complex elements that are functions of frequency [11,18-22]. However, the currently used transmission line models in transient programs such as the EMTP [1] and EMTDC [2] utilize modal decomposition assuming a real constant transformation matrix, $\mathbf{T}_0$, calculated at a user defined frequency ω_0. By assuming a constant transformation matrix, a considerable increase in the computational efficiency of the time domain simulation is attained.

This approach can be justified for many overhead lines of interest (in particular, horizontal line configurations with a plane of symmetry) because the frequency-dependence of the transformation matrix is weak. Therefore, at frequency values other

than ω_0 the non-diagonal elements will not be zero, but are in general small compared to the diagonal and can be neglected [39].

If the transformation matrix is assumed constant, then the relationships defined in (2.12) and (2.13) can be transformed directly into the time domain to give,

$$\mathbf{v}^m(t) = \mathbf{t}_{\mathrm{v}0}^{-1}\mathbf{v}(t) \tag{2.17}$$

$$\mathbf{i}^m(t) = \mathbf{t}_{i0}^{-1}\mathbf{i}(t) \tag{2.18}$$

Therefore, only a series of multiplications are required to transform the solution back and forth between the modal and phase domains at each time step during the simulation, making this approach very computationally efficient. However, for multi-circuit lines, asymmetrical line configurations and cable systems, the frequency-dependence of the transformation matrix may be strong and should therefore be taken into account [18-32].

In principle, the frequency dependence of the transformation matrix can be included in the time domain simulation by introducing numerical convolutions, albeit with a decrease in the computational efficiency of the model. This method has been undertaken successfully for the simulation of electromagnetic transients in underground high voltage cable systems [18-19]. However, for overhead lines it may not always be possible to obtain an accurate rational function approximation of the elements of the transformation matrix using stable poles only [20,32].

An alternative approach, which is recommended in this thesis, is to formulate the line model directly in the phase domain, thereby avoiding the problem of frequency-dependent transformation matrices completely [21-32]. The development of this phase domain transmission line model is discussed in greater detail in the next chapter.

2.2.2.1 Transposed Transmission Lines

In the case of completely balanced lines, further simplifications can be made regarding the choice of the transformation matrix. For a transposed line, the system can be decoupled by means of real, constant matrices that are independent of the particular line under investigation [38]. Examples of these matrices are the Clark Transformation and Karrenbauer transformation, which is defined as,

$$\mathbf{T}_{\mathrm{v}} = \mathbf{T}_{\mathrm{i}} = \begin{bmatrix} 1 & 1 & \cdots & 1 \\ 1 & 1-n & \cdots & 1 \\ \vdots & \vdots & \ddots & \vdots \\ 1 & 1 & \cdots & 1-n \end{bmatrix} \tag{2.19}$$

where n is the number of phases. The Karrenbauer transformation has the advantage that it is not restricted to three-phase systems, but can be applied to any number of phases.

2.3 Frequency-Independent Transmission Line Model

If the losses are neglected (R=G=0), assuming the transmission system to be lossless, then the modal travelling wave equations, (2.15) and (2.16), can be transformed directly into the time domain to give,

$$\frac{\partial^2 \mathrm{v}(x,t)}{\partial x} = \mathrm{LC}\frac{\partial^2 \mathrm{v}(x,t)}{\partial t^2} \tag{2.20}$$

$$\frac{\partial^2 \mathrm{i}(x,t)}{\partial x^2} = \mathrm{CL}\frac{\partial^2 \mathrm{i}(x,t)}{\partial t^2} \tag{2.21}$$

where for convenience the subscript m is dropped. The solution of the above wave equations was first derived in the eighteenth century by d'Alembert and describes the solution as a sum of forward, $f_1(x\text{-}\upsilon t)$, and backward, $f_2(x+\upsilon t)$, travelling waves, moving with a velocity, υ [1,3-4]

$$\mathrm{i}(x,t) = f_1(x-\upsilon t) + f_2(x+\upsilon t) \tag{2.22}$$

$$\mathrm{v}(x,t) = \mathrm{Z} f_1(x-\upsilon t) - \mathrm{Z} f_2(x+\upsilon t) \tag{2.23}$$

The functions $f_1(x\text{-}\upsilon t)$ and $f_2(x+\upsilon t)$ are defined completely from boundary and intial conditions. The parameters υ and Z are defined as the velocity of propagation and surge impedance, respectively,

$$\upsilon = \sqrt{\frac{1}{\mathrm{LC}}} \tag{2.24}$$

$$\mathrm{Z} = \sqrt{\frac{\mathrm{L}}{\mathrm{C}}} \tag{2.25}$$

Dommel [3] observed that the relation between the current and voltage at one end of the line (node 1) at a given time t is known from the past values of the corresponding quantities at the opposite end of the line (node 2) at τ units of time earlier,

$$\mathrm{v}_1(t) + \mathrm{Z}[-\mathrm{i}_1(t)] = \mathrm{v}_2(t-\tau) + Z\,\mathrm{i}_2(t-\tau) \tag{2.26}$$

and vice-versa,

$$\mathrm{v}_2(t) + \mathrm{Z}[-\mathrm{i}_2(t)] = \mathrm{v}_1(t-\tau) + Z\,\mathrm{i}_1(t-\tau) \tag{2.27}$$

where, for a line of length l, the quantity τ is termed the travel time and can be defined as the time taken for a wave to propagate from one end of the line to the other,

$$\tau = \frac{l}{\upsilon} \tag{2.28}$$

Re-arranging (2.26) and (2.27) gives,

$$\mathrm{i}_1(t) = \frac{1}{\mathrm{Z}}\mathrm{v}_1(t) + \mathrm{I}_1(t-\tau) \tag{2.29}$$

$$\mathrm{i}_2(t) = \frac{1}{\mathrm{Z}}\mathrm{v}_2(t) + \mathrm{I}_2(t-\tau) \tag{2.30}$$

where the current sources, $\mathrm{I}_1(t\text{-}\tau)$ and $\mathrm{I}_2(t\text{-}\tau)$ are completely defined from past history values of the line end voltages and currents,

$$\mathrm{I}_1(t-\tau) = -\frac{1}{\mathrm{Z}}\mathrm{v}_2(t-\tau) - \mathrm{i}_2(t-\tau) \tag{2.31}$$

$$\mathrm{I}_2(t-\tau) = -\frac{1}{\mathrm{Z}}\mathrm{v}_1(t-\tau) - \mathrm{i}_1(t-\tau) \tag{2.32}$$

Figure 2.1 shows the corresponding equivalent impedance network, which describes the lossless line at its terminals.

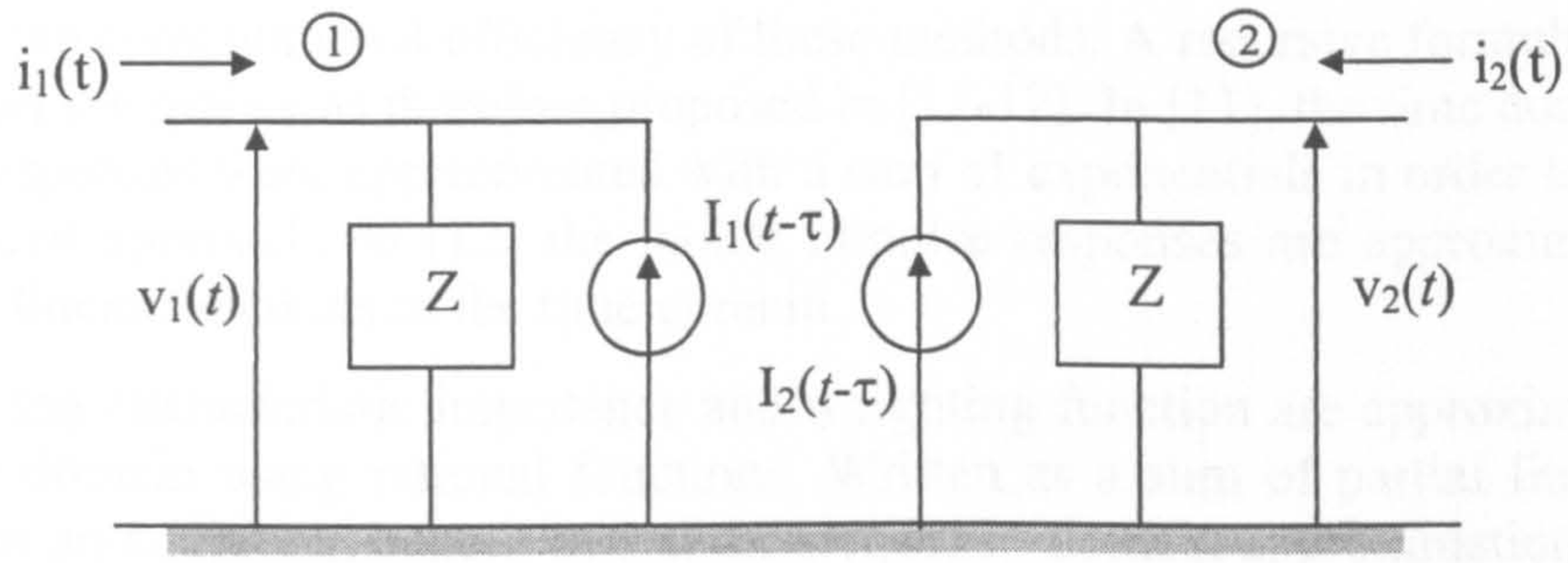

Figure 2.1. Lossless line equivalent circuit in the time domain

2.4 Frequency-dependent Transmission Line Model

The transmission system cannot be assumed lossless if accurate results are needed, since the waves become distorted as they propagate along the line, due to the complex field phenomena in the ground and inside the transmission line conductors [39]. This results in the parameters of the line exhibiting a dependence on frequency. For example, the zero sequence resistance can increase by a factor of 10^3 as the frequency varies from 60Hz to 1MHz [7,13].

The travelling wave method must therefore be modified to include these frequency-dependent characteristics of the line parameters. Indeed, the accurate and efficient modelling of multiphase transmission lines, taking into account this frequency-dependence, has been the subject of much effort in the EMTP development since its beginning [1,3,5-12]. The line model in these methods is embedded in the electrical network by means of convolutions between the line end quantities and impulse responses, which approximate the propagating characteristics of the line. In transient calculations, these models can be treated in much the same way as lossless lines, in the sense that they are interfaced to the electrical network by means of a constant resistance and a time-dependent current source.

Budner [6] developed one of the earliest models for the frequency-dependent transmission line that could be introduced into general electromagnetic transient programs such as EMTP [1]. However, the time domain form of the weighting functions used in this model are made up of a series of peaks which tend to zero as time proceeds, but only after many travel times of the line have elapsed [7,9-10]. Evaluation of the convolution integrals, which is undertaken at each time step of the solution, therefore becomes very computationally expensive.

Snelson [7] extended Bergeron's representation of the lossless, frequency-independent line model (as described in section 2.3), by defining a set of forward and backward travelling wave functions. The new set of weighting functions obtained using this approach attenuate more rapidly than those of [6], leading to a more efficient evaluation of the convolution integrals. However, the characteristic impedance of the line is approximated by its limiting value at high frequency. Snelson's analysis was further developed in [8], where again the characteristic impedance is approximated by a real constant, and the current sources are obtained from the weighted sum of the past history of the currents and voltages at both ends of the line.

It was suggested in [9-10] that an equivalent network could represent the characteristic impedance of the line. The parameters of the network are chosen so that the frequency response of the approximating equivalent network, match closely the frequency response of the characteristic impedance of the line. This results in a simplification of one of the weighting functions and completely eliminates the need for a second.

The direct numerical evaluation of the convolution integrals in [5-8] significantly

decreases the computational efficiency of these methods. A recursive formulation of the convolution integrals was therefore proposed in [11-12]. In [11], the time domain modal impulse responses were approximated with a sum of exponentials in order to formulate the recursive approach. In [12] the modal impulse responses are approximated using piecewise linear functions in the time domain.

In [9-10], the characteristic impedance and weighting function are approximated in the frequency domain using rational functions. Written as a sum of partial fractions, this method has an additional benefit in that the frequency domain approximation of the line responses can be obtained directly in closed form in the time domain, without requiring numerical inverse Fourier Transforms. In the time domain, the approximations are obtained as a sum of exponentials, directly leading to a recursive formulation of the convolution integrals. A more detailed derivation of the line model presented in [7-8] is given below:

The solution of the modal wave equations, (2.15) and (2.16), can be written directly in the frequency domain as [9,10,13],

$$V_1(\omega) = \cosh[\gamma(\omega)l]V_2(\omega) - Z_c(\omega)\sinh[\gamma(\omega)l]I_2(\omega) \tag{2.33}$$

$$I_1(\omega) = \frac{1}{Z_c(\omega)}\sinh[\gamma(\omega)l]V_2(\omega) - \cosh[\gamma(\omega)l]I_2(\omega) \tag{2.34}$$

where the characteristic impedance, $Z_c(\omega)$, and wave propagation constant, $\gamma(\omega)$, are defined as,

$$Z_c(\omega) = \sqrt{\frac{Z(\omega)}{Y(\omega)}} \tag{2.35}$$

$$\gamma(\omega) = \sqrt{Z(\omega)Y(\omega)} \tag{2.36}$$

A set of forward and backward travelling functions, to relate the currents and voltages in the time domain in a way which is analogous to Bergeron's interpretation of the simplified wave equations, are defined. The new variables can be expressed in the frequency domain as follows [9-10]:

$$F_1(\omega) = V_1(\omega) + Z_{eq}(\omega)I_1(\omega) \tag{2.37}$$

$$F_2(\omega) = V_2(\omega) + Z_{eq}(\omega)I_2(\omega) \tag{2.38}$$

and

$$B_1(\omega) = V_1(\omega) - Z_{eq}(\omega)I_1(\omega) \tag{2.39}$$

$$B_2(\omega) = V_2(\omega) - Z_{eq}(\omega)I_2(\omega) \tag{2.40}$$

where the equivalent network $Z_{eq}(\omega)$ is approximately equal to the characteristic impedance, $Z_c(\omega)$ of the line. Substituting the general solution of the wave equations in the frequency domain (2.33) and (2.34) into (2.39) and re-arranging leads to the following relationship,

$$B_1(\omega) = A(\omega)F_1(\omega) \tag{2.41}$$

and analogously at the far end of the line,

$$B_2(\omega) = A(\omega)F_2(\omega) \tag{2.42}$$

where, in both (2.41) and (2.42) the weighting function A(ω) (or impulse response function) is defined by,

$$A(\omega) = e^{-\gamma(\omega)l} = \frac{1}{\cosh[\gamma(\omega)l] + \sinh[\gamma(\omega)l]} \tag{2.43}$$

Transferring both (2.41) and (2.42) into the time domain yields the following convolution integrals,

$$b_1(t) = \int_{\tau}^{\infty} f_2(t-u)\,a(u)\,du \tag{2.44}$$

$$b_2(t) = \int_{\tau}^{\infty} f_1(t-u)\,a(u)\,du \tag{2.45}$$

The lower limit in the integrals of (2.44) and (2.45) is equal to τ since this represents the travelling time (delay) of the fastest frequency component of the injected impulse [10]. The values of the functions $b_1(t)$ and $b_2(t)$ at a time t, are completely defined by the past history values of the functions f_2 and f_1.

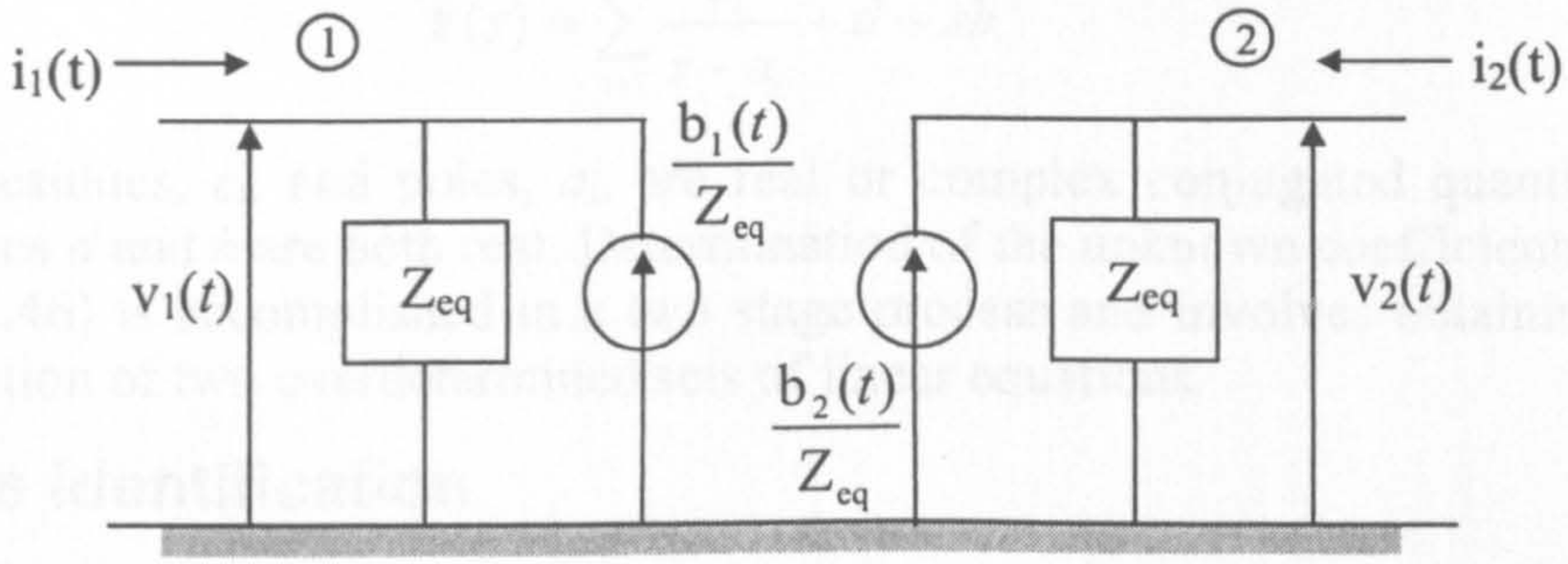

Figure 2.2. Equivalent circuit in the time domain for frequency-dependent model

Transferring (2.37-2.40) into the time domain, the corresponding equivalent circuit is shown in Figure 2.2, with $b_1(t)$ and $b_2(t)$ computed using (2.44) and (2.45), respectively. This has the same form as that for the lossless line model (Figure 2.1) and can be incorporated directly into general purpose electromagnetic transient programs in the time domain, such as EMTP [1].

2.5 Synthesis of the Transmission Line Responses

The inclusion of the time domain impulses, through the convolution integrals of (2.44) and (2.45) can significantly decrease the computational efficiency of frequency-dependent models, if at each time step, direct numerical evaluation of (2.44) and (2.45) is undertaken. Therefore, as mentioned previously, the concept of recursive convolutions [11-12] was proposed to increase the efficiency of the travelling wave method. In Marti's [9-10] approach, the transmission line responses are approximated with rational functions in the frequency domain. Expansion of the rational functions into a sum of partial fractions allows a closed form equivalent approximation to be obtained in the time domain. Each partial fraction block in the frequency domain is directly obtained as a weighted exponential in the time domain. In this form, a recursive formulation of the convolution integrals can be made. The process of evaluating (2.44) and (2.45) in a recursive manner is discussed in great detail in [9,10].

In this thesis, the method of Vector Fitting [33] has been used to obtain the rational function approximations of the transmission line responses.

2.5.1 Vector Fitting

Vector Fitting [33] can be used to calculate a rational function approximation of a given frequency domain response. The method can be used to approximate both scalar and vector functions. In the latter case, all the elements of the vector will be fitted using the same set of poles, leading to an increase in efficiency when evaluating the time domain convolutions [33].

Vector Fitting has been found to be extremely useful for the modelling of frequency-dependent effects in power systems, e.g. for transformer modelling, network equivalents and transmission line modelling. One of the advantages of Vector Fitting is that it is possible to obtain a high-order approximation for data over a wide frequency range, without suffering from numerical instability problems [33]. Methods that rely on fitting a ratio of two polynomials to the given data are usually limited to low order approximations, particularly when the fitting is performed over a wide frequency range, due to ill-conditioning [33]. A general outline of the theory is presented below:

For a given frequency response, $\mathbf{F}(s)$, Vector Fitting approximates the response with rational functions, expressed in the form of a sum of partial fractions,

$$\mathbf{F}(s) = \sum_{i=1}^{N} \frac{c_i}{s - a_i} + d + sh \tag{2.46}$$

where the residues, c_i, and poles, a_i, are real or complex conjugated quantities. The optional terms d and h are both real. Determination of the unknown coefficients (c_i, a_i, d and h) in (2.46) is accomplished in a two stage process and involves obtaining a least squares solution of two overdetermined sets of linear equations.

2.5.2 Pole Identification

The unknown set of poles, a_i, in (2.46) is replaced with a set of starting poles, $\bar{a}_i$, which are logarithmically distributed in the frequency range of interest. In addition, the frequency response, $\mathbf{F}(s)$, is multiplied with an unknown function $\eta(s)$. The unknown function is itself approximated by a rational function, yielding the following expanded problem,

$$\left.\begin{aligned} \eta(s)\mathbf{F}(s) &\approx \sum_{i=1}^{N} \frac{c_i}{s - \bar{a}_i} + d + sh \\ \eta(s) &\approx \sum_{i=1}^{N} \frac{\tilde{c}_i}{s - \bar{a}_i} + 1 \end{aligned}\right\} \tag{2.47}$$

Multiplying the second row in (2.47) with $\mathbf{F}(s)$ and re-arranging gives rise to the following relation,

$$\left(\sum_{i=1}^{N} \frac{c_i}{s - \bar{a}_i} + d + sh\right) \approx \left(\sum_{i=1}^{N} \frac{\tilde{c}_i}{s - \bar{a}_i} + 1\right)\mathbf{F}(s) \tag{2.48}$$

(2.48) can be expressed in a more convenient form as,

$$(\eta\mathbf{F})_{fit}(s) = \eta_{fit}(s)\mathbf{F}(s) \tag{2.49}$$

On re-arranging (2.48), over the full frequency range of interest, the following set of overdetermined linear equations can be obtained,

$$\mathbf{Ax} = \mathbf{b} \tag{2.50}$$

where the unknown terms are contained in the solution vector **x**. (2.50) can be solved as a least squares problem using Singular Value Decomposition (SVD) techniques [35-37].

If the partial fraction form of $(\eta\mathbf{F})_{fit}(s)$ and $\eta_{fit}(s)$ in (2.48/49) is re-written in a factorized form of the original rational functions then a rational function approximation for $\mathbf{F}(s)$ can be deduced immediately from (2.49),

$$\mathbf{F}(s) = \frac{(\eta\mathbf{F})_{fit}(s)}{\eta_{fit}(s)} = h\frac{\prod_{i=1}^{N+1}(s - z_i)}{\prod_{i=1}^{N}(s - \tilde{z}_i)} \tag{2.51}$$

Thus, an improved set of poles for fitting the original frequency response, **F**(s), is obtained by calculating the zeros of $\eta_{fit}(s)$. The calculation of the zeros in (2.51) from the partial fraction representations of $(\eta\mathbf{F})_{fit}(s)$ and $\eta_{fit}(s)$ in (2.48/49) can be undertaken as described in [33].

2.5.3 Residue Identification

The residues for **F**(s) can be obtained directly from (2.51). However, for improved accuracy it is recommended [33] to solve the original overdetermined set of linear equations in (2.46) with the zeros of $\eta(s)$ used as new poles, a_i, for **F**(s). In this case, the solution vector **x** contains the unknown terms, c_i, d and h.

If necessary, the overall process can be repeated in an iterative procedure with the poles obtained at each iteration used as the starting poles in the next iterative cycle.

2.6 Fitting Results

The method of Vector Fitting [33], as described in the previous section, is used to approximate the frequency domain responses of the characteristic impedance and weighting functions. In order to illustrate the accuracy of the method, results are presented for the 345kV transposed single circuit line shown in Figure 2.3. The line is 398km in length. The physical data for the transmission line is described in Appendix III [13,34].

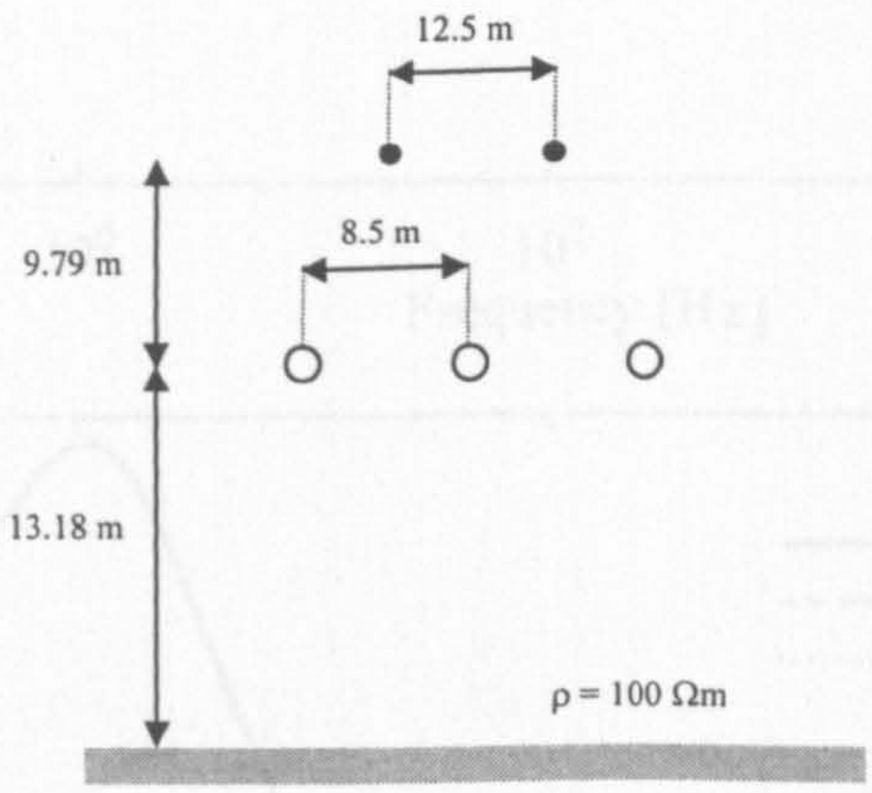

Figure 2.3. 345kV single-circuit transmission line

The fitting for both $\mathbf{Z}_c(\omega)$ and $\mathbf{A}(\omega)$ is undertaken in the frequency interval 10^{-2}Hz - 10^{6}Hz. In all cases presented, real starting poles, logarithmically distributed in the given frequency range of interest are used.

2.6.1 Synthesis of the Characteristic Impedance $\mathbf{Z}_c(\omega)$

Figure 2.4 shows the real and imaginary parts of the positive sequence characteristic

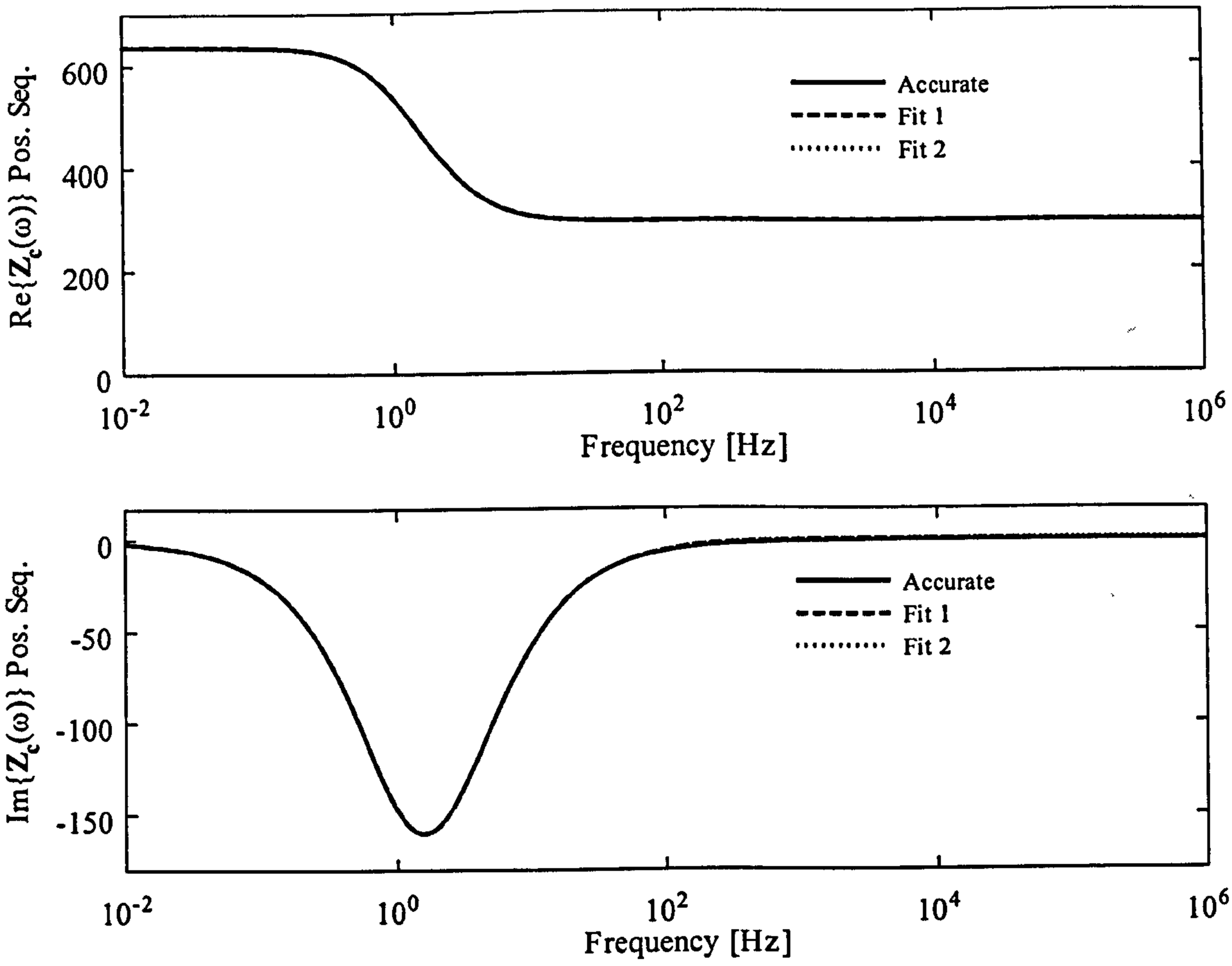

Figure 2.4 Real (top) and imaginary (bottom) parts of $\mathbf{Z}_c(\omega)$ for positive sequence

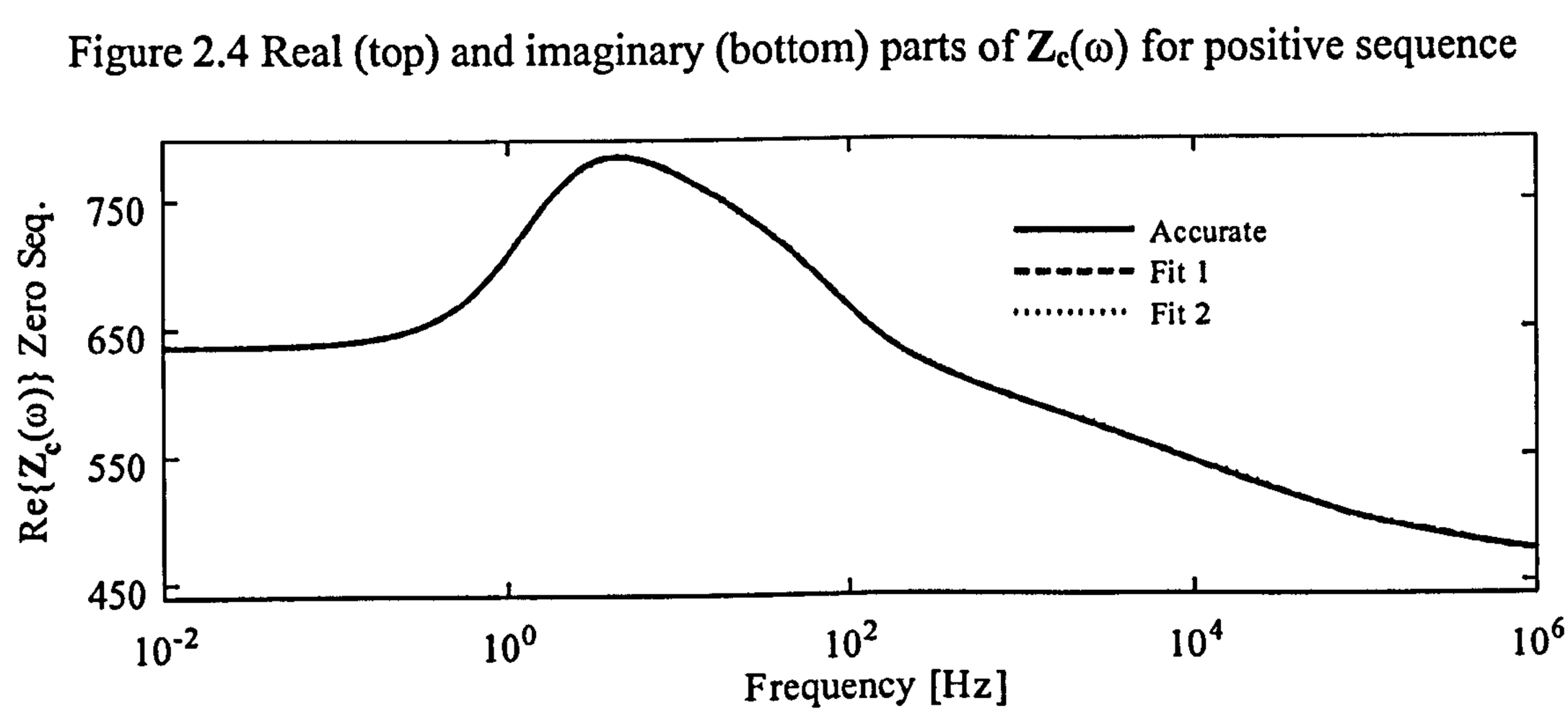

Figure 2.5 Real (top) and imaginary (bottom) parts of $\mathbf{Z}_c(\omega)$ for zero sequence

impedance function for two different fitting orders. Table 2.1 summarises the details of the two fits. It can be seen from Figure 2.4 that both approximations are very accurate, despite the reduced number of poles used in Fit 2.

Figure 2.5 shows the real and imaginary parts corresponding to the zero sequence characteristic impedance function using the same fitting orders as summarised in Table 2.1. Again, a high degree of accuracy is observed for both fits.

Table 2.1 Summary of Approximation Orders for $Z_c(\omega)$ and $P(\omega)$

FIT	$Z_c(\omega)$ ZERO SEQ.	$Z_c(\omega)$ POS. SEQ.
Fit 1	12	12
Fit 2	8	2
	P(ω) ZERO SEQ.	P(ω) POS. SEQ.
Fit 1	12	12
Fit 2	6	6

2.6.2 Synthesis of the Weighting Function A(ω)

While the weighting function in (2.43) is less oscillatory than the corresponding functions used in [6,7], the high frequency region is still very oscillatory (this is illustrated in more detail in the next chapter). Subsequently, it is very difficult to fit this function directly in the frequency domain using a low-order rational function approximation. However, it was noted in [9-10] that the time domain form of the weighting function, a(t), can be expressed as,

$$a(t) = p(t - \tau) \tag{2.52}$$

where p(t) has the same form as a(t), but is delayed by τ (the travel time of the fastest frequency component) units of time. In the frequency domain this can be written as

$$A(\omega) = P(\omega)e^{-j\omega\tau} \tag{2.53}$$

The function P(ω) is then given by,

$$P(\omega) = A(\omega)e^{j\omega\tau} \tag{2.54}$$

The real and imaginary parts of the function P(ω) are much smoother than those of the original weighting function A(ω), in the frequency range of interest, and can therefore be approximated without using excessively large order rational function approximations.

Figure 2.6 shows the real and imaginary parts of the positive sequence 'shifted weighting function', P(ω), for two different fitting orders. A summary of the order of the approximation functions can be seen in Table 2.1. Again, there is a good agreement with the rational function approximations and the original function, although a slight decrease in the accuracy of both fits can be observed in the higher frequency range (10^3-10^6) for the imaginary part of P(ω).

Figure 2.7 shows the real and imaginary parts corresponding to the zero sequence shifted weighting function using the same fitting orders as summarised in Table 2.1. Both approximations agree very well with the original function in this case, over the entire frequency range considered.

It is interesting to note that complex poles are usually obtained at high frequencies near the 'toe portion' of the response, appearing better suited to approximating this region of the response than with real poles only.

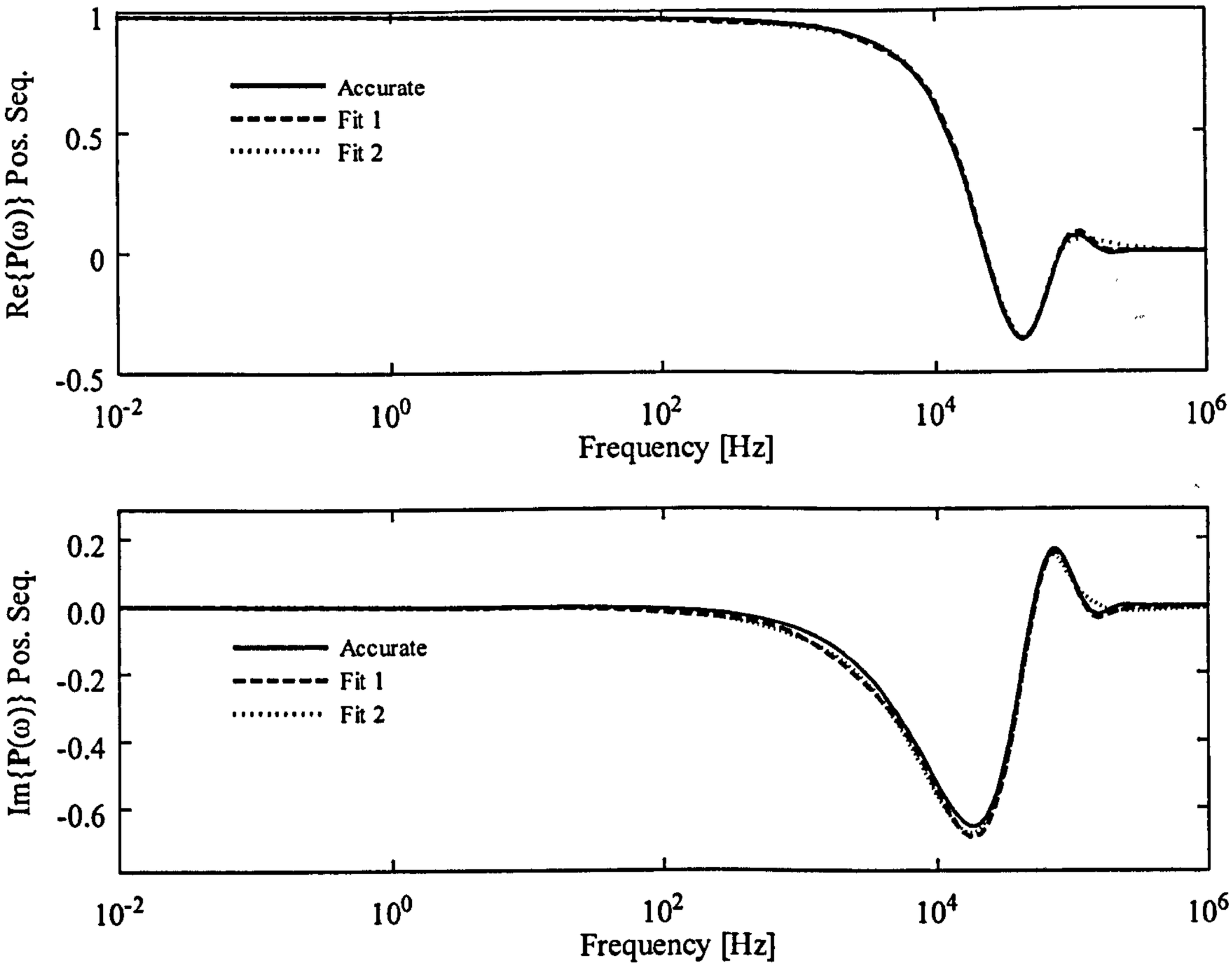

Figure 2.6 Real (top) and imaginary (bottom) parts of P(ω) for positive sequence

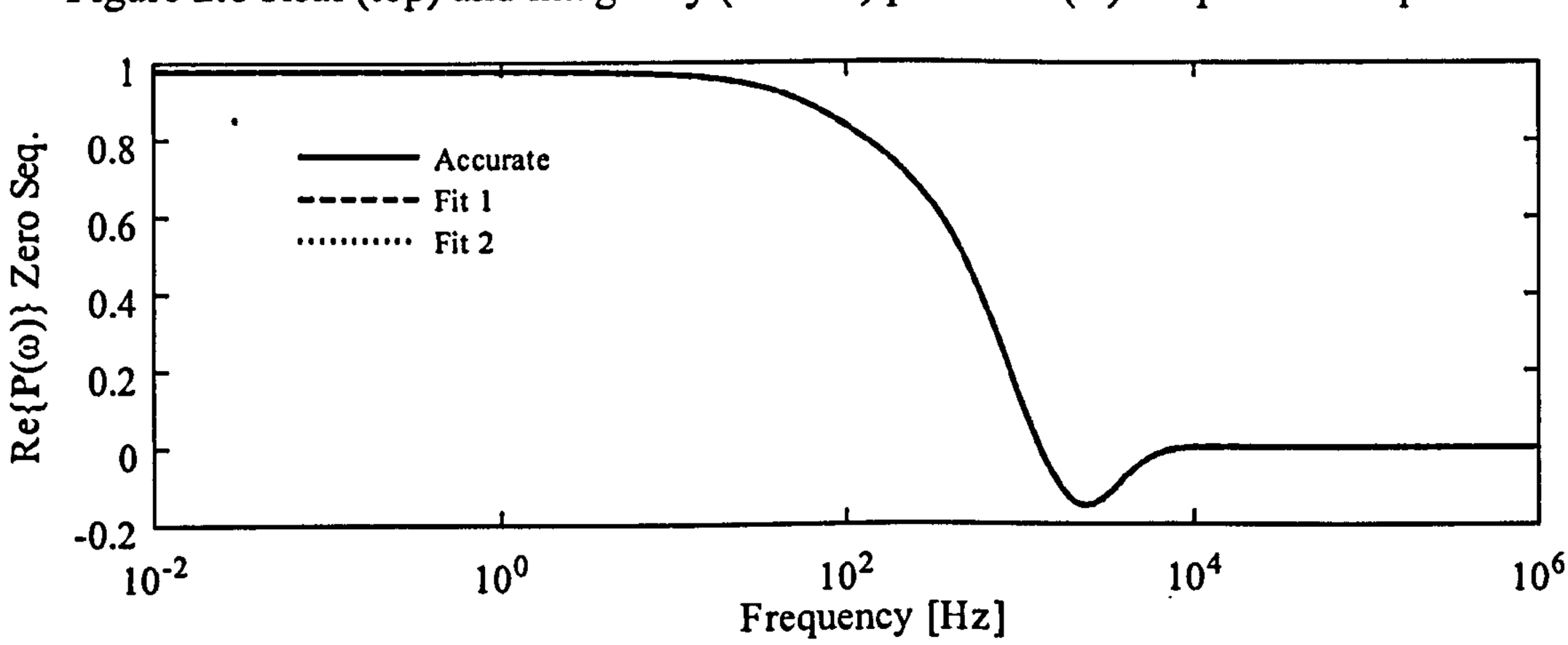

Figure 2.7 Real (top) and imaginary (bottom) parts of P(ω) for zero sequence

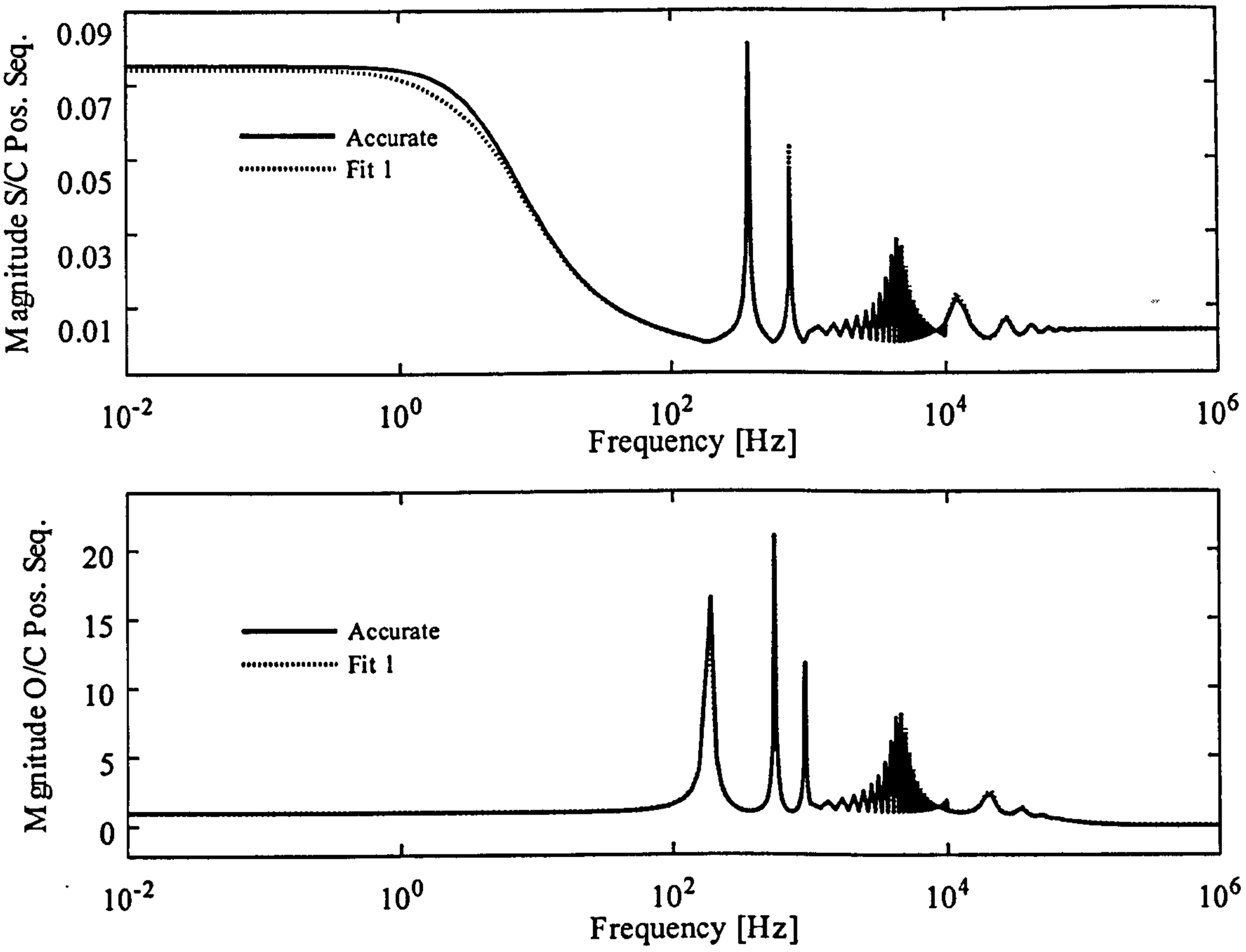

Figure 2.8 S/C (top) and O/C (bottom) response for positive sequence

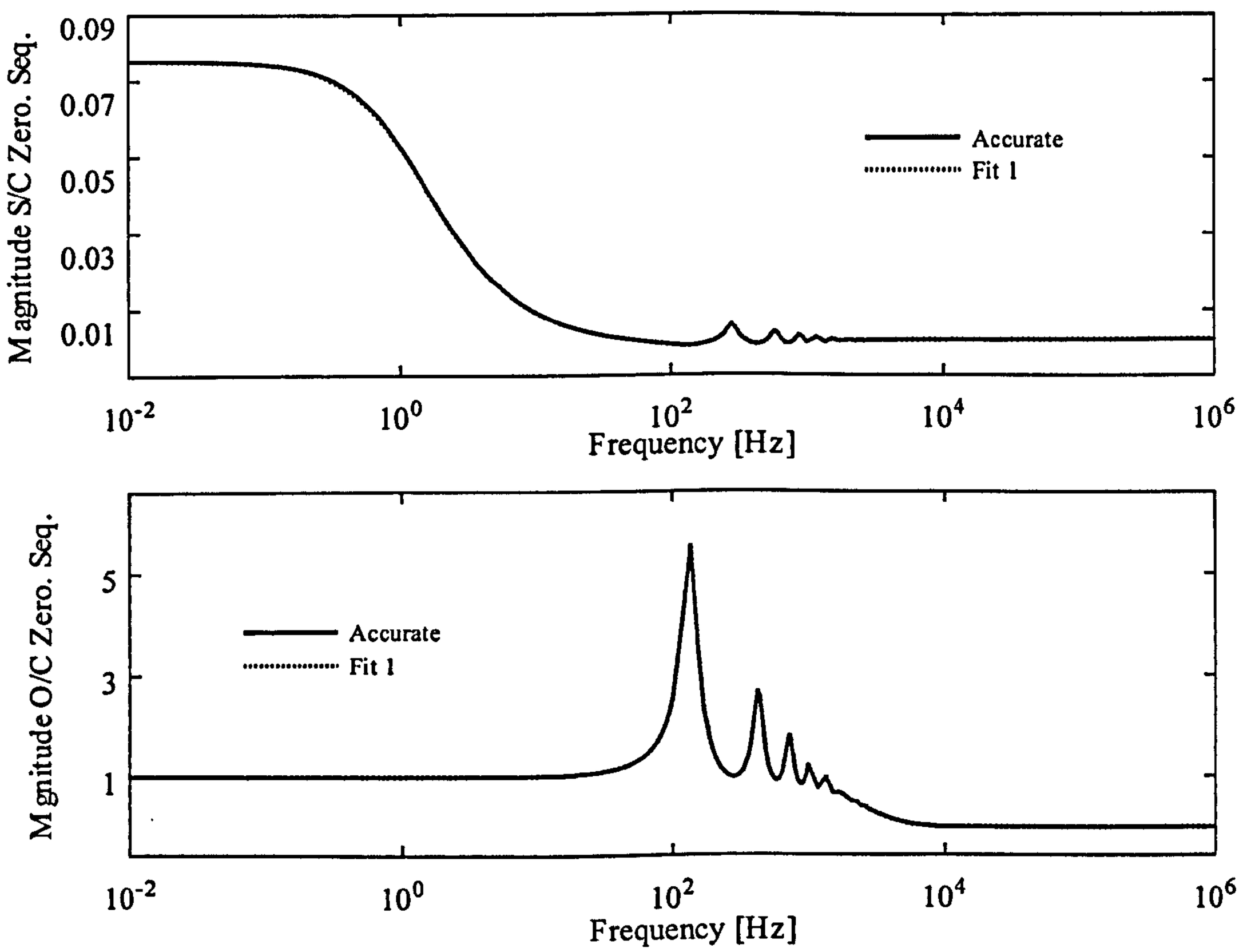

Figure 2.9 S/C (top) and O/C (bottom) response for zero sequence

2.7 Open/Short Circuit Tests in the Frequency Domain

In order to further analyse the accuracy of the rational function approximations of the characteristic impedance and weighting function, open and short circuit tests are performed in the frequency domain. The open and short circuit terminations represent extreme loading conditions in a transmission system and provide a very effective way of assessing the accuracy of the rational function approximations in simulating the line responses. [9-10,18-19,23-24,31].

Open and short circuit responses are calculated for the single-circuit overhead transmission line shown previously in Figure 2.3 and described in Appendix III, for a line length of 398km.

2.7.1 Open Circuit Response

From the general solution of the line equations in the frequency domain (2.33) and (2.34), if the receiving end of the line is open, the receiving end voltage, V_2, is given by,

$$V_2(\omega) = \frac{2A(\omega)V_0}{1+(A(\omega))^2} \tag{2.55}$$

Equation (2.55) represents the open circuit response of the transmission system at a given frequency ω. A constant 1 p.u. magnitude voltage source, V_0, is connected at the sending end of the line. From (2.55) the open circuited response of the line using the exact values of the modal characteristic impedance and weighting function can be compared with the responses obtained when these functions are approximated with rational functions using the method of Vector Fitting.

Figure 2.8 shows the magnitude of the open circuit response for the positive sequence. The order of the rational function approximations for $Z_c(\omega)$ and $A(\omega)$ in (2.55) correspond to those of Fit 1 for the positive sequence parameters, summarized earlier in Table 2.1. It can be seen from Figure 2.8 that the approximation is in general in good agreement with the exact value of (2.55).

The magnitude of the open circuit response for the zero sequence is shown in Figure 2.9. Again, the order of the rational function approximations for $Z_c(\omega)$ and $A(\omega)$ in (2.55) correspond to those of Fit 1 for the zero sequence parameters. From Figure 2.9 it can be seen that the approximated value of the receiving end voltage compares extremely well with the exact values over the entire frequency range under consideration.

2.7.2 Short Circuit Response

If the receiving end of the line is short circuited (V_2=0), then the current at the receiving end of the line, I_2, is given by,

$$I_2(\omega) = \frac{2V_0 A(\omega)}{Z_c(1-A^2(\omega))} \tag{2.56}$$

Equation (2.56) represents the short cicuit response of the transmission system at a given frequency ω. The voltage source, V_0, as with the rational function approximations of, $Z_c(\omega)$ and $A(\omega)$, are the same as those used for the open circuit case presented above.

Figure 2.8 also shows the magnitude of the short circuit currents for the positive sequence component. As for the open circuit case, the approximation matches the exact function quite well over the frequency range of interest. The magnitude of the short

circuit currents for the zero sequence component can be seen in Figure 2.9. Again, the approximation is seen to compare very well with the exact function.

2.8 Time Domain Simulations

The theory related to the modelling of frequency-independent and frequency-dependent transmission lines using model decomposition has been discussed so far in this chapter. Both models presented are based on those which have been widely used for analysing electromagnetic transient problems in power networks, having been incorporated in general transient programs such as EMTP [1] and EMTDC [2]. The frequency-independent line model represents the line as a pure delay and a characteristic impedance. The model assumes that the parameters of the transmission line are frequency-independent. However, in general, the series resistance and inductance are dependent upon frequency and this must be taken into account in the time domain simulation in order to avoid a significant loss of accuracy. This is accomplished in the second line model by approximating the frequency domain variation in the transmission line parameters with low-order rational functions using the method of Vector Fitting [33]. The accuracy of these approximations has been confirmed by performing open and short circuit tests in the frequency domain and comparing the results with the exact functions.

To further validate the two line models and to demonstrate the relative accuracy of both transmission line representations, time domain simulations under transient conditions have been performed. The test cases and corresponding results, including a comparison with field measurements, are discussed in the following sections.

2.8.1 Time Domain Implementation

Both transmission line models discussed in this chapter have been implemented in a computer program for the purpose of testing the models in time domain electromagnetic transient simulations. The FORTRAN programming language was adopted since it provides a convenient means to export the transmission line models for execution within the Applied Dynamics International (ADI) real-time simulation environment. The development of these models for real-time simulations is discussed in chapter six.

The developed program allows the line models to be embedded in a simulated power network in which the elements are represented as current sources in parallel with a conductance, in accordance with the approach in the EMTP [1]. The line models are introduced into this network model using their associated equivalent circuits, as discussed earlier in sections 2.3 and 2.4 (see Figures 2.1 and 2.2).

2.8.2 Sequential Energization Test

In the following section the calculated results of a sequential energization of the 345kV Jaguara-Taquaril power transmission system in the State of Minas Gerais, Brazil are presented. The transmission system is illustrated in Figure 2.10. The single-circuit transmission line is 398km in length and is assumed to be transposed. The transformation from phase to modal components and vice-versa is undertaken using the Karrenbauer transformation matrix (2.19). Details of the transmission system can be found in Appendix III [13,34].

The sequential energization is performed for both the frequency-independent and frequency-dependent transmission line models. The line parameters for the frequency-independent model are calculated at 60Hz. Table 2.2 provides a summary of the 60Hz data used. The contacts of the circuit breakers are closed according to the sequence given in Table 2.3. The simulations were conducted initially with the frequency-

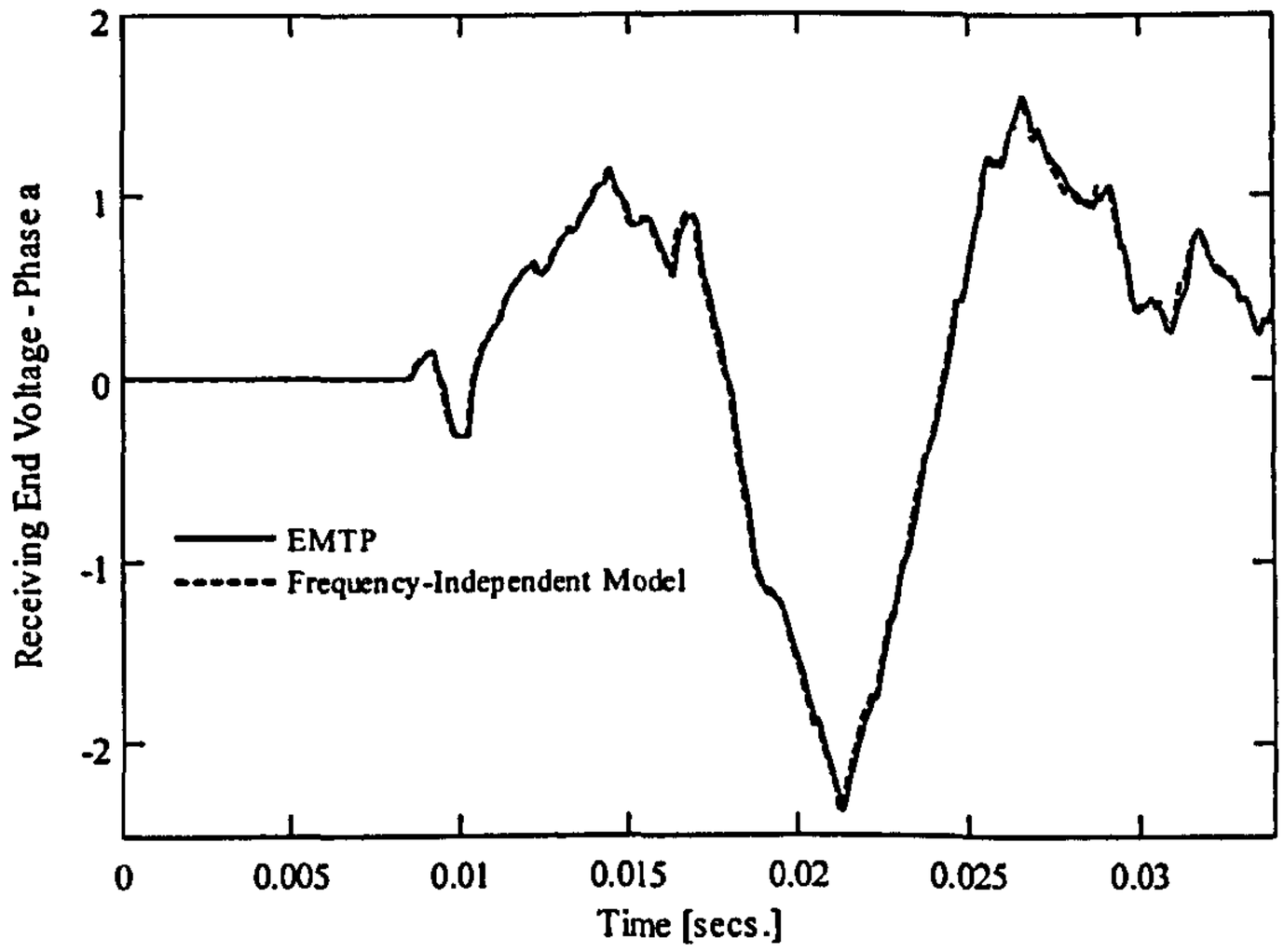

Figure 2.11. Receiving end voltage after simulated sequential energization - Phase a (Frequency-independent model)

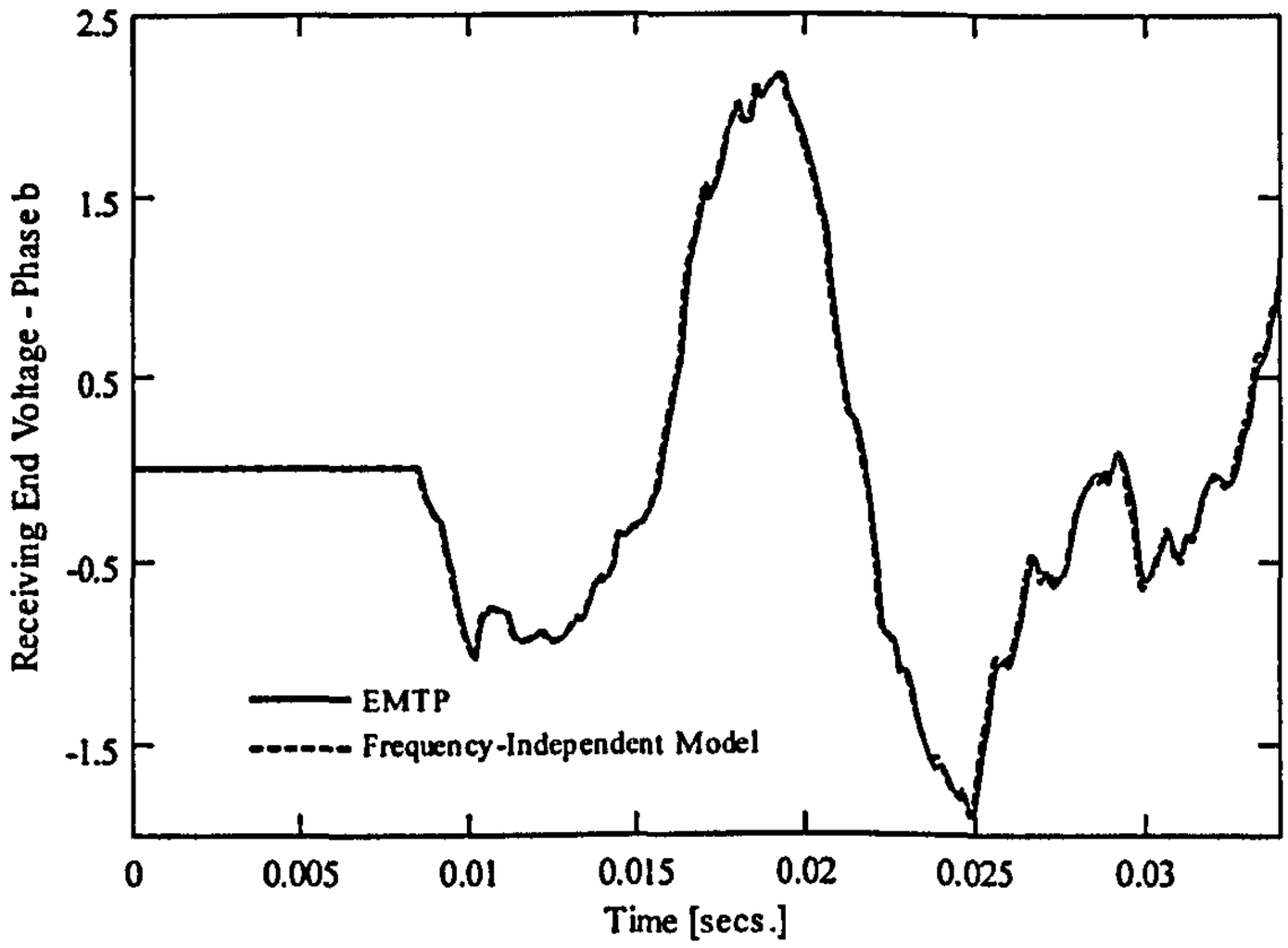

Figure 2.12. Receiving end voltage after simulated sequential energization - Phase b (Frequency-independent model)

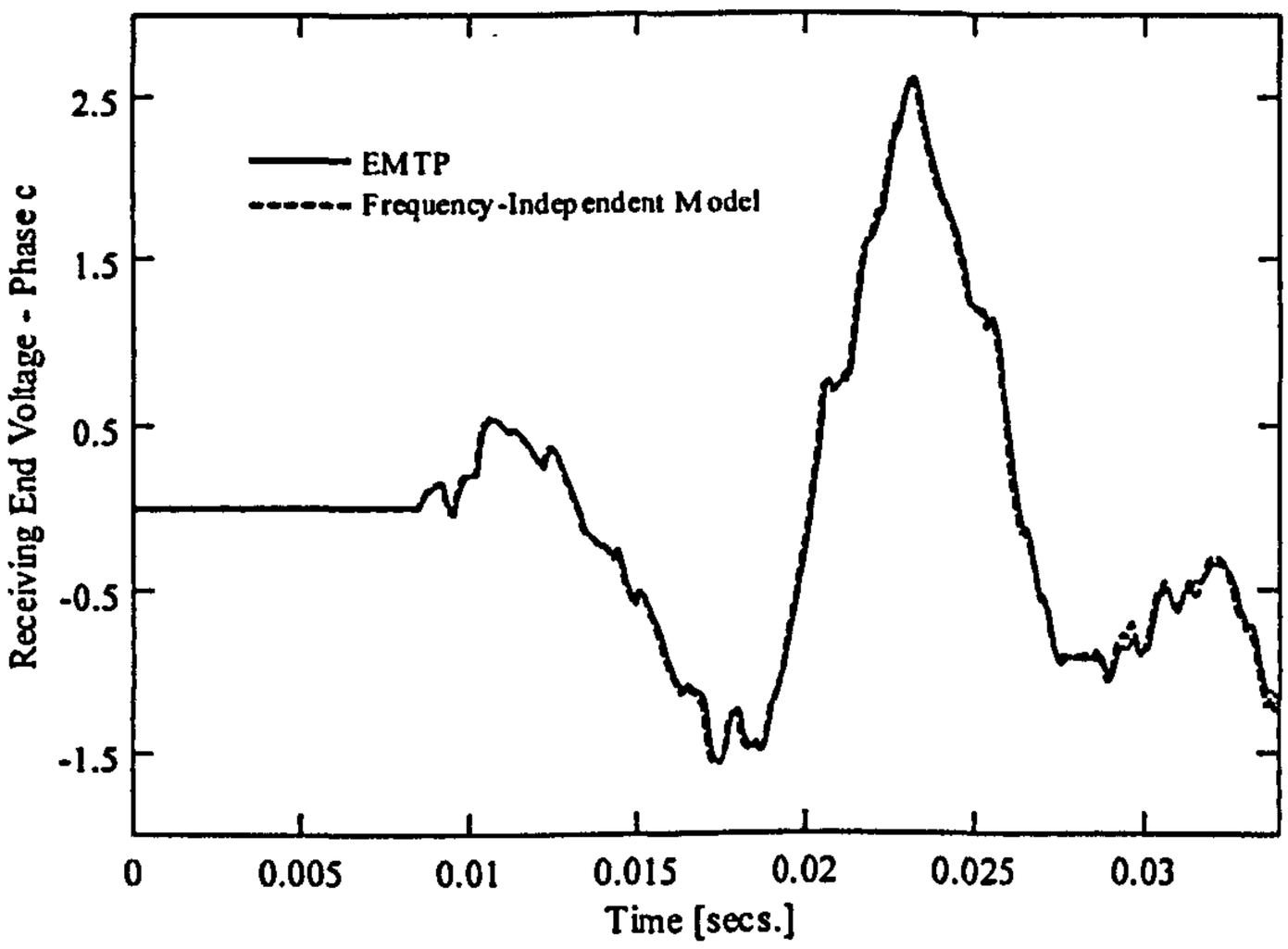

Figure 2.13. Receiving end voltage after simulated sequential energization - Phase c (Frequency-independent model)

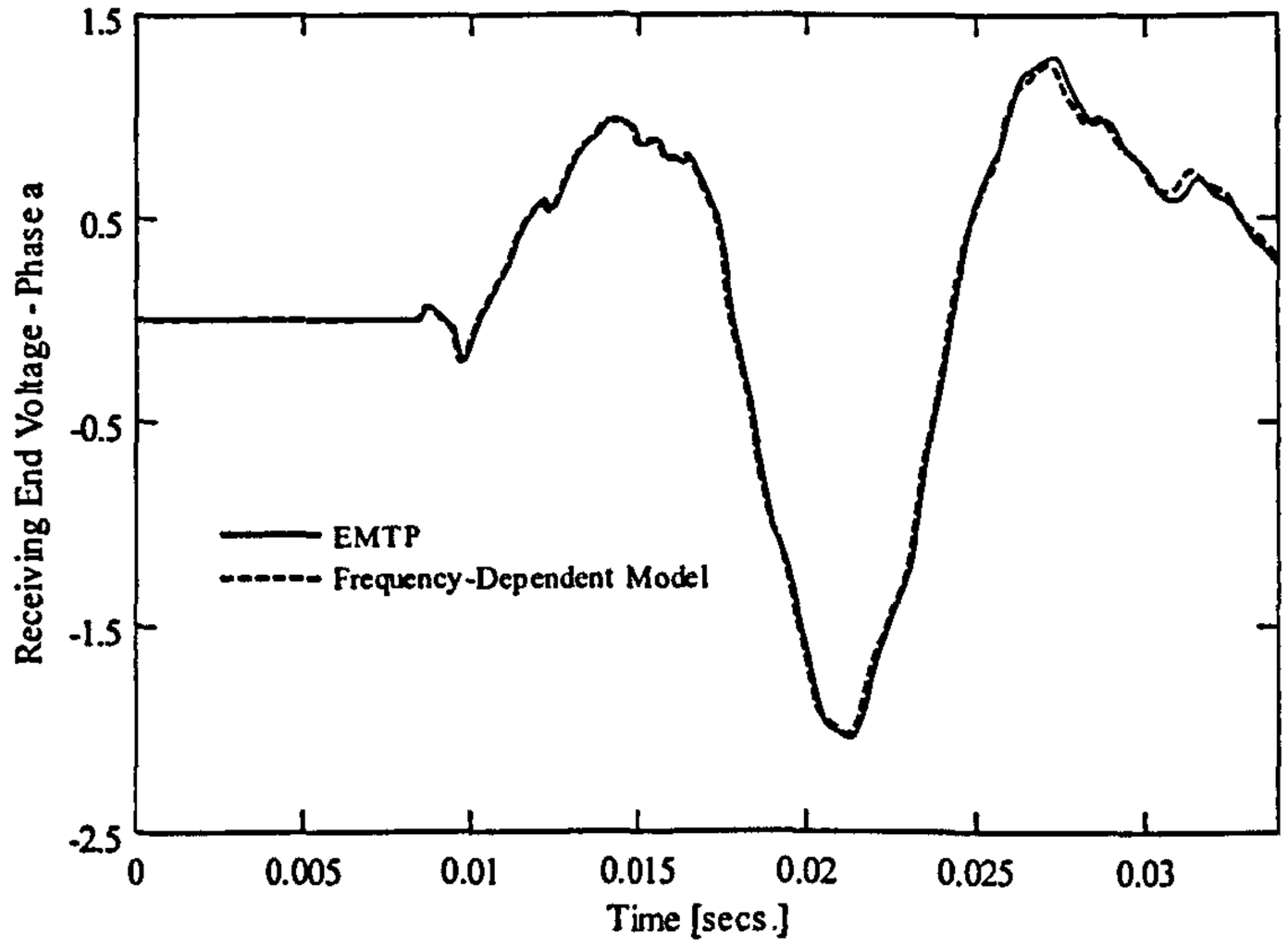

Figure 2.14. Receiving end voltage after simulated sequential energization - Phase a (Frequency-dependent model)

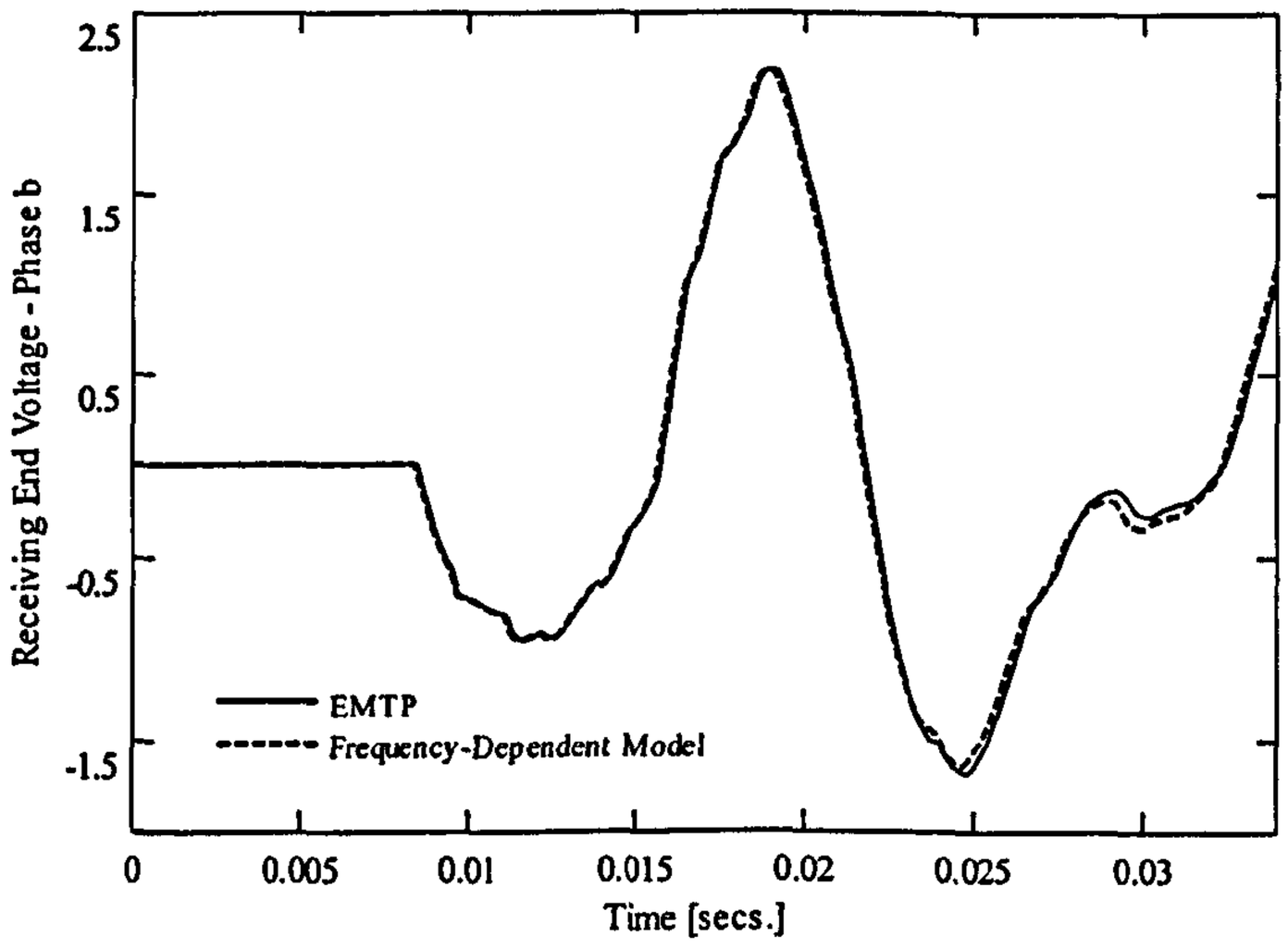

Figure 2.15. Receiving end voltage after simulated sequential energization - Phase b (Frequency-dependent model)

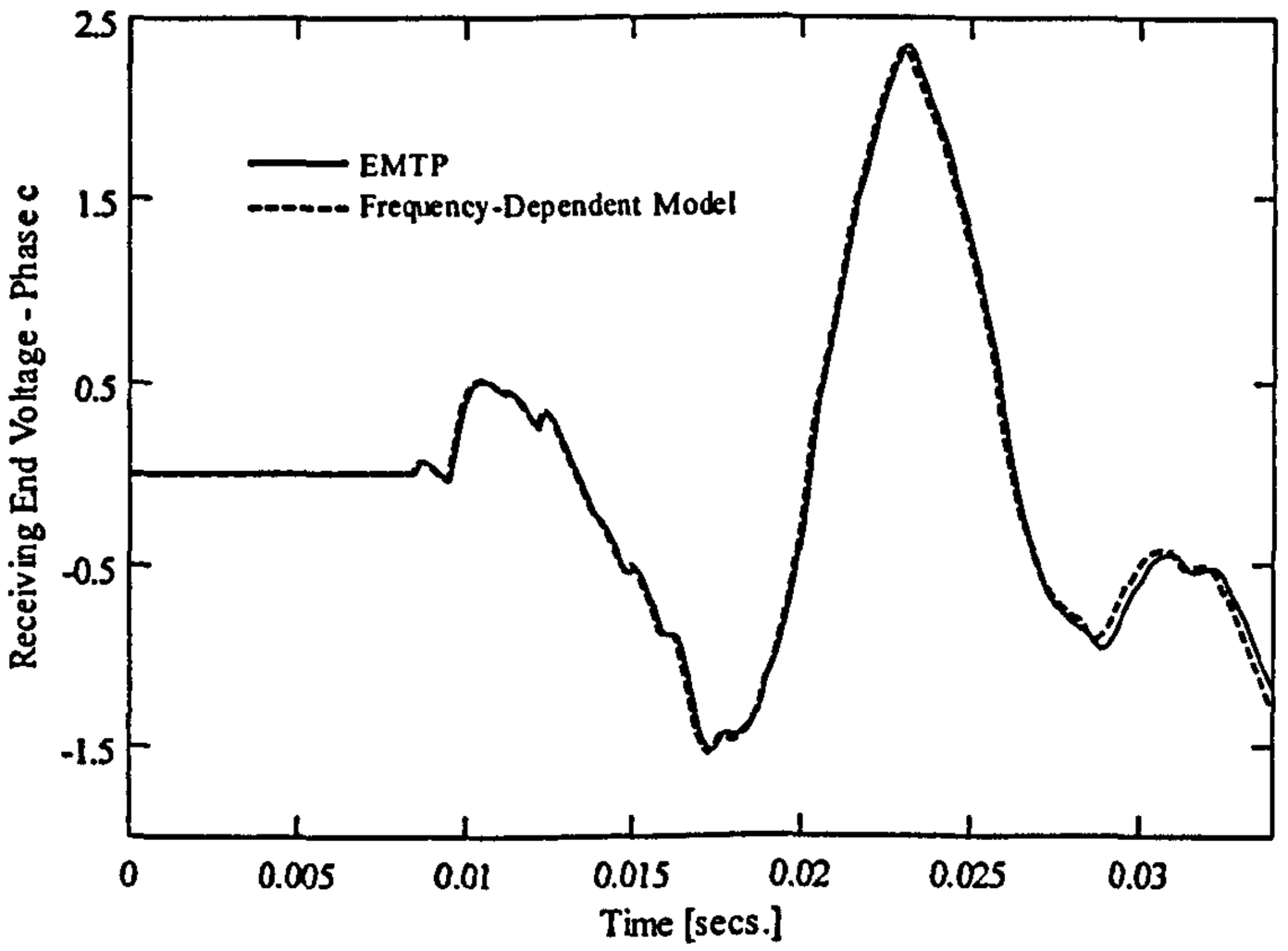

Figure 2.16. Receiving end voltage after simulated sequential energization - Phase c (Frequency-dependent model)

independent line model and then subsequently repeated using the frequency-dependent transmission line model. A time step of 34μsec was used for both line models in the time domain simulation.

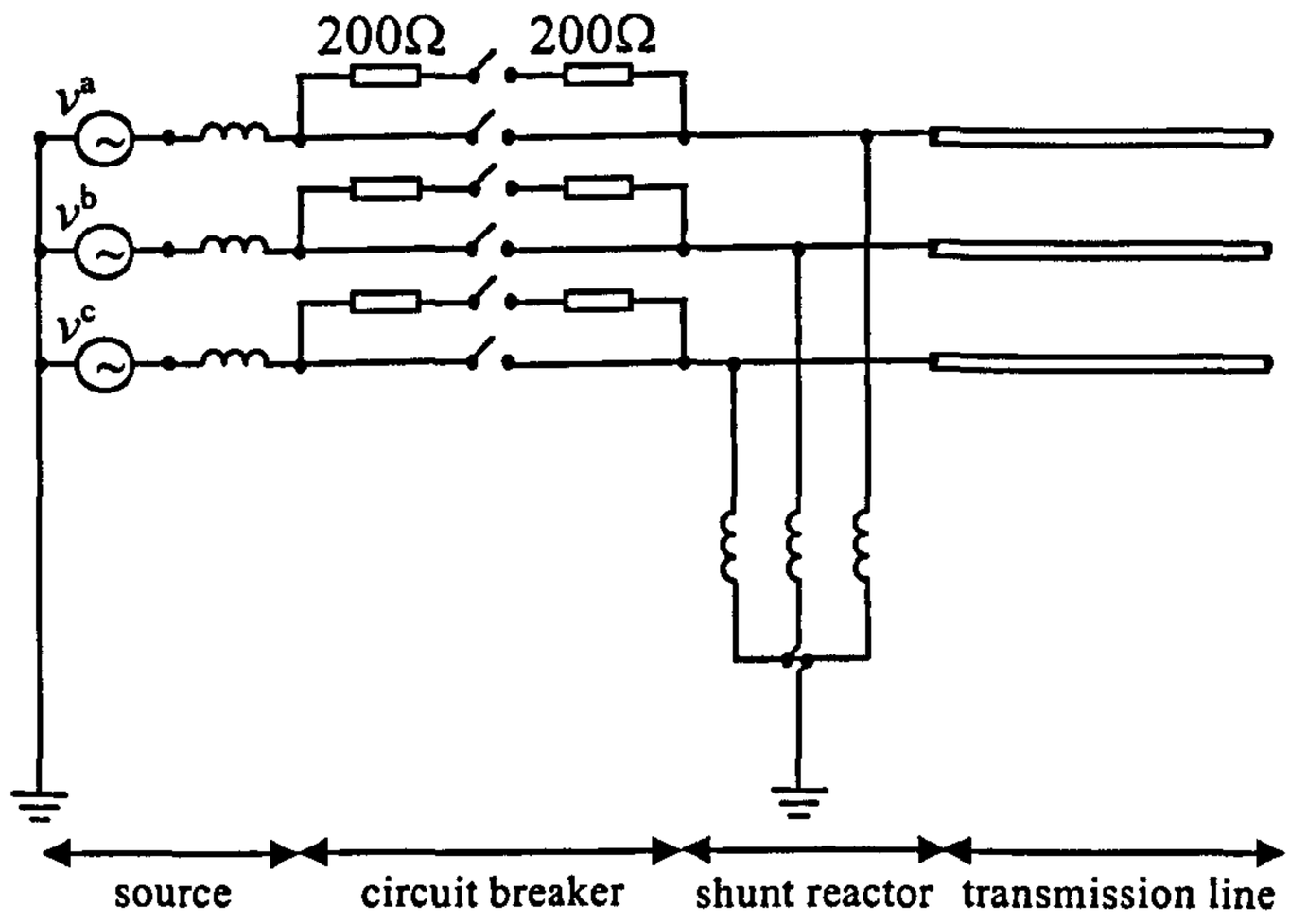

Figure 2.10. Jaguara-Taquaril 345kV transmission system

Table 2.2 Line parameters calculated at 60Hz.

PARAMETER	ZERO SEQ.	POS. SEQ.
R	0.32183 Ω/km	0.03419 Ω/km
X	1.26693 Ω/km	0.37478 Ω/km
C	0.008 μF/km	0.0118 μF/km

Table 2.3 Circuit breaker switching data

PHASE	AUX. CONTACTS	MAIN CONTACTS
a	8.50 ms	15.98 ms
b	7.14 ms	14.28 ms
c	8.16 ms	14.96 ms

Figures 2.11, 2.12 and 2.13 show the simulated transient voltages for phase a, b and c respectively, obtained at the far end of the line due to the sequential energization of the Jaguara-Taquaril transmission system, as outlined above. The corresponding results for the frequency-dependent transmission line model are shown in Figures 2.14, 2.15 and 2.16, respectively. The order of the rational function approximations for the modal characteristic impedance and weighting functions correspond to those of Fit 1, as described in Table 2.1. The results from both models are superimposed upon those obtained using the frequency-independent and dependent transmission line representations in the EMTP [1].

Both sets of results compare well with those obtained using the EMTP for all phases, confirming the accuracy of the line models implemented in this chapter. The attenuation of all three phases, due to the inclusion of the frequency-dependent effects of the line parameters, can clearly be seen from a comparison of Figures 2.11-13 and 2.14-16. The peak voltages for all three phases of the frequency-independent model are higher than those of the corresponding frequency-dependent model. It can also be seen that there is, in general, a magnification of the higher harmonics contained within the voltage waveforms using the frequency-independent model.

2.8.3 Comparison with Field Measurements

In order to further assess the accuracy of the above results, a comparison with the actual

field recordings of the sequential energization of the Jaguara-Taquaril transmission system, as described in [34], can be made.

Figure 2.17 (top) shows the receiving end voltages for all three phases, obtained using the frequency-dependent model. The bottom graph corresponds to the results obtained from the field measurements, superimposed with those calculated using an electromagnetic transients program [13].

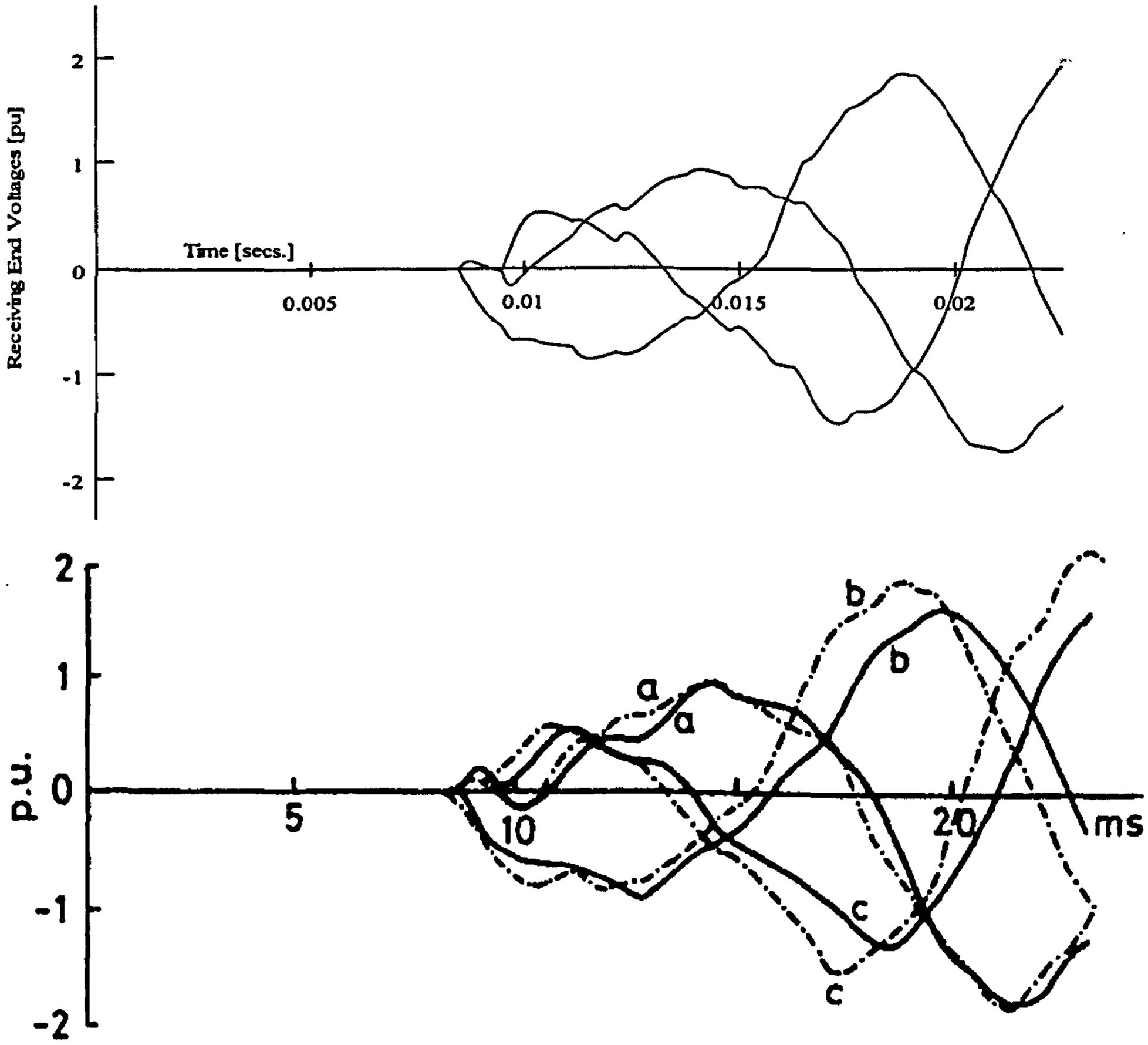

Figure 2.17. (Top) Energization results for frequency-dependent line model (Bottom) Actual field measurements (solid line) and EMTP results (dotted line)

It can be seen from Figure 2.17 that there is, in general, a good agreement with the results obtained from the frequency-dependent transmission line model and the field measurements. The measured peak voltages after energization show a greater attenuation and an approximate 1ms delay than the voltages obtained with the frequency-dependent model. The differences could be due a variety of sources, such as the assumption of constant earth conductivity, assumption of a perfectly transposed line, losses in the reactor and generator-transformer source and inaccuracies in the actual field measurements.

2.9 Conclusions

This chapter has focused on the modelling of multiconductor transmission lines for electromagnetic transient studies using modal decomposition methods. Wedepohl [14] and Hedman [15] first applied numerical linear algebra techniques to the analysis of multiconductor transmission lines over forty years ago. The method transforms the governing wave equations in the coupled phase domain to the uncoupled modal domain. Each independent mode is then solved in a similar manner to that of a single-phase system. The solution is then back transformed from modal co-ordinates to the phase

domain where the overall network solution is obtained. The transformation between modal and phase quantities is performed at each time step of the simulation.

Two transmission line models, which differ significantly in model complexity, are described and implemented. The first model simplifies the line somewhat by assuming the parameters of the transmission line are constant and represents the line by a time delay and a characteristic impedance. The method is based on a travelling wave approach. However, the presence of an imperfect ground return path for the travelling waves and the skin effect in the conductors result in the line parameters displaying a strong dependence with frequency. Therefore, models which assume constant parameters cannot adequately simulate the response of the line over the wide range of frequencies that are present in the transient voltages and currents. Thus, in order to avoid a significant loss of accuracy, the frequency-dependent characteristics of the line parameters must be taken into account.

This is accomplished in the second model by approximating the characteristic impedance, $Z_c(\omega)$, and weighting function, $A(\omega)$ with partial fraction approximations. By fitting the transmission line responses in this way, a closed form approximation is obtained directly in the time domain, circumventing the need for numerical inverse Fourier Transforms. The rational function approximations are represented in the time domain by a sum of exponentials. In this form, a recursive formulation of the convolution integrals can be directly performed, significantly increasing the overall efficiency of the algorithm.

The method of Vector fitting has been applied to approximate the transmission line responses with rational functions. Unlike conventional Marti-type fitting, which is restricted to negative, real poles, Vector Fitting allows both real and complex conjugated poles to be used in the fitting process. This has been found to be particularly advantageous in obtaining accurate low order approximations of the weighting function. The complex poles are well suited to fitting the 'toe portion' of the weighting, or impulse response function.

Open and short circuit tests have been performed in the frequency domain to confirm the accuracy of the rational function approximations. The time domain energization of a 345kV test transmission system has been performed to assess the validity and accuracy of the two line models. The results from both models are compared with those obtained from the EMTP and are shown to be in good agreement.

2.10 References

[1] Dommel, H. W.: 'Electromagnetic Transients Program (EMTP) Rule Book', EPRI EL6421-1, Vol. 1, June 1989.

[2] Manitoba HVDC Research Centre: 'EMTDC Reference – Theory Manual', 1988.

[3] Dommel, H. W.: 'Digital Computer Solution of Electromagnetic Transients in Single-and Multiphase Networks', IEEE Transactions on Power Apparatus and Systems, Vol. PAS-88, No. 4, April 1969, pp. 388-399.

[4] Dommel, H. W. and Meyer, W. S.: 'Computation of Electromagnetic Transients', Proceedings of the IEEE, Vol. 62, No. 7, July 1974, pp. 983-993.

[5] Carroll, D. P. and Nozari, F.: 'An Efficient Computer Method for Simulating Transients on Transmission Lines with Frequency Dependent Parameters', IEEE Transactions on Power Apparatus and Systems, Vol. PAS-94, No. 4, July/August 1975, pp. 1167-1176.

[6] Budner, A.: 'Introduction of Frequency-Dependent Line Parameters into an

Electromagnetic Transients Program', IEEE Transactions on Power Apparatus and Systems, Vol. PAS-89, No. 1, January 1970, pp. 88-97.

[7] Snelson, J. K.: 'Propagation of Travelling Waves on Transmission Lines – Frequency Dependent Parameters', IEEE Transactions on Power Apparatus and Systems, Vol. PAS-91, January/February 1972, pp. 85-91.

[8] Meyer, W. S. and Dommel, H. W.: 'Numerical Modelling of Frequency-Dependent Transmission-Line Parameters in an Electromagnetic Transients Program', IEEE Transactions on Power Apparatus and Systems, Vol. PAS-93, September/October 1974, pp. 1401-1409.

[9] Marti, J.: 'Accurate Modelling of Frequency-Dependent Transmission Lines in Electromagnetic Transient Simulations', IEEE Transactions on Power Apparatus and Systems, Vol. PAS-101, No. 1, January 1982, pp. 147-157.

[10] Marti, J.: 'The Problem of Frequency Dependence in Transmission Line Modelling', PhD Thesis, The University of British Columbia, Canada, April 1981.

[11] Semlyen, A. and Dabuleanu, A.: 'Fast and Accurate Switching Transient Calculations on Transmission Lines with Ground Return Using Recursive Convolutions', IEEE Transactions on Power Apparatus and Systems, Vol. PAS-94, No. 2, March/April 1975, pp. 561-571.

[12] Ametani, A.: 'A Highly Efficient Method for Calculating Transmission Line Transients', IEEE Transactions on Power Apparatus and Systems, Vol. PAS-95, No. 5, September/October 1976, pp. 1545-1551.

[13] Naidu, S. R. and de Lima, F. N.: 'A Frequency-Dependent Transmission Line Model for Electromagnetic Transient Studies', IEE Proceedings, Vol. 132, Pt. C, No. 6, November 1985, pp. 294-297.

[14] Wedepohl, L. M.: 'Application of Matrix Methods to the Solution of Travelling-Wave Phenomena in Polyphase Systems', Proceedings of the IEE, Vol. 100, No. 12, 1963, pp. 2200-2212.

[15] Hedman, D. E.: 'Propagation on Overhead Transmission Lines I-Theory of Modal Analysis', IEEE Transactions on Power Apparatus and Systems, Vol. PAS-84, March 1965, pp. 200-205.

[16] Brandão, J. A. and Borges da Silva, J. F.: 'Wave Propagation in Polyphase Transmission Lines a General Solution to Include Cases Where Ordinary Modal Theory Fails', IEEE Transactions on Power Delivery, Vol. PWRD-1, No. 2, April 1986, pp. 182-189.

[17] Brandão, J. A.: 'Overhead Three-Phase Transmission Lines – Non-Diagonalizable Situations', IEEE Transactions on Power Delivery, Vol. 3, No. 4, October 1988, pp. 1348-1355.

[18] Marti, L.: 'Simulation of Electromagnetic Transients in Underground Cables with Frequency-Dependent Modal Transformation Matrices', PhD Thesis, The University of British Columbia, Canada, November 1986.

[19] Marti, L.: 'Simulation of Transients in Underground Cables with Frequency-Dependent Modal Transformation Matrices', IEEE Transactions on Power Delivery, Vol. 3, No. 3, July 1988, pp. 1099-1110.

[20] Gustavsen, B. and Semlyen, A.: 'Simulation of Transmission Line Transients Using Vector Fitting and Modal Decomposition', IEEE Transactions on Power

Delivery, Vol. 13, No. 2, pp. 605-614.

[21] Gustavsen, B. and Semlyen, A.: 'Combined Phase and Modal Calculation of Transmission Line Transients Based on Vector Fitting', IEEE Transactions on Power Delivery, Vol. 13, No. 2, April 1998, pp. 596-604.

[22] Gustavsen, B., Sletbak, J., and Henriksen, T.: 'Calculation of Electromagnetic Transients in Transmission Line Cables and Lines Taking Frequency Dependent Effects Accurately Into Account', IEEE Transactions on Power Delivery, Vol. 10, No. 2, April 1995, pp. 1076-1084.

[23] Nguyen, H. V., Dommel, H. W. and Marti, J. R.: 'Direct Phase Domain Modelling of Frequency-Dependent Overhead Transmission Lines', IEEE Transactions on Power Delivery, Vol. 12, No. 3, July 1997, pp. 1335-1342.

[24] Nguyen, H.: 'Simulation of Lightning Surges on Transmission Lines', PhD Thesis, The University of British Columbia, Canada, February 1996.

[25] Marcano, F. J.: 'Modelling of Transmission Lines Using Idempotent Decomposition', M.Sc Thesis, August 1996, The University of British Columbia.

[26] Castellanos, F. and Marti, J. R.: 'Phase-Domain Multiphase Transmission Line Models', International Conference on Power System Transients, Lisbon, 3-7 September 1995.

[27] Castellanos, F., Marti, J. R. and Marcano, F.: 'Phase-Domain Multiphase Transmission Line Models', Electrical Power & Energy Systems, Vol. 19, No. 4, 1997, pp. 241-248.

[28] Noda, T., Nagaoka, N. and Ametani, A.: 'Phase Domain Modeling of Frequency-Dependent Transmission Lines by Means of an ARMA Model', IEEE Transactions on Power Delivery, Vol. 11, No. 1, January 1996, pp. 401-411.

[29] Noda, T., Nagaoka, N. and Ametani, A.: 'Further Improvements to a Phase-Domain ARMA Line Model in Terms of Convolution, Steady-State Initialization, and Stability', IEEE Transactions on Power Delivery, Vol. 12, No. 3, July 1997, pp. 1327-1334.

[30] Angelidis, G. and Semlyen, A.: 'Direct Phase-Domain Calculation of Transmission Line Transients Using Two-Sided Recursions', IEEE Transactions on Power Delivery, Vol. 10, No. 2, April 1995, pp. 941-949.

[31] Gustavsen, B: 'A Study of Overvoltages in High Voltage Cables With Emphasis on Sheath Overvoltages', Dr. Ing. Thesis, The Norwegian Institute of Technology, Trondheim, Norway, 1993.

[32] Morched, A., Gustavsen, B. and Tartibi, M.: 'A Universal Model for Accurate Calculation of Electromagnetic Transients on Overhead Lines and Underground Cables', IEEE Transactions on Power Delivery, Vol. 14, No. 3, July 1999, pp. 1032-1038.

[33] Gustavsen, B. and Smelyen, A.: 'Rational Approximation of Frequency Domain Responses by Vector Fitting', IEEE Transactions on Power Delivery, Vol. 14, No. 3, July 1999, pp. 1052-1061.

[34] Dommel, H. W., Yan, A., Ortiz de Marcano, R. J. and Miliani, A. B.: 'Case Studies for Electromagnetic Transients', Internal Report, The Department of Electrical Engineering, The University of British Columbia, Canada, May 1983.

[35] Anderson, A. *et al.*: 'Lapack User's Guide', Second Edition, Society for Industrial

and Applied Mathematics (SIAM), 1995, pp. 19.

[36] Press, W. H., Teukolsky, S. A., Vetterling, W. T. and Flannery, B. P.: 'Numerical Recipes in FORTRAN – The Art of Scientific Computing', Second Edition, Cambridge University Press, 1992, pp. 51.

[37] Golub, G. H. and Van Loan, C. F.: 'Matrix Computations', Second Edition, The John Hopkins University Press, 1991, pp. 427.

[38] Stagg, G. W. and El-Abiad, A. H.: 'Computer Methods in Power System Analysis', McGraw-Hill Book Company, 1968, pp. 123.

[39] Soysal, A. O. and Semlyen, A.: 'State Equation Approximation of Transfer Matrices and its Applications to the Phase Domain Calculation of Electromagnetic Transients', IEEE Transactions on Power Systems, Vol. 9, No. 1, February 1994, pp. 420-428.

CHAPTER 3

PHASE DOMAIN TRANSMISSION LINE MODELLING - FREQUENCY DOMAIN FORMULATION

The following chapter introduces a model for overhead power transmission lines in which the analysis is performed entirely in phase co-ordinates. This differs from the approach adopted in the phase domain models presented in the open literature, in which the initial evaluation of the line responses in the frequency domain is performed using established modal decomposition techniques. The phase domain analysis in these models is restricted to the final time domain simulations. These models can in effect be considered as a hybrid of the modal and phase domain methods. Algorithms are presented which allow accurate and efficient determination of both the phase domain characteristic admittance and wave propagation matrices for physically realizable transmission line configurations over the frequency range considered for electromagnetic transient studies. The algorithm for evaluating the characteristic admittance matrix is derived by exploiting a relationship between the matrix sign function and the matrix square root. The wave propagation matrix is evaluated directly in phase co-ordinates by applying a Padé approximation technique to the matrix exponential function. The properties of both algorithms are thoroughly analysed, frequently making use of matrix decomposition techniques to highlight specific algorithm characteristics. However, it should be emphasised that explicit computation of eigenvalues or eigenvectors is not required when applying these methods. Results are presented for single, double and highly asymmetrical transmission line configurations to highlight the accuracy, efficiency and robustness of the proposed phase domain methods.

3.1 Introduction

Accurate simulation of electromagnetic transients in power systems requires the frequency-dependent effects of transmission lines to be taken into account [1-23]. The currently used frequency-dependent modal domain approaches, as discussed in chapter two, have long been used for this type of analysis [13-23]. In these methods, the numerical calculations are conducted in the modal domain with the solution transformed into the phase domain by means of a real and constant transformation matrix. Under this assumption, these algorithms attain a high level of computational efficiency. However, though these models provide a very dependable way of analysing many overhead lines of interest, the solution accuracy can deteriorate substantially when modelling, for example, multi-circuit overhead lines, strongly asymmetrical configurations and underground cable systems [1-12,21-22]. In these cases, the transformation matrix may depend strongly on frequency and therefore the assumption of a constant transformation matrix is no longer valid.

In principle, this problem can be overcome by introducing a convolution for the transformation matrix in the time domain, albeit with a reduction in the overall

efficiency of the algorithm. This method was applied successfully to underground cable systems in [21-22]. One of the difficulties with this approach is that the elements of the transformation matrix, in general, are not obtained as smooth functions of frequency. This is due to eigenvector switchovers taking place in the diagonalization process at a new frequency point, causing abrupt changes to be observed in the calculated elements. Therefore, 'tracking' [21-22] or special diagonalization routines [3-4,21-22] are required so that the elements of the transformation matrix can be obtained as smooth functions of frequency. It has also been shown that, unlike cable systems, for overhead lines it may not always be possible to obtain an accurate rational function approximation for the elements of the transformation matrix using stable poles only [12-13].

An alternative approach, which has seen considerable interest in recent years, is to model the transmission line system directly in the phase domain [1-12]. This frame of reference offers the most natural co-ordinates for modelling the transmission line, since the rest of the network is also represented in phase quantities. As there is no requirement to transfer the transmission line solution between modal and phase domains, the problem of including frequency-dependent transformation matrices is completely avoided. Also, since the number of convolutions to be evaluated in the solution is reduced, the method is more computationally efficient than full frequency-dependent modal decomposition methods [8,13].

However, despite the recent attention phase domain transmission line modelling has received, the situation remains somewhat unsatisfactorily resolved. The phase domain method implies that evaluation of the transmission line responses does not require the calculation of eigenvalues and eigenvectors at any stage in the analysis, as in modal decomposition techniques. However, in all of the models presented thus far, the phase domain analysis refers only to the solution of the equations in the time domain simulation. In the formulation of the transmission line equations in the frequency domain the transmission line responses are still evaluated using established eigenvector/eigenvalue based methods [24-25] before being transformed into phase co-ordinates using frequency-dependent transformation matrices. In essence these models can be considered as a hybrid of the modal and phase domain based methods.

A further limitation concerns the unwinding of the wave propagation matrix, $\mathbf{H}(\omega)$, in the phase domain. The function can be thought of as being composed of modal components which are, in general, associated with different time delays [12]. However, for many practical overhead lines of interest, the modal time delays are very similar, which makes it possible to unwind the elements of $\mathbf{H}(\omega)$ using a common scalar phase shift function, corresponding to the fastest mode [1,3,7,12]. However, for multi-circuit lines, asymmetrical configurations and cable systems, this assumption may not hold and the elements of the wave propagation matrix will still contain a significant oscillatory component as a function of frequency. Subsequently it is not possible to fit the elements of $\mathbf{H}(\omega)$ with low order rational functions [1,12].

The following chapter introduces a model for overhead transmission lines in which the analysis is performed entirely in phase co-ordinates. Algorithms are presented which allow accurate and efficient determination of both the characteristic admittance and wave propagation matrices, without restrictions on the transmission line topology, over the entire frequency range required for electromagnetic transient studies. The determination of these transmission line responses does not require the eigenvalues or eigenvectors of the matrices to be evaluated at any point in the solution process. The algorithms are based on Padé approximation techniques for approximating the matrix square root and the matrix exponential functions.

The new phase domain transmission line model will be developed over several chapters, with the emphasis in the following chapter on the frequency domain formulation of the problem. Chapter four will discuss the development of the time domain analysis, including a method to unwind the wave propagation matrix in the phase domain, and chapter five will present the time domain numerical results obtained. Application of the model for undertaking closed loop, real-time digital power system simulations will be presented in chapter six.

3.2 Wave Propagation in Transmission Lines

The series impedance matrix, $\mathbf{Z}(\omega)$, and the shunt admittance matrix, $\mathbf{Y}(\omega)$, as defined in chapter two, exhibit a dependence on frequency in the range analysed for electromagnetic transient studies. A closed form solution to the differential equations that describe the propagation of waves along the transmission line cannot, therefore, be obtained directly in the time domain due to the frequency domain characteristics of the line responses. Indeed, the time domain form of the governing equations is still very complicated even when the frequency-dependent nature of $\mathbf{Z}(\omega)$ and $\mathbf{Y}(\omega)$ is neglected [17,18].

In the frequency domain, however, a solution for the wave propagation equations can be constructed. The time domain solution is then found by transforming the solution into the time domain by means of the inverse Fourier transform. The following section presents a brief analysis of the formulation of the wave equations in the frequency domain:

Consider the *n*-conductor transmission line system of length l as shown in Figure 3.1. Let $\mathbf{Z}(\omega)$ be the series impedance matrix and $\mathbf{Y}(\omega)$ the shunt admittance matrix per unit length of the line. The electromagnetic behaviour of the system can be described in the frequency domain by $\mathbf{Z}(\omega)$ and $\mathbf{Y}(\omega)$, defined in the following set of partial differential equations [4-6,7-8,11,18,22],

$$-\frac{\partial \mathbf{V}(x,\omega)}{\partial x} = \mathbf{Z}(\omega)\mathbf{I}(x,\omega) \tag{3.1}$$

$$-\frac{\partial \mathbf{I}(x,\omega)}{\partial x} = \mathbf{Y}(\omega)\mathbf{V}(x,\omega) \tag{3.2}$$

where $\mathbf{V}(x,\omega)$ and $\mathbf{I}(x,\omega)$ are the voltages and currents at a distance x from the sending end of the transmission line. $\mathbf{V}(x,\omega)$ and $\mathbf{I}(x,\omega)$ are complex vectors of dimension n. $\mathbf{Z}(\omega)$ and $\mathbf{Y}(\omega)$ are complex, symmetric matrices of dimension n x n.

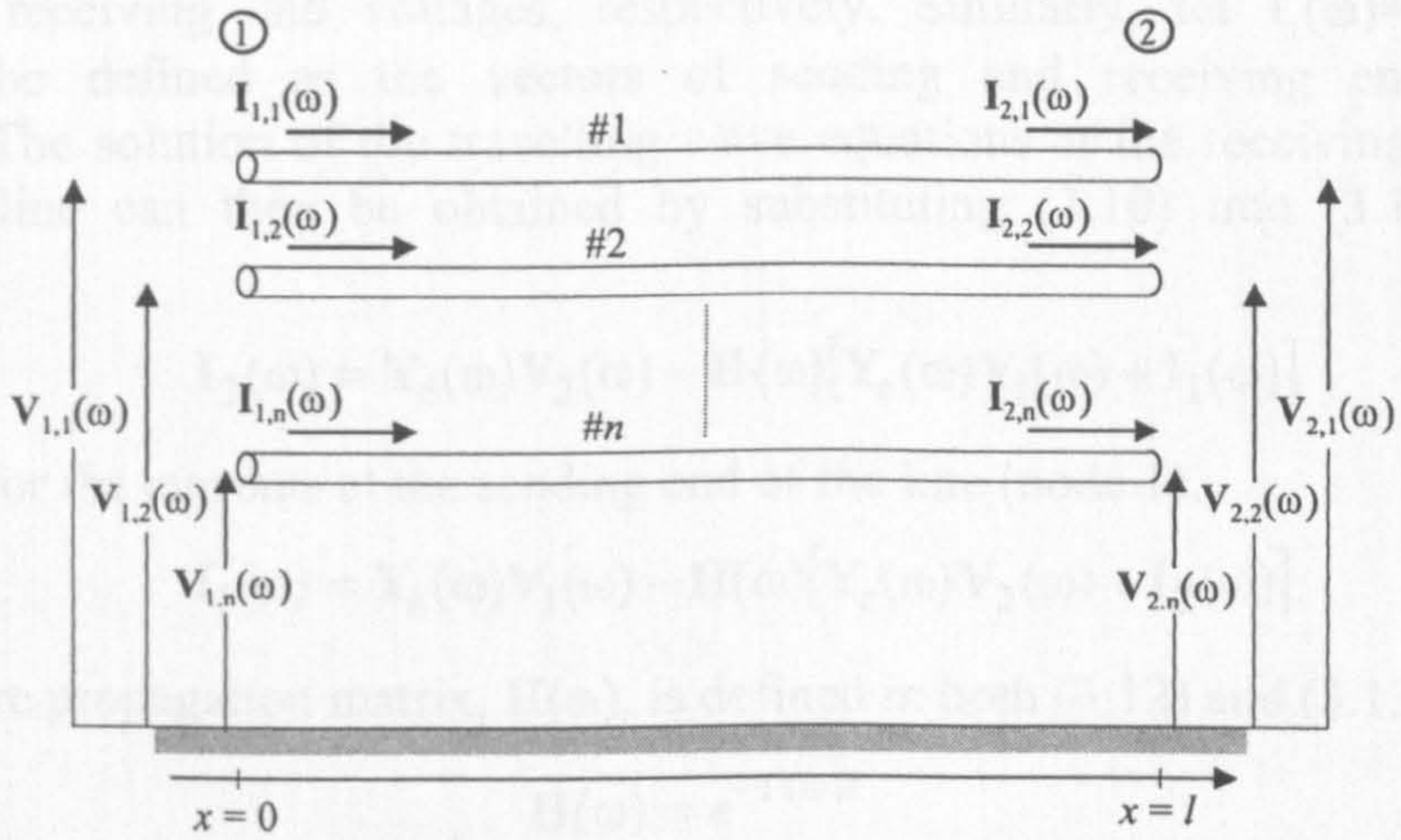

Figure 3.1. Multiphase distributed-parameter transmission line system

Differentiating (3.1) and (3.2) with respect to x, yields the following wave propagation equations,

$$\frac{\partial^2 \mathbf{V}(x,\omega)}{\partial x^2} = [\mathbf{Z}(\omega)\mathbf{Y}(\omega)]\mathbf{V}(x,\omega) \tag{3.3}$$

$$\frac{\partial^2 \mathbf{I}(x,\omega)}{\partial x^2} = [\mathbf{Y}(\omega)\mathbf{Z}(\omega)]\mathbf{I}(x,\omega) \tag{3.4}$$

The general solution for (3.4) in the frequency domain can be obtained as,

$$\mathbf{I}(x,\omega) = e^{-\Gamma(\omega)x}\mathbf{I}^+ + e^{\Gamma(\omega)x}\mathbf{I}^- \tag{3.5}$$

where $\mathbf{I}^+$ and $\mathbf{I}^-$ are the vectors of forward and backward travelling currents, with respect to the positive x direction and are defined by the boundary conditions at both ends of the transmission line (x=0 and x=l). The propagation constant matrix, $\Gamma(\omega)$, is defined as,

$$\Gamma(\omega) = \sqrt{\mathbf{Y}(\omega)\mathbf{Z}(\omega)} \tag{3.6}$$

The voltage vectors of the line can be obtained by substituting (3.5) into (3.2) to give,

$$\mathbf{V}(x,\omega) = \mathbf{Y}_c^{-1}(\omega)\left(e^{-\Gamma(\omega)x}\mathbf{I}^+ - e^{\Gamma(\omega)x}\mathbf{I}^-\right) \tag{3.7}$$

where the characteristic admittance matrix, $\mathbf{Y}_c(\omega)$, is defined as,

$$\mathbf{Y}_c(\omega) = \sqrt{[\mathbf{Y}(\omega)\mathbf{Z}(\omega)]^{-1}}\,\mathbf{Y}(\omega) \tag{3.8}$$

Multiplying (3.7) by $\mathbf{Y}_c(\omega)$ and adding the result to (3.5) gives,

$$\mathbf{Y}_c(\omega)\mathbf{V}(x,\omega) + \mathbf{I}(x,\omega) = 2e^{-\Gamma(\omega)x}\mathbf{I}^+ \tag{3.9}$$

Applying the boundary conditions at the sending and receiving ends of the transmission line, respectively, gives rise to the following set of equations,

$$\mathbf{Y}_c(\omega)\mathbf{V}(0,\omega) + \mathbf{I}(0,\omega) = 2\mathbf{I}^+ \qquad ; x = 0 \tag{3.10}$$

$$\mathbf{Y}_c(\omega)\mathbf{V}(l,\omega) - \mathbf{I}(l,\omega) = 2e^{-\Gamma(\omega)l}\mathbf{I}^+ \qquad ; x = l \tag{3.11}$$

For convenience, let $\mathbf{V}_1(\omega)$=$\mathbf{V}(0,\omega)$ and $\mathbf{V}_2(\omega)$=$\mathbf{V}(l,\omega)$ be defined as the vectors of sending and receiving end voltages, respectively. Similarly, let $\mathbf{I}_1(\omega)$=$\mathbf{I}(0,\omega)$ and $\mathbf{I}_2(\omega)$=$\mathbf{I}(l,\omega)$ be defined as the vectors of sending and receiving end currents, respectively. The solution of the travelling wave equations at the receiving end of the transmission line can then be obtained by substituting (3.10) into (3.11) and re-arranging,

$$\mathbf{I}_2(\omega) = \mathbf{Y}_c(\omega)\mathbf{V}_2(\omega) - \mathbf{H}(\omega)[\mathbf{Y}_c(\omega)\mathbf{V}_1(\omega) + \mathbf{I}_1(\omega)] \tag{3.12}$$

Analogously for the currents at the sending end of the line (node 1),

$$\mathbf{I}_1(\omega) = \mathbf{Y}_c(\omega)\mathbf{V}_1(\omega) - \mathbf{H}(\omega)[\mathbf{Y}_c(\omega)\mathbf{V}_2(\omega) + \mathbf{I}_2(\omega)] \tag{3.13}$$

where the wave propagation matrix, $\mathbf{H}(\omega)$, is defined in both (3.12) and (3.13) as,

$$\mathbf{H}(\omega) = e^{-\Gamma(\omega)l} \tag{3.14}$$

The remainder of this chapter is devoted to the calculation of the characteristic admittance matrix (3.8) and the wave propagation matrix (3.14) directly in phase co-ordinates for electromagnetic transient studies.

3.3 Phase Domain Evaluation of $\mathbf{Y_c}(\omega)$ and $\mathbf{H}(\omega)$

A transmission line can be characterized by the characteristic admittance, $\mathbf{Y_c}(\omega)$, and wave propagation functions, $\mathbf{H}(\omega)$. Both matrix transfer functions exhibit a significant dependence on frequency over the frequency range of interest for typical electromagnetic transient studies (10^{-2}-10^{6}Hz). In practice, $\mathbf{Y_c}(\omega)$ and $\mathbf{H}(\omega)$ are calculated as discrete functions in the frequency domain using the line parameters, which are evaluated from well known formulations [26-29]. A time domain simulation can then be carried out using convolutions involving the transmission line end quantities and the time domain impulse responses of the characteristic admittance matrix, $\mathbf{y_c}(t)$, and the wave propagation matrix, $\mathbf{h}(t)$, which are obtained via an inverse Fourier transform.

In all the phase domain methods presented thus far [1-12], $\mathbf{Y_c}(\omega)$ and $\mathbf{H}(\omega)$ are evaluated using matrix decomposition techniques in a similar fashion to that used in modal domain models [13-23]. The modal analysis of overhead transmission lines was pioneered by Wedepohl [24] and Hedman [25] over forty years ago. This analysis is based on the matrix eigenvalue-eigenvector problem (involving the matrix product of the per unit length shunt admittance matrix and the series impedance matrix of the line), whose numerical solution provides, for a given frequency, the characteristics of the propagation modes travelling along the line. A brief review of modal analysis for evaluating $\mathbf{Y_c}(\omega)$ and $\mathbf{H}(\omega)$ is given below (see section 2.2.1 of chapter two for more details):

The matrix product $\mathbf{Y}(\omega)\mathbf{Z}(\omega)$ is first diagonalized, at every frequency point of interest, using eigenvector theory:

$$\mathbf{Y}(\omega)\mathbf{Z}(\omega) = \mathbf{T}(\omega)\gamma^{2}(\omega)\mathbf{T}^{-1}(\omega) \tag{3.15}$$

where $\gamma(\omega)$ is a diagonal matrix containing the eigenvalues of $\mathbf{Y}(\omega)\mathbf{Z}(\omega)$ and $\mathbf{T}(\omega)$ is the corresponding transformation matrix of eigenvectors which depends on frequency. The elements of $\gamma(\omega)$ can be expressed as a modal attenuation $\alpha(\omega)$ and a modal velocity $\upsilon(\omega)$:

$$\gamma_{i,i}(\omega) = \alpha_i(\omega) + j\frac{\omega}{\upsilon_i(\omega)} \tag{3.16}$$

The wave propagation matrix, $\mathbf{H}(\omega)$, is then calculated as,

$$\mathbf{H}(\omega) = \mathbf{T}(\omega)e^{-\gamma(\omega)l}\mathbf{T}^{-1}(\omega) \tag{3.17}$$

where $\exp(-\gamma(\omega)l)$ is a diagonal matrix with diagonal elements $\exp(-\gamma_{i,i}(\omega)l)$. In a similar manner, the characteristic admittance, $\mathbf{Y_c}(\omega)$, can be evaluated as,

$$\mathbf{Y_c}(\omega) = \mathbf{T}(\omega)\gamma^{-1}(\omega)\mathbf{T}^{-1}(\omega)\mathbf{Y}(\omega) \tag{3.18}$$

3.3.1 Non-Diagonalization Situations

The above modal decomposition analysis assumes that the matrix product $\mathbf{Y}(\omega)\mathbf{Z}(\omega)$ is diagonalizable for every frequency point considered in the evaluation of (3.17) and (3.18). However, it has been shown in [30,31] that there are transmission lines for which it may not be possible to diagonalize $\mathbf{Y}(\omega)\mathbf{Z}(\omega)$. The theoretical difficulty occurs

when $\mathbf{Y}(\omega)\mathbf{Z}(\omega)$ does not have a complete set of linearly independent eigenvectors and is thus defective. In this case there is no invertible matrix of eigenvectors $\mathbf{T}(\omega)$ and conventional modal theory breaks down (in such cases a more generalized modal domain approach using Jordan decompositions can be used [30,31]). However, this situation may only occur at a single frequency (as discussed by Semlyen in [30]), so in practice a more likely difficulty will arise when $\mathbf{Y}(\omega)\mathbf{Z}(\omega)$ is 'nearly' defective over a range of frequencies. This can be defined more precisely using the matrix condition number with respect to inversion,

$$cond(\mathbf{T}(\omega)) = \|\mathbf{T}(\omega)\|\|\mathbf{T}^{-1}(\omega)\| \tag{3.19}$$

If $\mathbf{Y}(\omega)\mathbf{Z}(\omega)$ is nearly (exactly) defective, then cond($\mathbf{T}(\omega)$) is large (infinite). Any errors in $\mathbf{Y}(\omega)\mathbf{Z}(\omega)$, including roundoff errors in its computation and roundoff errors from the eigenvalue decomposition may be magnified in the final result by cond($\mathbf{T}(\omega)$). Consequently, when (3.19) is large, the computed $\mathbf{Y}_c(\omega)$ and $\mathbf{H}(\omega)$ will most likely be inaccurate.

Transmission line models that are conducted in phase co-ordinates will not be affected by the above considerations, since explicit calculation of eigenvalues and eigenvectors are not required to evaluate (3.8) and (3.14). However, as discussed previously, all the current phase domain models available today make use of the above analysis to evaluate $\mathbf{Y}_c(\omega)$ and $\mathbf{H}(\omega)$, and as such, would suffer the same problems associated with this method under non-diagonalization conditions.

3.3.2 Padé Approximation

The Padé approximant to a function, $f(x)$, is the rational function constructed from the coefficients of the Taylor series expansion of $f(x)$. Padé approximation has a long history (Baker [63] provides details of the development of these approximants from Cauchy (1821) through Jacobi (1846) and Frobenius (1881) to Padé (1892)) with applications in a variety of areas, such as theoretical physics [64], control theory [40,65], mechanics etc., [63]. A brief description of Padé approximation theory is given below.

If a given function $f(x)$ can be represented by a power series [40,63],

$$f(x) = \sum_{n=0}^{\infty} a_i x^n \tag{3.20}$$

then the $[L/M]$ Padé approximant to $f(x)$ can be denoted by the following rational function,

$$[L/M] = \frac{P_L(x)}{Q_M(x)} \tag{3.21}$$

where $P_L(x)$ and $Q_M(x)$ are polynomials of degree at most L and M, respectively, and can be defined as follows,

$$P_L(x) = p_0 + p_1 x + \cdots + p_L x^L \tag{3.22}$$

$$Q_M(x) = q_0 + q_1 x + \cdots + q_M x^M \tag{3.23}$$

The coefficients of (3.22) and (3.23) can be found by setting,

$$f(x) - \frac{P_L(x)}{Q_M(x)} = 0 \tag{3.24}$$

and equating coefficients. Since the numerator and denominator can be multiplied by any constant with [*L*/*M*] left unchanged, the normalization condition, $Q_M(0)=1$, can be imposed. Expanding (3.24) gives the following set of equations,

$$\begin{aligned}
a_0 &= p_0 \\
a_1 + a_0 q_1 &= p_1 \\
a_2 + a_1 q_1 + a_0 q_2 &= p_2 \\
&\vdots \\
a_L + a_{L-1} q_1 + \cdots + a_0 q_L &= p_L \\
a_{L+1} + a_L q_1 + \cdots + a_{L-M+1} q_M &= 0 \\
&\vdots \\
a_{L+M} + a_{L+M-1} q_1 + \cdots + a_L q_M &= 0
\end{aligned} \tag{3.25}$$

where $a_n \equiv 0$ if $n < 0$ and $q_n \equiv 0$ if $n > \mathrm{M}$. If the defining equations are nonsingular, then they can be solved directly to obtain [63],

$$[L/M] = \frac{\det \begin{vmatrix} a_{L-M+1} & a_{L-M+2} & \cdots & a_{L+1} \\ \vdots & \vdots & \ddots & \vdots \\ a_L & a_{L+1} & \cdots & a_{L+M} \\ \sum_{n=M}^{L} a_{n-M} x^n & \sum_{n=M-1}^{L} a_{n-M+1} x^n & \cdots & \sum_{n=0}^{L} a_n x^n \end{vmatrix}}{\det \begin{vmatrix} a_{L-M+1} & a_{L-M+2} & \cdots & a_{L+1} \\ \vdots & \vdots & \ddots & \vdots \\ a_L & a_{L+1} & \cdots & a_{L+M} \\ x^M & x^{M-1} & \cdots & 1 \end{vmatrix}} \tag{3.26}$$

where summations are replaced with zero if the lower index exceeds the upper and the equivalence conditions stated above hold.

3.4 Phase Domain Calculation of $Y_c(\omega)$

The characteristic admittance matrix, $\mathbf{Y}_c(\omega)$, is a complex, symmetric matrix which defines the relation between the current and voltage waves propagating in the same direction. From (3.8) it can be seen that in order to evaluate $\mathbf{Y}_c(\omega)$ directly in phase co-ordinates requires evaluation of the matrix square root of,

$$\mathbf{A} = \left[\mathbf{Y}(\omega)\mathbf{Z}(\omega)\right]^{-1} \tag{3.27}$$

A number of methods have been proposed to evaluate the square root of a matrix. These methods are usually based on applying Newton's method, either directly, or via the matrix sign function [42-48,50-53]. These methods have the advantage of not requiring knowledge of the eigenvalues or eigenvectors of the matrix, which may even be defective.

Other methods are based on eigen-analysis techniques, such as performing a Schur decomposition [49], however, this involves evaluation of the matrix eigenvalues, and is thus not desirable for the proposed phase domain model.

The proposed method to evaluate the square root of (3.27), in this research is a Padé approximation to the matrix square root. The method can be derived from an iteration

for the matrix sign function, which itself is derived from Newton's iteration to compute (3.27). The following sections provide an introduction to the matrix square root, with an explanation of how to calculate the principle square root of a matrix. A definition of the matrix sign function is given and the Padé iteration to the matrix square root is then derived from the iteration for the matrix sign function. It is then shown how manipulation of the algorithm for computing the square root of a matrix can be used to evaluate the phase domain characteristic admittance matrix.

3.4.1 The Matrix Square Root

Given the matrix $\mathbf{A} \in \mathbf{C}^{n \times n}$, as defined in (3.27), a matrix $\mathbf{X}$ is a square root of $\mathbf{A}$ if it is a solution of the quadratic matrix equation [42-53],

$$F(\mathbf{X}) = \mathbf{X}^2 - \mathbf{A} = \mathbf{0} \tag{3.28}$$

For n=1, the square root of any complex number exists and every nonzero complex number has two distinct square roots, but for $n \geq 2$ the problem is less straightforward, and a solution to (3.28) may not even exist [42-45,49].

If $\mathbf{A}$ is nonsingular and has s distinct eigenvalues then it has precisely 2^s square roots [45]. To illustrate this, consider the overhead line configuration given in Figure 3.4 (see page 54). At an arbitrary frequency, f= 1kHz, the matrix in (3.27) is,

$$\mathbf{A} = \begin{pmatrix} -5.4444e-04+3.5393e-05i & -7.8137e-05+2.5878e-05i & -8.2577e-05+3.0142e-05i \\ -8.8737e-05+2.9687e-05i & -5.2886e-04+3.1373e-05i & -8.8519e-05+2.9665e-05i \\ -8.2645e-05+3.0149e-05i & -7.8010e-05+2.5863e-05i & -5.4404e-04+3.5361e-05i \end{pmatrix} \tag{3.29}$$

which has three distinct eigenvalues, λ_1=-7.0529e-04+9.1187e-05i, λ_2=-4.6163e-04+5.2315e-06i and λ_3=-4.5042e-04+5.7089e-06i. In this case, $\mathbf{A}$ has eight square roots, four of which are given by,

$$\mathbf{X}_1 = \begin{pmatrix} 6.8144e-04+2.3224e-02i & 4.7716e-04+1.6518e-03i & 5.5948e-04+1.7336e-03i \\ 5.4813e-04+1.8762e-03i & 6.0696e-04+2.2882e-02i & 5.4785e-04+1.8716e-03i \\ 5.5955e-04+1.7350e-03i & 4.7697e-04+1.6492e-03i & 6.8107e-04+2.3216e-02i \end{pmatrix}$$

$$\mathbf{X}_2 = \begin{pmatrix} -5.5867e-04+4.7461e-03i & -5.0946e-04-1.4651e-02i & -6.8946e-04-1.6698e-02i \\ -6.2963e-04-1.6653e-02i & -3.2437e-04+6.5337e-03i & -6.3892e-04-1.6611e-02i \\ -6.8668e-04-1.6711e-02i & -5.1524e-04-1.4625e-02i & -5.7395e-04+4.8172e-03i \end{pmatrix}$$

$$\mathbf{X}_3 = \begin{pmatrix} 5.5492e-04+1.7455e-03i & 4.7089e-04+1.6909e-03i & 6.8300e-04+2.3211e-02i \\ 5.4044e-04+1.9194e-03i & 6.0699e-04+2.2881e-02i & 5.5554e-04+1.8284e-03i \\ 6.7954e-04+2.3230e-02i & 4.8325e-04+1.6101e-03i & 5.6408e-04+1.7232e-03i \end{pmatrix}$$

$$\mathbf{X}_4 = \begin{pmatrix} -6.8519e-04-1.6733e-02i & -5.1572e-04-1.4612e-02i & -5.6593e-04+4.7794e-03i \\ -6.3731e-04-1.6610e-02i & -3.2434e-04+6.5336e-03i & -6.3123e-04-1.6654e-02i \\ -5.6670e-04+4.7839e-03i & -5.0896e-04-1.4664e-02i & -6.9094e-04-1.6676e-02i \end{pmatrix} \tag{3.30}$$

The remaining four roots are given by $-\mathbf{X}_1$, $-\mathbf{X}_2$, $-\mathbf{X}_3$ and $-\mathbf{X}_4$. Thus, a further problem arises with regards to the selection of the 'correct' square root for the physical system under investigation. This can be undertaken as outlined in section 3.4.2.

3.4.2 Obtaining the Principal Matrix Square Root

As shown above, if the matrix square root exists then it is never unique. However, if the matrix product given in (3.27) has no negative real eigenvalues, then there is a unique square root for which every eigenvalue has positive real part (this can be verified by obtaining the eigenvalues of all the roots above) [44-45,47,50]. This square root is called the principal square root, denoted by $\mathbf{A}^{1/2}$, and is the square root that is required. The principle square root can be defined formally as,

$$\left(\mathbf{A}^{1/2}\right)^2 = \mathbf{A} \quad \text{and} \quad \mathrm{Re}\,\lambda_k\left(\mathbf{A}^{1/2}\right) > 0 \quad \text{for all } k, \tag{3.31}$$

where $\lambda_k(\mathbf{A})$ denotes an eigenvalue of $\mathbf{A}$. To clarify the issue of which square root is required, it is necessary to re-examine the eigenvalues given in (3.16) for the modal case.

It was shown in (3.16) that the eigenvalues of $\gamma(\omega)$ can be expressed as a modal attenuation, $\alpha(\omega)$, and a modal velocity $\upsilon(\omega)$. This represents the propagating mode as a wave travelling with a positive velocity which is attenuated along the length of the line. If, $\alpha(\omega)$ is not positive, clearly from the definition of the wave propagation function, $\mathbf{H}(\omega)$ in (3.14), the wave will be amplified rather than attenuated, which for a lossy transmission system cannot be the case. Thus, the eigenvalues of the calculated matrix square root must have positive real part, which, if none of the eigenvalues of the original matrix (3.27) are negative and real, corresponds to the principal square root, $\mathbf{A}^{1/2}$, which in this case, as stated above, is unique.

3.4.3 The Matrix Sign Function

The matrix sign function, introduced by Roberts[1] [54], has many interesting algebraic properties which can be used to determine solutions to problems which frequently arise in systems and control theory applications, such as solving the Lyapunov and algebraic Ricatti equations [54,57-59,61,66].

One of the most unique features of the matrix sign function is that it partitions the space spanned by the eigenvectors of a matrix into two subspaces, according to the sign of the real part of the eigenvalues of the matrix [54-56,58,61]. This partitioning allows the determination of the solutions of several algebraic matrix equations without explicit knowledge of the individual eigenvectors. In particular, positive definite solutions of algebraic Ricatti equations can be found without knowledge of the corresponding eigenvectors. In addition to the algebraic matrix equations, the sign function can be used for the computation of the positive definite square root of a matrix [44-45,58,61]. This result is of particular interest in power transmission line modelling, since it enables the wave propagation matrix and characteristic admittance matrix to be determined directly in phase co-ordinates without resorting to model decomposition techniques.

A Newton-Raphson type algorithm, proposed by Roberts [54], has been a standard algorithm for computing the matrix sign function. The sign of the matrix $\mathbf{B}$ is defined constructively as the limit of the iteration,

$$\mathbf{X}_{k+1} = \frac{1}{2}\left(\mathbf{X}_k + \mathbf{X}_k^{-1}\right), \qquad \mathbf{X}_0 = \mathbf{A} \tag{3.32}$$

which converges quadratically to sign($\mathbf{A}$) for any $\mathbf{A} \in \mathbf{C}^{n\,x\,n}$ having no pure imaginary eigenvalues. From (3.32) it can be seen that an additional advantage of using the matrix

[1] [54] is based on a technical report concerning the matrix sign function, written by Roberts in 1971 at Cambridge University.

sign function is that it can be evaluated efficiently using relatively simple numerical methods.

3.4.4 Matrix Sign Function Definition

The matrix sign function is an extension of its scalar counterpart, which, for a complex scalar, z, with $\mathrm{Re}(z)\neq 0$, is defined as follows [45,48,54,56-57,59-61],

$$\mathrm{sign}(z)=\begin{cases}+1 & \text{if } \mathrm{Re}(z)>0\\ -1 & \text{if } \mathrm{Re}(z)<0\end{cases} \tag{3.33}$$

The corresponding matrix sign function is restricted to square matrices, **A**, and is defined only for $\mathbf{A}\in\mathbf{C}^{n\times n}$ having no pure imaginary eigenvalues. The matrix sign function can be defined in several different ways e.g. making use of eigen decompositions such as the Jordan canonical form or Schur form, matrix iteration based definitions, etc., [61]. In a recent paper [44], a new representation of the matrix sign function was introduced in terms of the matrix square root, using the following matrix sign decomposition,

$$\mathbf{A}=\mathbf{SN} \tag{3.34}$$

where $\mathbf{S}=\mathrm{sign}(\mathbf{A})$ and $\mathbf{A}\in\mathbf{C}^{n\times n}$ assuming **A** has no pure imaginary eigenvalues. The decomposition (3.34) is uniquely defined because $\mathbf{S}=\mathrm{sign}(\mathbf{A})$ is uniquely defined and nonsingular (its eigenvalues are ± 1), so that $\mathbf{N}=\mathbf{S}^{-1}\mathbf{A}$. Since **S** is involutary ($\mathbf{S}^2=\mathbf{I}$), $\mathbf{N}=\mathbf{SA}$ [44]. This is similar to the polar decomposition, $\mathbf{A}=\mathbf{UH}$, where **U** is orthogonal and **H** is Hermitian.

For the matrix sign decomposition, (3.34), $\mathbf{A}^2=\mathbf{SNSN}=\mathbf{S}^2\mathbf{N}^2=\mathbf{N}^2$, and since **A** is assumed to have no pure imaginary eigenvalues, $\mathbf{A}^2$ is nonsingular and has no real, negative eigenvalues. Therefore, $\mathbf{N}=(\mathbf{A}^2)^{1/2}$, where for a nonsingular matrix **B** with no real, negative eigenvalues, $\mathbf{B}^{1/2}$ denotes the unique square root all of whose eigenvalues lie in the open right half plane. This characterization of **N** provides the following definition of the matrix sign function [44-45,61],

$$\mathrm{sign}(\mathbf{A})=\mathbf{A}\left(\mathbf{A}^2\right)^{-1/2} \tag{3.35}$$

where $\mathbf{A}^2$ has no negative real eigenvalues. Hence, from (3.31) there is a unique square root of $\mathbf{A}^2$ (the principle root) which has all its eigenvalues in the open right-half complex plane.

In [48,59-60] an algorithm is presented for computing the sign of a matrix based on a Padé approximation to the hypergeometric function $f(\xi)=(1-\xi)^{-1/2}$, which leads to a rational function approximation of the sign function. By expanding the rational function into partial fraction form it is possible to obtain an algorithm for computing the matrix sign function, which is particularly suitable for parallel implementation [45,48,59-60]. The iterates have the form,

$$\mathbf{X}_{k+1}=\frac{1}{p}\mathbf{X}_k\sum_{i=1}^{p}\frac{1}{\xi_i}\left(\mathbf{X}_k^2+\alpha_i^2\mathbf{U}\right)^{-1},\mathbf{X}_0=\mathbf{A} \tag{3.36}$$

where

$$\left.\begin{aligned}\xi_i &= \frac{1}{2}\left[1+\cos\left(\frac{(2i-1)\pi}{2p}\right)\right] \\ \alpha_i^2 &= \frac{1}{\xi_i}-1\end{aligned}\right\} \quad \text{for } i = 1{:}\,p \tag{3.37}$$

3.4.5 Padé Iteration for Evaluating $\mathbf{Y_c}(\omega)$

The above iteration for computing the matrix sign function using Padé approximation can be used to obtain an iteration for computing the characteristic admittance, $\mathbf{Y_c}(\omega)$, by exploiting the relationship between the matrix sign function and the matrix square root given in (3.35). Consider the following block 2x2 matrix [45],

$$\mathbf{B}(\omega)=\begin{bmatrix}\mathbf{0} & \mathbf{Y}(\omega)\\ \mathbf{Z}(\omega) & \mathbf{0}\end{bmatrix} \tag{3.38}$$

where, as before, $\mathbf{Y}(\omega)$ and $\mathbf{Z}(\omega)$ are defined as the per unit length shunt admittance and series impedance matrices, respectively. Substitution of (3.38) into (3.35) gives the following relation,

$$\begin{aligned}\operatorname{sign}\left(\begin{bmatrix}\mathbf{0} & \mathbf{Y}(\omega)\\ \mathbf{Z}(\omega) & \mathbf{0}\end{bmatrix}\right) &= \begin{pmatrix}\mathbf{0} & \mathbf{Y}(\omega)\\ \mathbf{Z}(\omega) & \mathbf{0}\end{pmatrix}\left[\begin{pmatrix}\mathbf{0} & \mathbf{Y}(\omega)\\ \mathbf{Z}(\omega) & \mathbf{0}\end{pmatrix}^2\right]^{-1/2} \\ &= \begin{pmatrix}\mathbf{0} & \mathbf{Y}(\omega)\\ \mathbf{Z}(\omega) & \mathbf{0}\end{pmatrix}\begin{bmatrix}\begin{pmatrix}\mathbf{Y}(\omega)\mathbf{Z}(\omega) & \mathbf{0}\\ \mathbf{0} & \mathbf{Z}(\omega)\mathbf{Y}(\omega)\end{pmatrix}\end{bmatrix}^{-1/2} \\ &= \begin{pmatrix}\mathbf{0} & \mathbf{Y}(\omega)\\ \mathbf{Z}(\omega) & \mathbf{0}\end{pmatrix}\begin{pmatrix}\left[\mathbf{Y}(\omega)\mathbf{Z}(\omega)\right]^{-1/2} & \mathbf{0}\\ \mathbf{0} & \left[\mathbf{Z}(\omega)\mathbf{Y}(\omega)\right]^{-1/2}\end{pmatrix} \\ &= \begin{pmatrix}\mathbf{0} & \mathbf{Y}(\omega)\left[\mathbf{Z}(\omega)\mathbf{Y}(\omega)\right]^{-1/2}\\ \mathbf{Z}(\omega)\left[\mathbf{Y}(\omega)\mathbf{Z}(\omega)\right]^{-1/2} & \mathbf{0}\end{pmatrix}\end{aligned} \tag{3.39}$$

Thus, if we calculate the matrix sign function for the 2x2 block matrix given in (3.38) it is possible to obtain the characteristic admittance matrix $\mathbf{Y_c}(\omega)=\mathbf{Y}(\omega)[\mathbf{Z}(\omega)\mathbf{Y}(\omega)]^{-1/2}$ (which is equivalent to (3.8)), and the characteristic impedance matrix $\mathbf{Z_c}(\omega)=\mathbf{Z}(\omega)[\mathbf{Y}(\omega)\mathbf{Z}(\omega)]^{-1/2}$ directly. Hence, the Padé iteration for the matrix sign function discussed above can be manipulated to obtain an iteration for evaluating the characteristic admittance matrix, $\mathbf{Y_c}(\omega)$, directly in phase co-ordinates.

Applying the Padé iteration to the matrix sign function (3.36-3.37) to the 2x2 block matrix in (3.38) we find the iterates have the form,

$$\mathbf{X}_k=\begin{bmatrix}\mathbf{0} & \mathbf{Y}_{c_k}(\omega)\\ \mathbf{Z}_{c_k}(\omega) & \mathbf{0}\end{bmatrix} \tag{3.40}$$

and the following Padé iteration for evaluating the phase domain characteristic admittance, $\mathbf{Y_c}(\omega)$, is obtained,

$$\left.\begin{aligned}\mathbf{Y}_{c_{k+1}}(\omega) &= \frac{1}{p}\mathbf{Y}_{c_k}(\omega)\sum_{i=1}^{p}\frac{1}{\xi_i}\left[\mathbf{Z}_{c_k}(\omega)\mathbf{Y}_{c_k}(\omega)+\alpha_i^2\mathbf{U}\right]^{-1}\\ \mathbf{Z}_{c_{k+1}}(\omega) &= \frac{1}{p}\mathbf{Z}_{c_k}(\omega)\sum_{i=1}^{p}\frac{1}{\xi_i}\left[\mathbf{Y}_{c_k}(\omega)\mathbf{Z}_{c_k}(\omega)+\alpha_i^2\mathbf{U}\right]^{-1}\end{aligned}\right\} \quad k=0,1,2,\ldots \quad (3.41)$$

with $\mathbf{Y}_{c0}(\omega)=\mathbf{Y}(\omega)$ and $\mathbf{Z}_{c0}(\omega)=\mathbf{Z}(\omega)$.

3.4.6 Convergence Characteristics

In order to determine a value for the order of the Padé iteration in (3.41) that will provide computational efficiency and accuracy, it is necessary to analyse the convergence characteristics of the algorithm for different values of p, over the entire frequency range of interest. This can be done at each iteration by monitoring the convergence using the relative residual,

$$res(\mathbf{X}_k)=\frac{\left\|\mathbf{U}-\mathbf{X}_k^2\right\|_F}{\left\|\mathbf{U}\right\|_F} \quad (3.42)$$

where $||\ .\ ||_F$ is the Frobenius[2] norm, $\mathbf{U}$ is the unit matrix and,

$$\mathbf{X}_k=\mathbf{Z}_{c_k}.\mathbf{Y}_{c_k} \quad (3.43)$$

denotes the iterate converging to the product of the characteristic admittance, $\mathbf{Y}_c$, and characteristic impedance, $\mathbf{Z}_c$, so that $\mathbf{X}_k \rightarrow \mathbf{U}$ as $k\rightarrow\infty$.

Consider the single-circuit transmission line configuration as described in section 3.5.1. The characteristic admittance is calculated using iteration (3.41) with the order of the Padé approximation varied from p=1 to p=7. The tolerance to measure converge is set at 1.0E-15. The convergence characteristics are shown in Figure 3.2.

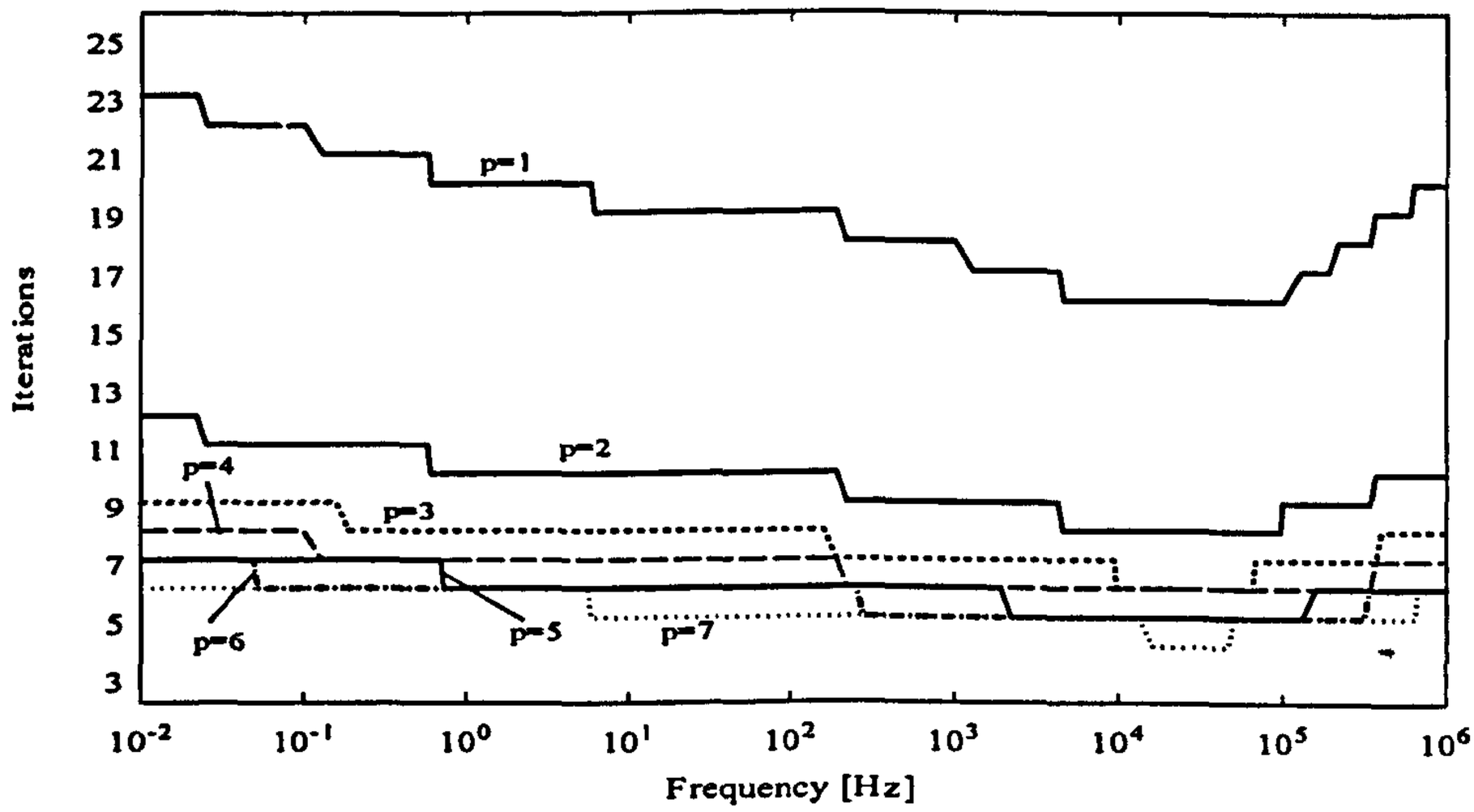

Figure 3.2. Convergence characteristics for a single-circuit transmission line with a varying order, p, Padé approximation.

---

[2] The Frobenius norm is defined as $\|\mathbf{A}\|=\sqrt{\sum_{i=1}^{m}\sum_{j=1}^{n}\left|a_{ij}\right|^2}$

It can be seen from Figure 3.2 that convergence is achieved in at most $2p$ iterations, over the entire frequency range, for values of $p > 3$. Furthermore, as the frequency increases, a more rapid convergence is observed. Figure 3.2 also highlights the stability of the algorithm - even for very small orders, p=1 and p=2, convergence is achieved, albeit with an increased number of iterations, with no instability problems occurring at any stage in the frequency interval. A similar result was obtained using a double-circuit transmission line configuration, with convergence obtained for all values of p used in (3.41).

3.4.7 Scaling

As discussed above, although the algorithm in (3.41) has at most a convergence of $2p$ for $p > 3$, accelerated convergence is not guaranteed since the method may not necessarily converge rapidly in the initial stages. This is because the error can take several iterations to become small enough for rapid convergence to be observed. However, if required, the number of iterations can be reduced by introducing scaling techniques into the algorithm of (3.41).

Several different scaling strategies have been suggested for the matrix sign function [45], and these can be used for the iteration of (3.41) by making use of the relationship between the matrix sign function and matrix square root (3.35). The scaled Padé iteration has the form,

$$\left.\begin{aligned}
\mathbf{Y}_{c_{k+1}}(\omega) &= \frac{1}{p}\gamma_k \mathbf{Y}_{c_k}(\omega)\sum_{i=1}^{p}\frac{1}{\xi_i}\left[\gamma_k^2 \mathbf{Z}_{c_k}(\omega)\mathbf{Y}_{c_k}(\omega) + \alpha_i^2 \mathbf{U}\right]^{-1} \\
\mathbf{Z}_{c_{k+1}}(\omega) &= \frac{1}{p}\gamma_k \mathbf{Z}_{c_k}(\omega)\sum_{i=1}^{p}\frac{1}{\xi_i}\left[\gamma_k^2 \mathbf{Y}_{c_k}(\omega)\mathbf{Z}_{c_k}(\omega) + \alpha_i^2 \mathbf{U}\right]^{-1} \\
\gamma_k &= \left|\left[\left(\det(\mathbf{Y}_{c_k})\right)\left(\det(\mathbf{Z}_{c_k})\right)\right]^{-\frac{1}{2n}}\right|
\end{aligned}\right\} \quad k = 0,1,2,\ldots \quad (3.44)$$

where the initial conditions are also $\mathbf{Y}_{c0}(\omega)=\mathbf{Y}(\omega)$ and $\mathbf{Z}_{c0}(\omega)=\mathbf{Z}(\omega)$.

Applying the scaled iteration (3.44) to the single-circuit transmission line configuration the convergence characteristics of the new iteration can be examined in a similar manner as above. The results are shown in Figure 3.3.

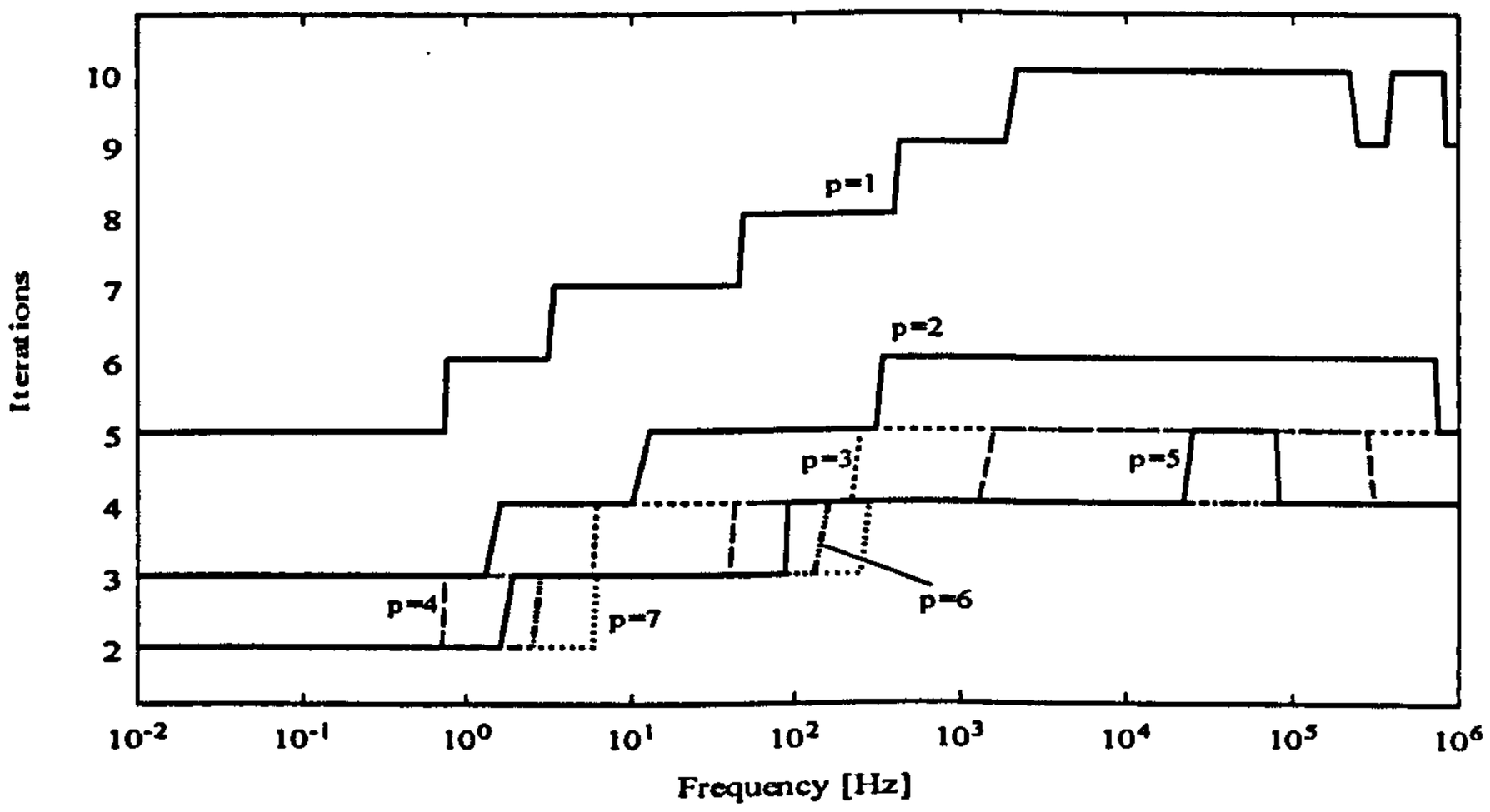

Figure 3.3. Convergence characteristics for a single-circuit transmission line with a varying order, p, Padé approximation using scaling

It can be seen from Figure 3.3 that the introduction of scaling has a dramatic effect on the number of iterations required for convergence. For $p < 3$, the effect of introducing scaling is significant over the entire frequency range. For p=3,4,5,6 and 7 convergence is achieved in just four iterations, up to frequencies of ~ 200Hz.

3.5 Test Examples

To illustrate the accuracy, efficiency and robustness of the Padé iteration (3.41) for calculating the characteristic admittance matrix, $\mathbf{Y}_c(\omega)$, directly in phase co-ordinates, the results for several test cases are presented in this section. The test cases correspond to single, double and asymmetrical transmission line configurations.

For all the results presented, the order of the Padé approximation is taken to be p=4. The frequency interval considered has been taken to be 10^{-2}Hz-10^{6}Hz, with 241 frequency points and 30 frequency points per decade.

The tolerance used for measuring convergence in each test case, and at all frequencies, is taken to be 10^{-15}.

3.5.1 Single-Circuit Transmission Line Configuration

Consider the case of the 345kV, single-circuit untransposed overhead transmission line system, with a bilateral symmetry, as shown in Figure 3.4. The physical data for the system can be found in Appendix III.

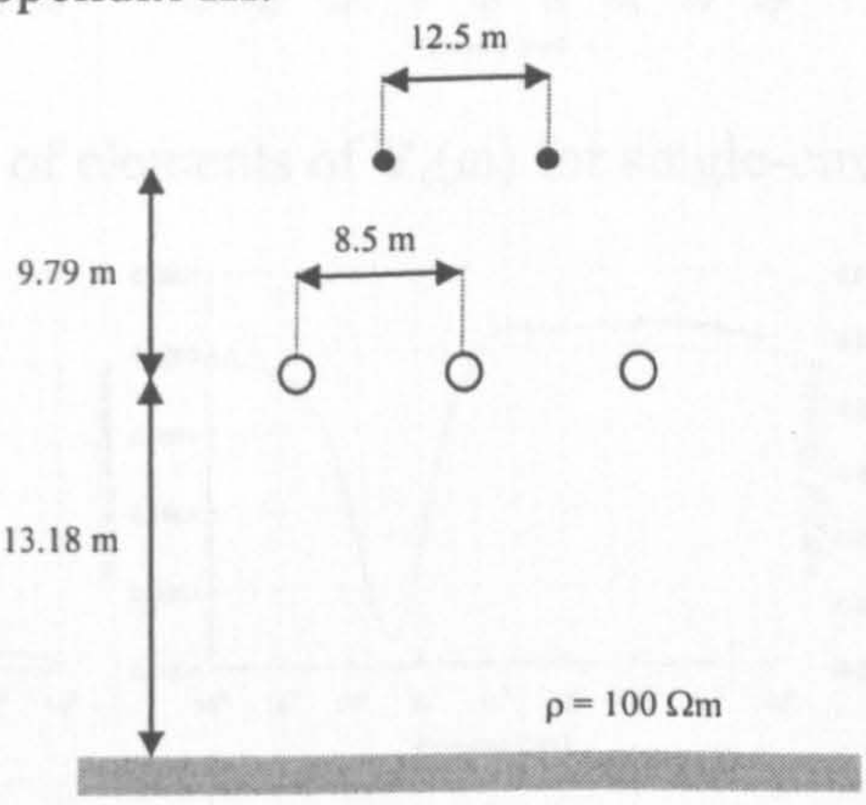

Figure 3.4. 345kV single-circuit overhead line

Figures 3.5 and 3.6 show the real and imaginary parts of the elements of the characteristic admittance matrix, $\mathbf{Y}_c(\omega)$, respectively, as calculated by iteration (3.41). The corresponding magnitude and phase angles are shown in Figures 3.7 and 3.8, respectively. An analysis of the results can be made as follows:

The definition of the characteristic admittance in (3.8) can be re-written in the following form (assuming the conductance is zero) as follows,

$$\mathbf{Y}_c(\omega) = \left[j\omega\mathbf{C}(\omega)\left(\mathbf{R}(\omega) + j\omega\mathbf{L}(\omega)\right)\right]^{-1/2} j\omega\mathbf{C}(\omega) \tag{3.45a}$$

As the frequency tends to zero, series impedance converges to the DC value of the resistance and the elements become complex, and proportional to the square root of the frequency. In this case, (3.45a) is reduced to,

$$\mathbf{Y}_c(\omega \to 0) = \sqrt{j\omega}\left(\mathbf{C}\mathbf{R}_{DC}\right)^{-1/2}\mathbf{C} \tag{3.45b}$$

At high frequencies (above approximately 100Hz for this example) the significant contribution to the series impedance, $\mathbf{Z}(\omega)$, arises from the reactance. As the frequency tends to infinity the series inductance matrix tends to a constant, since the complex

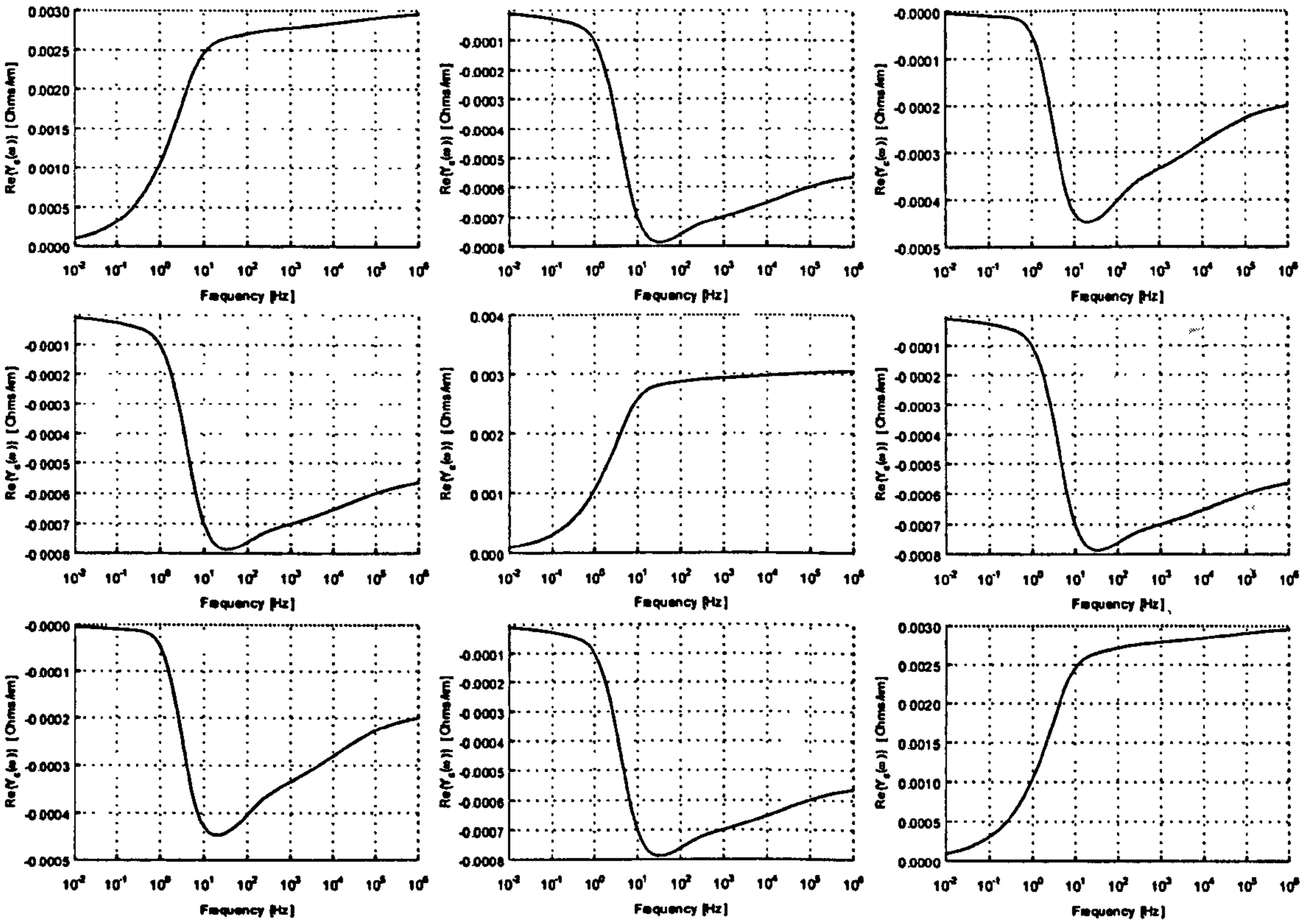

Figure 3.5. Real part of elements of $\mathbf{Y_c}(\omega)$ for single-circuit transmission line

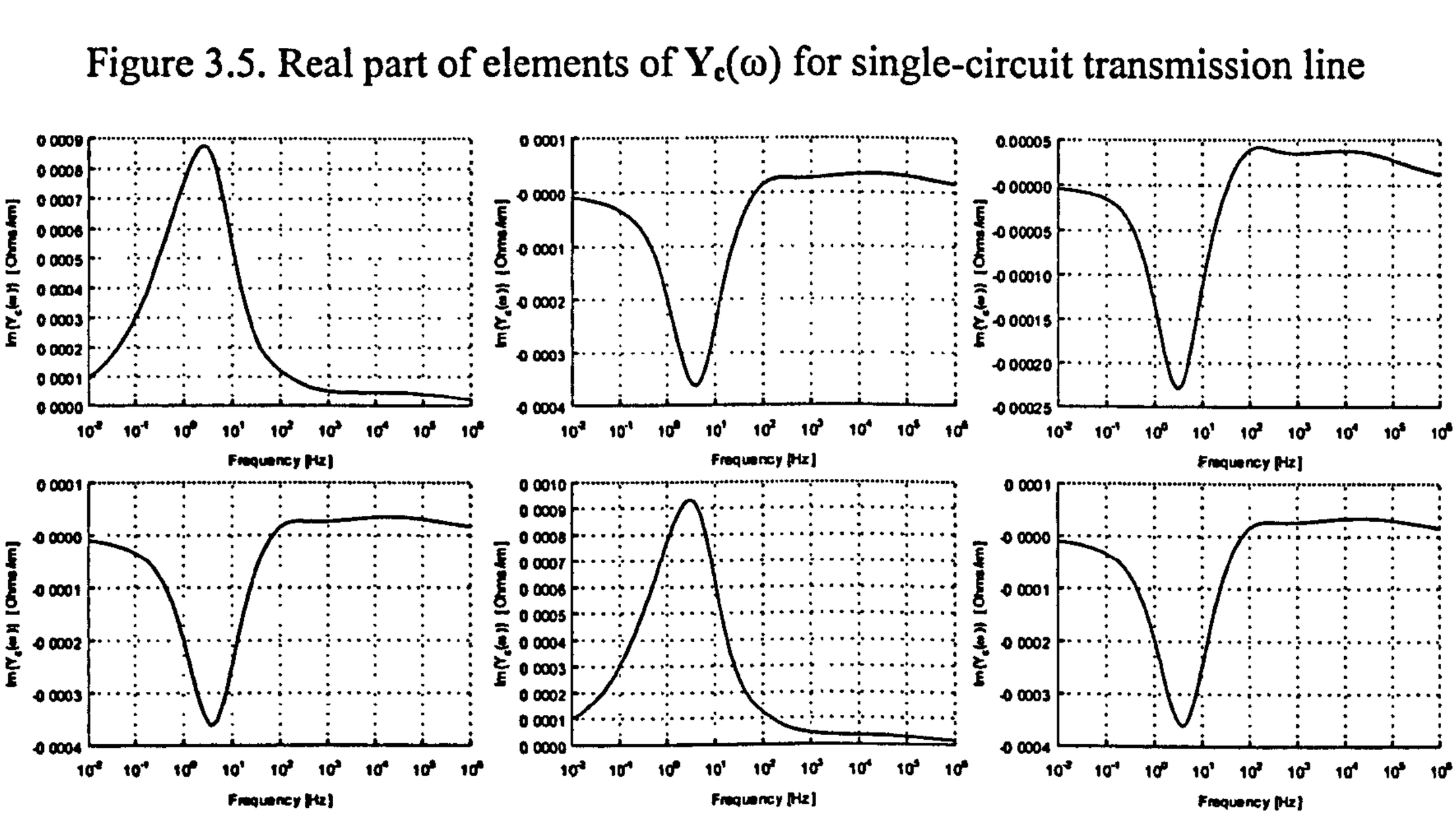

Figure 3.6. Imaginary part of elements of $\mathbf{Y_c}(\omega)$ for single-circuit transmission line

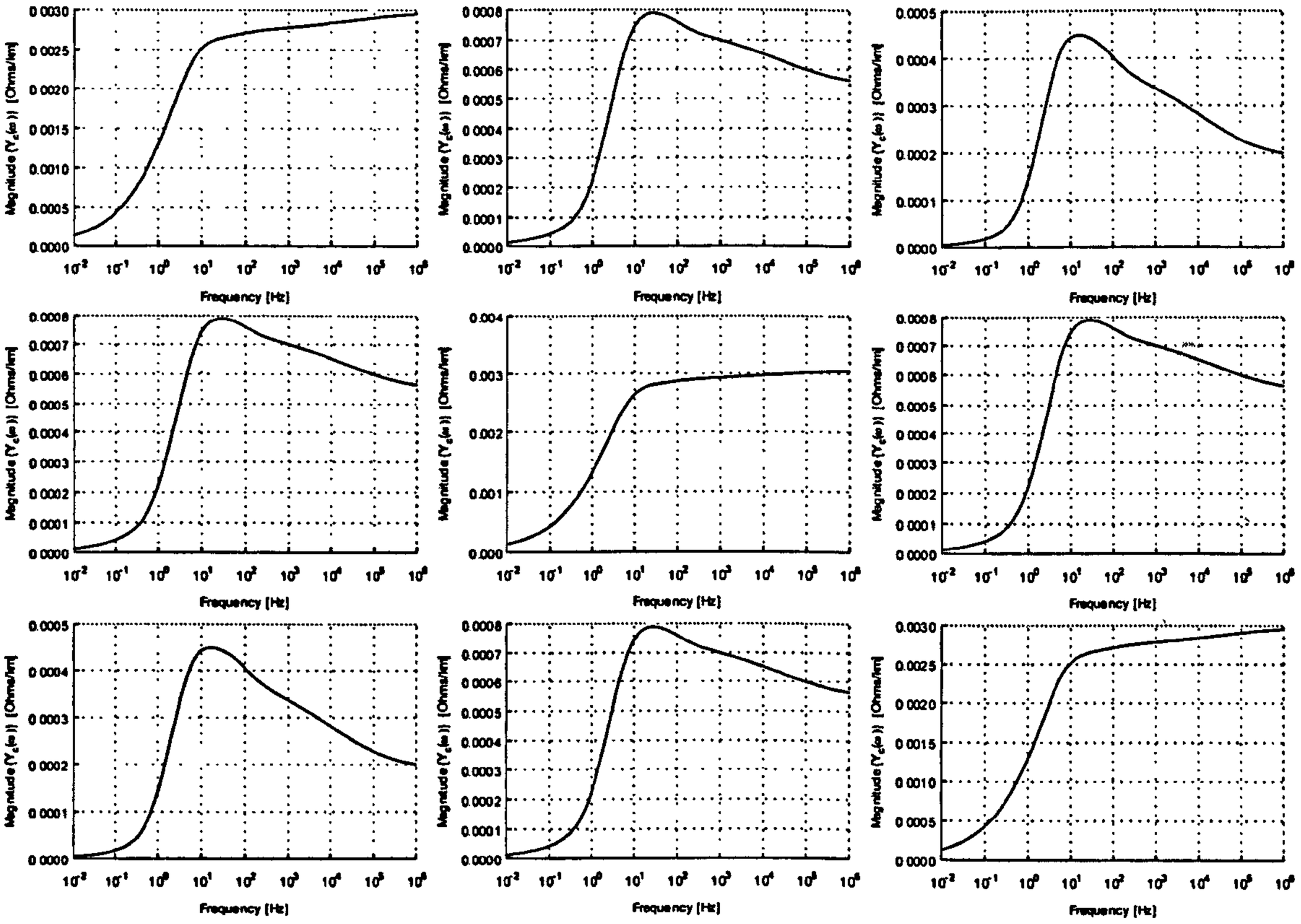

Figure 3.7. Magnitude of elements of $\mathbf{Y_c}(\omega)$ for single-circuit transmission line

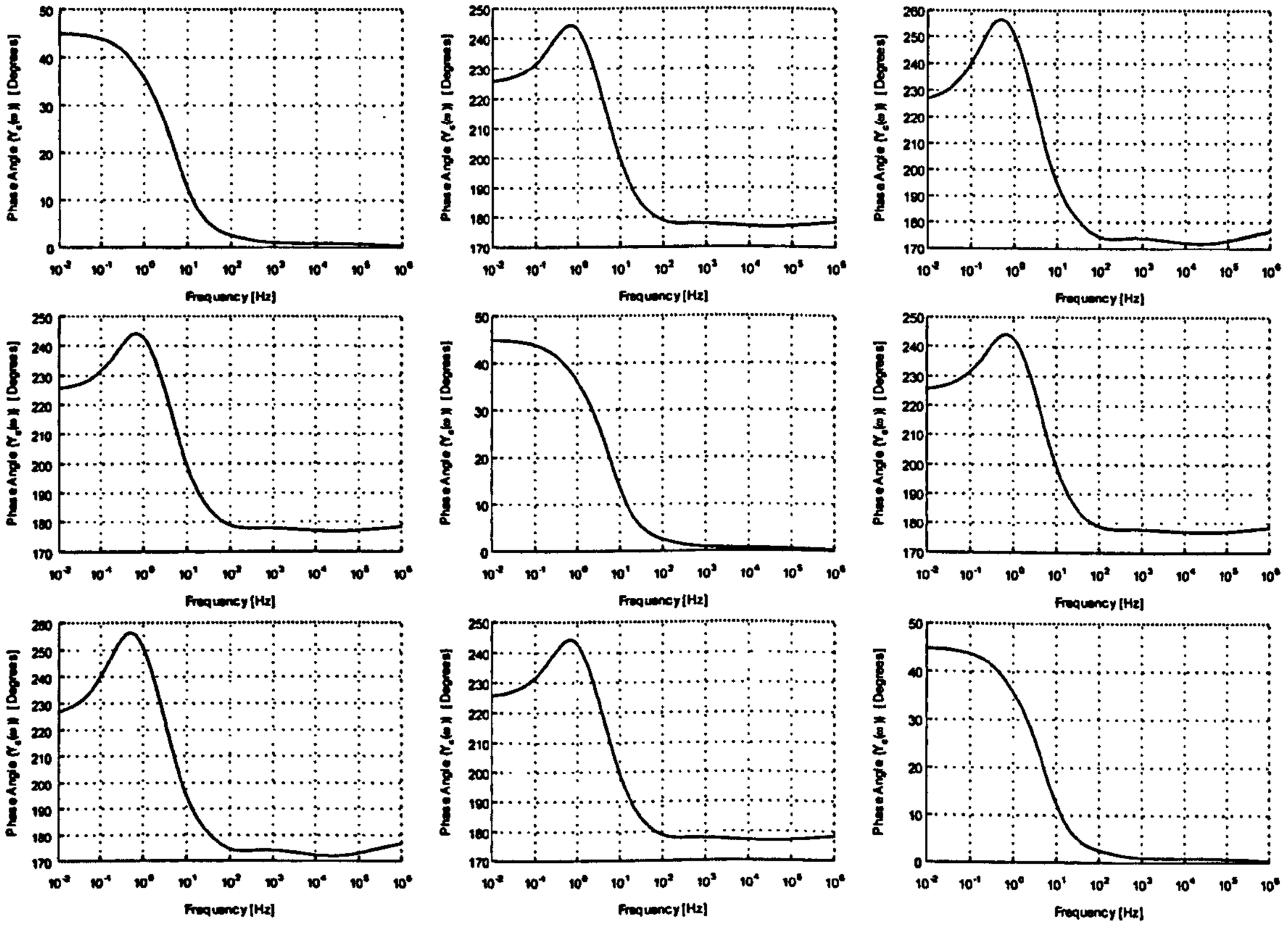

Figure 3.8. Phase Angle of elements of $\mathbf{Y_c}(\omega)$ for single-circuit transmission line

depth in the conductors and ground approach zero. The characteristic admittance matrix can therefore be written as [11],

$$\mathbf{Y_c}(\omega \to \infty) = \left(\mathbf{CL}_\infty\right)^{-1/2}\mathbf{C} \tag{3.46}$$

From (3.46) it follows that at high frequency the elements of $\mathbf{Y_c}(\omega)$ become real and constant. It can be seen from Figures 3.5 and 3.6 that the behaviour of the elements of $\mathbf{Y_c}(\omega)$ follows that of the above discussion. However, at 10^6Hz, the complex depth in the ground is still sufficiently high, so that the elements of $\mathbf{Y_c}(\omega)$ are still tending towards a constant.

3.5.2 Double-Circuit Transmission Line Configuration

Consider the case of the 220kV, double-circuit untransposed overhead transmission line system, as shown in Figure 3.9. The physical data for the system can be found in Appendix III.

The real and imaginary elements of the first column of the characteristic admittance matrix, $\mathbf{Y_c}(\omega)$, as calculated by iteration (3.41) are shown in Figure 3.11. The corresponding magnitude and phase angle is shown in Figure 3.12. The results can be seen to agree with the theoretical considerations discussed previously for the single-circuit case.

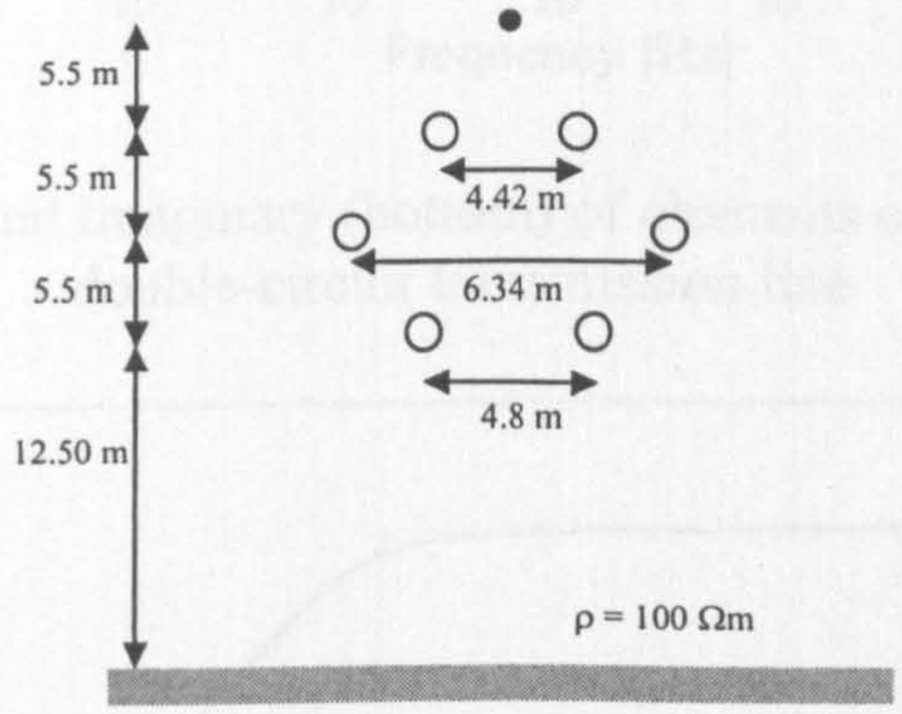

Figure 3.9. 220kV double-circuit overhead line

3.5.3 Asymmetrical Transmission Line Configuration

Figure 3.10 shows a 6-circuit (18 phase conductor), 230kV overhead transmission line system on the same right-of-way [12]. The physical data for the system can be found in Appendix III.

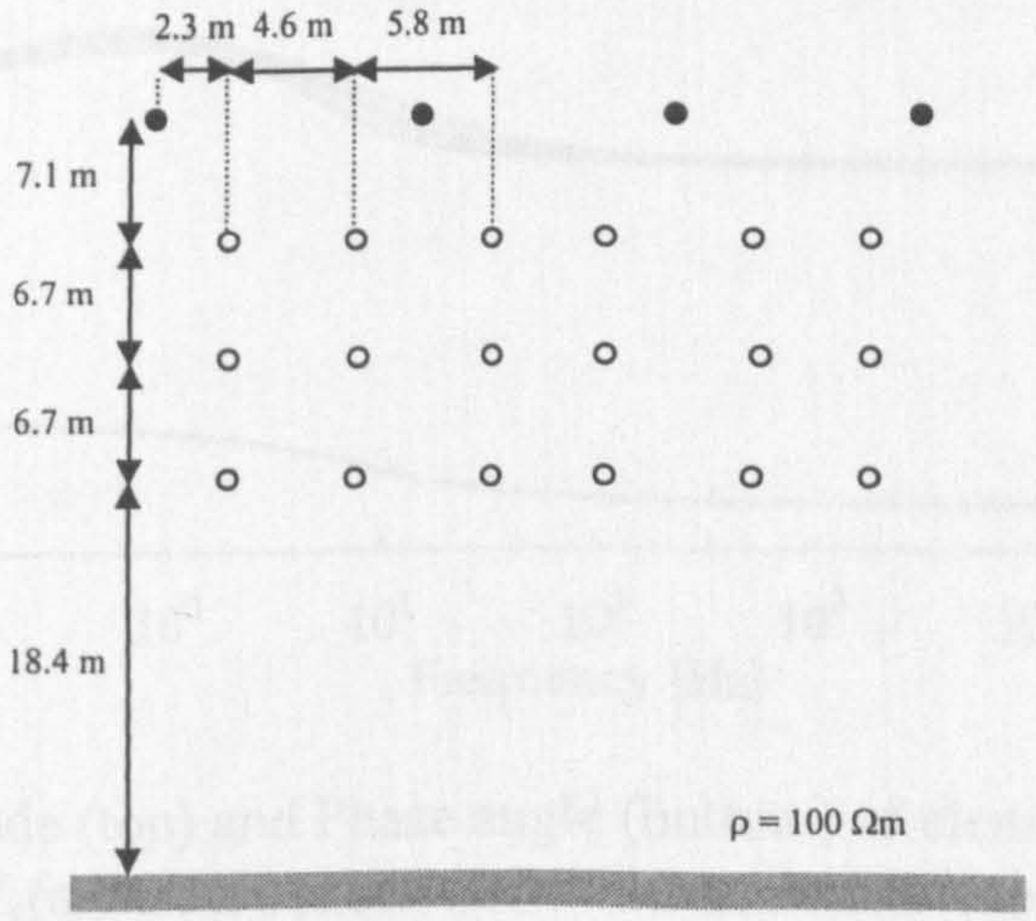

Figure 3.10. 230kV 6-circuit overhead line

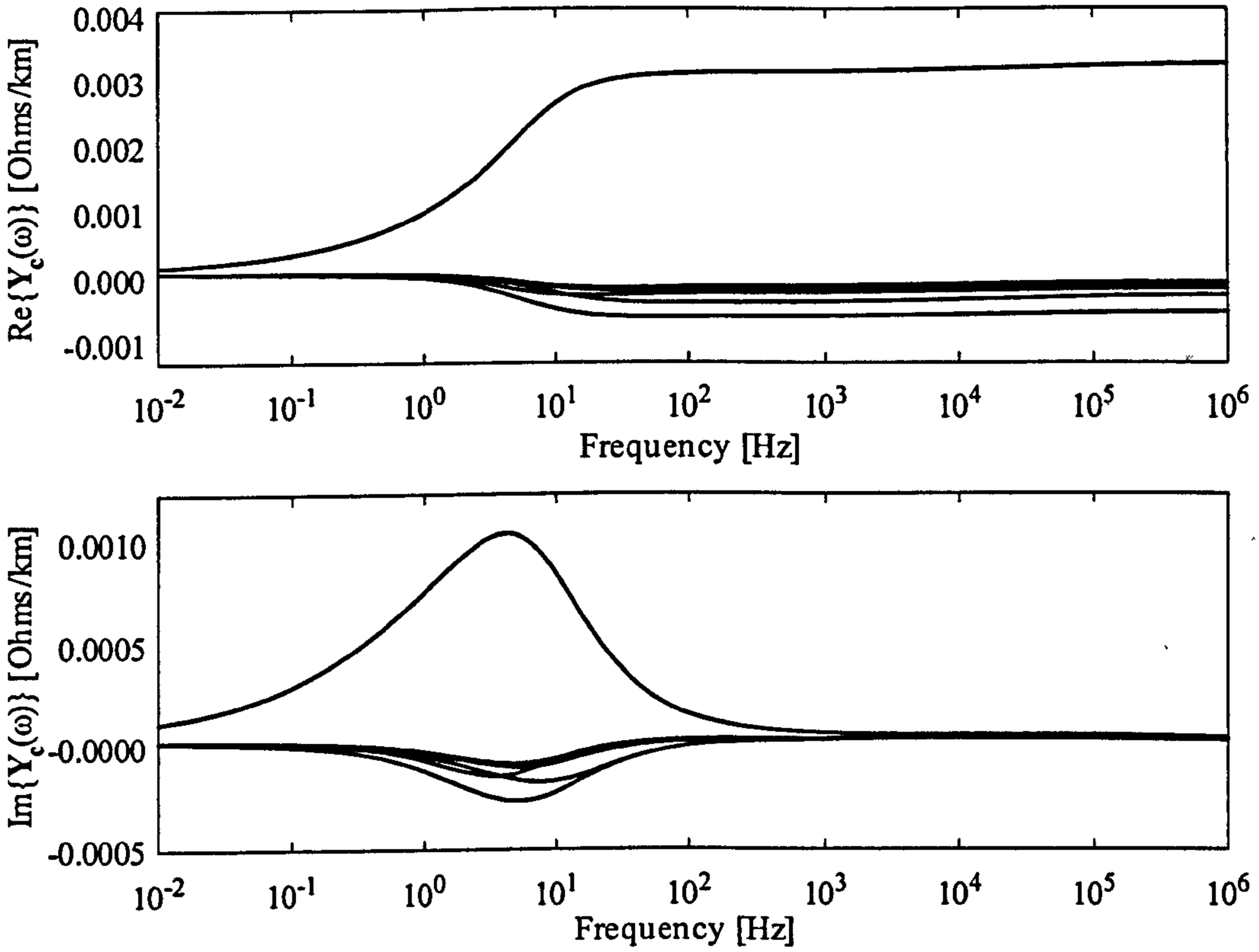

Figure 3.11. Real (top) and Imaginary (bottom) of elements of column 1 of $\mathbf{Y}_c(\omega)$ for a double-circuit transmission line

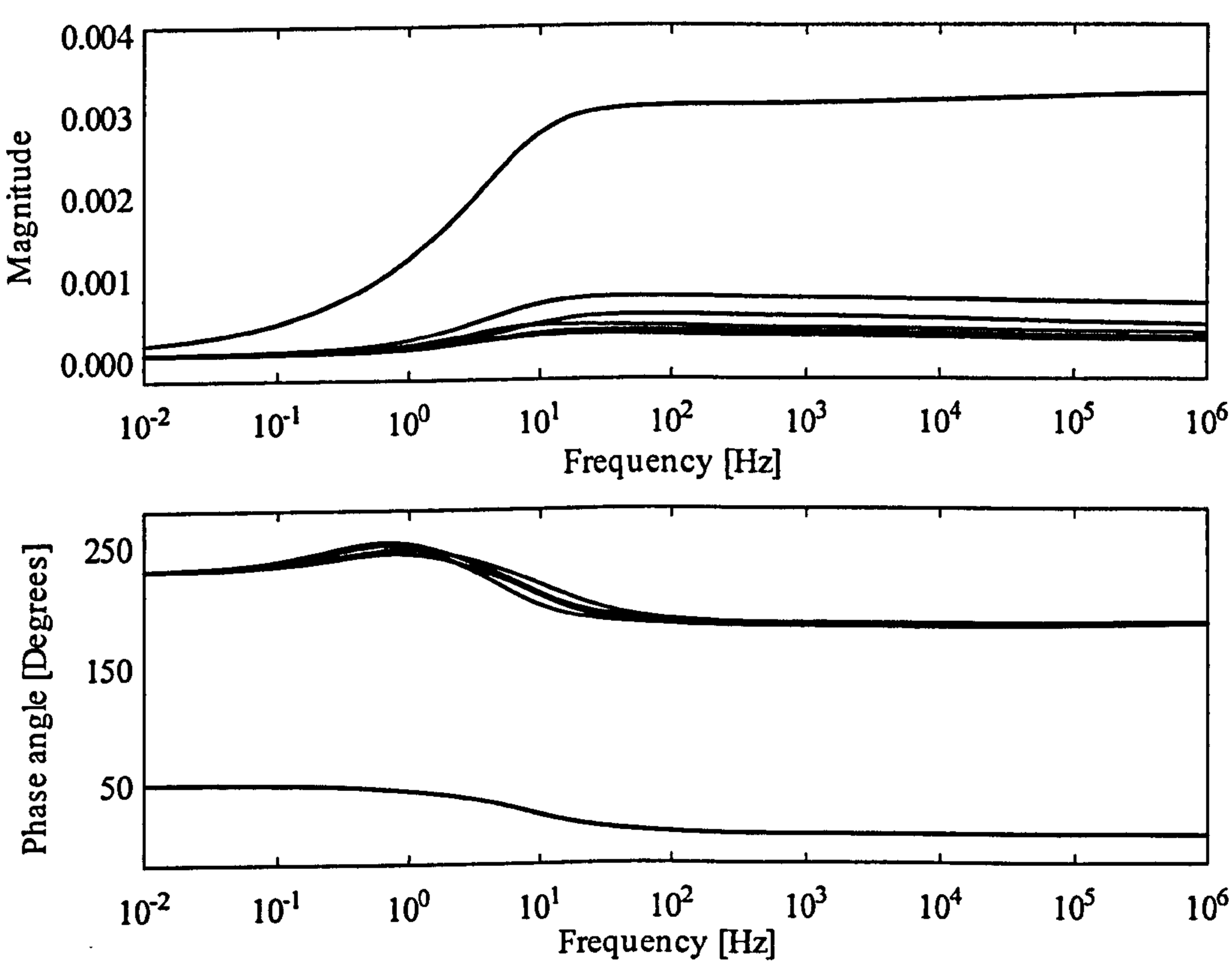

Figure 3.12. Magnitude (top) and Phase angle (bottom) of elements of column 1 of $\mathbf{Y}_c(\omega)$ for a double-circuit transmission line

Despite the increased size (18x18 matrix) of, $\mathbf{Y}_c(\omega)$, in this test case, the proposed algorithm for evaluating the phase domain characteristic admittance, $\mathbf{Y}_c(\omega)$ performs very well. The algorithm does not fail to converge for any order of the Padé approximant. Using the scaled version of the iteration (3.44), the maximum number of iterations required, using an order of p=1, was 13 iterations. Using an order of p=4, the maximum number of iterations occurring throughout the entire frequency interval is just 6 iterations.

3.6 Phase Domain Calculation of H(ω)

The propagation matrix, $\mathbf{H}(\omega)$, defines the transfer of travelling waves from one end of the transmission line to the other. The matrix is complex, and unlike the characteristic admittance matrix, it is unsymmetric. From (3.14) and the definition of $\Gamma(\omega)$ in (3.6), it can be seen that in order to evaluate the wave propagation matrix directly in the phase domain requires evaluation of the matrix square root and matrix exponential functions, at each frequency point of interest. The matrix square root in (3.6) can be obtained directly from the result for the characteristic admittance (3.8) after some matrix manipulation. The following section focuses on the approximation of the matrix exponential operator so that $\mathbf{H}(\omega)$ can be accurately and reliably evaluated directly in phase co-ordinates.

3.6.1 The Matrix Exponential

Like its scalar counterpart, the matrix exponential can be defined directly through a convergent power series expansion [32-33,36,38-39,41,62],

$$e^{\mathbf{A}} = \sum_{k=0}^{\infty} \frac{\mathbf{A}^k}{k!} \tag{3.47}$$

The evaluation of this matrix function is an important problem that arises in the solution of many physical, biological and economic processes that are modelled with systems of ordinary differential equations [32]. A variety of different methods have been proposed to evaluate the matrix exponential based on truncated power series representations, rational function approximations, as well as matrix decomposition methods [32-39,41,62]. However, there are few numerical methods that can be applied in a reliable and efficient way to any class of matrix [32]. The choice of which method to use is therefore very much dependent upon the particular problem under investigation. For example, for problems involving very large sparse and symmetric matrices, matrix decomposition techniques are very efficient. However, as discussed earlier, for matrices that do not have a complete set of linearly independent eigenvectors, these methods are likely to produce inaccurate results due to roundoff error [32].

With these considerations in mind it is proposed in the following sections to apply a Padé approximation technique to evaluate the wave propagation matrix in (3.14).

3.6.2 Padé Approximation for Evaluating H(ω)

The (p, q) Padé approximation to (3.14) can be defined by [32,34-37,41,62]

$$R_{pq}(\mathbf{A}) = \frac{N_{pq}(\mathbf{A})}{D_{pq}(\mathbf{A})} \tag{3.48}$$

where

$$\mathbf{A} = -\sqrt{[\mathbf{Y}(\omega)\mathbf{Z}(\omega)]}\,l \tag{3.49}$$

and

$$N_{pq}(\mathbf{A}) = \sum_{k=0}^{p} \frac{(p+q-k)!\,p!}{(p+q)!\,k!\,(p-k)!}\mathbf{A}^k \tag{3.50}$$

and

$$D_{pq}(\mathbf{A}) = \sum_{k=0}^{q} \frac{(p+q-k)!\,q!}{(p+q)!\,k!\,(q-k)!}(-\mathbf{A})^k \tag{3.51}$$

Several important points should be made about the above algorithm.

(1) $N_{pq}(\mathbf{A})$ approaches the series for exp(**A**/2) as p tends to infinity whereas $[D_{pq}(\mathbf{A})]^{-1}$ approaches the series for exp(-**A**/2) as q tends to infinity, for the argument matrix **A**, as defined in (3.49) [32].

(2) The explicit computation of the matrix exponential function is difficult when the eigenvalues of the argument matrix (3.49) are widely spread, the norm of the argument matrix is large and also when the order of the argument matrix is high [32]. The latter problem is of little consequence for transmission line modelling, since the argument matrix will always be of a relatively low order. However, the two former problems can severely affect the accuracy of the Padé approximation technique for evaluating $\mathbf{H}(\omega)$. This is particularly true in the mid to high frequency range, and for lines of very long length, as discussed below.

3.6.3 Widely Spread Eigenvalues

If the argument matrix (3.49) has widely spread eigenvalues, then (3.48) will most likely produce an inaccurate result because the denominator matrix $D_{pq}(\mathbf{A})$ becomes very poorly conditioned with respect to inversion. In order to better illustrate the effect of widely spread eigenvalues on the conditioning of the matrix $D_{pq}(\mathbf{A})$, consider again the single circuit overhead transmission line configuration given in Figure 3.4.

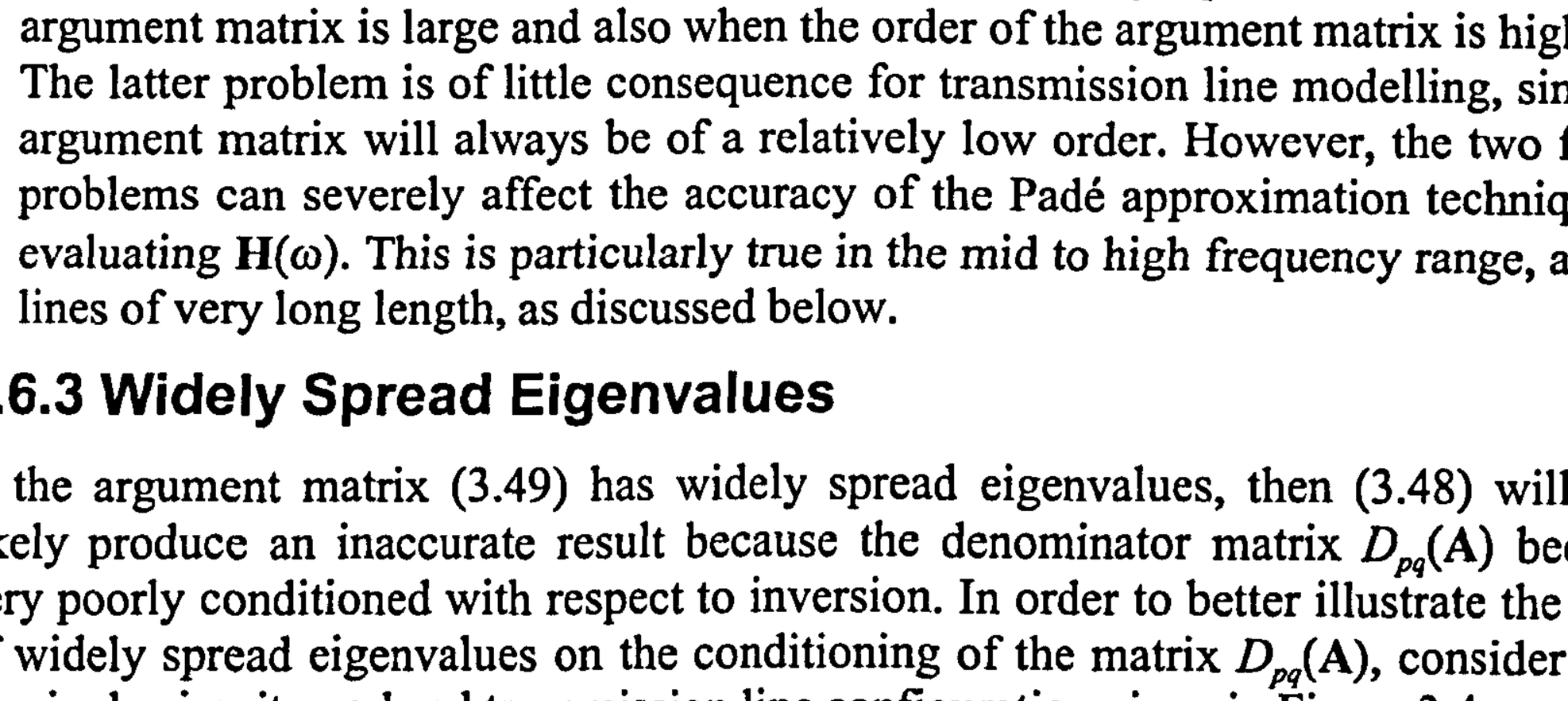

Figure 3.13. Spread of the eigenvalues of the wave propagation constant

The eigenvalues of the propagation constant matrix $\Gamma(\omega)$, as defined in (3.6), can be calculated by diagonalizing $\Gamma(\omega)$ over the whole frequency range of interest. The behaviour of the eigenvalues as functions of frequency is shown in Figure 3.13. The

separation of the eigenvalues (at ~ 300Hz) as the frequency increases is very evident. This separation can be attributed to the presence of the ground, which causes the mode associated with ground to be greatly attenuated as compared with the remaining aerial modes.

As mentioned above, the denominator matrix, $D_{pq}(\mathbf{A})$ tends to the series for the function

$$\mathbf{H}_{l/2} = e^{-\mathbf{A}/2} \tag{3.52}$$

with A defined as in (3.49). At an arbitrary frequency, $f = 250000$Hz, the eigenvalues of the diagonalized wave propagation constant, $\Gamma(\omega)$, are λ_1=2.0659e-01+5.4657e+00i, λ_2=2.3105e-02+5.3321e+00i and λ_3=2.9448e-03+5.3051e+00i. These eigenvalues can be used to obtain a diagonalized version of (3.52). At 250kHz we have,

$$\begin{aligned}
\mathbf{H}_{l/2(i,i)} &= e^{-\mathbf{A}(i,i)/2} \\
&= \begin{pmatrix} e^{-\sqrt{\mathbf{Y}(\omega)\mathbf{Z}(\omega)_{(1,1)}}l} & 0 & 0 \\ 0 & e^{-\sqrt{\mathbf{Y}(\omega)\mathbf{Z}(\omega)_{(2,2)}}l} & 0 \\ 0 & 0 & e^{-\sqrt{\mathbf{Y}(\omega)\mathbf{Z}(\omega)_{(3,3)}}l} \end{pmatrix} \\
&= \begin{pmatrix} 5.5715e+17+4.4836e+17i & 0 & 0 \\ 0 & 7.1438e+01-6.8931e+01i & 0 \\ 0 & 0 & 1.7784e+00+2.5639e-01i \end{pmatrix}
\end{aligned} \tag{3.53}$$

It is clear from (3.53) that $\mathbf{H}_{l/2(1,1)} >> \mathbf{H}_{l/2(2,2)}$ and $\mathbf{H}_{l/2(3,3)}$. Subsequently, when matrix (3.53) is transformed into phase co-ordinates we obtain the following matrix,

$$D_{pq}(\mathbf{A}) = \begin{pmatrix} 1.8743e+17+0.5427e+17i & 1.9454e+17+1.5713e+17i & 1.8728e+17+1.5307e+17i \\ 1.7604e+17+1.4020e+17i & 1.8267e+17+1.4275e+17i & 1.7588e+17+1.3909e+17i \\ 1.8721e+17+1.5254e+17i & 1.9430e+17+1.5535e+17i & 1.8705e+17+1.5135e+17i \end{pmatrix} \tag{3.54}$$

which is very nearly singular, with a condition number with respect to inversion of cond($D_{pq}(\mathbf{A})$)=6.3609e+16.

The reciprocal of the condition number, rcond(A), of the denominator matrix $D_{pq}(\mathbf{A})$ over the whole frequency range is shown in Figure 3.14. For frequencies below 1Hz, it can be seen that rcond(A) is approximately equal to one and $D_{pq}(\mathbf{A})$ is well conditioned. However, as the frequency increases and the eigenvalues begin to separate, rcond(A)$\rightarrow$0 and $D_{pq}(\mathbf{A})$ becomes increasingly badly-conditioned with respect to inversion so that the accuracy of (3.48) deteriorates significantly.

3.6.4 Large Matrix Norm

The problem associated with widely spread eigenvalues will most likely not be observed in practice due to an additional problem concerning the magnitude of the norm of the argument matrix (3.49). This problem manifests itself in the summation of the series for both $N_{pq}(\mathbf{A})$ and $D_{pq}(\mathbf{A})$.

Figure 3.14 clearly illustrates the frequency-dependent nature of the magnitude of the norm of the argument matrix (3.48). This frequency-dependent behaviour can be expected since the elements of (3.48) are increasing with frequency.

In the summation of the series for both $N_{pq}(\mathbf{A})$ and $D_{pq}(\mathbf{A})$ the argument matrix is repeatedly raised to the power of the corresponding term in the summation, up to the

order of the approximation, p. However, when the magnitude of the norm of the argument matrix is relatively large, intermediate matrices in the summation will have elements with large magnitude, but possibly of opposite sign. This results in cancellation of the intermediate terms in the series causing the final result to be corrupted with errors.

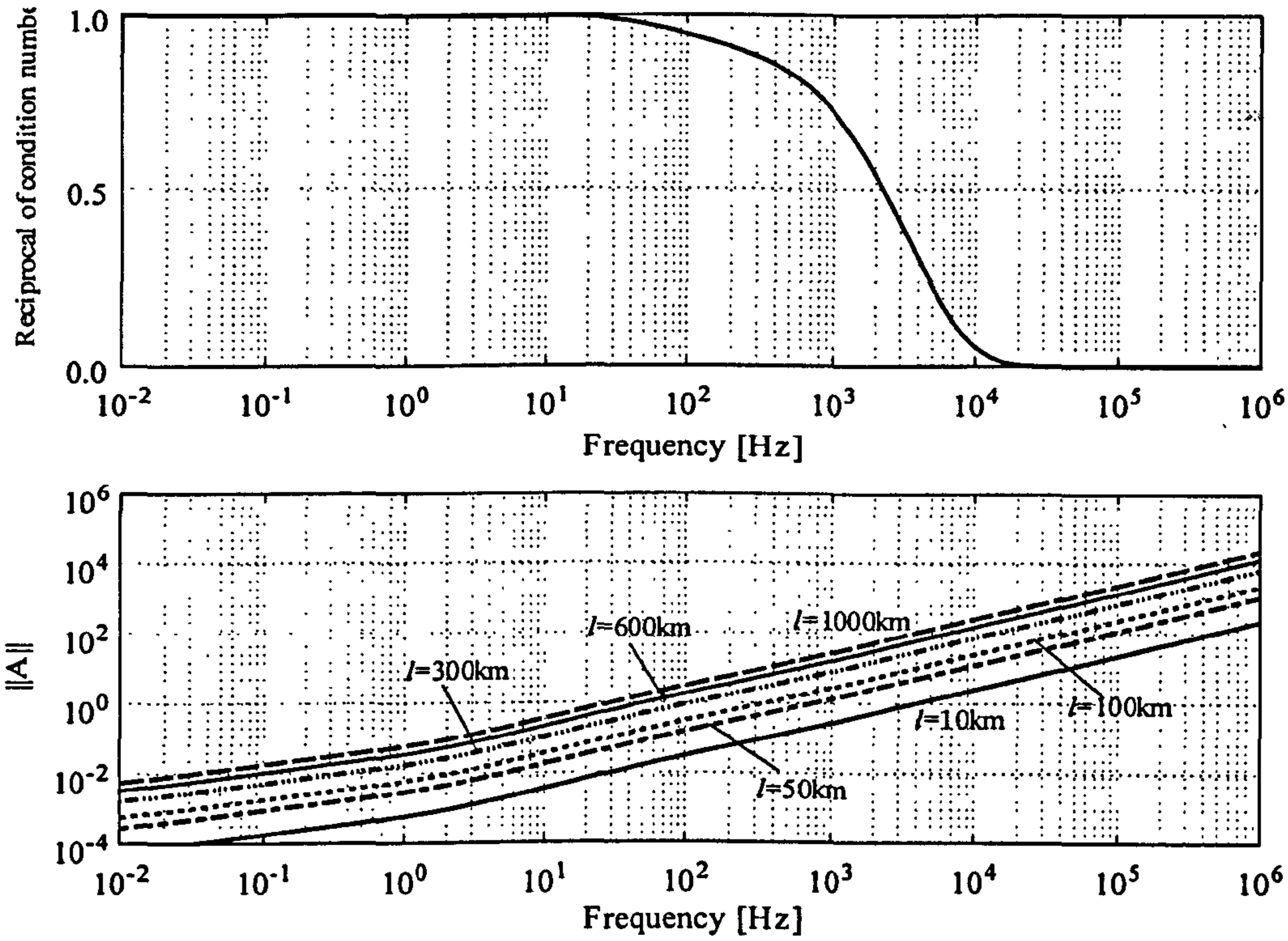

Figure 3.14. (Top) Condition number of $D_{pq}(\mathbf{A})$ over the frequency range of interest, (Bottom) 2-Norm of the argument matrix of $\mathbf{H}(\omega)$ for different line lengths

3.6.5 Scaling and Squaring

Fortunately, the numerical problems discussed above can be overcome by exploiting a fundamental property unique to the exponential function, namely,

$$e^{\mathbf{A}} = e^{\left(\frac{\mathbf{A}}{m}\right)^m} \tag{3.55}$$

where $\mathbf{A}$ is defined as in (3.49), a method which is referred to as 'Scaling and Squaring' [32,41,62]. The general idea is to scale the argument matrix, $\mathbf{A}$, by dividing it by some power of two, denoted by m, so that the wave propagation matrix, $\exp(\mathbf{A}/m)$, can be reliably and efficiently computed [32,62]. This can be visualized as dividing the transmission line, of length l, into N identical segments of length $\Delta l = l/N$. The original wave propagation matrix is then obtained by repeated squaring. The value of m can be chosen by making it the smallest power of two for which the following inequality,

$$\frac{\mathbf{A}}{m} \leq 1 \tag{3.56}$$

holds [32,62]. With this restriction, Padé approximation provides a very accurate means of evaluating $\mathbf{H}(\omega)$ over the entire frequency range of interest for electromagnetic transient analysis.

As discussed in the previous section, since the norm of the arugment matrix (3.49) increases with frequency, it follows that the value of m required for inequalty (3.56) to hold will similarly increase. The amount of scaling required will be further dependent

on the length of the transmission line under consideration, since the magnitude of the elements of the argument matrix, **A**, are proportional to the length of the line.

In order to give an indication as to the number of squaring operations typically required to evaluate $\mathbf{H}(\omega)$, the wave propagation function for the single-circuit transmission line described in section 3.5.1 is evaluated for line lengths of l=10km, 50km, 100km, 300km, 600km and 1000km in the frequency interval 10^{-2}Hz-10^{6}Hz. The choice of a 1000km line, though unrealistic, is useful for the purposes of analysing the characteristics of the algorithm. The results are shown in Figure 3.15.

The algorithm is clearly at its most efficient when no squaring operations are required. For the shortest line length considered (l=10km) this is the case up to frequencies of approximately 1.1kHz. This 'no squaring' limit is reduced steadily as the length of the line increases, with the limit for the longest line length (l=1000km) at approximately 11Hz. After these respective frequencies, the number of squaring operations increases so that the inequality of (3.56) is always satisfied. For the 10km line the maximum number of squaring operations required is eight, rising to 16 for the 1000km transmission line.

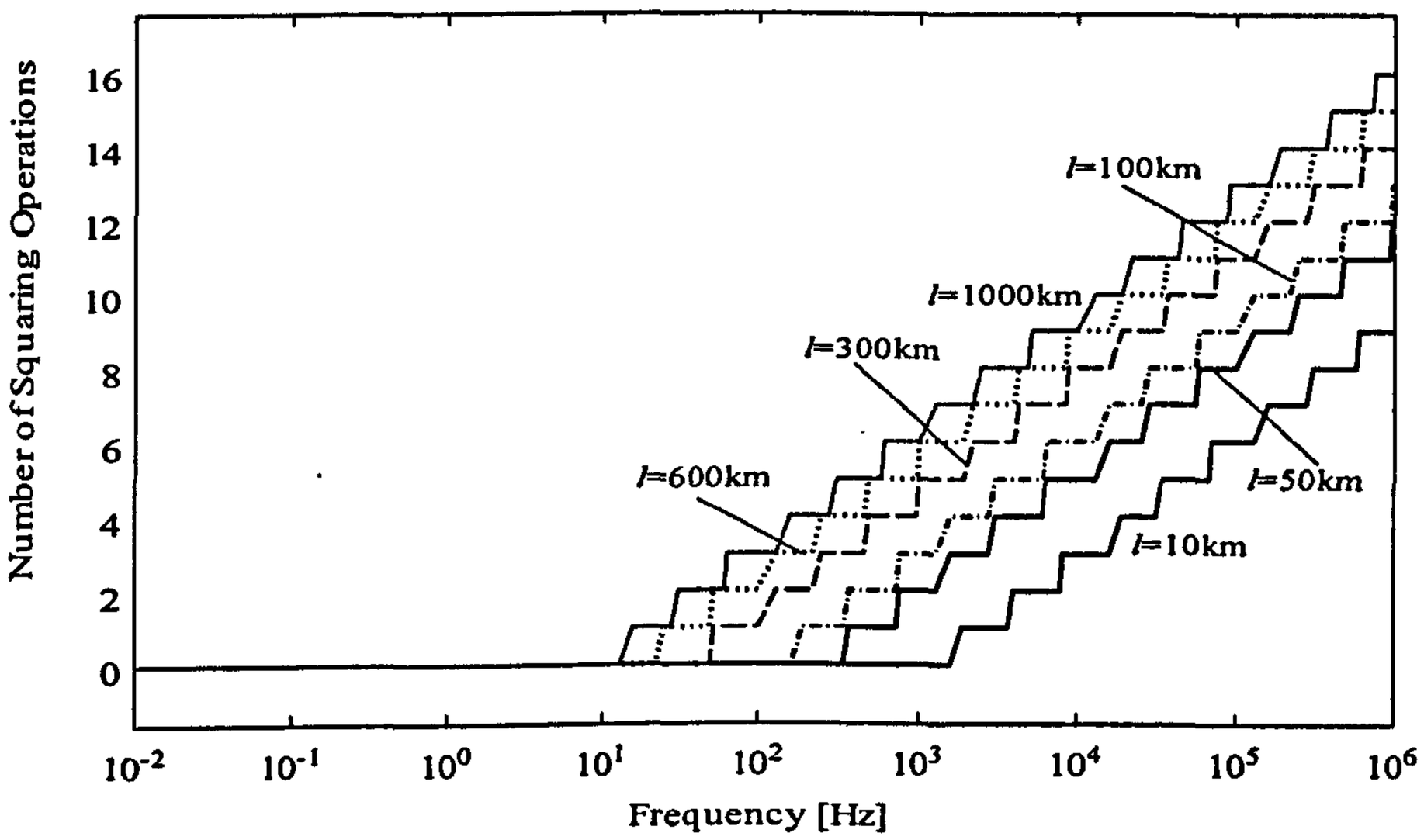

Figure 3.15. Number of squaring operations required for different line lengths as a function of frequency

Though the squaring results presented in Figure 3.15 are for a single-circuit line configuration, the results can be regarded as fairly well representative for most transmission line configurations. For the double-circuit transmission line configuration of section 3.5.2, the number of squaring operations required follows a similar trend to that of Figure 3.15.

3.6.6 Order of the (p, q) Padé Approximant

There are several reasons why the diagonal Padé approximants (p=q) should be used in (3.48) rather than the off-diagonal approximants ($p \neq q$). In terms of stability, if all the eigenvalues of the argument matrix are in the left hand side of the complex plane, then the computed approximants with $p>q$ tend to have larger rounding errors due to cancellation of the terms in the summation of the series (3.50) and (3.51). For approximants with $p<q$, the problem of a badly-conditioned denominator matrix, $D_{pq}(\mathbf{A})$, is increased further [32,62].

From the discussion of section 3.4.2, it is known that the eigenvalues of the wave propagation constant (3.6) have both positive real and imaginary parts. Therefore, the argument matrix (3.49) of the wave propagation matrix, $\mathbf{H}(\omega)$, can be expected to have eigenvalues lying in the left hand side of the complex plane. Thus, in this case, and from the discussion above it is recommended to use a diagonal Padé approximant for evaluating $\mathbf{H}(\omega)$.

In terms of efficiency, it is further recommended to use the diagonal Padé approximants, since they yield a higher order approximation than the off-diagonal approximants, for the same amount of computation time [32,62]. For example, suppose $p < q$, about qn^3 flops are required to evaluate $R_{pq}(\mathbf{A})$, an approximation of order $p+q$. However, the same amount of work is needed to compute $R_{pp}(\mathbf{A})$ and this approximation has order $2p > p+q$ [32,62]. A similar argument can be applied to the superdiagonal approximants ($p > q$).

Assuming a diagonal Padé approximant ($p=q$), then (3.48) can be re-defined as follows,

$$R_{pp}(\mathbf{A}) = \frac{N_{pp}(\mathbf{A})}{N_{pp}(-\mathbf{A})} \tag{3.57}$$

where,

$$N_{pp}(\mathbf{A}) = \sum_{k=0}^{p} c_k \mathbf{A}^k \tag{3.58}$$

and

$$c_k = c_{k-1} \frac{p+1-k}{(2p+1-k)k} \tag{3.59}$$

and $c_0=1$. The algorithm can be quickened further by applying Horner's Rule to evaluate the numerator and denominator in (3.57) [62].

3.6.6.1 Horner's Rule

Horner's Rule is a method for polynomial calculation which reduces the number of necessary multiplications. The rule factors out powers of x, giving [62],

$$a_n x^n + a_{n-1} x^{n-1} + \cdots + a_0 = ((a_n x + a_{n-1})x + \ldots)x + a_0 \tag{3.60}$$

3.6.6.2 Error Analysis

The accuracy of (3.57) over the full frequency region of interest for a given order p can be investigated by calculating the following relative error,

$$\mathbf{E} = \frac{\left\| R_{pp}^{h}(\mathbf{A}) - R_{pp}(\mathbf{A}) \right\|}{\left\| R_{pp}^{h}(\mathbf{A}) \right\|} \tag{3.61}$$

where $R_{pp}^{h}(\mathbf{A})$ is a high order approximation to $\mathbf{H}(\omega)$ and $R_{pp}(\mathbf{A})$ is as defined in (3.57). The order of (3.57) is varied from $p=1$ to $p=9$ and $\mathbf{H}(\omega)$ is evaluated for both the single and double-circuit transmission line configurations as described in sections 3.5.1 and 3.5.2, respectively. The results can be seen in Figure 3.16.

It can be seen from Figure 3.16, that for both transmission line cases, for $p>4$, (3.57) provides a very accurate method for evaluating the wave propagation matrix, $\mathbf{H}(\omega)$ over

the whole frequency interval. For the shorter (l=152.9km) double-circuit line, values of p=3 and p=4 still provide very accurate results up to a frequency of almost 100kHz.

For all the cases presented in this research, a value of p=6 has been used in (3.57) and provides a very accurate and efficient order for the Padé approximation method for evaluating **H**(ω).

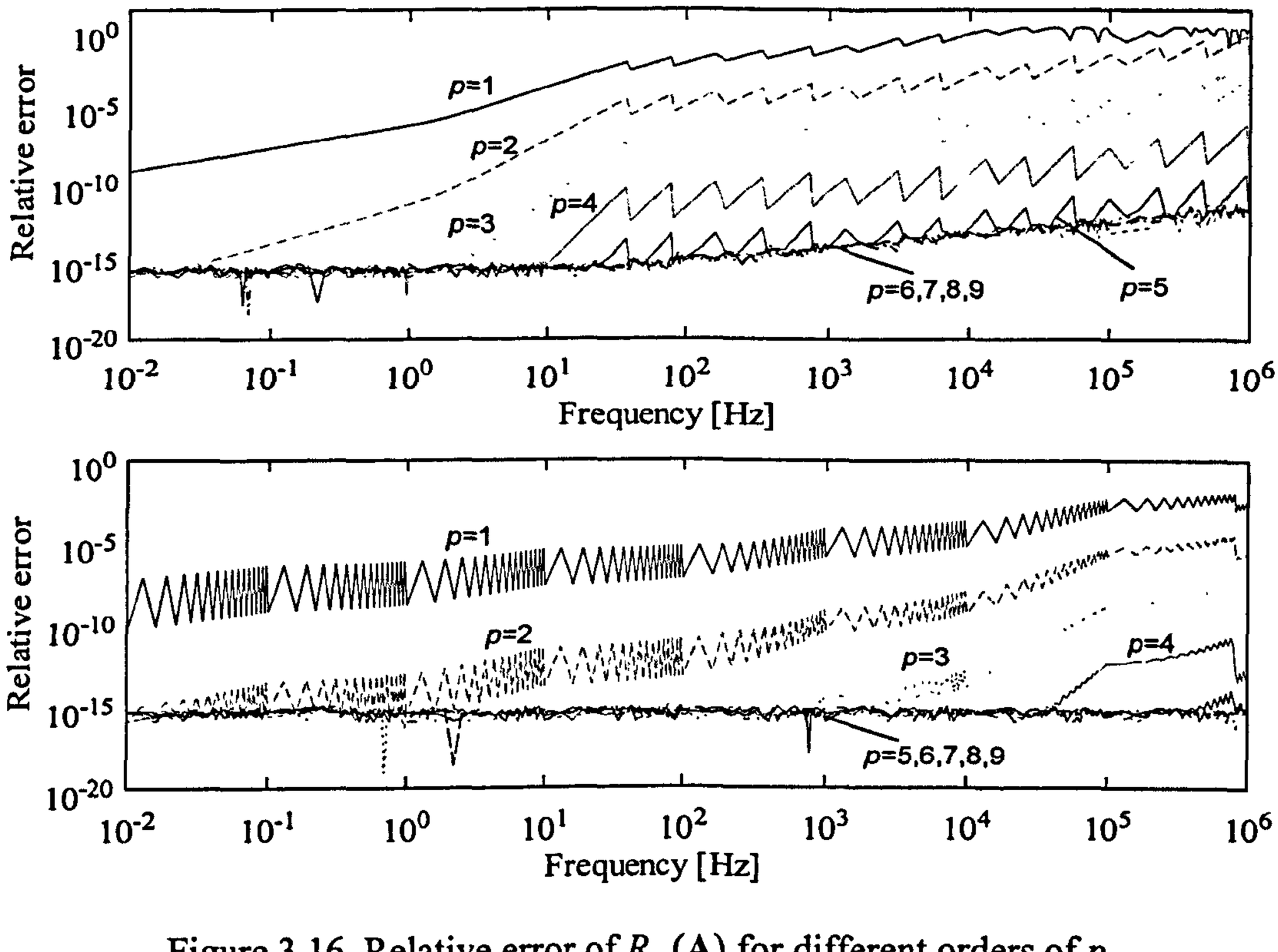

Figure 3.16. Relative error of R_{pp}(**A**) for different orders of p.

A principal drawback of the algorithm may come from the fact that if $s >> 1$ then, computed squares can be contaminated by rounding errors and the cost becomes large. However, in all the cases considered, s has never exceeded 16, and high values of s are restricted only to the high frequency range, so that the overall algorithm remains efficient and the result obtained accurate.

3.7 Test Examples

The accuracy, efficiency and robustness of the Padé scheme (3.57) for evaluating the wave propagation matrix, **H**(ω), directly in phase co-ordinates, can be illustrated by returning to the single, double and asymmetrical line of sections (3.5.1), (3.5.2) and (3.5.3).

For all the results presented, the order of the Padé approximant is taken to be p=6. The frequency range under consideration is again assumed to be 10^{-2}Hz-10^{6}Hz, with 241 frequency points and 30 frequency points per decade.

3.7.1 Single-Circuit Transmission Line Configuration

Consider the 345kV, single-circuit untransposed overhead transmission line system, as shown in Figure 3.4. The physical data for the system can be found in Appendix III. Figures 3.17 and 3.18 show the real and imaginary parts of the elements of **H**(ω), as calculated by (3.57). Figures 3.19 and 3.20 show the corresponding magnitude and phase angles.

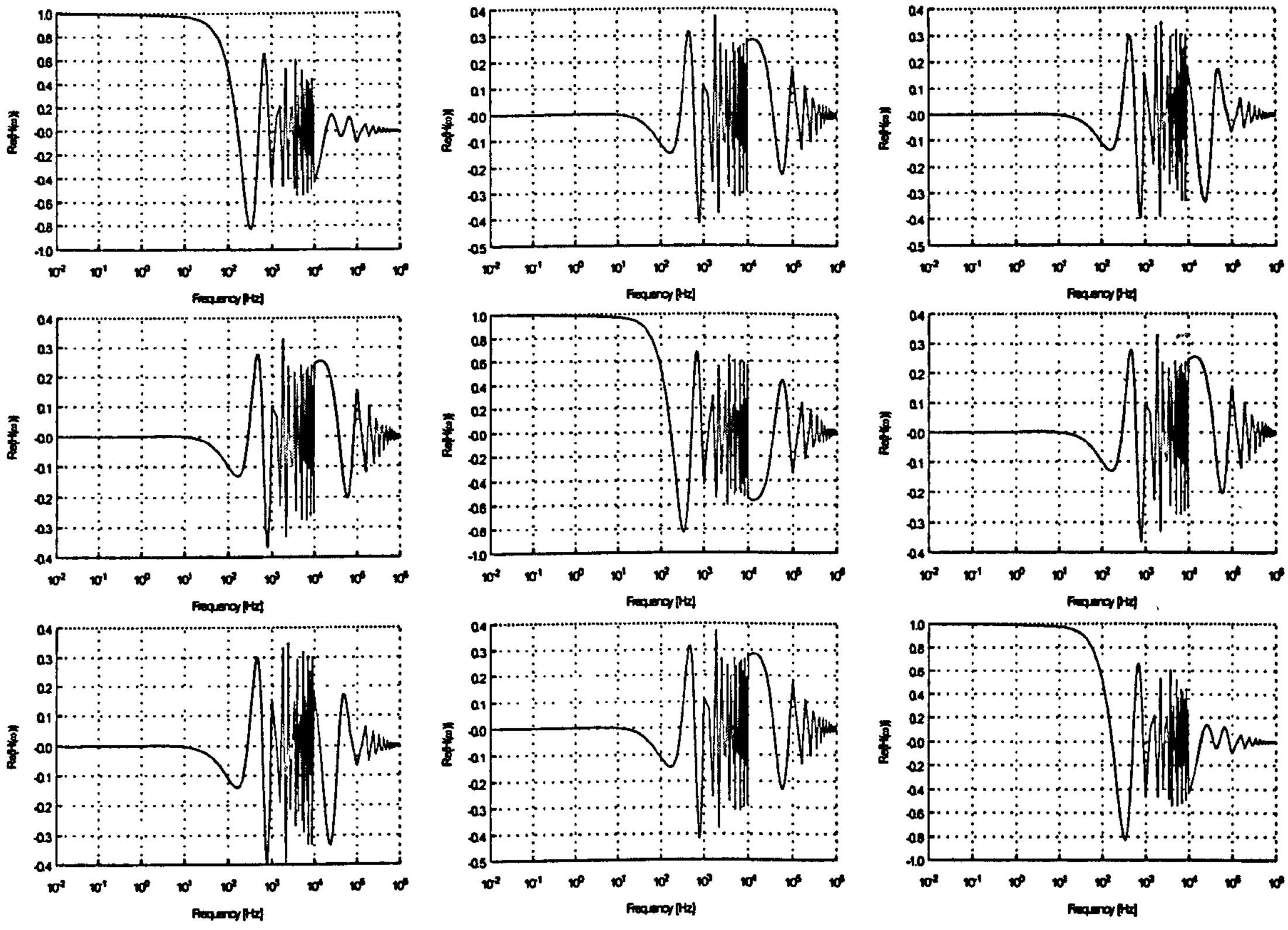

Figure 3.17. Real part of the elements of **H**(ω) for a single-circuit transmission line

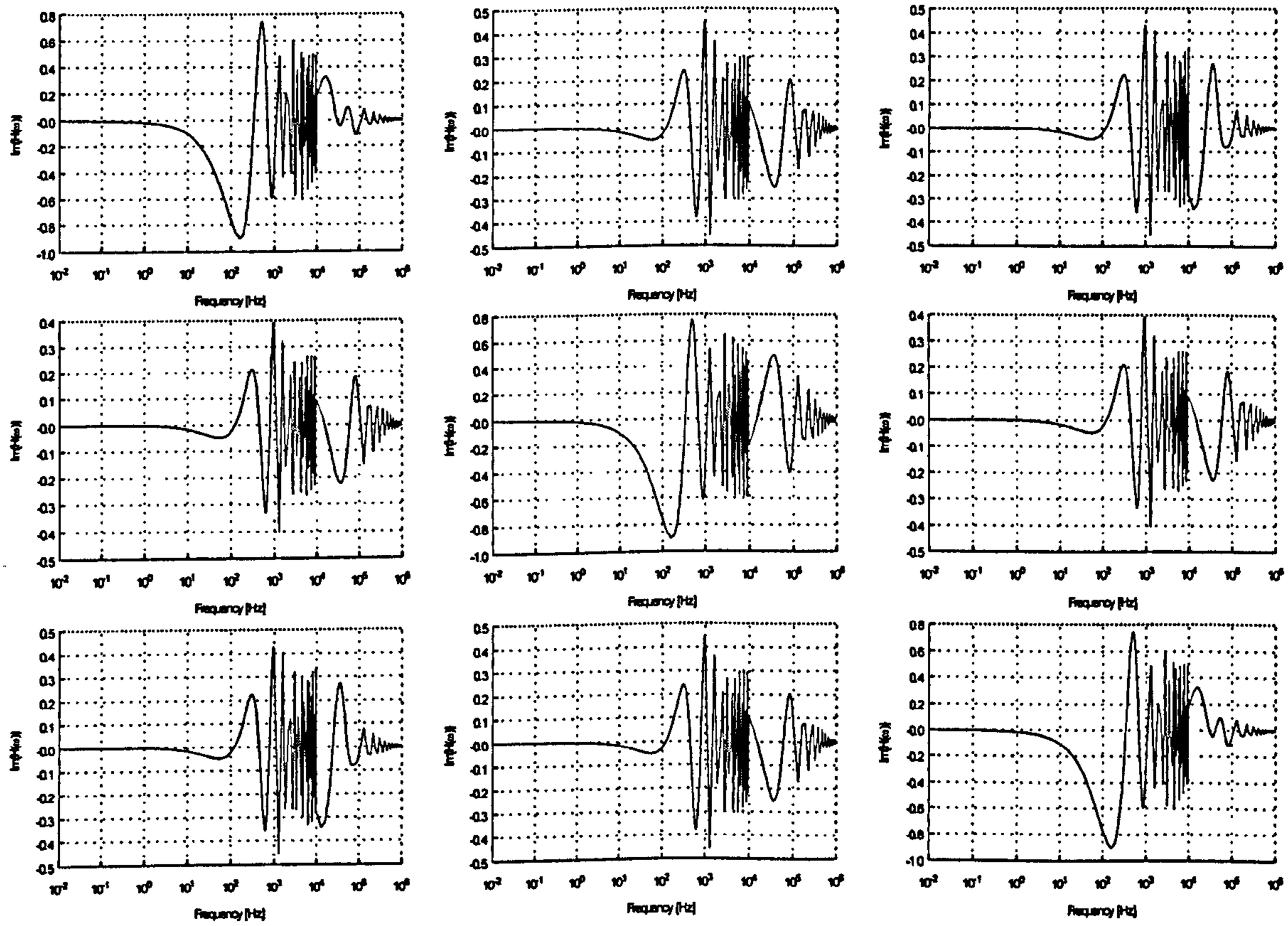

Figure 3.18. Imaginary part of the elements of **H**(ω) for a single circuit-transmission line

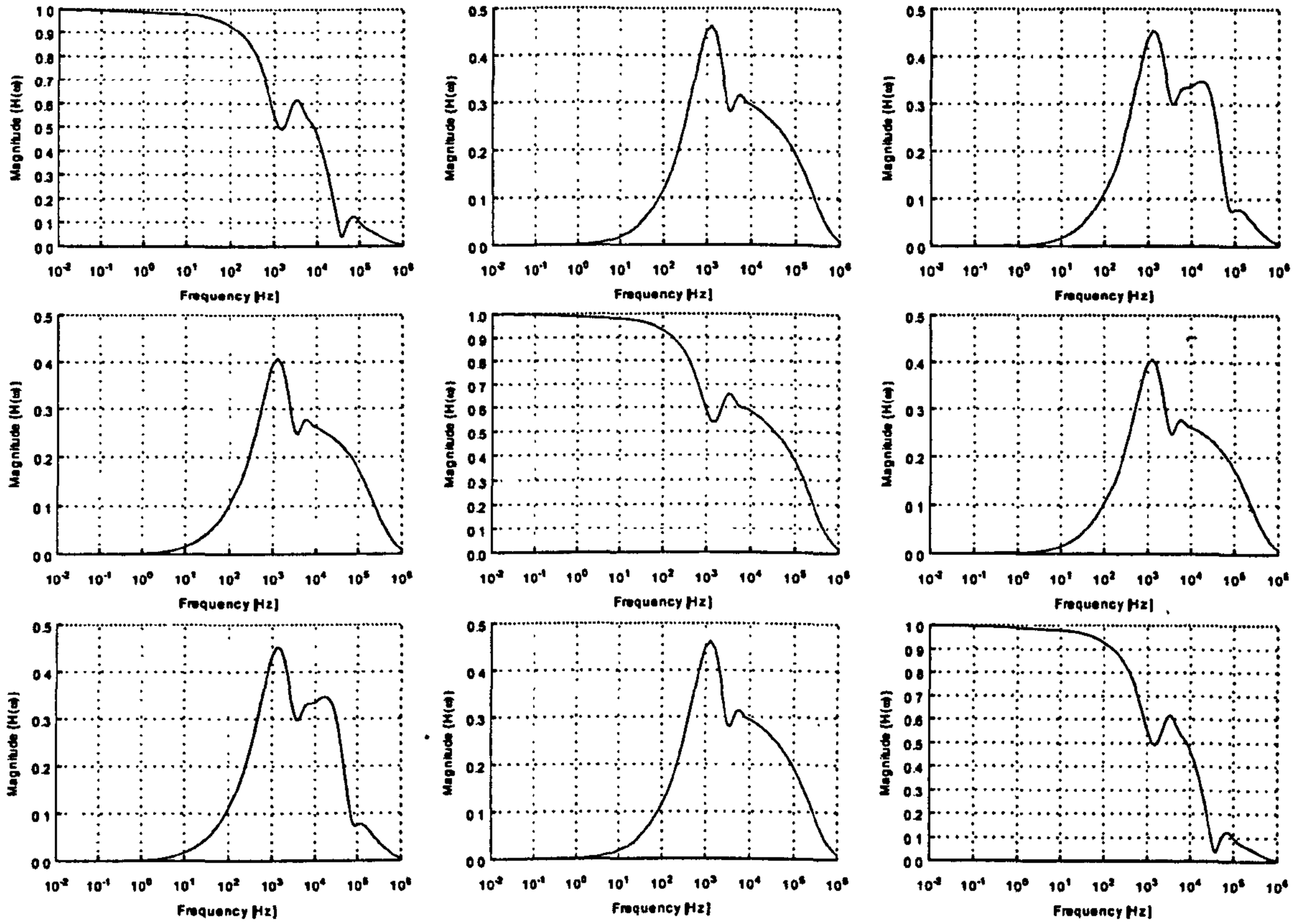

Figure 3.19 Magnitude of the elements of **H**(ω) for a single-circuit transmission line

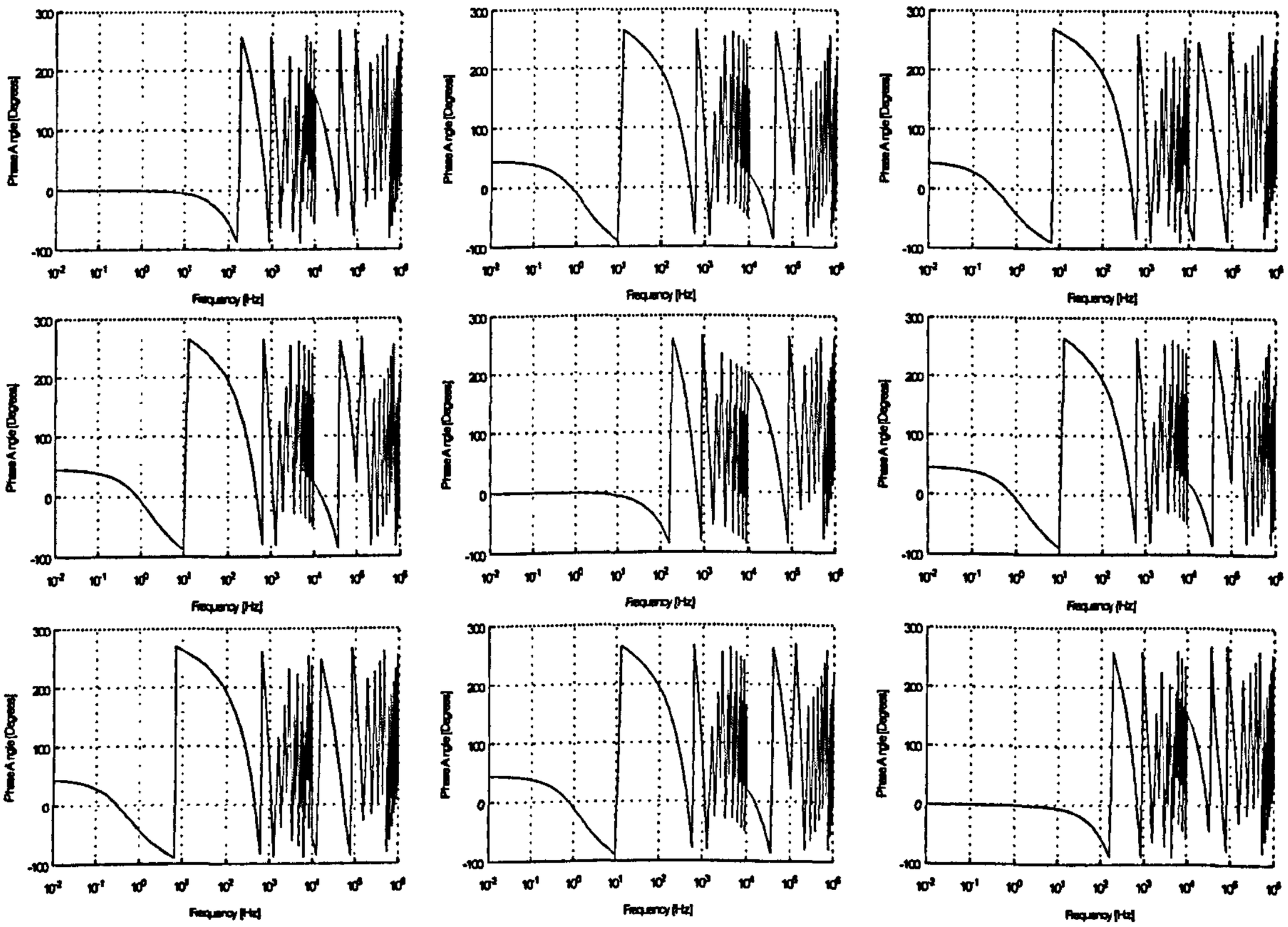

Figure 3.20. Phase angle of the elements of **H**(ω) for a single-circuit transmission line

Expanding the wave propagation matrix using the matrix exponential power series (3.47) for the argument matrix defined in (3.49) gives [11],

$$\mathbf{H}(\omega) = e^{-\sqrt{\mathbf{Y}(\omega)\mathbf{Z}(\omega)}l} = \mathbf{U} - \left[j\omega\mathbf{CR} - \omega^2\mathbf{CL}\right]^{1/2} l + \left[j\omega\mathbf{CR} - \omega^2\mathbf{CL}\right]\frac{l^2}{2!} - \left[j\omega\mathbf{CR} - \omega^2\mathbf{CL}\right]^{3/2}\frac{l^3}{3!} + \cdots \tag{3.62}$$

where **U** is defined as the identity matrix and $\mathbf{Z}(\omega)$ and $\mathbf{Y}(\omega)$ are defined as in (2.3) and (2.4) respectively, assuming the conductance $\mathbf{G}(\omega)$ is negligible. From (3.62) it can be seen that as the frequency tends to zero, $\mathbf{H}(\omega)$ becomes real and tends toward the identity matrix with the real off-diagonal and imaginary elements becoming zero. This is clearly evident from Figures 3.17 and 3.18. As the frequency increases, the travelling waves are subjected to increasing attenuation due to the skin effect in the conductors and earth, such that all the elements of $\mathbf{H}(\omega)$ tend to zero. Again this can be clearly seen in Figures 3.17 and 3.18.

Also evident from Figures 3.17 and 3.18 is the oscillatory component of the wave propagation matrix in the high frequency region, due to the time delays of the line. As discussed in the introduction, $\mathbf{H}(\omega)$, can be thought of as being composed of a sum of modal components that, in general, have different time delays. It is proposed in the next chapter to apply a matrix phase shift function to smooth the elements of $\mathbf{H}(\omega)$, in the frequency range of interest. A rational function approximation for $\mathbf{H}(\omega)$ can then be obtained without using an excessively large number of poles.

3.7.2 Double-Circuit Transmission Line Configuration

A further test of the accuracy and efficiency of the algorithm can be performed using the 220kV untransposed, double-circuit transmission line system as described in section (3.5.2) and illustrated in Figure 3.9. The physical data for the system can be found in Appendix III.

By way of example, Figure 3.21 shows the real and imaginary parts of element (1,1) of $\mathbf{H}(\omega)$, as calculated by (3.57). Figure 3.22 shows the magnitude of the elements of the first column of $\mathbf{H}(\omega)$ and, for ease of viewing, only the phase angle of element (1,1). As expected, the behaviour of the wave propagation function follows a similar pattern to that described above for the single-circuit transmission line.

The remaining elements of the $\mathbf{H}(\omega)$ (36 elements in total) show a similar degree of accuracy to that of element (1,1), although for practicality reasons they are not shown. The behaviour of the these elements follows a pattern as expected from the theoretical discussion of above.

3.7.3 Asymmetrical Transmission Line Configuration

Consider again the 230kV, 6-circuit (18 conductor) transmission line system as described in section (3.5.3) [12]. The physical data for the system can be found in Appendix III.

As for the algorithm for computing the characteristic admittance, it has been found that the accuracy and efficiency of (3.57) for evaluating this test case is maintained at a high level, despite the increased size of the system under investigation. In this case, the maximum number of squaring operations required was found to be 13. The 'no squaring' limit is attained at approximately 130Hz.

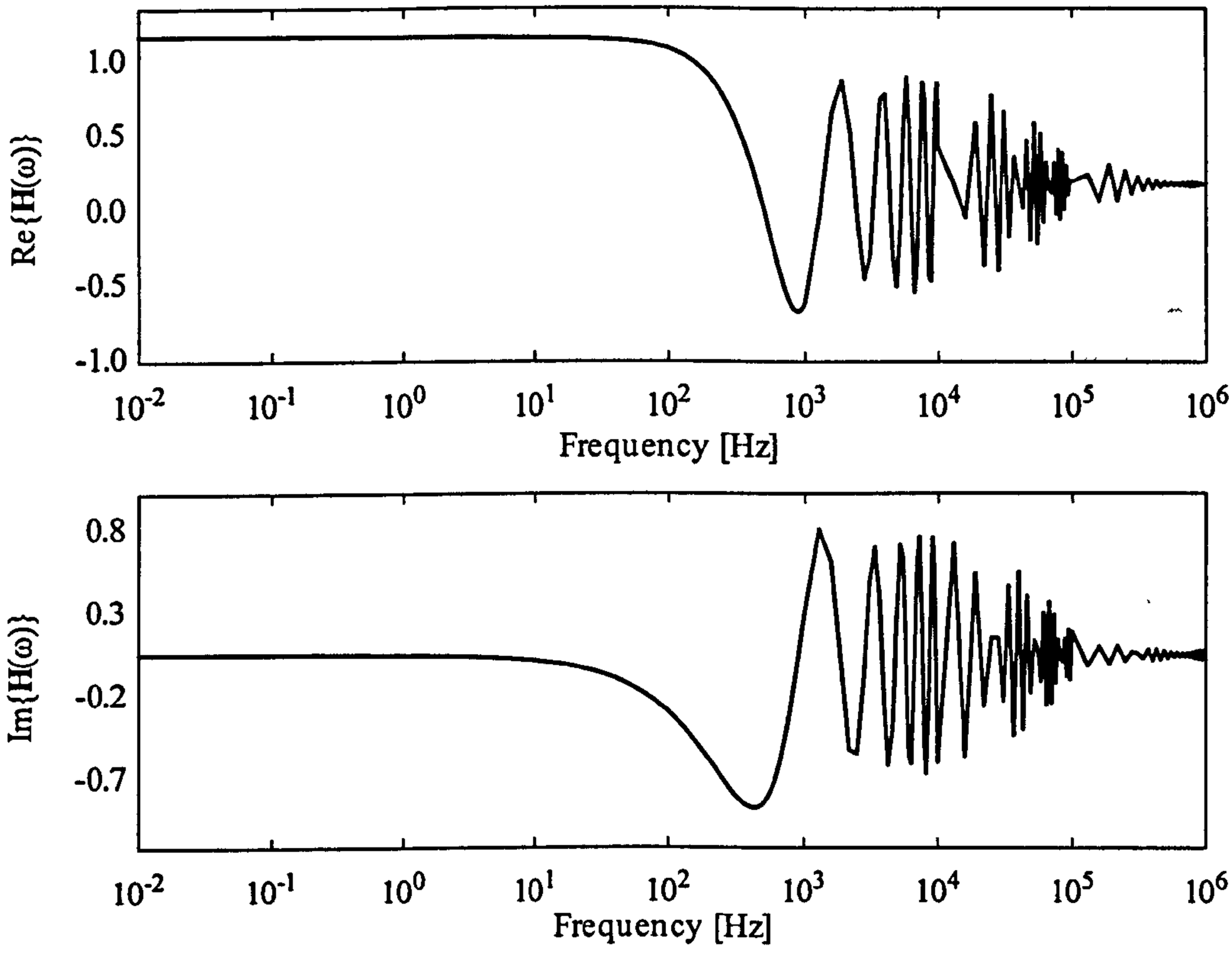

Figure 3.21. Real part (top) and Imaginary part (bottom) of element (1,1) of **H**(ω) for a double-circuit transmission line

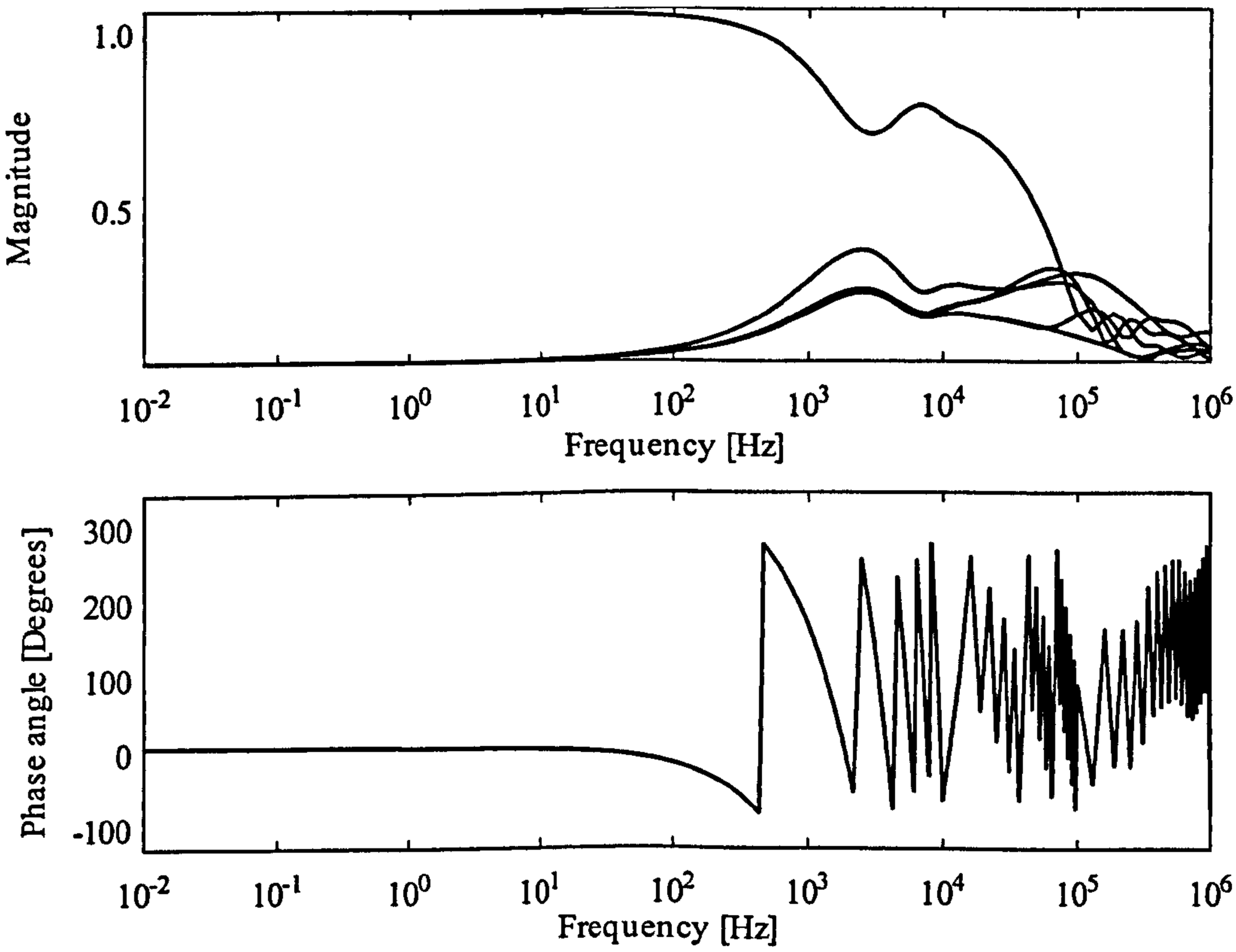

Figure 3.22. Magnitude (top) and Phase angle (bottom) of element (1,1) of **H**(ω) for a double-circuit transmission line

3.8 Conclusions

The frequency domain implementation of a new phase domain transmission line model suitable for electromagnetic transient studies has been presented in this chapter. Algorithms are introduced for calculating the characteristic admittance matrix and wave propagation matrices. In contrast to current methods reported in open literature, the proposed algorithms do not require the evaluation of frequency-dependent modal transformation matrices in order to evaluate the functions in the modal domain before transforming the solution into the phase domain. Instead, the proposed algorithms perform all the calculations directly in phase co-ordinates. Both algorithms have the added advantage of having a very simplistic form, making them very easy to implement in a computer program.

The algorithm for calculating the characteristic admittance matrix is derived by exploiting a relationship between the matrix sign function and the matrix square root. The efficiency of the algorithm, particularly in the lower frequency range, can be further enhanced by introducing scaling techniques.

The algorithm proposed for evaluating the wave propagation matrix is based on a Padé approximation to the matrix exponential function. A 'scaling and squaring' technique is employed by exploiting a fundamental property of the exponential function. The efficiency of the algorithm is investigated for lines of different length and an error analysis is presented to enable the optimum order of approximation to be chosen for a given transmission line configuration.

Although extensive use has been made of matrix decomposition techniques to analyse the properties and behaviour of the algorithms presented, it should be stressed that calculation of eigenvalues and eigenvectors is not required in either algorithm.

Test cases corresponding to single, double and a highly asymmetrical transmission line configuration have been used to test the robustness of the proposed algorithms. The accuracy of both algorithms compare well with conventional modal decomposition techniques. The test cases also serve to confirm the generality of the methods.

The efficiency of the proposed algorithms have not been tested against the alternative methods, i.e. performing a modal decomposition at each frequency point. However, due to the very simplistic form of the algorithms, it is expected that they would be comparable to existing methods in terms of computational efficiency.

3.9 References

[1] Gustavsen, B. and Semlyen, A.: 'Combined Phase and Modal Calculation of Transmission Line Transients Based on Vector Fitting', IEEE Transactions on Power Delivery, Vol. 13, No. 2, April 1998, pp. 596-604.

[2] Gustavsen, B., Sletbak, J., and Henriksen, T.: 'Calculation of Electromagnetic Transients in Transmission Line Cables and Lines Taking Frequency Dependent Effects Accurately Into Account', IEEE Transactions on Power Delivery, Vol. 10, No. 2, April 1995, pp. 1076-1084.

[3] Nguyen, H. V., Dommel, H. W. and Marti, J. R.: 'Direct Phase Domain Modelling of Frequency-Dependent Overhead Transmission Lines', IEEE Transactions on Power Delivery, Vol. 12, No. 3, July 1997, pp. 1335-1342.

[4] H. Nguyen: 'Simulation of Lightning Surges on Transmission Lines', PhD Thesis, The University of British Columbia, Canada, February 1996.

[5] Marcano, F. J.: 'Modelling of Transmission Lines Using Idempotent Decomposition', M.Sc Thesis, August 1996, The University of British Columbia.

[6] Castellanos, F. and Marti, J. R.: 'Phase-Domain Multiphase Transmission Line Models', International Conference on Power System Transients, Lisbon, 3-7 September 1995.

[7] Cstellanos, F., Marti, J. R. and Marcano, F.: 'Phase-Domain Multiphase Transmission Line Models', Electrical Power & Energy Systems, Vol. 19, No. 4, 1997, pp. 241-248.

[8] Noda, T., Nagaoka, N. and Ametani, A.: 'Phase Domain Modeling of Frequency-Dependent Transmission Lines by Means of an ARMA Model', IEEE Transactions on Power Delivery, Vol. 11, No. 1, January 1996, pp. 401-411.

[9] Noda, T., Nagaoka, N. and Ametani, A.: 'Further Improvements to a Phase-Domain ARMA Line Model in Terms of Convolution, Steady-State Initialization, and Stability', IEEE Transactions on Power Delivery, Vol. 12, No. 3, July 1997, pp. 1327-1334.

[10] Angelidis, G. and Semlyen, A.: 'Direct Phase-Domain Calculation of Transmission Line Transients Using Two-Sided Recursions', IEEE Transactions on Power Delivery, Vol. 10, No. 2, April 1995, pp. 941-949.

[11] Gustavsen, B: 'A Study of Overvoltages in High Voltage Cables With Emphasis on Sheath Overvoltages', Dr. Ing. Thesis, The Norwegian Institute of Technology, Trondheim, Norway, 1993.

[12] Morched, A., Gustavsen, B. and Tartibi, M.: 'A Universal Model for Accurate Calculation of Electromagnetic Transients on Overhead Lines and Underground Cables', IEEE Transactions on Power Delivery, Vol. 14, No. 3, July 1999, pp. 1032-1038.

[13] Gustavsen, B. and Semlyen, A.: 'Simulation of Transmission Line Transients Using Vector Fitting and Modal Decomposition', IEEE Transactions on Power Delivery, Vol. 13, No. 2, pp. 605-614.

[14] Budner, A.: 'Introduction of Frequency-Dependent Line Parameters into an Electromagnetic Transients Program', IEEE Transactions on Power Apparatus and Systems, Vol. PAS-89, No. 1, January 1970, pp. 88-97.

[15] Snelson, J. K.: 'Propagation of Travelling Waves on Transmission Lines – Frequency Dependent Parameters', IEEE Transactions on Power Apparatus and Systems, Vol. PAS-91, January/February 1972, pp. 85-91.

[16] Meyer, W. S. and Dommel, H. W.: 'Numerical Modelling of Frequency-Dependent Transmission-Line Parameters in an Electromagnetic Transients Program', IEEE Transactions on Power Apparatus and Systems, Vol. PAS-93, September/October 1974, pp. 1401-1409.

[17] Marti, J.: 'Accurate Modelling of Frequency-Dependent Transmission Lines in Electromagnetic Transient Simulations', IEEE Transactions on Power Apparatus and Systems, Vol. PAS-101, No. 1, January 1982, pp. 147-157.

[18] Marti, J.: 'The Problem of Frequency Dependence in Transmission Line Modelling', PhD Thesis, The University of British Columbia, Canada, April 1981.

[19] Semlyen, A. and Dabuleanu, A.: 'Fast and Accurate Switching Transient Calculations on Transmission Lines with Ground Return Using Recursive

Convolutions', IEEE Transactions on Power Apparatus and Systems, Vol. PAS-94, No. 2, March/April 1975, pp. 561-571.

[20] Ametani, A.: 'A Highly Efficient Method for Calculating Transmission Line Transients', IEEE Transactions on Power Apparatus and Systems, Vol. PAS-95, No. 5, September/October 1976, pp. 1545-1551.

[21] Marti, L.: 'Simulation of Transients in Underground Cables with Frequency-Dependent Modal Transformation Matrices', IEEE Transactions on Power Delivery, Vol. 3, No. 3, July 1988, pp. 1099-1110.

[22] Marti, L.: 'Simulation of Electromagnetic Transients in Underground Cables with Frequency-Dependent Modal Transformation Matrices', PhD Thesis, The University of British Columbia, Canada, November 1986.

[23] Naidu, S. R. and de Lima, F. N.: 'A Frequency-Dependent Transmission Line Model for Electromagnetic Transient Studies', IEE Proceedings, Vol. 132, Pt. C, No. 6, November 1985, pp. 294-297.

[24] Wedepohl, L. M.: 'Application of Matrix Methods to the Solution of Travelling-Wave Phenomena in Polyphase Systems', Proceedings of the IEE, Vol. 100, No. 12, 1963, pp. 2200-2212.

[25] Hedman, D. E.: 'Propagation on Overhead Transmission Lines I-Theory of Modal Analysis', IEEE Transactions on Power Apparatus and Systems, Vol. PAS-84, March 1965, pp. 200-205.

[26] Carson, J. R.: 'Wave Propagation in Overhead Wires with Ground Return', Bell System Technical Journal, Vol. 5, 1926, pp. 539-554.

[27] Deri, A., Tevan, G., Semlyen A. and Castanheria, A.: 'The Complex Ground Return Plane, a Simplified Model for Homogeneous and Multi-Layer Earth Return', IEEE Transactions on Power Apparatus and Systems, Vol. 100, 1981, pp. 3686-3693.

[28] Lewis, V. A. and Tuttle, P. D.: 'The Resistance and Reactance of Aluminium Conductors Steel Reinforced', Trans. AIEE PAS, Vol. 77, 1958, pp. 1189-1215.

[29] Semlyen A. and Deri, A.: 'Time Domain Modelling of Frequency Dependent Three Phase Transmission Line Inductance', IEEE Transactions on Power Apparatus and Systems, Vol. 104, 1985, pp. 1549-1555.

[30] Brandão, J. A. and Borges da Silva, J. F.: 'Wave Propagation in Polyphase Transmission Lines a General Solution to Include Cases Where Ordinary Modal Theory Fails', IEEE Transactions on Power Delivery, Vol. PWRD-1, No. 2, April 1986, pp. 182-189.

[31] Brandão, J. A.: 'Overhead Three-Phase Transmission Lines – Non-Diagonalizable Situations', IEEE Transactions on Power Delivery, Vol. 3, No. 4, October 1988, pp. 1348-1355.

[32] Moler, C. and Van Loan, C.: 'Nineteen Dubious Ways to Compute the Matrix Exponential', SIAM Review, Vol. 20, No. 4, October 1978, pp. 801-836.

[33] Hon-Wing, C. and Yau, S. T.: 'More Explicit Formulas for the Matrix Exponential', Linear Algebra and its Applications, Vol. 262, 1997, pp. 131-163.

[34] Wragg, A. and Davies, C.: 'Computation of the Exponential of a Matrix I: Theoretical Considerations', J. Inst. Maths Applics, Vol. 11, 1973, pp. 369-375.

[35] Wragg, A. and Davies, C.: 'Computation of the Exponential of a Matrix I: Practical Considerations', J. Inst. Maths Applics, Vol. 15, 1975, pp. 273-278.

[36] Gallopoulos, E. and Saad, Y.: 'On the Parallel Solution of Parabolic Equations', Proceedings of ACM/SIGARCH International Conference on Supercomputing, Crete, Greece, 1989, pp. 17-28.

[37] Underhill, C. and Wragg, A.: 'Convergence Properties of Padé Approximants to exp(*z*) and Their Derivatives', J. Inst. Maths Applics, Vol. 11, 1973, pp. 361-367.

[38] Leonard, I. E.: 'The Matrix Exponential', SIAM Review, Vol. 38, No. 3, September 1996, pp. 507-512.

[39] Healey, M.: 'Study Methods of Computing Trasition Matrices', Proceedings of the IEE, Vol. 120, No. 8, August 1973, pp. 905-912.

[40] Kenney, C. and Laub, A. J.: ' Padé Error Estimates for the Logarithm of a Matrix', International Journal of Control, Vol. 50, No. 3, 1989, pp. 707-730.

[41] Ward, R. C.: 'Numerical Computation of the Matrix Exponential with Accuracy Estimate', SIAM Journal on Numerical Analysis, Vol. 14, No. 4, September 1977, pp. 600-610.

[42] Higham, N. J.: 'Computing Real Square Roots of a Real Matrix', Linear Algebra and its Applications, Vol. 88/89, 1987, pp. 405-430.

[43] Higham, N. J.: 'Newton's Method for the Matrix Square Root', Mathematics and Computation, Vol. 46, No. 174, April 1986, pp. 537-549.

[44] Higham, N. J.: 'The Matrix Sign Decomposition and its Relation to the Polar Decomposition', Linear Algebra and its Applications, Vol. 212/213, 1994, pp. 3-20.

[45] Higham N. J.: 'Stable Iterations for the Matrix Square Root', Numerical Algorithms, Vol. 15, No. 2, 1997, pp. 227-242.

[46] Cross, G. W. and Lancaster, P.: 'Square Roots of Complex Matrices', Linear and Multilinear Algebra, Vol. 1, 1974, pp. 289-293.

[47] Shieh, L. S., Lian, S. R. and McInnis, B. C.: 'Fast and Stable Algorithms for Computing the Principal Square Root of a Complex Matrix', IEEE Transactions on Automatic Control, Vol. AC-32, No. 9, September 1987, pp. 820-822.

[48] Pandey, P., Kenney, C. and Laub, A. J.: 'A Parallel Algorithm for the Matrix Sign Function', International Journal of High Speed Computing, Vol. 2, No. 2, 1990, pp. 181-191.

[49] Björck, Å. and Hammarling, S.: 'A Schur Method for the Square Root of a Matrix', Linear Algebra and its Applications, Vol. 52/53, 1983, pp. 127-140.

[50] Shieh, L. S., Tsay, Y. T. and Yates, R. E.: 'Computation of the Principal *n*th Roots of Complex Matrices', IEEE Transactions on Automatic Control, Vol. AC-30, No. 6, June 1985, pp. 606-608.

[51] Hoskins, D. and Walton, D. J.: 'A Faster, More Stable Method for Computing the *p*th Roots of Positive Definite Matrices', Linear Algebra and its Applications, Vol. 26, 1979, pp. 139-163.

[52] Denman, E. D.: 'Roots of Real Matrices', Linear Algebra and its Applications, Vol. 36, 1981, pp. 133-139.

[53] Alefeld, G. and Schneider, N.: 'On Square Roots of *M*-Matrices', Linear Algebra and its Applications, Vol. 42, 1982, pp. 119-132.

[54] Roberts, J. D.: 'Linear Model Reduction and Solution of the Algebraic Riccati Equation by Use of the Sign Function', International Journal of Control, Vol. 32, No. 4, 1980, pp. 677-687.

[55] Shieh, L. S., Tsay, Y. T. and Yates, R. E.: 'Some Properties of Matrix Sign Functions Derived from Continued Fractions', Proceedings of the IEE, Vol. 130, Part D, No. 3, May 1983, pp. 111-118.

[56] Shieh, L. S., Tsay, Y. T. and Wang, C. T.: 'Matrix Sector Functions and Their Applications to Systems Theory', Proceedings of the IEE, Vol. 131, Part D, No. 5, September 1984, pp. 171-181.

[57] Stickel, E. U.: 'Separating Eigenvalues Using the Matrix Sign Function', Linear Algebra and its Applications, Vol. 148, 1991, pp. 75-88.

[58] Denman, E. D. and Beavers Jr., A. N.: 'The Matrix Sign Function and Computations in Systems', Applied Mathematics and Computation, Vol. 2, 1976, pp. 63-94.

[59] Kenney, C. and Laub, A. J.: 'Rational Iterative Methods for the Matrix Sign Function', SIAM Journal on Matrix Analysis and Applications, Vol. 12, No. 2, April 1991, pp. 273-291.

[60] Kenney, C. and Laub, A. J.: 'A Hyperbolic Tangent Identity and the Geometry of Padé Sign Function Iterations', Numerical Algorithms, Vol. 7, 1994, pp. 111-128.

[61] Kenney, C. and Laub, A. J.: 'The Matrix Sign Function', IEEE Transactions on Automatic Control, Vol. 40, No. 8, August 1995, pp. 1330-1348.

[62] Golub, G. and Van Loan, C. F.: 'Matrix Computations', The John Hopkins University Press, Second Edition, 1989.

[63] Baker Jr., G. A.: 'Essentials of Padé Approximants', Academic Press, 1975.

[64] Baker Jr., G. A. and Gammel, J. L.: 'The Padé Approximant in Theoretical Physics', Academic Press, 1970.

[65] Gong, W.: 'Padé Approximation for Stochastic Discrete-Event Systems', IEEE Transactions on Automatic Control, Vol. 40, No. 8, August 1995, pp. 1349-1358.

[66] Byers, R.: 'Solving the Algebraic Riccati Equation with the Matrix Sign Function', Linear Algebra and its Applications, Vol. 85, 1987, pp. 267-279.

CHAPTER 4

PHASE DOMAIN TRANSMISSION LINE MODELLING - TIME DOMAIN FORMULATION

This chapter describes the time domain formulation of a new phase domain model to study electromagnetic transient phenomena on multiphase power transmission lines. One of the main difficulties in conducting the analysis directly in the phase domain concerns the unwinding of the wave propagation matrix. The elements of this matrix are associated with coupled time delays that, in general, differ in magnitude. At present, a common scalar time delay, corresponding to the fastest mode of the system, is used to unwind the wave propagation matrix in the phase domain. However, for multi-circuit and asymmetrical transmission lines, the modal travel times may be widely different and compensating for a common time delay will not completely remove the oscillations present in these functions. In order to overcome this, a matrix phase shift function is proposed to unwind the elements of the wave propagation matrix. The function is evaluated directly in the phase domain, intrinsically taking into account the time delays of the line. The elements of the wave propagation matrix are then obtained as relatively smooth functions of frequency, and as such can be approximated with comparatively low-order rational functions. The method of Vector Fitting is used to obtain the rational function approximations of the characteristic admittance and wave propagation matrix. A columnwise realization can be obtained using this method, which increases the computational efficiency for the time domain simulation. The final phase domain model can be represented in the time domain by a Norton equivalent circuit.

4.1 Introduction

Power transmission lines may be characterized in the phase domain by two matrix response functions, namely the characteristic admittance matrix, $Y_c(\omega)$, and the wave propagation matrix, $H(\omega)$ [11,12]. The frequency-dependent behaviour of both functions can be taken into account in a time domain simulation by introducing numerical convolutions between the electrical quantities at the ends of the line and the transmission line responses [1]. A recursive formulation of the convolution integrals can be obtained in phase co-ordinates if both the characteristic admittance and the wave propagation matrices are approximated using either rational functions in the frequency domain [1,3,4,12,14-18], *z*-domain [7-9] or piecewise linear functions in the time domain [10,19]. With the frequency responses approximated in this way, a recursive formulation of the convolution integrals can be realized, greatly increasing the computational efficiency of the resulting time domain model [19,20].

The elements of the characteristic admittance matrix are in general smooth functions of frequency and can therefore be accurately fitted with low-order rational functions directly in phase co-ordinates. However, for multi-conductor systems, the elements of the wave propagation matrix are obtained as oscillating functions of frequency, due to

the time delays of the line. For convenience, the elements of $\mathbf{H}(\omega)$ can be regarded as being composed of a sum of modal contributions that, in general, are associated with different time delays [1,3,7,8,11]. As a result, it is very difficult, if not impossible, to obtain an accurate approximating function without using an excessively large number of poles in the fitting process.

For single or multiphase modal domain models, this problem can be overcome with relative ease since there is only a single time delay associated with each mode of propagation [15]. The modal time delays can therefore be removed from each independent modal wave propagation function by multiplying each mode with a scalar phase shift factor, $\exp(j\omega\tau)$, in the frequency domain, where τ corresponds to the fastest frequency component of the corresponding mode [1,15]. The elements of the 'unwinded' modal propagation function are subsequently obtained as smooth functions of frequency that can be fitted with low-order approximating functions, e.g. with rational functions [14,15]. Note that, for the case of a line containing a single-phase conductor the unwinding of the wave propagation function in the phase domain would also be relatively easy to perform, since only a single travel time would be required.

For multiconductor systems the problem becomes somewhat more involved since, for the purposes of description, each element of the wave propagation matrix is associated with a sum of modal travel times. However, almost all of the phase domain transmission line models proposed thus far in the open literature [1,3,4,7,8] attempt to unwind $\mathbf{H}(\omega)$ in the phase domain using a single phase shift, $\exp(j\omega\tau)$, where τ in this case corresponds to a common time delay, usually determined as the shortest travel time of all the system modes. For single-circuit transmission lines, this approach will invariably succeed in unwinding the elements of $\mathbf{H}(\omega)$ since the magnitude of each corresponding modal travel time is usually very similar. The elements of the phase domain wave propagation matrix are then unwound in a similar way to that proposed for modal domain methods [1,3,7,8]. However, if the transmission system under investigation has very different travel times associated with each mode, as will in general be the case for multi-circuit or asymmetrical overhead line configurations, and cable systems, application of a single common time delay to all the elements of $\mathbf{H}(\omega)$ will not completely remove all these oscillations. In these cases, compensating for a common time delay may not permit a low-order fitting of $\mathbf{H}(\omega)$, due to the uncompensated part of the time delays [1].

In this chapter, a direct phase domain solution to this problem is introduced. The method is based on the evaluation, in the phase domain, of a *matrix* phase shift function. A coupled matrix of time delays is evaluated in phase co-ordinates to intrinsically take into account the effect of non-confluent travel times. The method is therefore applicable to line configurations in which the time delays of the system are very different from each other, such as multi-circuit and asymmetrical line systems. As a result of introducing the matrix phase shift function, the wave propagation matrix is obtained as a smooth function of frequency. This enables an accurate fitting of $\mathbf{H}(\omega)$ to take place, using a reduced-order approximating function.

The characteristic admittance and wave propagation matrices are accurately approximated in the frequency domain using rational function approximations. The method of Vector Fitting [18] is employed to fit these functions directly in phase co-ordinates. Vector Fitting, as described in chapter two, allows the elements of each column of $\mathbf{Y}_c(\omega)$ and $\mathbf{H}(\omega)$ to be fitted with the same set of poles. A columnwise realization for $\mathbf{Y}_c(\omega)$ and $\mathbf{H}(\omega)$ can then be obtained, leading to an approximately 2-fold increase in efficiency as compared to an element-by-element realization [11].

The final transmission line model is represented in the time domain by means of a Norton equivalent representation, making it compatible with general purpose electromagnetic transient programs such as EMTP [21].

4.2 Time Domain Formulation

Consider the multiphase distributed-parameter transmission system described in section 3.2 and illustrated again in Figure 4.1. As described in the previous chapter, the solution of the travelling wave equations at the sending and receiving ends of the line can be written in the frequency domain as [7,8],

$$\mathbf{I}_1(\omega) = \mathbf{Y}_c(\omega)\mathbf{V}_1(\omega) - \mathbf{H}(\omega)\left[\mathbf{Y}_c(\omega)\mathbf{V}_2(\omega) + \mathbf{I}_2(\omega)\right] \tag{4.1}$$

$$\mathbf{I}_2(\omega) = \mathbf{Y}_c(\omega)\mathbf{V}_2(\omega) - \mathbf{H}(\omega)\left[\mathbf{Y}_c(\omega)\mathbf{V}_1(\omega) + \mathbf{I}_1(\omega)\right] \tag{4.2}$$

where $\mathbf{I}_1(\omega)$ and $\mathbf{I}_2(\omega)$ are the vectors of sending and receiving end currents, respectively, $\mathbf{V}_1(\omega)$ and $\mathbf{V}_2(\omega)$ are the vectors of sending and receiving end voltages, respectively, $\mathbf{Y}_c(\omega)$ is the characteristic admittance matrix and $\mathbf{H}(\omega)$ is the wave propagation matrix.

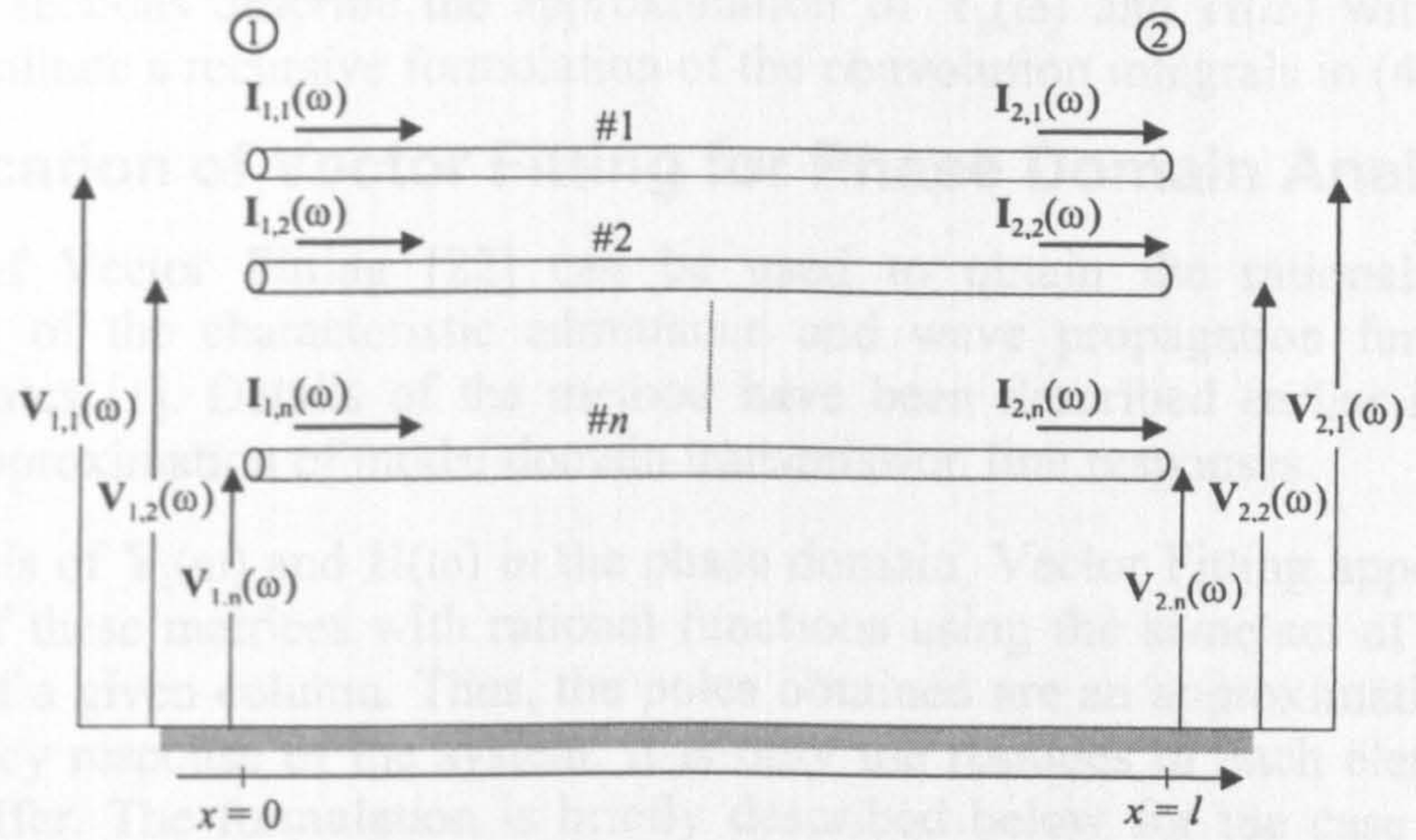

Figure 4.1. Multiphase distributed-parameter transmission line system

Transforming (4.1) and (4.2) into the time domain yields the following equations,

$$\mathbf{i}_1(t) = \mathbf{y}_c(t) * \mathbf{v}_1(t) - \mathbf{J}_1(t) \tag{4.3}$$

$$\mathbf{i}_2(t) = \mathbf{y}_c(t) * \mathbf{v}_2(t) - \mathbf{J}_2(t) \tag{4.4}$$

where,

$$\mathbf{J}_1(t) = \mathbf{h}(t) * \left[\mathbf{y}_c(t) * \mathbf{v}_2(t) + \mathbf{i}_2(t)\right] = \mathbf{h}(t) * \mathbf{f}_2(t) \tag{4.5}$$

$$\mathbf{J}_2(t) = \mathbf{h}(t) * \left[\mathbf{y}_c(t) * \mathbf{v}_1(t) + \mathbf{i}_1(t)\right] = \mathbf{h}(t) * \mathbf{f}_1(t) \tag{4.6}$$

and $\mathbf{y}_c(t)$ and $\mathbf{h}(t)$ correspond to the time domain impulse responses of $\mathbf{Y}_c(\omega)$ and $\mathbf{H}(\omega)$ respectively and the symbol '*' represents matrix-vector convolutions. Thus, from (4.3)-(4.6), it can be seen that the frequency-dependent characteristics of the transmission line responses, $\mathbf{Y}_c(\omega)$ and $\mathbf{H}(\omega)$, are taken into account in the time domain by means of numerical convolutions between the electrical quantities at both ends of the line and the line impulse responses, $\mathbf{y}_c(t)$ and $\mathbf{h}(t)$.

A direct evaluation of the numerical convolution integrals in (4.3)-(4.6) is always possible [1,11,18]. However, the computational effort required can become excessive

for calculations requiring a large number of time steps since these integrals must be evaluated at each discrete time step of the simulation [18]. In order to increase the computational efficiency of the time domain model it is recommended to develop a recursive formulation of the convolution integrals [19,20].

4.3 Rational Function Approximations

In this research, a recursive formulation of the convolution integrals is obtained by approximating the time domain impulse responses ($\mathbf{y}_c(t)$ and $\mathbf{h}(t)$) with a sum of exponentials. The fitting is performed in the frequency domain, where the corresponding approximation can be written as a rational function in partial fraction form. Thus, the advantage of performing the approximation in the frequency domain, is that the time domain form of the functions, $\mathbf{y}_c(t)$ and $\mathbf{h}(t)$ can be obtained directly in a closed form, without having to apply inverse Fourier transform techniques [14,15].

A further advantage is that the actual approximation of $\mathbf{Y}_c(\omega)$ and $\mathbf{H}(\omega)$ with rational functions in the frequency domain is much easier to perform than the corresponding time domain approximation of $\mathbf{y}_c(t)$ and $\mathbf{h}(t)$ with a sum of exponentials [10,15].

The following sections describe the approximation of $\mathbf{Y}_c(\omega)$ and $\mathbf{H}(\omega)$ with rational functions to facilitate a recursive formulation of the convolution integrals in (4.3)-(4.6).

4.3.1 Application of Vector Fitting for Phase Domain Analysis

The method of Vector Fitting [22] can be used to obtain the rational function approximations of the characteristic admittance and wave propagation functions in phase co-ordinates [1]. Details of the method have been described earlier in section 2.5.1, for the approximation of modal domain transmission line responses.

For the synthesis of $\mathbf{Y}_c(\omega)$ and $\mathbf{H}(\omega)$ in the phase domain, Vector Fitting approximates each column of these matrices with rational functions using the same set of poles for each element of a given column. Thus, the poles obtained are an approximation of the natural frequency response of the system. It is only the residues of each element in a column that differ. The formulation is briefly described below for the case of a two element vector, further details of the formulation can be found in [22].

For a two element vector, the rational function approximation given in (2.46) can be replaced with the following [22],

$$\mathbf{F}(s)=\begin{bmatrix}\mathbf{F}_1(s)\\ \mathbf{F}_2(s)\end{bmatrix}=\begin{bmatrix}\sum_{i=1}^{N}\frac{c_i^1}{s-a_i}\\ \sum_{i=1}^{N}\frac{c_i^2}{s-a_i}\end{bmatrix} \tag{4.7}$$

Assuming the optional terms d and h in (2.46) are zero and the residue superscripts 1 and 2 refer to the corresponding elements of the frequency responses $\mathbf{F}_1(\omega)$ and $\mathbf{F}_2(\omega)$ respectively. If the same set of starting poles are selected for both vector elements, and a common unknown scaling function, $\eta(s)$, is multiplied to both frequency responses, then, on introducing a rational function approximation for the unknown scaling function the expanded problem of (2.47) now becomes [22],

$$\begin{bmatrix}\sum_{i=1}^{N}\frac{c_i^1}{s-a_i}\\ \sum_{i=1}^{N}\frac{c_i^2}{s-a_i}\end{bmatrix}-\begin{bmatrix}\mathbf{F}_1(s)\sum_{i=1}^{N}\frac{\tilde{c}_i}{s-a_i}\\ \mathbf{F}_2(s)\sum_{i=1}^{N}\frac{\tilde{c}_2}{s-a_i}\end{bmatrix}\approx\begin{bmatrix}\mathbf{F}_1(s)\\ \mathbf{F}_2(s)\end{bmatrix} \tag{4.8}$$

For each frequency point of interest, (4.8) can be written as a set of overdetermined linear equations (**Ax=b**), analogously to (2.50). After solving this set of linear equations, an improved set of poles for fitting the original frequency response, $\mathbf{F}(\omega)$ can be obtained from the zeros of the unknown scaling function, $\eta(s)$, the details of which are described [22].

Finally, in order to obtain a set of residues for each frequency response, $\mathbf{F}_1(\omega)$ and $\mathbf{F}_2(\omega)$, the elements are fitted independently using the new poles as known quantities in (4.7). As for the scalar case, the overall process can be repeated in an iterative procedure with the poles obtained at each iteration used as starting poles in the next iterative cycle.

4.3.2 Synthesis of the Characteristic Admittance Matrix $\mathbf{Y}_c(\omega)$

As stated in the introduction, the elements of the characteristic admittance matrix $\mathbf{Y}_c(\omega)$ are in general very smooth functions of frequency over the range of interest for electromagnetic transient studies. This has been shown in the previous chapter, where the characteristic admittance is evaluated for both single and double-circuit transmission line configurations (c.f. Figures 3.5-3.8). The elements of $\mathbf{Y}_c(\omega)$ can therefore be accurately approximated using very low-order rational functions in the phase domain.

In the following section, the results of fitting the characteristic admittance matrix with rational functions using the method of Vector Fitting [22] are presented. As discussed previously, Vector Fitting allows each individual column of the matrix to be approximated by the same set of poles, which leads to a more efficient time domain formulation [1,11,18] as compared to element-by-element fitting.

The results described below correspond to a 220kV, 152.90km double-circuit transmission line configuration. The physical data for the transmission system can be found in Appendix III.

4.3.3 Double-Circuit Transmission Line Configuration

Figures 4.3 and 4.4 show the magnitude and phase angle of columns 1, 3, 4 and 6, respectively, of $\mathbf{Y}_c(\omega)$ for the vertical double-circuit line configuration shown in Figure 4.2, when each column is approximated by a 10th order rational function using the method of Vector Fitting. The approximated results are superimposed on the accurate results, as calculated using the algorithm described in section 3.4.5. The starting poles used in the fitting process are, for all columns of $\mathbf{Y}_c(\omega)$, real and negative, logarithmically distributed between 1Hz and 1MHz.

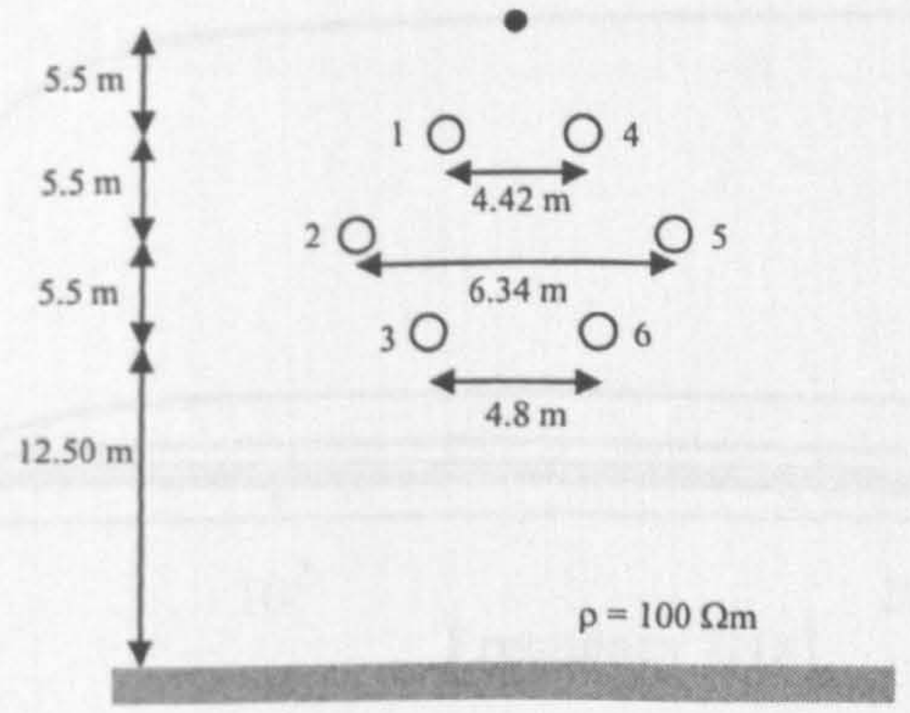

Figure 4.2. 220kV Double-circuit transmission line

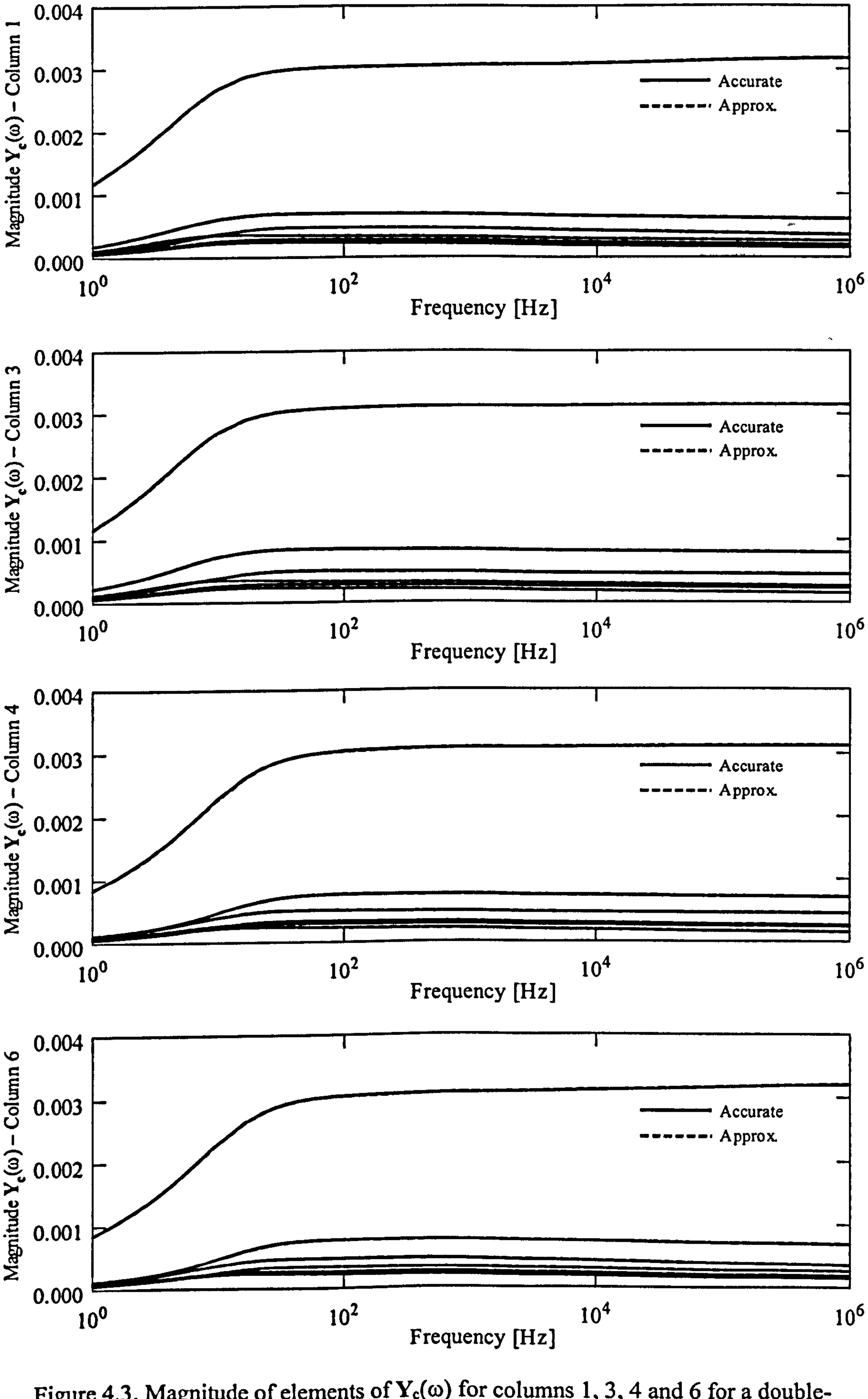

Figure 4.3. Magnitude of elements of $\mathbf{Y}_c(\omega)$ for columns 1, 3, 4 and 6 for a double-circuit line

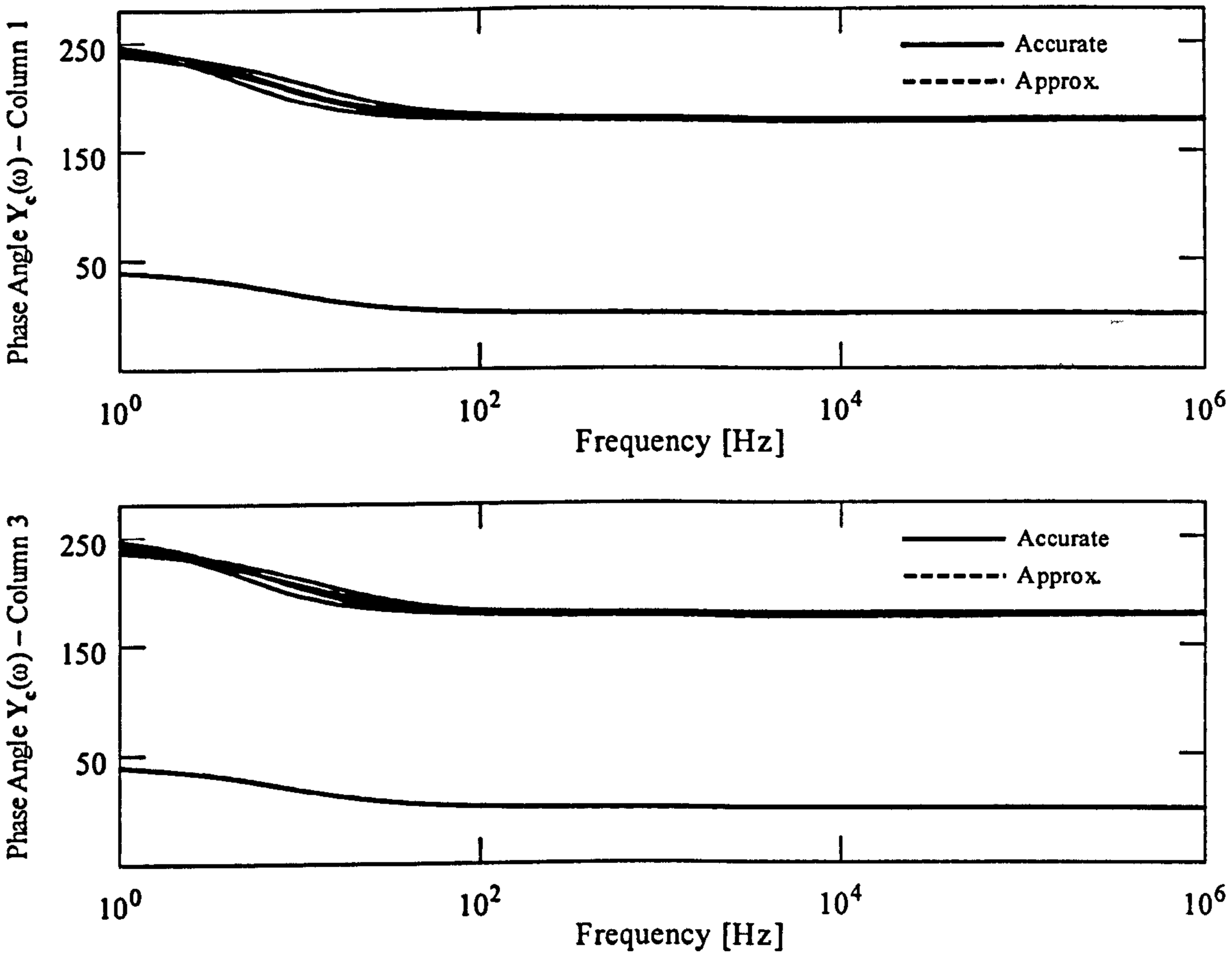

Figure 4.4. Phase angle (degrees) of elements of $\mathbf{Y}_c(\omega)$ for columns 1, 3, 4 and 6 for a double-circuit line

As can be seen from Figures 4.3 and 4.4, the approximation is very accurate for each column of the matrix $\mathbf{Y}_c(\omega)$, for both the magnitude and the phase angle. A similar degree of accuracy is obtained for the remaining columns (2 and 5) of $\mathbf{Y}_c(\omega)$ (not shown). Real poles and residues were obtained for all the columns of $\mathbf{Y}_c(\omega)$, which is to be expected since the elements of the function are smooth throughout the frequency range considered. In general, complex conjugated poles will only be obtained in the rational function approximation if the frequency response to be fitted contains resonance peaks [1,22].

4.3.4 Equivalent Circuit in the Time Domain

If the elements of the characteristic admittance matrix, $\mathbf{Y}_c(\omega)$, are approximated with rational functions in the frequency domain, as outlined in the previous section, then each element of $\mathbf{y}_c(t)$ can be written as a sum of exponentials in the time domain with a constant term. With $\mathbf{y}_c(t)$ approximated in this form, it is shown in Appendix I that the matrix-vector convolution of the impulse response and the vector of voltages, $\mathbf{y}_c(t)*\mathbf{v}(t)$, can be performed recursively as,

$$\mathbf{y}_c(t) * \mathbf{v}(t) = \boldsymbol{\zeta}(t) = \mathbf{y}_{eq}\mathbf{v}(t) + \mathbf{J}_a(t) \tag{4.9}$$

where $\mathbf{y}_{eq}$ is a real, constant and symmetric matrix of order n x n. The second term on the right hand side of (4.9), $\mathbf{J}_a(t)$, is a history current vector, evaluated from the known values of $\boldsymbol{\zeta}(t)$ and $\mathbf{v}(t)$ at the previous time step. By way of example, the convolution between element $y_{c11}(t)$ and the first element of $\mathbf{v}(t)$ can be given in a more detailed form as shown below,

$$y_{c11}(t) * v^a(t) = \zeta_{11}(t) = zv^a(t) + J_{a11}(t) \tag{4.10}$$

where,

$$z = d + \sum_{i=1}^{N} p_i \tag{4.11}$$

and,

$$J_{a11}(t) = \sum_{i=1}^{N} q_i \zeta_{11_i}(t - \Delta t) + r_i v^a(t - \Delta t) \tag{4.12}$$

The coefficients p_i, q_i and r_i are constants which depend on the time step, Δt, for a given simulation (see Appendix I for details) [14]. Note from (4.12), and as stated above, $J_{a11}(t)$ is determined exclusively from the known values of $\zeta_{11}(t)$ and $v^a(t)$ at the previous time step.

From (4.9), equation (4.3) and (4.4) can be re-written as follows,

$$\mathbf{i}_1(t) = \mathbf{y}_{eq}\mathbf{v}_1(t) - \overline{\mathbf{J}}_1(t) \tag{4.13}$$

$$\mathbf{i}_2(t) = \mathbf{y}_{eq}\mathbf{v}_2(t) - \overline{\mathbf{J}}_2(t) \tag{4.14}$$

where,

$$\overline{\mathbf{J}}_1(t) = \mathbf{J}_1(t) - \mathbf{J}_{a1}(t) \tag{4.15}$$

$$\overline{\mathbf{J}}_2(t) = \mathbf{J}_2(t) - \mathbf{J}_{a2}(t) \tag{4.16}$$

Equations (4.13)-(4.16) can be represented in the time domain by an equivalent circuit expressed at each end of the line by an n-terminal admittance in parallel with an n-

terminal current source, as shown in Figure 4.5 [7,8]. With this representation, the model can be introduced into general purpose electromagnetic transient programs, such as EMTP [21], based on a nodal admittance representation. The constant admittance matrix, $\mathbf{y}_{eq}$, is added to the network conductance matrix before the time domain simulation is executed.

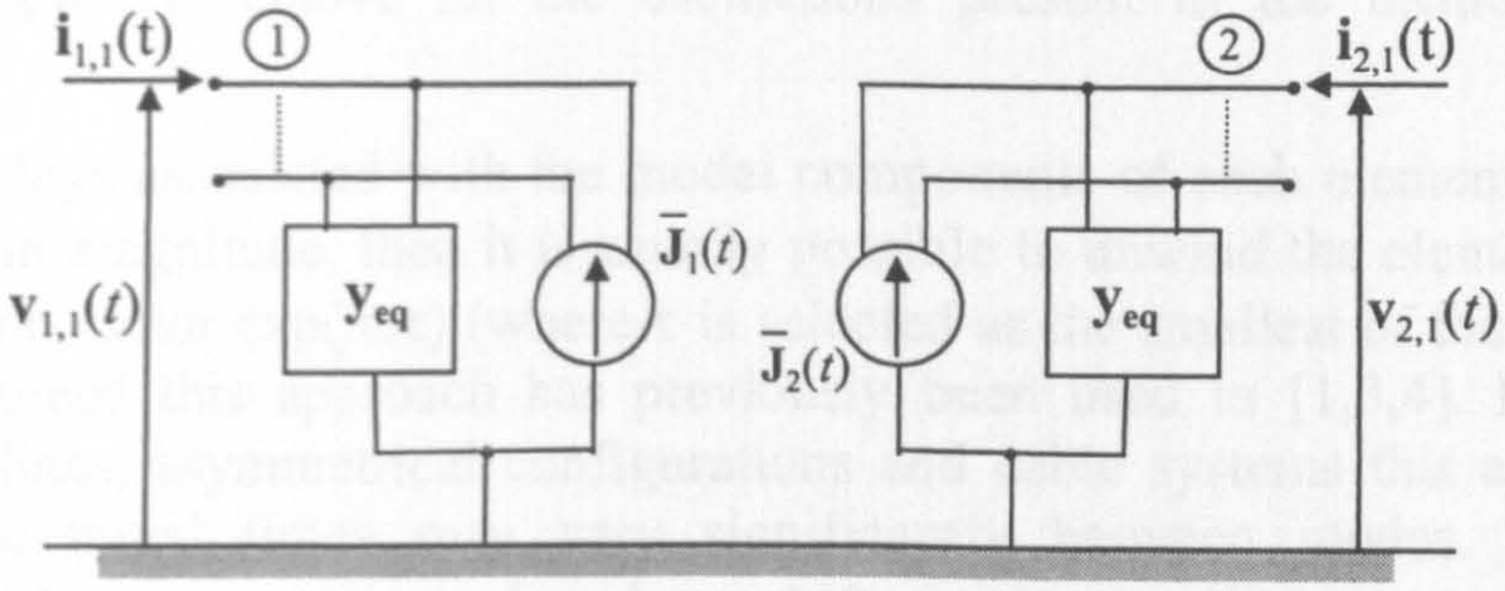

Figure 4.5. Multiphase transmission line equivalent in the time domain

4.4 Synthesis of the Wave Propagation Matrix H(ω)

As stated in the introduction, one of the most difficult aspects of modelling multiphase power transmission lines directly in the phase domain concerns the fitting of the elements of the wave propagation matrix, $\mathbf{H}(\omega)$ [1,3,7,8,11,17]. The elements of $\mathbf{H}(\omega)$ exhibit a highly oscillatory nature in the frequency domain, due to the time delays of the line [1,3,7,8,11]. For the purposes of description, each element of $\mathbf{H}(\omega)$ can be thought of as being composed of a sum of modal components that will in general have different travel times. In this form therefore, it is extremely difficult, if not impossible, to fit the elements of $\mathbf{H}(\omega)$ directly in the phase domain, without using very high-order rational function approximations [11].

Thus, in order to obtain an accurate approximation of the elements of $\mathbf{H}(\omega)$, it is necessary to remove these oscillations before the fitting process takes place [1,3,4,7-9,11]. If the elements of $\mathbf{H}(\omega)$ can be obtained as smooth functions of frequency, then it follows that relatively low-order rational function approximations can be obtained. With the elements of the wave propagation matrix approximated with in this form, then a recursive formulation of the convolutions integrals, (4.5)-(4.6), can be obtained, greatly increasing the computational efficiency of the proposed line model. The process of unwinding the wave propagation matrix directly in the phase domain is the subject of the following sections.

4.4.1 Unwinding the elements of H(ω)

In order to facilitate a low order rational function approximation of the elements of $\mathbf{H}(\omega)$, the elements must be 'unwound' before the fitting process takes place. The elements are then obtained as relatively smooth functions of frequency and more amenable to approximation by low-order rational functions. Current phase domain transmission line models [1-13] make use of modal components in order to unwind the elements of the propagation matrix. It is proposed in this research to formulate a solution to this problem directly in the phase domain, without resorting to modal components, making use of the inherent coupling between phases to unwind the elements of $\mathbf{H}(\omega)$.

In modal domain based models, each mode of the weighting function $A(\omega)$ can be unwound with relative ease, since a single time delay can be associated with each mode [14]. The procedure for unwinding the elements of $A(\omega)$ has been discussed previously in section 2.6.2 of chapter two.

In the phase domain, the situation is somewhat more complicated. Each element of $\mathbf{H}(\omega)$ can be thought of as being composed as a sum of modal components which in general will have different time delays. Therefore, applying a common scalar phase shift, $\exp(j\omega\tau)$, in a similar manner to that undertaken for modal domain based models, will not completely remove all the oscillations present in the elements of $\mathbf{H}(\omega)$ [1,3,4,7,8,11].

If the time delays associated with the modal components of each element of $\mathbf{H}(\omega)$ are quite similar in magnitude, then it is usually possible to unwind the elements of $\mathbf{H}(\omega)$, with a common factor $\exp(j\omega\tau)$ (where τ is selected as the smallest of the modal travel times) and indeed this approach has previously been used in [1,3,4]. However, for multi-circuit lines, asymmetrical configurations and cable systems this approach may fail since the travel times may vary significantly between modes. As a result, multiplication by a common *scalar* phase shift, $\exp(j\omega\tau)$, will not remove all these oscillations from the elements of $\mathbf{H}(\omega)$ and it will not be possible to obtain a low order approximation [11].

Several alternative approaches have been suggested to solve this problem, however, since explicit computation of modal parameters is required, these methods cannot be regarded as a direct phase domain approach. In [7,8], the wave propagation matrix $\mathbf{H}(\omega)$ is expressed as a sum on n modal components so that a separate time delay can be assigned to each mode. Since the process is undertaken in the z-domain, if the time step for the time domain simulation is changed, it is necessary to re-fit the elements of the wave propagation matrix. A similar approach has been undertaken in [11] with the analysis performed in the frequency domain, however, modal parameters are again required in the formulation.

In order to overcome these difficulties, it is therefore proposed in this work to unwind the elements of $\mathbf{H}(\omega)$ directly in the phase domain. This is achieved by evaluating a *matrix* phase shift function in phase co-ordinates that enables relatively low-order rational function approximations of the elements of $\mathbf{H}(\omega)$ to be obtained. The method is described in more detail in the following sections.

4.4.2 Matrix Phase Shift Function

When evaluated in phase co-ordinates, the travel time function, τ, is a real $n \times n$ matrix (where n is the number of conductors) containing off-diagonal elements due to the mutual coupling that exists between the phase conductors.

Intuitively, rather than seeking a common scalar phase factor, it is proposed in this research to unwind the elements of $\mathbf{H}(\omega)$ directly in the phase domain using a coupled matrix phase shift function. Since the matrix phase shift is evaluated directly in phase co-ordinates, the travel times of the transmission system are intrinsically taken into account in the unwinding process. The method is therefore applicable to a wide variety of transmission systems, including multi-circuit and asymmetrical line systems, in which the travel times may vary significantly in magnitude for each mode

When evaluated directly in phase co-ordinates, the elements of $\mathbf{H}(\omega)$ can be unwound by multiplication with the matrix phase shift function, $\Phi(\omega)$, as follows,

$$\mathbf{P}(\omega) = e^{j\omega\boldsymbol{\tau}}\,\mathbf{H}(\omega) = \Phi(\omega)\mathbf{H}(\omega) \tag{4.17}$$

The matrix $\boldsymbol{\tau}$ may be regarded as the phase domain "equivalent" of the modal travel time function, τ, however, the function is used here purely as a mathematical tool, rather than an attempt to provide a physical description of the problem.

The elements of the resulting matrix $\mathbf{P}(\omega)$ are relatively smooth throughout the required frequency range and can thus be approximated with relatively low-order rational functions. The original function is then obtained as follows,

$$\mathbf{H}(\omega) = e^{-j\omega\tau}\mathbf{P}(\omega) = \Phi^{-}(\omega)\mathbf{P}(\omega) \tag{4.18}$$

4.4.2.1 Evaluation of the Phase Domain Travel Time Function τ

For a transmission line of length, l, the phase domain travel time matrix (or PDTT), τ, can be defined directly in phase co-ordinates as follows,

$$\tau = l\upsilon^{-1}(\omega_0) = l\sqrt{\mathbf{C}(\omega_0)\mathbf{L}(\omega_0)} \tag{4.19}$$

where $\mathbf{L}(\omega_0)$ and $\mathbf{C}(\omega_0)$ are the series inductance and shunt capacitance matrices, respectively, evaluated at some high frequency point ω_0. $\mathbf{L}(\omega_0)$ and $\mathbf{C}(\omega_0)$ are both n x n matrices, where n is the number of equivalent phase conductors of the system. Finally, $\upsilon(\omega_0)$ is the phase velocity of the system (assuming: $\mathbf{R}(\omega_0)=0$ and $\mathbf{G}(\omega_0)=0$) defined as,

$$\upsilon(\omega_0) = \sqrt{[\mathbf{C}(\omega_0)\mathbf{L}(\omega_0)]^{-1}} \tag{4.20}$$

It can be seen from (4.19) that in order to evaluate the PDTT function at the specified frequency point ω_0, requires the evaluation of a matrix square root. This can be accomplished by exploiting the relationship between the matrix sign function and the matrix square root [23-25], in a similar manner as that proposed to evaluate the characteristic admittance matrix, described in section 3.4.5. The result is an accurate and efficient iteration for evaluating τ, directly in phase co-ordinates. The procedure is described below:

Consider the following block 2x2 matrix [24],

$$\mathbf{B} = \begin{bmatrix} \mathbf{0} & \mathbf{C}(\omega_0)\mathbf{L}(\omega_0) \\ l^{-2}\mathbf{U} & \mathbf{0} \end{bmatrix} \tag{4.21}$$

where $\mathbf{U}$ is the n x n unit matrix and l is the length of the line. By substituting (4.21) into (3.35), the sign of the matrix can be defined in terms of the PDTT function, giving the following relationship,

$$\operatorname{sign}\left(\begin{bmatrix} \mathbf{0} & \mathbf{C}(\omega_0)\mathbf{L}(\omega_0) \\ l^{-2}\mathbf{U} & \mathbf{0} \end{bmatrix}\right) = \begin{pmatrix} \mathbf{0} & l\mathbf{U}[\mathbf{C}(\omega_0)\mathbf{L}(\omega_0)]^{1/2} \\ l^{-1}\mathbf{U}[\mathbf{C}(\omega_0)\mathbf{L}(\omega_0)]^{-1/2} & \mathbf{0} \end{pmatrix} \tag{4.22}$$

Applying the Padé iteration scheme, as described in section 3.4.4 to evaluate the matrix sign function, to the 2x2 block matrix in (4.21) leads to the following algorithm for computing the PDTT function,

$$\left.\begin{aligned} \mathbf{Y}_{k+1}(\omega) &= \frac{1}{p}\mathbf{Y}_k(\omega)\sum_{i=1}^{p}\frac{1}{\xi_i}\left[\mathbf{Z}_{k_i}(\omega)\mathbf{Y}_{k_i}(\omega) + \alpha_i^2\mathbf{U}\right]^{-1} \\ \mathbf{Z}_{k+1}(\omega) &= \frac{1}{p}\mathbf{Z}_k(\omega)\sum_{i=1}^{p}\frac{1}{\xi_i}\left[\mathbf{Y}_{k_i}(\omega)\mathbf{Z}_{k_i}(\omega) + \alpha_i^2\mathbf{U}\right]^{-1} \end{aligned}\right\} \quad k = 0,1,2,\ldots \tag{4.23}$$

In this case, algorithm (4.23) converges to the following: $\mathbf{Y}_k \rightarrow \tau$ and $\mathbf{Z}_k \rightarrow \tau^{-1}$, with initial conditions given by $\mathbf{Y}_0=\mathbf{L}(\omega_0)\mathbf{C}(\omega_0)$ and $\mathbf{Z}_0=l^{-2}\mathbf{U}$.

4.4.2.2 Convergence Properties

A summary of the convergence characteristics of algorithm (4.23), for evaluating the PDTT function for different orders, p, of the Padé approximation, is shown in Table 4.1.

Two sets of results are presented in Table 4.1, corresponding to the evaluation of τ for both single and double-circuit transmission line systems. The single-circuit line corresponds to that of section 3.5.1 (c.f. Figure 3.4) and is 398km in length. The double-circuit line in comparison is 152.90km in length and is illustrated in section 4.3.3 (c.f. Figure 4.2).

A pre-specified tolerance of 1.0E-15 was selected to measure convergence for all the cases presented.

Table 4.1. No. of iterations required to evaluate τ

	Double-circuit line		Single-circuit line	
p	Unscaled	Scaled	Unscaled	Scaled
1	30	4	31	3
2	15	2	16	2
3	12	2	12	1
4	10	2	11	1
5	9	1	10	1

As for the case of evaluating the characteristic admittance matrix, it can be seen from Table 4.1 that algorithm (4.23) will always converge, irrespective of the order of the Padé approximation. Again, employing the same scaling strategy of section 3.4.7 significantly decreases the number of iterations required to obtain convergence and it is recommended to employ this scaling strategy when evaluating τ [24]. For the remainder of the results presented in this thesis, the evaluation of the PDTT function, τ, is performed using a value of p=3, for the Padé approximation order in (4.23). The scaling technique described in section 3.4.7 is also applied in the evaluation of τ.

4.5 Evaluation of the Matrix Phase Shift Function $\Phi(\omega)$

In order to unwind the elements of the wave propagation matrix, $\mathbf{H}(\omega)$, directly in phase co-ordinates, it is proposed to calculate a matrix phase shift function, $\Phi(\omega)$, formerly defined as follows,

$$\Phi(\omega) = e^{j\omega\tau} \tag{4.24}$$

where τ, is a $n \times n$ matrix. The evaluation of (4.24) can be undertaken using the Padé approximation scheme developed in the previous chapter to calculate the wave propagation matrix. The argument matrix in this case is defined as follows,

$$\mathbf{S}(\omega) = j\omega l\sqrt{\mathbf{C}(\omega_0)\mathbf{L}(\omega_0)} \tag{4.25}$$

where $\mathbf{L}(\omega_0)$ and $\mathbf{C}(\omega_0)$ are n x n matrices evaluated at some high frequency point ω_0 and l is the length of the line. Again, the diagonal Padé approximants (p=q) are used in order to increase the overall efficiency and stability of the algorithm (see section 3.6.6 for more details) [26,27]. Assuming a diagonal Padé approximant (p=q), then the following algorithm is obtained for evaluating $\Phi(\omega)$, directly in the phase domain [26],

$$R_{pp}(\mathbf{S}) = \frac{N_{pp}(\mathbf{S})}{N_{pp}(-\mathbf{S})} \tag{4.26}$$

where,

$$N_{pp}(\mathbf{S}) = \sum_{k=0}^{p} c_k \mathbf{S}^k \tag{4.27}$$

and,

$$c_k = c_{k-1}\frac{p+1-k}{(2p+1-k)k} \tag{4.28}$$

with c_0=1. Again, Horner's Rule can be applied to increase the efficiency of the algorithm when evaluating the numerator and denominator in (4.26) [27].

It was found that numerical stability problems arise when evaluating (4.26) directly. This can be attributed to norm of the argument matrix (4.25) increasing in magnitude with frequency [26]. A similar problem was found when evaluating the wave propagation matrix. This problem was discussed in detail in section 3.6.4 of the previous chapter.

From (4.25) it can be seen that the length of the transmission line will influence the magnitude of the norm of S(ω). Following the discussion of section 3.6.5, once the magnitude of the norm increases above a certain threshold value, the accuracy of algorithm (4.25) will deteriorate substantially.

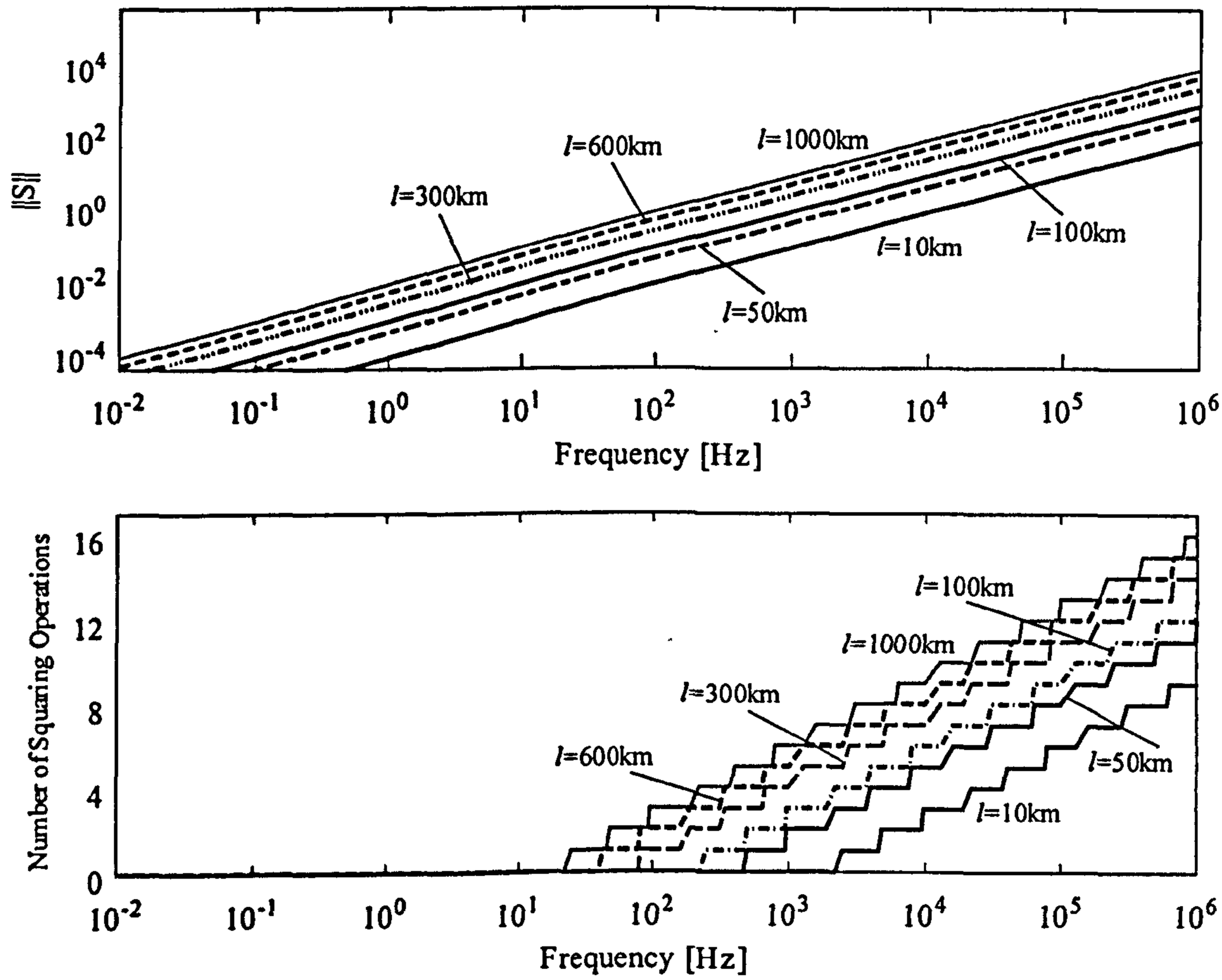

Figure 4.6 (Top) Norm of the matrix S(ω) and (Bottom) Number of squaring operations required to evaluate Φ(ω), for different line lengths.

Figure 4.6 highlights the variation of the norm of the argument matrix, S(ω), with frequency for line lengths of l=10km, 50km, 100km, 300km, 600km, and 1000km using the single-circuit transmission line described in section 3.5.1. The choice of the 1000km line, while unrealistic in a practical sense is useful for the purposes of analysing the characteristics of algorithm (4.26).

Again, following the discussion of section 3.6.5, the matrix phase shift function, Φ(ω), can only accurately be evaluated when the norm of the argument matrix is less than one

[26-28]. From Figure 4.6 it can be seen that this relationship is only satisfied up to frequencies in the approximate range 70Hz-8000Hz, the lower frequency point corresponding to the longest line investigated. Therefore, in order maintain a high level of accuracy over the entire frequency range of interest, the scaling and squaring technique described in section 3.6.5 must be applied at frequencies in which the norm of $S(\omega)$ exceeds one.

In order to give an indication as to the number of squaring operations required to accurately evaluate $\Phi(\omega)$, the function is evaluated for the same single-circuit transmission line configuration with different line lengths as described above. The order of the Padé approximation is set at p=4. With this value, $\Phi(\omega)$, can be accurately and efficiently evaluated over the entire frequency range of interest.

From Figure 4.6, the number of squaring operations, as a function of frequency, shows a similar pattern to that of the wave propagation matrix (c.f. figure 3.15). The maximum number of squaring operations required to accurately evaluate (4.26) can be anticipated to increase as power lines of longer length are considered. However, the number of squaring operations should be expected to reach some limiting value, irrespective of the transmission line configuration, frequency interval and line length under consideration.

4.6 Time Domain Form of the Matrix Phase Shift Function

After the elements of the matrix $\mathbf{P}(\omega)$ have been successfully synthesized with rational functions in the frequency domain, the approximated wave propagation matrix, $\mathbf{H}_f(\omega)$, can then be obtained as,

$$\mathbf{H}_f(\omega) = e^{-j\omega\tau}\mathbf{P}_f(\omega) = \Phi^{-}(\omega)\mathbf{P}_f(\omega) \tag{4.29}$$

where the subscript 'f' denotes the approximated function and $\Phi^{-}(\omega)$ is termed the negative phase shift function and is an n x n matrix. In the time domain, $\Phi^{-}(\omega)$ corresponds to a matrix of coupled, time delayed impulses.

To recap, in modal domain based methods, the weighting function, $A(\omega)$, is unwound in the frequency domain by introducing a scalar phase shift factor, $\exp(j\omega\tau_k)$, where τ_k corresponds to the fastest frequency component for each mode k [14,15,18]. The elements of $\mathbf{P}(\omega)$ are then obtained as relatively smooth functions of frequency and can be accurately approximated using low-order rational functions. The rational function approximation of $\mathbf{P}(\omega)$ is then multiplied with a negative phase shift $\exp(-j\omega\tau_k)$ to return an approximation of the original weighting function [14,15,18]. In the time domain, the factor $\exp(-j\omega\tau_k)$ corresponds to a unit impulse, $\delta(t-\tau_k)$, delayed by a interval equal to the modal travel time τ_k.

For multi-conductor transmission line systems, modelled directly in phase co-ordinates, the determination of the correct time delays for each element of the approximated wave propagation matrix is less straightforward. The difficulty arises in interpreting the time domain form of the negative phase shift function $\Phi^{-}(\omega)$. Each element of $\phi^{-}(t)$ is composed of n coupled time delays, where n is the number of phase conductors of the system, rather than with a single time delay as in the modal approach. The exact 'weight' of each impulse, and the corresponding delay cannot be pre-determined directly in phase co-ordinates from the frequency domain form of the function.

Therefore, in order to determine the appropriate phase shifts (time delays) that must be introduced into the elements of $\mathbf{P}_f(\omega)$ ($\mathbf{p}_f(t)$), to obtain a time domain approximation of the original wave propagation matrix, $\mathbf{H}(\omega)$, it is necessary to apply an inverse Fourier

transform on the elements of $\Phi^{-}(\omega)$. Since the elements of $\Phi^{-}(\omega)$ are obtained as discrete functions of frequency, a discrete form of the inverse Fourier transform is used.

Figure 4.7 shows the time domain form of four elements of the negative phase shift function, $\phi^{-}(t)$, evaluated for the 152.9km double-circuit transmission line illustrated in Figure 4.2. The PDTT function, τ, in this case is evaluated at a frequency of ω_0=1MHz, using the Padé iteration scheme of (4.23). The order of the Padé approximant in this case is p=3.

It can be seen from Figure 4.7 that each element of $\phi^{-}(t)$ is composed of a series of weighted impulses, with a different time delay associated with each impulse. The time delays of the impulses correspond exactly to the eigenvalues of the PDTT function, τ. For the double-circuit transmission line under consideration, τ, is 6 x 6 matrix and thus has six eigenvalues. It should be expected, therefore, that each element of $\phi^{-}(t)$ be composed of six impulses, each associated with a different time delay and weight.

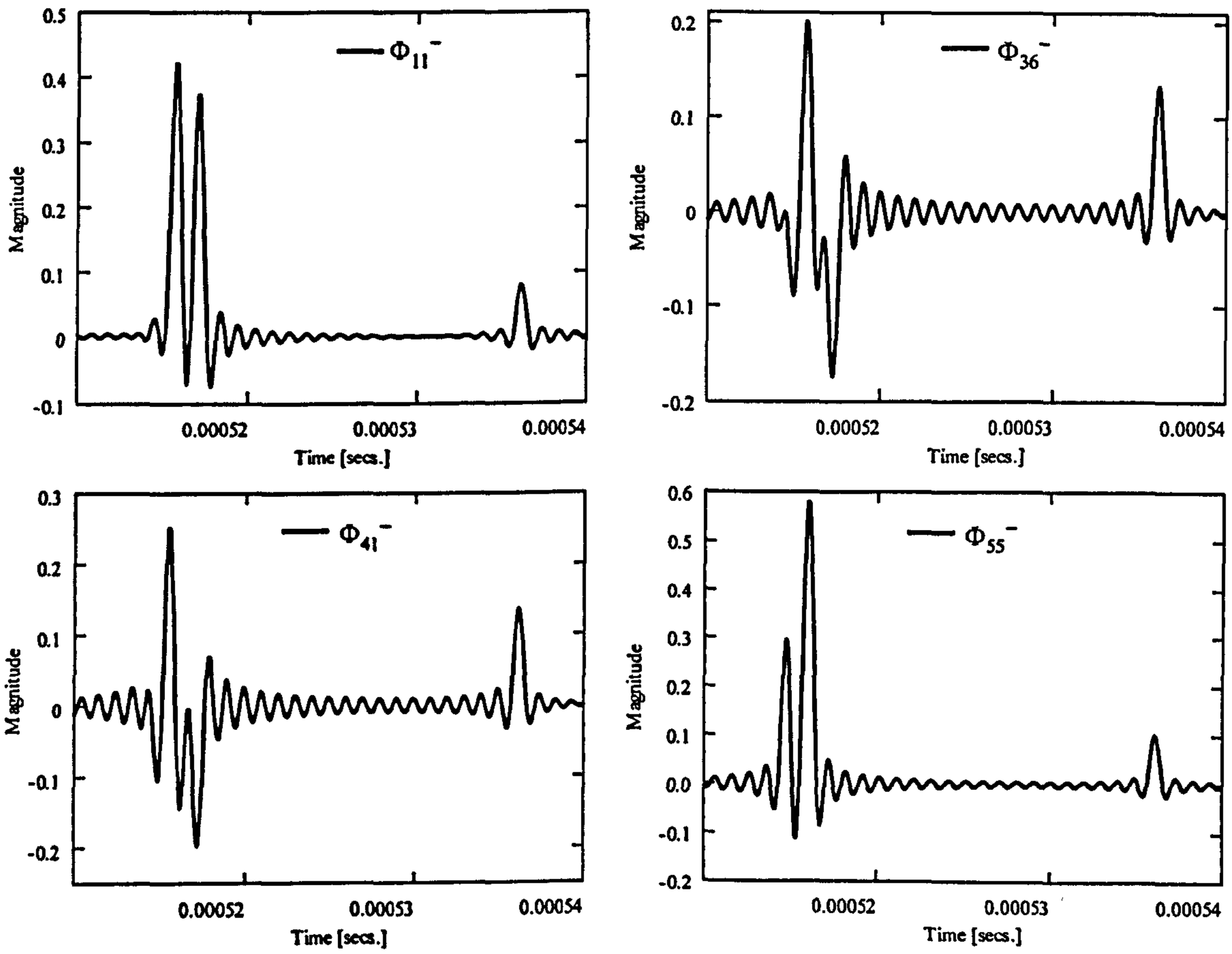

Figure 4.7 Elements of the time domain form of the negative phase shift function, $\phi^{-}(t)$, for a double-circuit overhead line

However, it can been see from Figure 4.7 (particularly evident from the diagonal elements shown) that there are less than six weighted impulses present. This can be attributed to the system possessing a group of confluent eigenvalues (the eigenvalues of τ can be regarded as 'equivalent' to the modal travel times of the system). For the diagonal elements, all the impulses have the same sign and are resolved as a lumped impulse, centred on the time delay of the dominant impulse in the group (in respect to the magnitude of the weights of the impulses). This is evident from the diagonal elements illustrated in Figure 4.7.

In contrast, the off-diagonal elements are composed of a series of positive and negative impulses. Again, not all the impulses in a confluent group will appear visible since the weight of any particular impulse may be negligible as compared to the remaining impulses of the group. This is illustrated for the off-diagonal elements shown in Figure 4.7.

In order to clarify the above comments and better describe the form of the elements of $\phi^-(t)$, in Figure 4.7, the negative phase shift function is defined below in the frequency domain, in terms of the eigenvalues of the system.

The matrix $\Phi^-(\omega)$ can be defined in terms of the eigenvalues of the PDTT function, τ, as follows (see Appendix II for details),

$$\Phi^-(\omega) = e^{-j\omega\tau} = \begin{pmatrix} \Phi_{11}^-(\omega) & \Phi_{12}^-(\omega) & \Phi_{13}^-(\omega) \\ \Phi_{21}^-(\omega) & \Phi_{22}^-(\omega) & \Phi_{23}^-(\omega) \\ \Phi_{31}^-(\omega) & \Phi_{32}^-(\omega) & \Phi_{33}^-(\omega) \end{pmatrix} \tag{4.30}$$

where,

$$\Phi_{ij}^-(\omega) = \sum_{k=1}^{n} T_{ik}(\omega) T_{kj}^I(\omega) e^{-j\omega\tau_k} \tag{4.31}$$

From (4.31), the composition of each element of $\Phi^-(\omega)$ can be seen to be made up of a series of weighted phase shifts. The values of τ_k are equal to the eigenvalues of the PDTT function, τ.

Thus, in the time domain, each element of $\phi^-(t)$ will be composed of n weighted $(T_{ik}(\omega)T_{kj}^I(\omega))$, delayed impulses, where n is the number of phase conductors of the system. However, if some of the eigenvalues of the matrix τ are very similar, then in practice there will be less than n impulses observable, due to the grouping of impulses. In the case of the diagonal elements, the confluent eigenvalues will generally form a single weighted impulse (all the weights are of positive sign), centred on the time delay of the dominant mode.

For the off-diagonal elements, the weights associated with each impulse will in general differ in sign and several dominant impulses will be seen to emerge.

This can be elaborated on further by analysing the actual eigenvalues of the PDTT function for the case of the double-circuit transmission line, discussed above. The eigenvalues of τ, are shown in Table 4.2.

Table 4.2. Eigenvalues of matrix τ for a double-circuit line

Eigenvalues of τ
τ_1=0.000536129
τ_2=0.000517175
τ_3=0.000514662
τ_4=0.000516173
τ_5=0.000515693
τ_6=0.000515975

From Figure 4.7, the last impulse for each element can be seen to be associated with τ_1. Observing element (4,1) in more detail, it can be seen that the first impulse is associated with eigenvalue τ_3, and is negative in sign. This is followed shortly after with a dominant positive impulse that is associated with eigenvalues τ_5 and τ_6. The final two

impulses in this confluent group are associated with eigenvalues τ_4 and τ_2 that are negative and positive in sign, respectively. The weight of the impulse associated with τ_5 is greater in this case.

The characteristics of the elements of $\phi^-(t)$, as described above, can clearly be seen in Figure 4.7. One additional observation that can be made concerns the sum of the weights for each element of $\phi^-(t)$. It can be see from Figure 4.7 that the sum of the weighted impulses for the diagonal elements is approximately equal to one, whereas that for the off-diagonal elements, is zero. This is consistent for the remaining elements of the matrix $\phi^-(t)$.

4.6.1 Scalar Impulse Functions

In the recursive formulation of the convolution integrals in (4.5) and (4.6) it is necessary to know the exact value of both the time delays, and weights of the impulses that make up each element of the negative phase shift function, $\Phi^-(\omega)$. This can be accomplished by approximating each element of $\phi^-(t)$ with a sum of weighted scalar impulse functions (or weighted negative phase shifts in the frequency domain). The time domain form, $\phi^-(t)$, of $\Phi^-(\omega)$ can be obtained by applying a discrete inverse Fourier transform routine on the elements of $\Phi^-(\omega)$, as described in the previous section. With the time delays and weights of each element that make up $\phi^-(t)$ known, the recursive formulation of (4.5) and (4.6) can then be obtained.

In the frequency domain, each element of $\Phi^-(\omega)$ can be approximated with a sum of weighted scalar phase shifts as written below,

$$\Phi_{ij}^-(\omega) = \sum_{k=1}^{n} w_{ijk} e^{-j\omega\tau_k} \tag{4.32}$$

where n is the number of phase conductors of the system, w is the weight of each impulse and τ_k is the approximation of the time delay of the k'th impulse. Each τ_k can be regarded as equivalent to the modal travel times of the system.

With experience, the values of w_k and τ_k in (4.32) can be determined in the frequency domain, in a 'trial and error' fashion, with relative ease. In the time domain this corresponds to a sum of scalar impulse functions, $\delta(t-\tau_k)$. It should be noted that a discrete inverse Fourier transform need not be applied to transform each approximating function into the time domain. In order to ascertain whether the sum of weighted phase shifts are an accurate approximation for each corresponding element of $\Phi^-(\omega)$ it is sufficient to observe both the functions in the frequency domain. If the approximation is sufficiently accurate as a function of frequency, then the corresponding time domain form of both functions will exhibit a similar degree of accuracy. This saves a considerable amount of computational effort, given the time required to perform the inverse Fourier transform with a sufficiently high degree of accuracy.

In order to compliment the above comments, consider the following example pertaining to the 345kV single-circuit transmission line system described earlier in section 3.5.1 (c.f. Figure 3.4). The line is taken to be 398km in length and is assumed untransposed in this example. The PDTT function, τ, is evaluated at 1MHz, using the algorithm described in section 4.4.2.1. As with previous examples, the order of the Padé approximant is taken to be p=3.

Four elements of the time domain form of the negative phase shift function, $\phi^-(t)$, are shown in Figure 4.8. Also, superimposed on the exact functions are the approximations using scalar impulse functions. In order to highlight the accuracy of the time domain

approximation of each element of $\Phi^{-}(\omega)$, the scalar impulse functions are also transformed into the time domain using an inverse Fourier transform routine. Although, as stated above, in practice this is not required. From Figure 4.8, the accuracy of each approximation can be seen to be very good. For the diagonal elements presented, three weighted impulses are clearly visible, however the magnitude of the first impulse in both cases is much less than that of the remaining two.

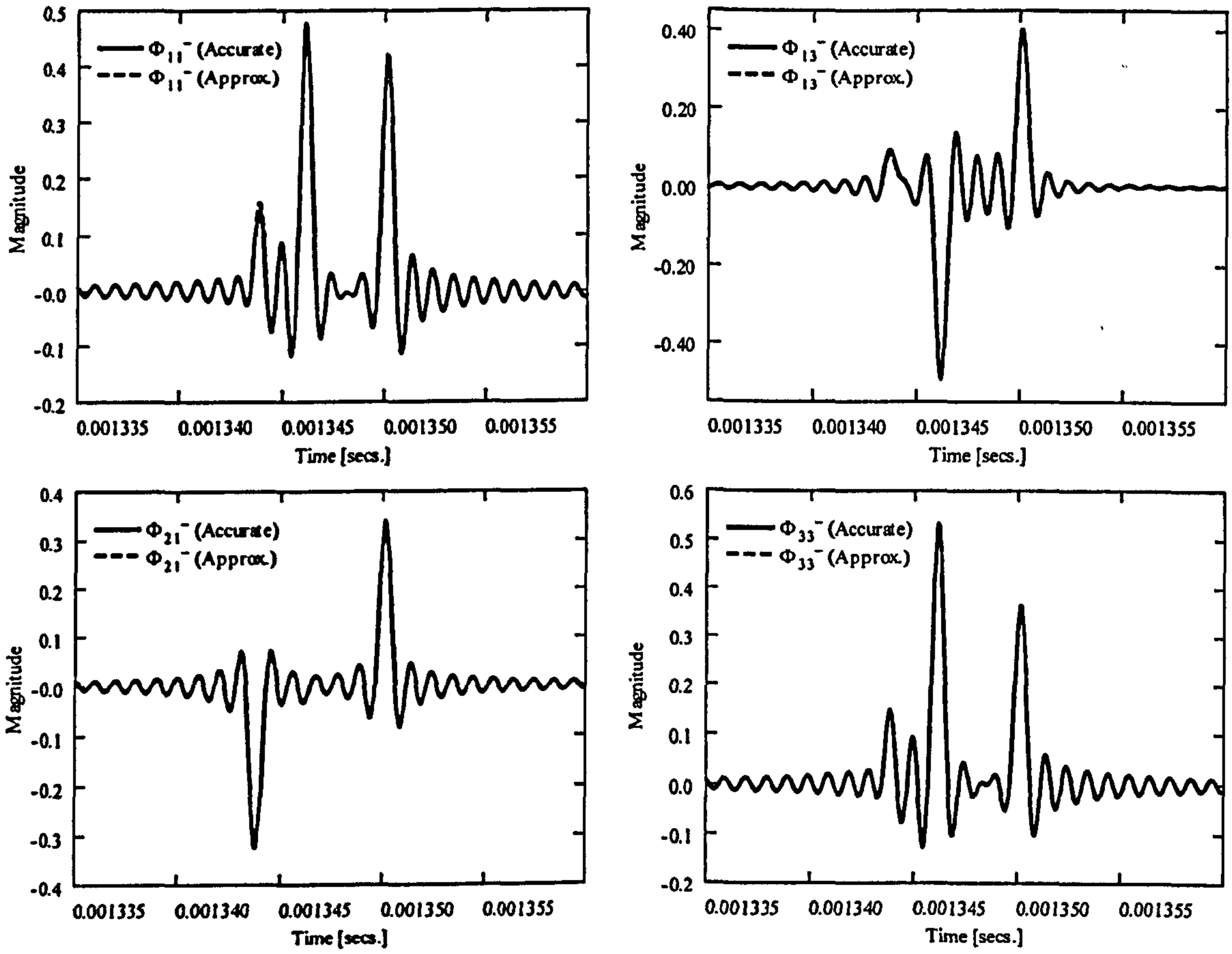

Figure 4.8. Approximation of the elements of $\phi^{-}(t)$ in the time domain with scalar impulse functions, for a single-circuit transmission line

For element $\phi_{13}^{-}(t)$, three impulses can be observed, again the magnitude of the first impulse is very small compared to the two subsequent impulses. Finally, for element $\phi_{21}^{-}(t)$, two impulses are can be observed. In this case, the magnitude of the third impulse can be assumed negligible

4.7 Synthesis of the Wave Propagation Matrix H(ω)

After multiplication of the matrix phase shift function, $\Phi(\omega)$, the elements of the shifted wave propagation matrix, $\mathbf{P}(\omega)$, are obtained as relatively smooth functions of frequency and can be synthesized using comparatively low-order rational functions.

In the following section, the results of fitting $\mathbf{P}(\omega)$ with rational functions using the method of Vector Fitting [22] are presented. As for the case of the characteristic admittance matrix, each individual column of the matrix is approximated by the same set of poles, only the residues for each element differ. This leads to a 2-fold increase in efficiency in the time domain formulation as compared to element-by-element fitting [11].

The results described below correspond to a 220kV double-circuit transmission line configuration. The line is 152.90km in length. The physical data for the transmission system can be found in Appendix III. The double-circuit transmission line system has been illustrated previously in section 4.3.3 (c.f. Figure 4.2).

4.7.1 Double-Circuit Transmission Line Configuration

Figures 4.9 and 4.10 show the magnitude and phase angle of columns 1, 3, 4 and 6, respectively, of $\mathbf{P}(\omega)$ for the vertical double-circuit line configuration shown in Figure 4.2, when each column is approximated by a 39th order rational function using the method of Vector Fitting. The approximated results are superimposed on the accurate results, as calculated using the algorithm described in section 3.6.6. The starting poles used in the fitting process are, for all columns of $\mathbf{P}(\omega)$, real and negative, logarithmically distributed between 1Hz and 1MHz.

As can be seen from Figures 4.9 and 4.10, a high degree of accuracy is achieved for each column of the matrix $\mathbf{P}(\omega)$, for both the magnitude and the phase angle. A similar level of accuracy is obtained for the remaining columns (2 and 5) of $\mathbf{P}(\omega)$ (not shown). Real and complex conjugated poles are obtained for all the elements of $\mathbf{P}(\omega)$, with the complex conjugated poles arising in the high frequency range.

4.8 Evaluation of the Phase Domain Convolution Integrals

As discussed previously, the computationally efficiency of the time domain model can be significantly increased if the numerical convolutions of (4.3)-(4.6) are formulated in a recursive manner. This is achieved in this research by fitting the elements of both the characteristic admittance and wave propagation matrices with rational functions using the method of Vector Fitting [22]. The recursive evaluation of the characteristic admittance function has already been addressed in section 4.3.4 and Appendix I. The following section therefore concentrates on the evaluation of the convolution integrals involving the wave propagation matrix, namely (4.5) and (4.6).

A sum of exponentials is obtained in the time domain if the fitting of the wave propagation matrix [4] (after the matrix phase shift has been applied as in (4.17)) is performed in the frequency domain using rational functions. With $\mathbf{h}(t)$ approximated in this way, it is shown in Appendix I that the matrix-vector convolution of the wave propagation matrix and the forcing function $\mathbf{f}(t)$, can be evaluated recursively as,

$$\mathbf{h}(t) * \mathbf{f}(t) = \xi(t) = \mathbf{J}_b(t) \tag{4.33}$$

where $\mathbf{J}_b(t)$ is a vector of past history determined from previous values of $\mathbf{f}(t)$ and $\xi(t)$. The convolution between the ij^{th} element of $\mathbf{h}(t)$ and the first element of the forcing function, $\mathbf{f}(t)$, can be expressed as

$$h_{ij}(t) * f^a(t) = \xi(t) = J_{b_{ij}}(t) \tag{4.34}$$

where,

$$J_{b_{ij}}(t) = \sum_{k=1}^{n}\sum_{m=1}^{N}\sum_{l=1}^{n} w_{ik_l} c_{kj_m} \left[\alpha_m \xi_{ij_l}(t-\Delta t) + \beta_m f^a(t-\tau_l) + \gamma_m f^a(t-\tau_l-\Delta t)\right] \tag{4.35}$$

The coefficients α_m, β_m and χ_m are constants that depend on the time step, Δt, for a given simulation [14], w corresponds to the weight of the respective scalar phase shift, and c_m are the residues for the ij^{th} element of $\mathbf{h}(t)$, obtained from the rational function approximation. Again, note that (4.35) is determined completely by past values of ξ

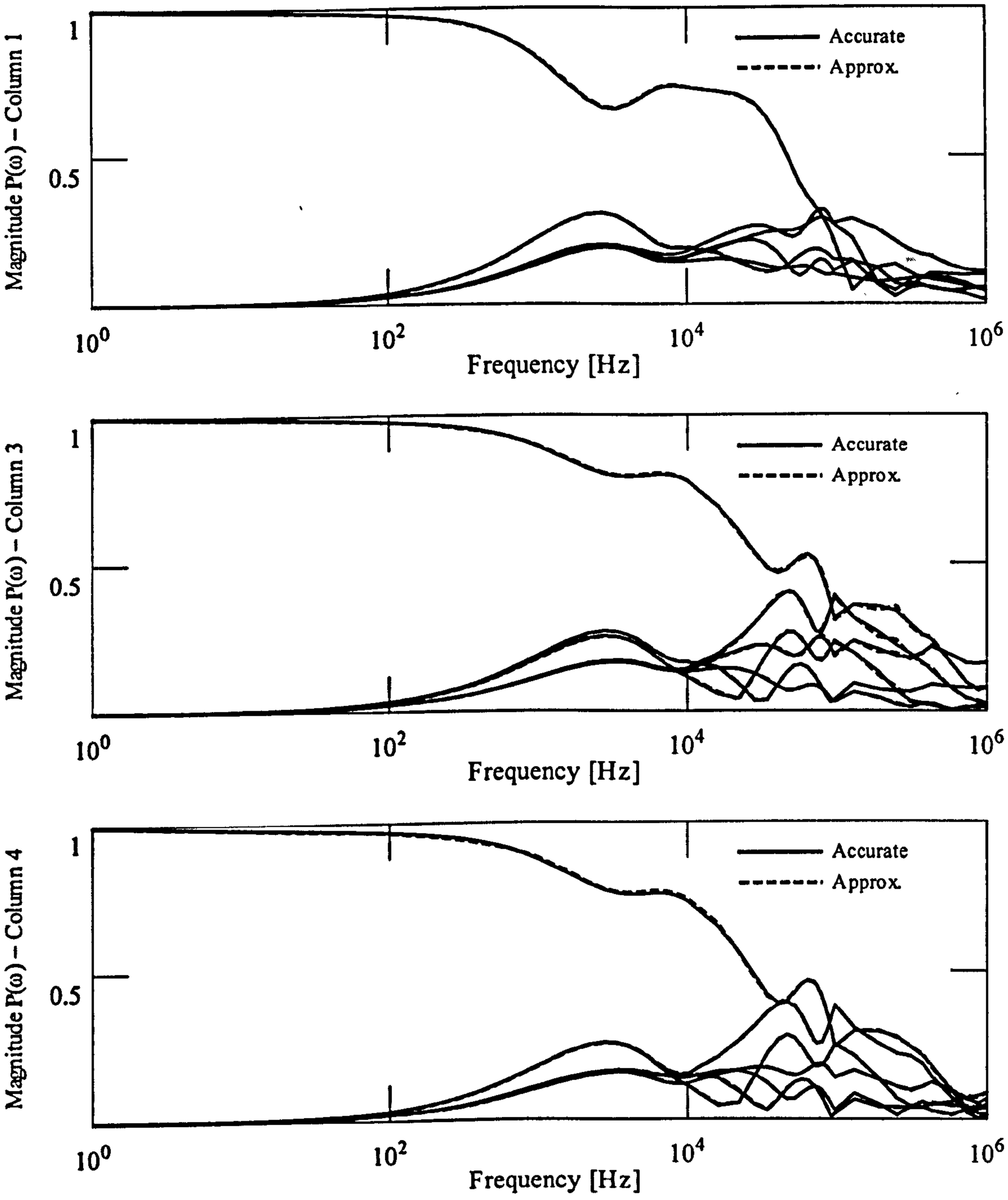

Figure 4.9. Magnitude of elements of P(ω) for columns 1, 3 ,4 and 6 for a double-circuit line

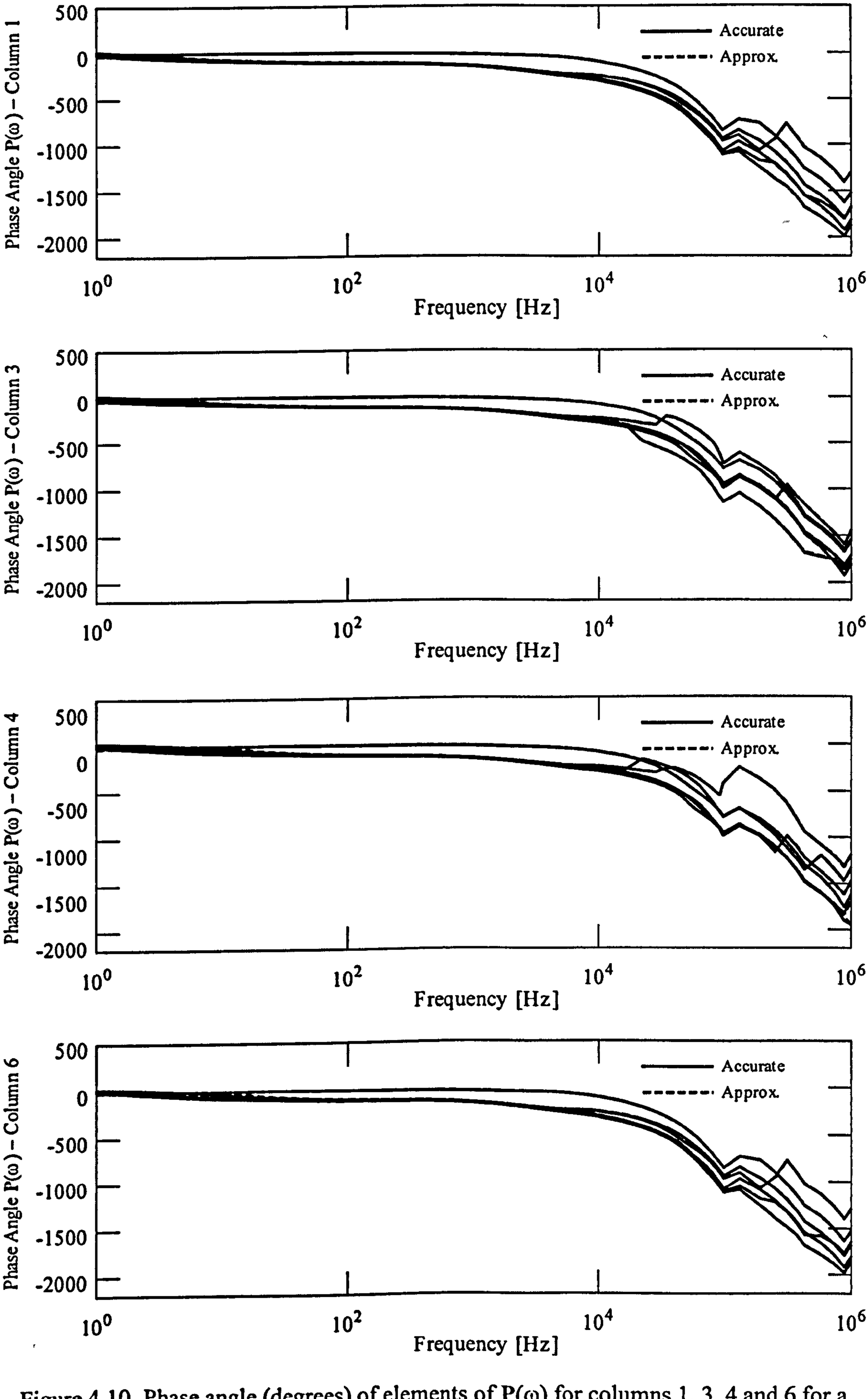

Figure 4.10. Phase angle (degrees) of elements of P(ω) for columns 1, 3, 4 and 6 for a double-circuit line

and $f^a(t)$. More detail of the derivation of (4.34) and (4.35) can be found in Appendix I.

Substituting (4.33) into (4.5) and (4.6) gives the following expression for the nodal equations, (4.3) and (4.4), at each end of the line,

$$\mathbf{i}_1(t) = \mathbf{y}_{eq}\mathbf{v}_1(t) - \overline{\overline{\mathbf{J}}}_1(t) \tag{4.36}$$

$$\mathbf{i}_2(t) = \mathbf{y}_{eq}\mathbf{v}_2(t) - \overline{\overline{\mathbf{J}}}_2(t) \tag{4.37}$$

where,

$$\overline{\overline{\mathbf{J}}}_1(t) = \mathbf{J}_{b1}(t) - \mathbf{J}_{a1}(t) \tag{4.38}$$

$$\overline{\overline{\mathbf{J}}}_2(t) = \mathbf{J}_{b2}(t) - \mathbf{J}_{a2}(t) \tag{4.39}$$

4.8.1 Final Time Domain Equivalent Circuit

As discussed in section 4.3.4, equation (4.36)-(4.39) can be represented in the time domain by a constant admittance in parallel with a time dependent current source, i.e. a Norton equivalent circuit, as illustrated in Figure 4.11.

Figure 4.11 represents the complete equivalent circuit representation of the newly developed phase domain transmission line model. With the model represented in this form, it can be introduced into general electromagnetic transient programs such as EMTP [21], based on a time dependent current source in parallel with a constant admittance. As stated previously, the constant equivalent admittance, $\mathbf{y}_{eq}$, is included in the network admittance matrix before the time domain simulation is executed.

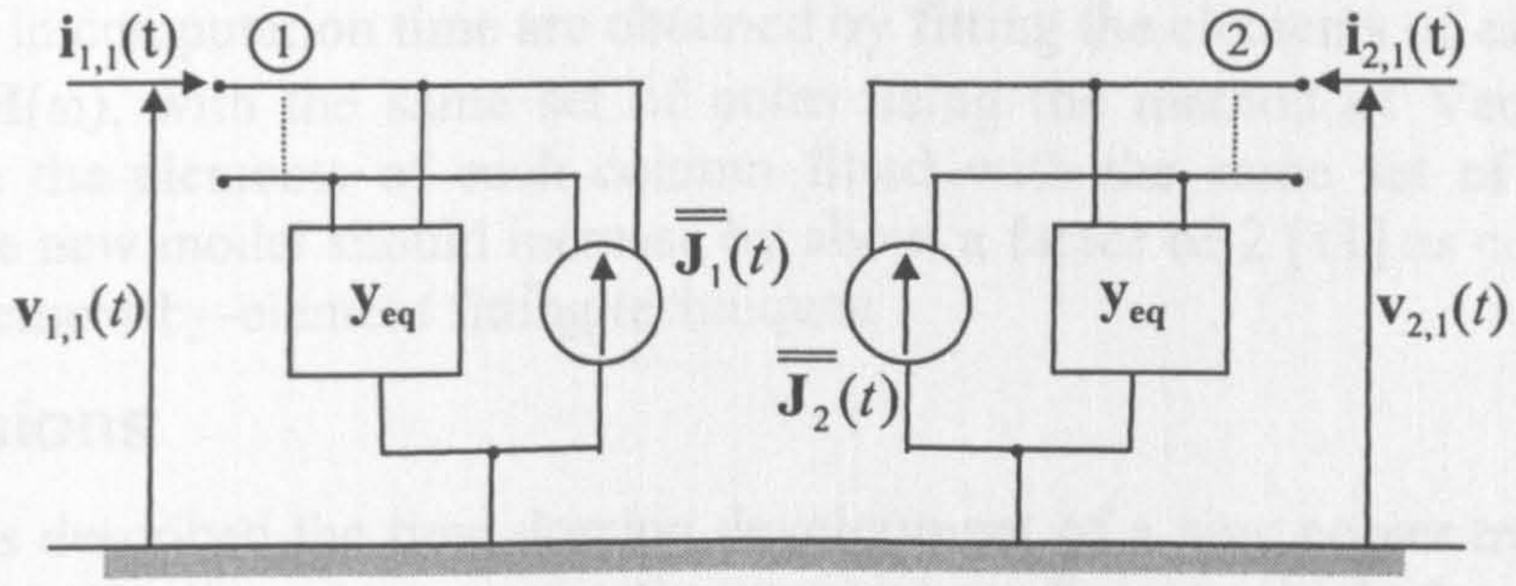

Figure 4.11 Norton equivalent representation for the phase domain transmission line model

4.8.2 Scalar Impulse Grouping

The phase domain convolutions involving the wave propagation matrix requires evaluation of n^3 scalar convolutions per line end. An additional n^2 convolutions are required for the characteristic admittance matrix, giving a total of (n^3+n^2) convolution operations per line end in the new model. For comparison, there are $(2n^2+2n)$ convolutions per line end in the modal domain model of [17] where the frequency-dependent transformation matrix is also approximated with rational functions. Using a constant transformation matrix, this is further reduced to $2n$ convolutions per line end [14]. Phase domain transmission line models using a common scalar phase shift to unwind the elements of the wave propagation function utilize $2n^2$ convolutions per line end.

However, in practice, the actual number of convolutions required to evaluate (4.5) and (4.6), is likely to be less than this maximum value. The time domain form, $\phi^{-}(t)$, of the negative phase shift function has been described and illustrated previously in section 4.6. Each element of $\phi^{-}(t)$ can be seen to be composed of a series of weighted impulses (c.f. Figures 4.7 and 4.8). The time delay of each impulse can be regarded as equivalent to the modal travel times of the system. If a group of travel times for a given system have a similar magnitude, then it is likely that the number of impulses observable will be less than that anticipated.

For an n conductor system, n weighted impulses should be anticipated in the time domain form of the negative phase shift function. However, a reduced number of weighted impulses will generally occur when one of the following situations arises:

1) A single impulse within a confluent group is dominant, in terms of the magnitude of its corresponding weight. In such cases, the remaining impulses will, in general, have negligible weights and for the purposes of analysis can be assumed zero.

2) If the travel times are very similar in magnitude the impulses will, in general, be lumped together, so that a reduced number of impulses are visible.

If either one of the above situations manifests itself, then it can generally be assumed that the number of scalar convolutions required to evaluate (4.5) and (4.6) will be less than n^3. This is illustrated in Figure (4.7) for a double-circuit line configuration. The number of weighted impulses expected in this case is six. However, for the diagonal elements, only three impulses are visible. A similar situation arises for the off-diagonal elements, where three peaks are evident. The remaining impulses in this case can be assumed negligible, without loss of accuracy. The computational efficiency of the proposed line model in these cases can therefore be expected to improve considerably.

Further savings in computation time are obtained by fitting the elements of each column of $\mathbf{Y}_c(\omega)$ and $\mathbf{H}(\omega)$, with the same set of poles using the method of Vector Fitting [1,18,22]. With the elements of each column fitted with the same set of poles, the efficiency of the new model should increase by about a factor of 2 [11] as compared to conventional element-by-element fitting techniques.

4.9 Conclusions

This chapter has described the time domain development of a new power transmission line model for conducting electromagnetic transient studies in which the analysis is undertaken entirely in frame of reference of the phases.

Both the characteristic admittance matrix, $\mathbf{Y}_c(\omega)$, and the wave propagation matrix, $\mathbf{H}(\omega)$, have been approximated with rational functions in the frequency domain using the method of Vector Fitting. The elements of $\mathbf{Y}_c(\omega)$ are in general smooth throughout the entire frequency range of interest and can therefore be approximated with low-order rational functions. However, for multi-conductor transmission systems, one of the main difficulties in conducting the analysis directly in the phase domain concerns the unwinding of the elements of $\mathbf{H}(\omega)$. Unlike the characteristic admittance, the elements of the wave propagation matrix exhibit a highly oscillatory behaviour in the frequency domain due to the time delays of the line. These oscillations must be removed from $\mathbf{H}(\omega)$ before the fitting process is undertaken in order to fit the elements of $\mathbf{H}(\omega)$ using relatively low-order rational functions.

The elements of $\mathbf{H}(\omega)$ have a series of travel times associated with them, due to the coupling between the phase conductors. In general, each coupled time delay will be associated with a different travel time. Therefore, unwinding the elements of $\mathbf{H}(\omega)$ with

a common, scalar phase shift corresponding to the fastest mode of the system (as is undertaken in current phase domain models) will not completely remove these oscillations.

In order to overcome these difficulties, a *matrix* phase shift function has been proposed to unwind the elements $\mathbf{H}(\omega)$ directly in phase co-ordinates. The coupled time delays of the line are intrinsically taken into account when the analysis is undertaken in the phase domain. The elements of the resulting shifted wave propagation matrix, $\mathbf{P}(\omega)$, are obtained as relatively smooth functions of frequency and can therefore be approximated using relatively low-order rational functions.

In the time domain, the approximation of the original wave propagation matrix is returned by assigning the appropriate time delays to the elements of $\mathbf{p}(t)$. At this point in time, a drawback with this approach is that in order to determine the appropriate coupled time delays, a negative phase shift function must be evaluated and transformed into the time domain using a discrete inverse Fourier transform routine. The corresponding time delays associated with each element of $\phi^{-}(t)$ can then be approximated in the time domain by weighted scalar impulse functions.

The final phase domain transmission line model can be implemented in general purpose electromagnetic transient programs, such as EMTP, by means of a Norton equivalent representation.

Notwithstanding its many advantages, the computational efficiency of the proposed method is less than that of existing methods (with the possible exception of [11]) since additional convolutions are required to be performed. However, in most cases, the number of convolutions involving the wave propagation matrix will be less than the maximum expected since travel time grouping reduces the number of time delayed impulses. Additional time savings are obtained because a columnwise realization for $\mathbf{H}(\omega)$ is utilized.

4.10 References

[1] Gustavsen, B. and Semlyen, A.: 'Combined Phase and Modal Calculation of Transmission Line Transients Based on Vector Fitting', IEEE Transactions on Power Delivery, Vol. 13, No. 2, April 1998, pp. 596-604.

[2] Gustavsen, B., Sletbak, J., and Henriksen, T.: 'Calculation of Electromagnetic Transients in Transmission Line Cables and Lines Taking Frequency Dependent Effects Accurately Into Account', IEEE Transactions on Power Delivery, Vol. 10, No. 2, April 1995, pp. 1076-1084.

[3] Nguyen, H. V., Dommel, H. W. and Marti, J. R.: 'Direct Phase Domain Modelling of Frequency-Dependent Overhead Transmission Lines', IEEE Transactions on Power Delivery, Vol. 12, No. 3, July 1997, pp. 1335-1342.

[4] Nguyen, H.: 'Simulation of Lightning Surges on Transmission Lines', PhD Thesis, The University of British Columbia, Canada, February 1996.

[5] Castellanos, F. and Marti, J. R.: 'Phase-Domain Multiphase Transmission Line Models', International Conference on Power System Transients, Lisbon, 3-7 September 1995.

[6] Castellanos, F., Marti, J. R. and Marcano, F.: 'Phase-Domain Multiphase Transmission Line Models', Electrical Power & Energy Systems, Vol. 19, No. 4, 1997, pp. 241-248.

[7] Noda, T., Nagaoka, N. and Ametani, A.: 'Phase Domain Modeling of Frequency-Dependent Transmission Lines by Means of an ARMA Model', IEEE Transactions on Power Delivery, Vol. 11, No. 1, January 1996, pp. 401-411.

[8] Noda, T., Nagaoka, N. and Ametani, A.: 'Further Improvements to a Phase-Domain ARMA Line Model in Terms of Convolution, Steady-State Initialization, and Stability', IEEE Transactions on Power Delivery, Vol. 12, No. 3, July 1997, pp. 1327-1334.

[9] Angelidis, G. and Semlyen, A.: 'Direct Phase-Domain Calculation of Transmission Line Transients Using Two-Sided Recursions', IEEE Transactions on Power Delivery, Vol. 10, No. 2, April 1995, pp. 941-949.

[10] Gustavsen, B: 'A Study of Overvoltages in High Voltage Cables With Emphasis on Sheath Overvoltages', Dr. Ing. Thesis, The Norwegian Institute of Technology, Trondheim, Norway, 1993.

[11] Morched, A., Gustavsen, B. and Tartibi, M.: 'A Universal Model for Accurate Calculation of Electromagnetic Transients on Overhead Lines and Underground Cables', IEEE Transactions on Power Delivery, Vol. 14, No. 3, July 1999, pp. 1032-1038.

[12] Soysal, A. O. and Semlyen, A.: 'State Equation Approximation of Transfer Matrices and its Applications to the Phase Domain Calculation of Electromagnetic Transients', IEEE Transactions on Power Systems, Vol. 9, No. 1, February 1994, pp. 420-428.

[13] Castellanos, F. and Marti, J. R.: 'Full Frequency-Dependent Phase-Domain Transmission Line Model', IEEE Transactions on Power Systems, Vol. 12, No. 3, August 1997, pp. 1331-1339.

[14] Marti, J.: 'Accurate Modelling of Frequency-Dependent Transmission Lines in Electromagnetic Transient Simulations', IEEE Transactions on Power Apparatus and Systems, Vol. PAS-101, No. 1, January 1982, pp. 147-157.

[15] Marti, J.: 'The Problem of Frequency Dependence in Transmission Line Modelling', PhD Thesis, The University of British Columbia, Canada, April 1981.

[16] Marti, L.: 'Simulation of Electromagnetic Transients in Underground Cables with Frequency-Dependent Modal Transformation Matrices', PhD Thesis, The University of British Columbia, Canada, November 1986.

[17] Marti, L.: 'Simulation of Transients in Underground Cables with Frequency-Dependent Modal Transformation Matrices', IEEE Transactions on Power Delivery, Vol. 3, No. 3, July 1988, pp. 1099-1110.

[18] Gustavsen, B. and Semlyen, A.: 'Simulation of Transmission Line Transients Using Vector Fitting and Modal Decomposition', IEEE Transactions on Power Delivery, Vol. 13, No. 2, pp. 605-614.

[19] Ametani, A.: 'A Highly Efficient Method for Calculating Transmission Line Transients', IEEE Transactions on Power Apparatus and Systems, Vol. PAS-95, No. 5, September/October 1976, pp. 1545-1551.

[20] Semlyen, A. and Dabuleanu, A.: 'Fast and Accurate Switching Transient Calculations on Transmission Lines with Ground Return Using Recursive Convolutions', IEEE Transactions on Power Apparatus and Systems, Vol. PAS-94, No. 2, March/April 1975, pp. 561-571.

[21] Dommel, H. W.: 'Electromagnetic Transients Program (EMTP) Rule Book', EPRI EL6421-1, Vol. 1, June 1989.

[22] Gustavsen, B. and Smelyen, A.: 'Rational Approximation of Frequency Domain Responses by Vector Fitting', IEEE Transactions on Power Delivery, Vol. 14, No. 3, July 1999, pp. 1052-1061.

[23] Higham, N. J.: 'The Matrix Sign Decomposition and its Relation to the Polar Decomposition', Linear Algebra and its Applications, Vol. 212/213, 1994, pp. 3-20.

[24] Higham N. J.: 'Stable Iterations for the Matrix Square Root', Numerical Algorithms, Vol. 15, No. 2, 1997, pp. 227-242.

[25] Kenney, C. and Laub, A. J.: 'The Matrix Sign Function', IEEE Transactions on Automatic Control, Vol. 40, No. 8, August 1995, pp. 1330-1348.

[26] Moler, C. and Van Loan, C.: 'Nineteen Dubious Ways to Compute the Matrix Exponential', SIAM Review, Vol. 20, No. 4, October 1978, pp. 801-836.

[27] Golub, G. and Van Loan, C. F.: 'Matrix Computations', The John Hopkins University Press, Second Edition, 1989.

[28] Ward, R. C.: 'Numerical Computation of the Matrix Exponential with Accuracy Estimate', SIAM Journal on Numerical Analysis, Vol. 14, No. 4, September 1977, pp. 600-610.

CHAPTER 5

TIME DOMAIN SIMULATIONS

This chapter is concerned with the time domain testing of the new phase domain model of power transmission lines suitable for conducting electromagnetic transient studies. The development of this phase domain model has been the theme of the previous two chapters. The model is formulated entirely in phase co-ordinates such that any geometric imbalances inherent in the line are automatically taken into account. The attenuation and distortion of the waves as they propagate along the line over a resistive ground are taken into account by fitting the transmission line responses as a function of frequency with rational functions using the method of Vector Fitting. The frequency-dependent nature of these functions is then included in the time domain simulation through convolutions between the line end quantities and the impulse responses. The model is finally incorporated within general purpose electromagnetic transient programs by means of a time dependent vector of current sources in parallel with a constant admittance matrix. This chapter details the simulation of a sequential energization of a real-life transmission circuit. The results obtained from the newly developed phase domain line model are compared against those obtained using frequency-independent and frequency-dependent transmission lines based on a modal decomposition methodology. The results compare favourably with available field measurements and highlight the accuracy attained when conducting the analysis entirely in phase co-ordinates.

5.1 Introduction

The formulation of a new phase domain model suitable for analysing electromagnetic transient phenomena arising in power transmission lines has been the main theme of the previous two chapters. The application of this phase domain transmission line for time domain simulations is the subject of this chapter.

Conducting the analysis entirely in the frame of reference of the phases has a number of advantages. Firstly, since the rest of the network is represented in phase co-ordinates, there is no requirement to introduce frequency-dependent modal decompositions [23,24] at any point in the analysis. However, all the phase domain models presented in the open literature thus far, make use of the modal domain at some stage in the initial formulation of the problem in the frequency domain [9-21]. The phase domain aspect of these models concerns the final time domain simulations. The models can therefore be regarded as a mixture of the phase and modal methodologies.

Formulating the problem directly in the phase domain also avoids any problems that might arise when the governing coupled equations describing the propagation of the travelling waves along the transmission line are non-diagonalizable, at which point conventional modal decomposition theory breaks down [4,5]. In such cases, a more generalised approach must be taken which involves the use of Jordan Decompositions [4,5].

The frequency domain data (the series impedance and shunt admittance) required to evaluate the transfer functions that may characterise a given line, namely the

characteristic admittance and the wave propagation matrices [19,20], is initially obtained directly in phase co-ordinates. Thus, since from this point forward the analysis remains in this frame of reference, any geometric imbalances that are naturally present in the original frequency domain data are inherently taken into account throughout the rest of the model formulation.

The ability to incorporate these imbalances is important, for example, when simulating transient overvoltages arising from the sequential energization of an overhead line [1]. The mutual coupling that exists between phase conductors can impinge on the magnitude and wave-shape of the transient overvoltages produced during such disturbances in the power network. The magnitude of induced voltages that may appear on the still open phases of the line during energization [1] are dependent upon the values of the off-diagonal terms of the characteristic impedance matrix, which is in turn dependent upon the spacing and configuration of the phase conductors [25-28].

This chapter presents the results of a sequential energization of a real-life 345kV single-circuit transmission network, obtained for the newly developed phase domain transmission line model and compared against those obtained using frequency-independent [2,3] and frequency-dependent [6,7] methods incorporating modal decomposition methodology [23,24]. Both models have been described previously in chapter two.

The 345kV single-circuit transmission system has been chosen since actual field measurements are available [8] with which to assess the accuracy of the proposed phase domain model. The results are shown to be in good agreement with these field measurements, and highlight the improved accuracy attained with this methodology as compared to those of conventional modal approaches that assume the transformation matrices are at a constant frequency.

5.2 Time Domain Implementation

The phase domain transmission line model that has been described over the previous two chapters has been written as a computer program for the purpose of testing the model in time domain electromagnetic transient simulations. As with previous models, the FORTRAN programming language has been adopted to provide a convenient means to export the phase domain transmission line model into the simulation environment required for real-time model execution. The incorporation of this model for real-time digital simulations is discussed in the next chapter.

The newly developed phase domain transmission line model can be embedded in a simulated power network in which the elements are represented as time dependent current sources in parallel with a constant admittance, in accordance with the approach in the EMTP [2,3]. The line model is then introduced into this network model using a Norton equivalent circuit, as discussed earlier in section 4.8.1 (c.f. Figure 4.11).

5.3 Sequential Energization Test

In the following section the calculated results of a sequential energization of the 345kV Jaguara-Taquaril power transmission system in the State of Minas Gerais, Brazil are presented. The transmission system is illustrated in Figure 5.1. The single-circuit transmission line is 398km in length and for the case of the frequency-independent and frequency-dependent transmission line models, it is assumed transposed. The transformation from phase to modal components and vice-versa is undertaken using the Karrenbauer transformation matrix (see section 2.2.2.1). Details of the transmission system can be found in Appendix III [8,29].

The contacts of the circuit breakers are closed during the energization according to the sequence given Table III.1 of Appendix III. The line parameters for the frequency-independent models are calculated as given in Table III.2, also shown in Appendix III. In this case, the earth is assumed homogeneous with a resistivity of 100Ωm.

The simulated transient voltages presented in this chapter have all been obtained assuming a time step of 34μs.

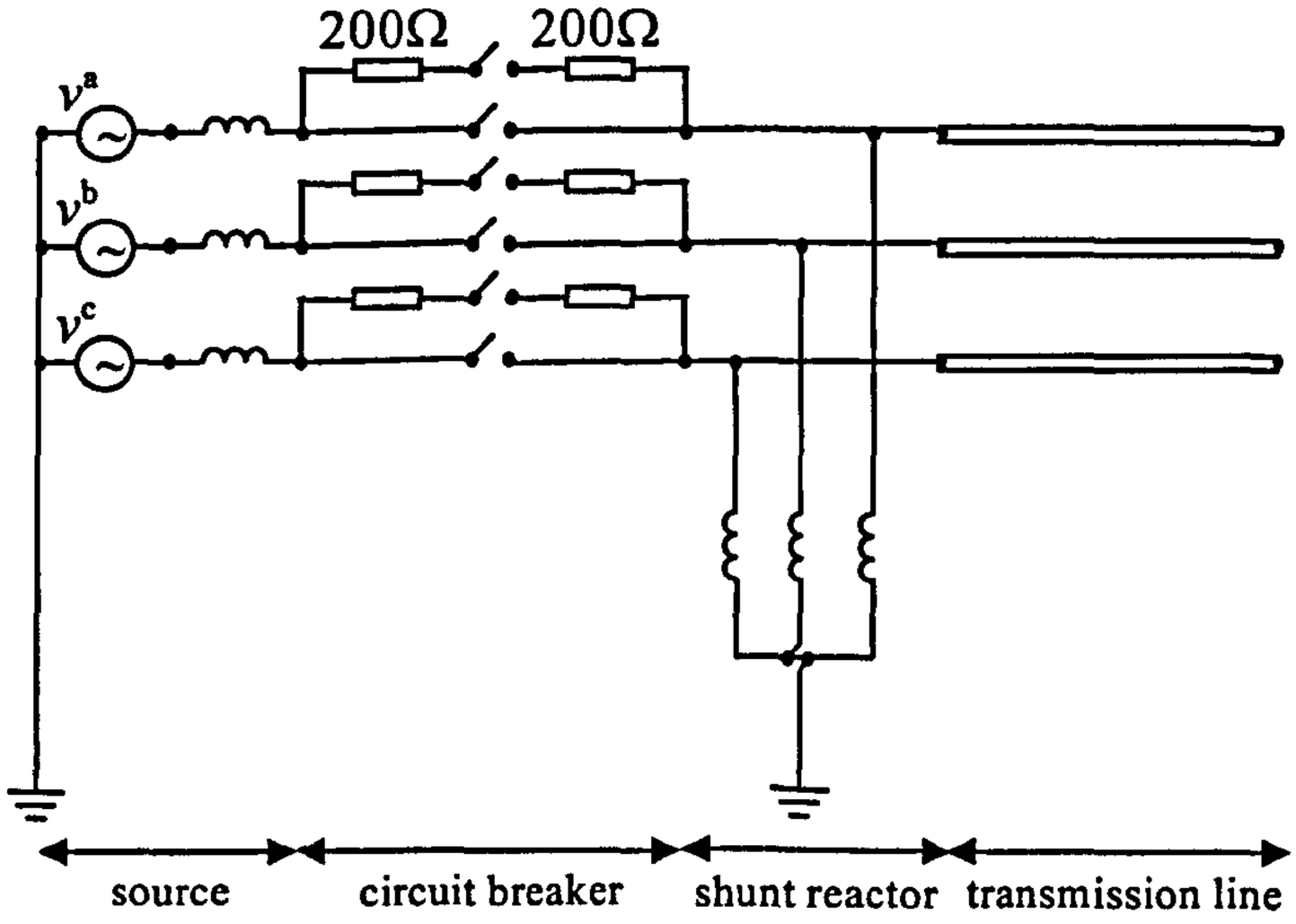

Figure 5.1. Jaguara-Taquaril 345kV transmission system

5.3.1 Order of the Rational Function Approximations

The order of the rational function approximations used to approximate the frequency domain variation of the line responses for the frequency-dependent and phase domain transmission line models are summarised in Tables 5.1 and 5.2, respectively. The frequency responses are calculated in the interval 10^{-2}Hz-10^{6}Hz.

The method of Vector Fitting [22] has been used to obtain the rational function approximations of the line responses for both models. In the case of the phase domain model, the characteristic admittance, $\mathbf{Y}_c(\omega)$, and the shifted wave propagation function, $\mathbf{P}(\omega)$, are approximated in the phase domain. The elements in each column of these matrices are fitted with the same set of poles, only the value of the residues for each element of a column differs in magnitude. This columnwise realization is expected to bring about a 2-fold increase in the computational efficiency of the time domain model when evaluating the time domain matrix-vector convolutions, as compared to element-by-element fitting [19].

Table 5.1. Summary of the approximation orders for $\mathbf{Z}_c(\omega)$ and $\mathbf{P}(\omega)$

Mode	$\mathbf{Z}_c(\omega)$	$\mathbf{P}(\omega)$
Zero	12	12
Positive	12	12

Table 5.2. Summary of the approximation orders for $\mathbf{Y}_c(\omega)$ and $\mathbf{P}(\omega)$

Column	$\mathbf{Y}_c(\omega)$	$\mathbf{P}(\omega)$
1	10	35
2	10	35
3	10	35

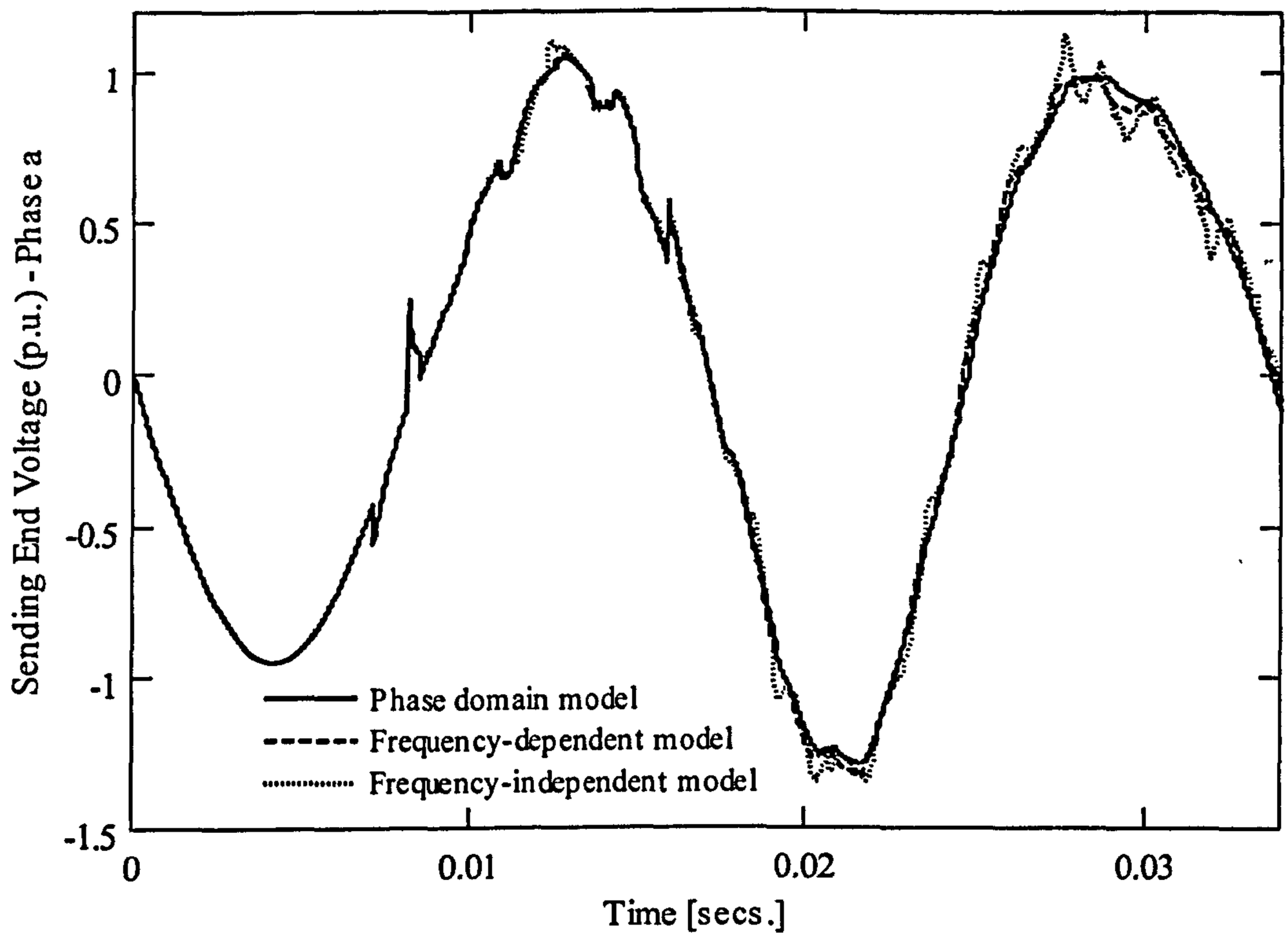

Figure 5.2. Sending end voltage after simulated sequential energization - Phase a

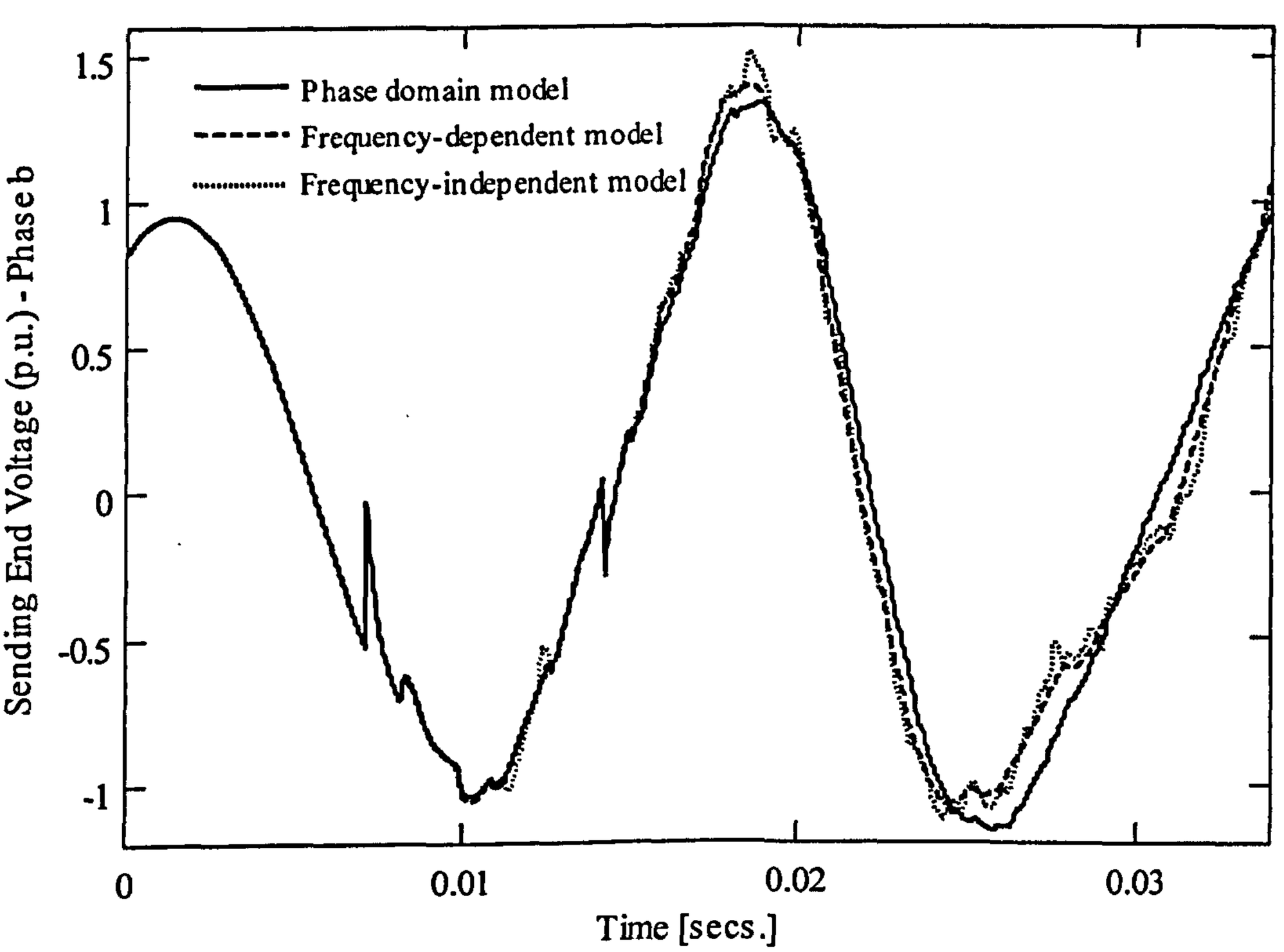

Figure 5.3. Sending end voltage after simulated sequential energization - Phase b

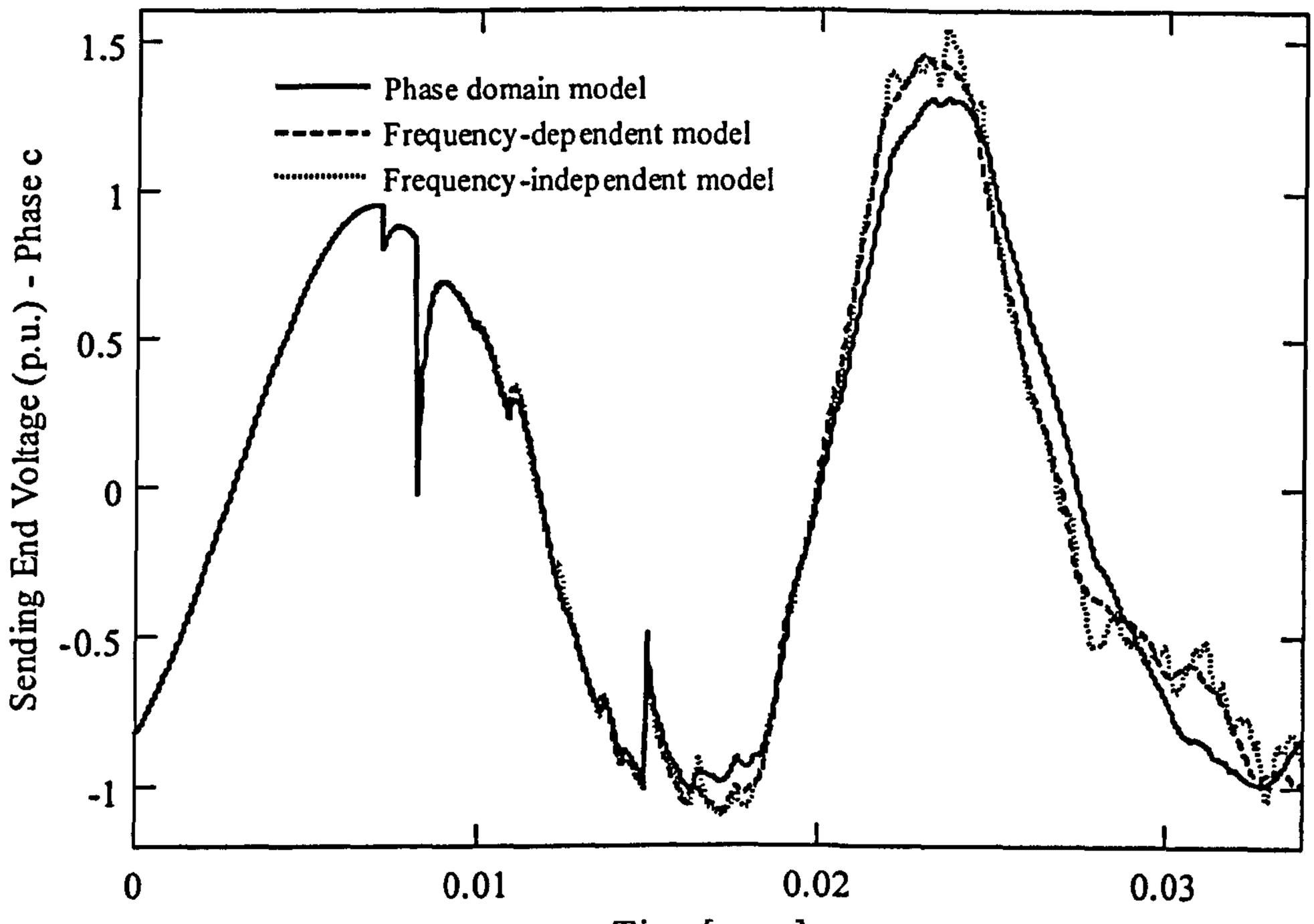

Figure 5.4. Sending end voltage after simulated sequential energization - Phase c

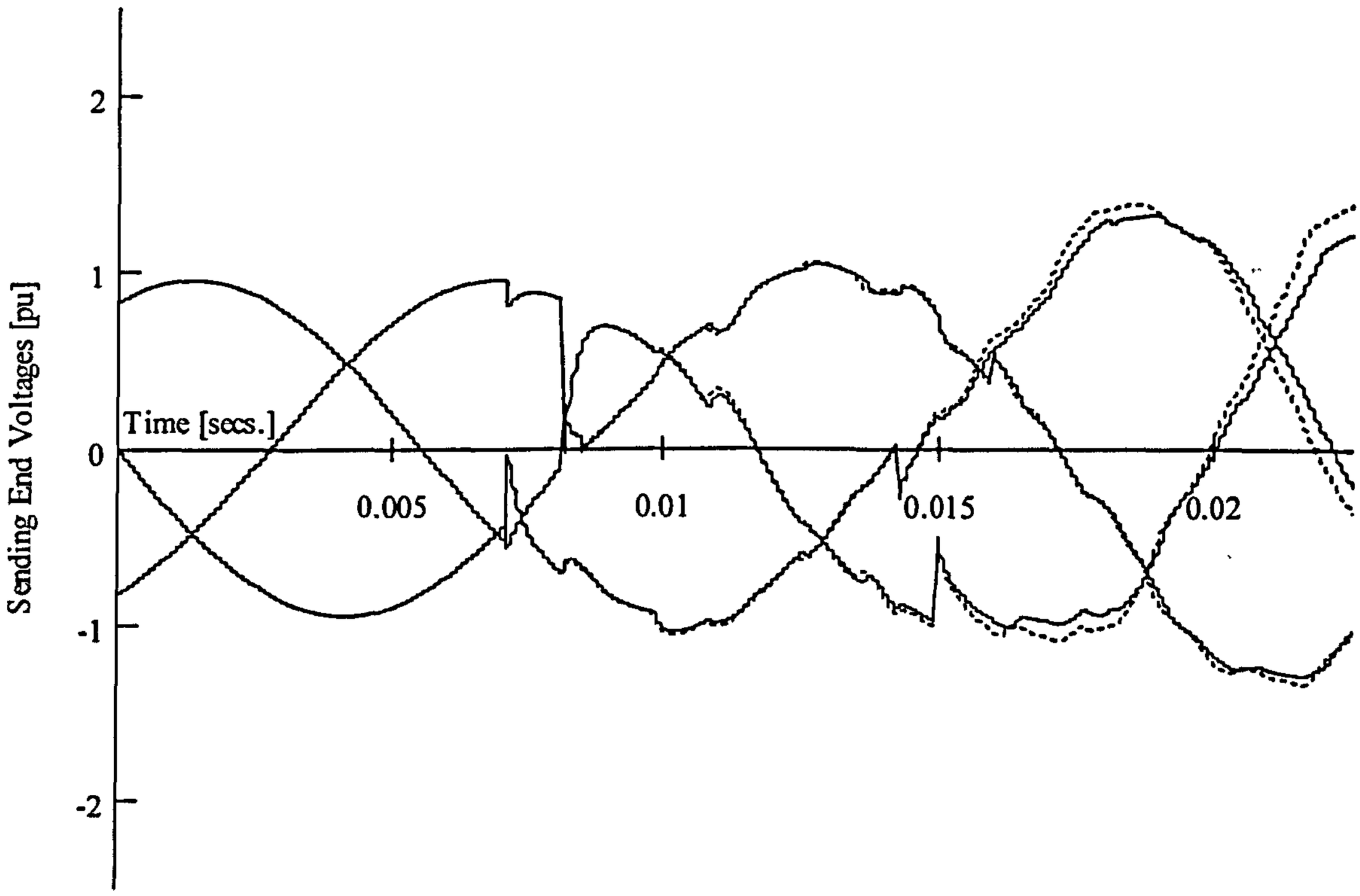

Figure 5.5 Sending end voltages after simulated sequential energization for phase domain model (solid line) and frequency-dependent model (dashed line)

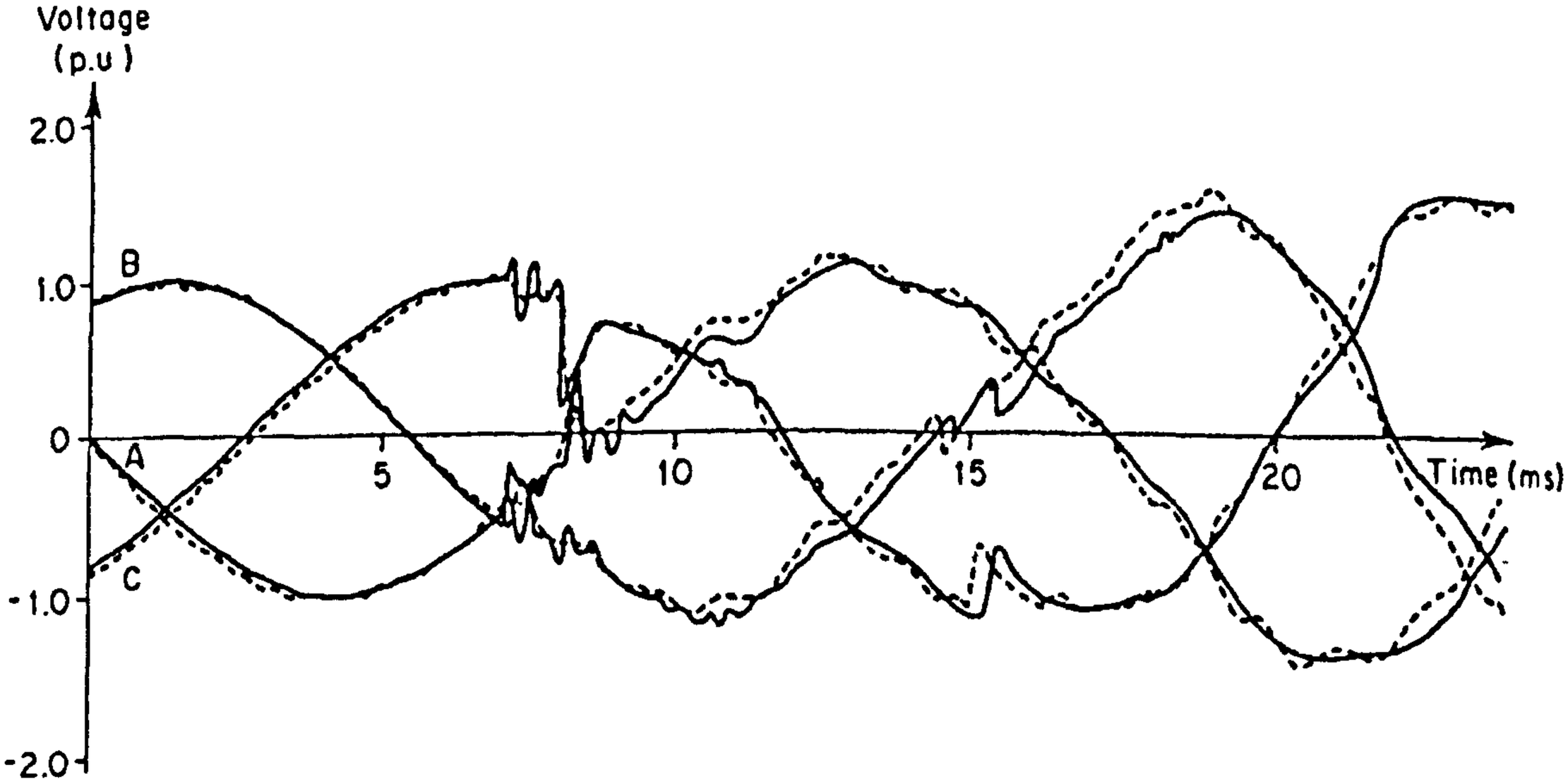

Figure 5.6 Sending end voltages after sequential energization for field measurements (solid line) and electromagnetic transient program (dashed line)

5.3.2 Sending End Results

Figures 5.2, 5.3 and 5.4 show the simulated transient voltages for phases a, b and c respectively, obtained at the sending end of the line for the frequency-independent, frequency-dependent and phase domain transmission line models, following the sequential energization of the line.

It can be seen that up until approximately 20ms, the simulated transients predicted from the three line models are very similar. In the time interval ~16-18ms, the phase c voltage predicted by the phase domain transmission line model shows a greater attenuation than that calculated by the frequency-independent and frequency-dependent line representations.

After this time period, it can be seen that the phase b and c transient voltages computed with the phase domain model are delayed by almost 1ms as compared to the other line models. It can also be seen that there is, in general, a magnification of the higher harmonics contained within the voltage waveforms of the frequency-independent model after 20ms. A summary of the peak phase voltages when calculated using the three different line representations is provided in Table 5.3.

Table 5.3. Peak voltage magnitude (sending end)

Method	Peak voltage magnitude (p.u.)		
	Phase a	Phase b	Phase c
Phase domain model	1.287	1.336	1.315
Frequency-dependent model	1.312	1.369	1.422
Frequency-independent model	1.345	1.505	1.45

5.3.3 Comparison with Field Measurements (Sending End)

The simulated phase voltages at the sending of the line for the frequency-dependent and phase domain transmission line models are compared further with the actual field recordings of the sequential energization of the Jaguara-Taquaril transmission system, as described in [8].

Figure 5.5 shows the computed transient voltages of the three phases at the sending end of the line for the phase domain transmission line model (solid line), superimposed on those of the frequency-dependent model (dashed line). Figure 5.6 shows the corresponding phase voltages obtained from the available field measurements [8] (solid line), superimposed on those from the EMTP (dashed line) [2].

From a comparison of Figures 5.5 and 5.6 it can be seen that there is, in general, a good agreement with the simulated transients obtained with both line models and those of the field measurements. After approximately 20ms there is a noticeable time delay in the waveforms of both the phase domain transmission line model and the actual field measurements, when compared against the transient voltages computed by the frequency-dependent line model.

5.3.4 Receiving End Results

Figures 5.7, 5.8 and 5.9 show the simulated transient voltages for phases a, b and c respectively, obtained at the receiving end of the line for the frequency-independent, frequency-dependent and phase domain line models, following the sequential energization of the line.

The amplification of the peak voltage magnitudes, as computed by the frequency-independent line model, is immediately noticeably from Figures 5.7, 5.8 and 5.9. This is

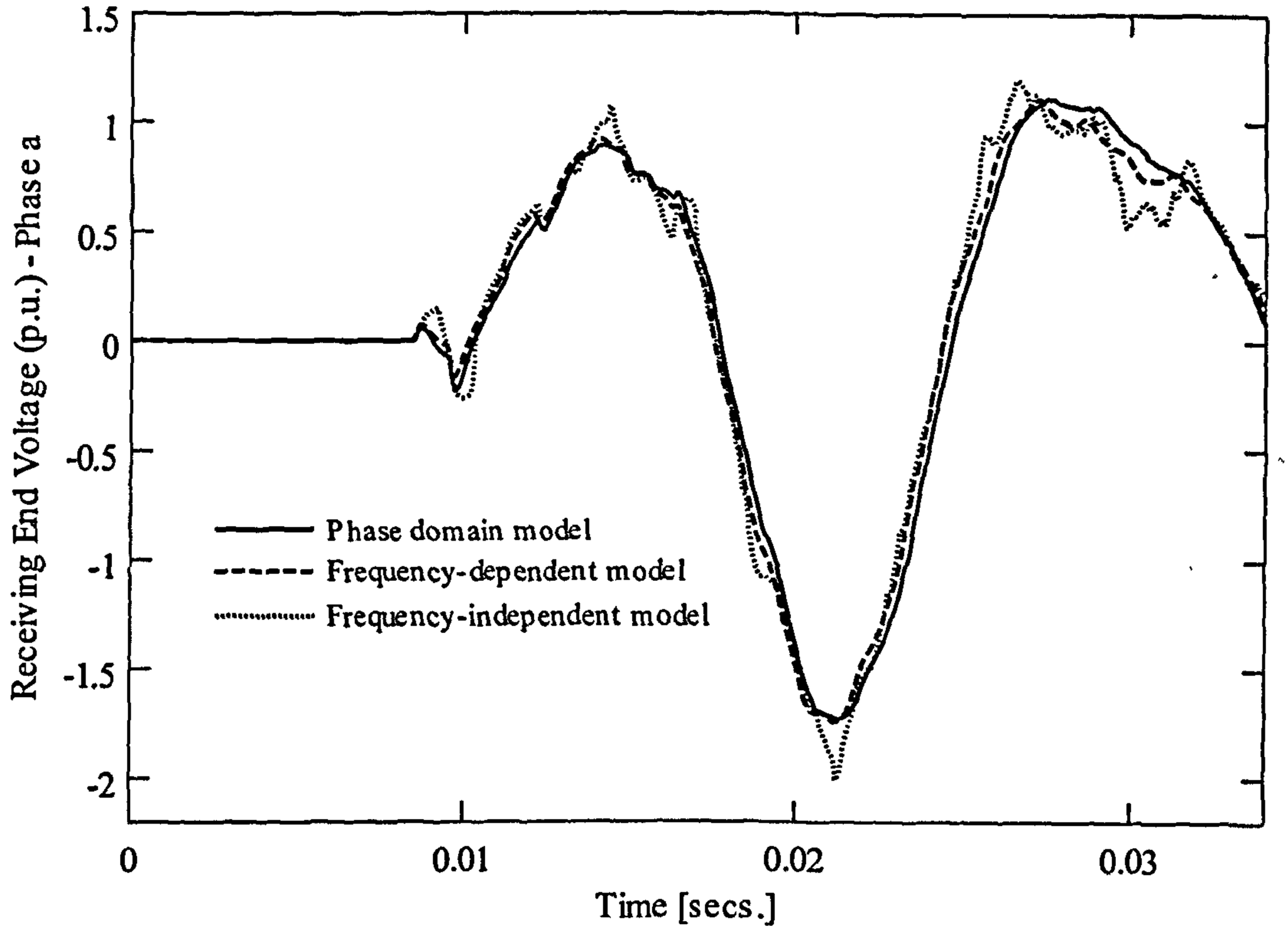

Figure 5.7. Receiving end voltage after simulated sequential energization - Phase a

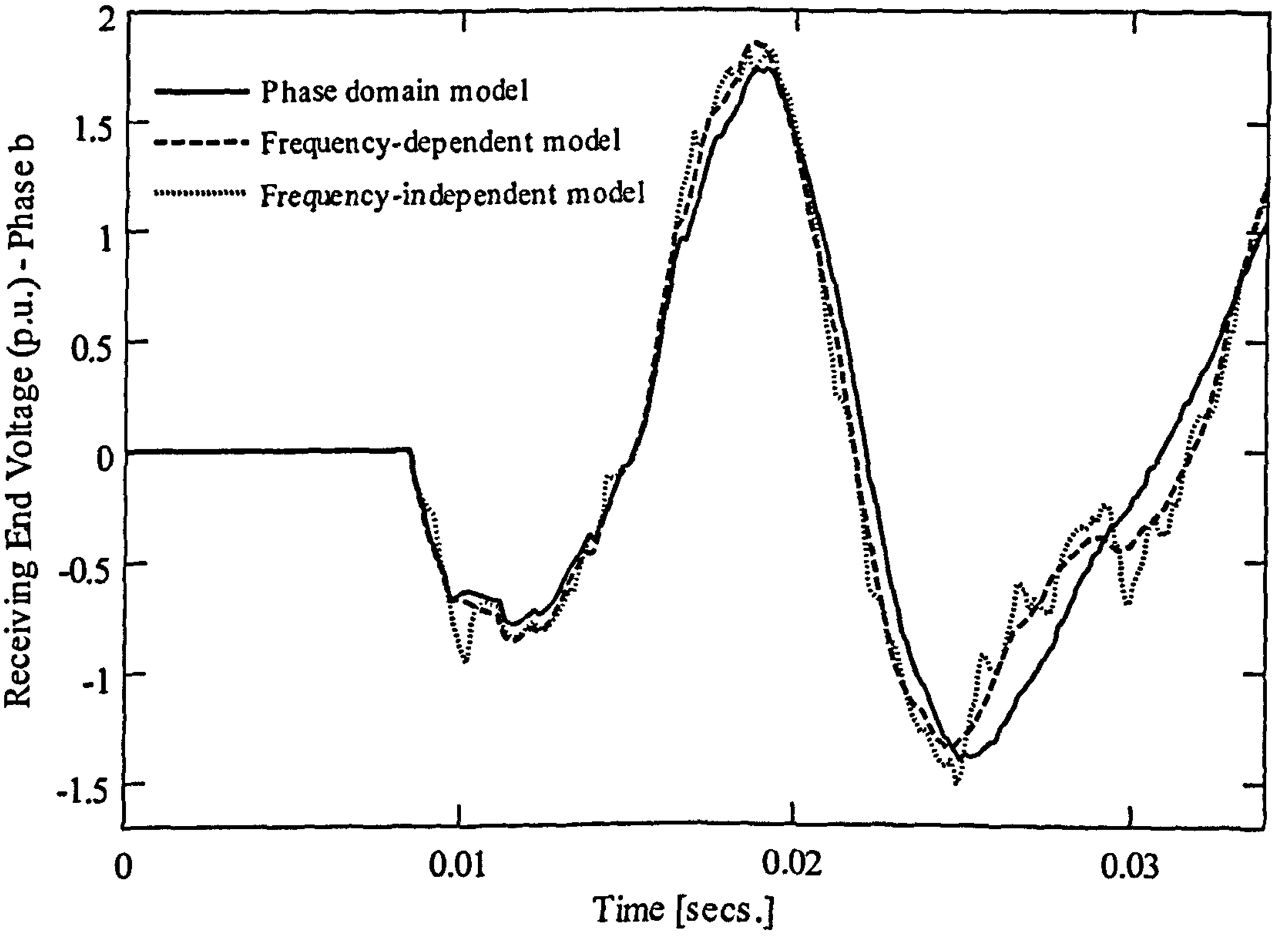

Figure 5.8. Receiving end voltage after simulated sequential energization - Phase b

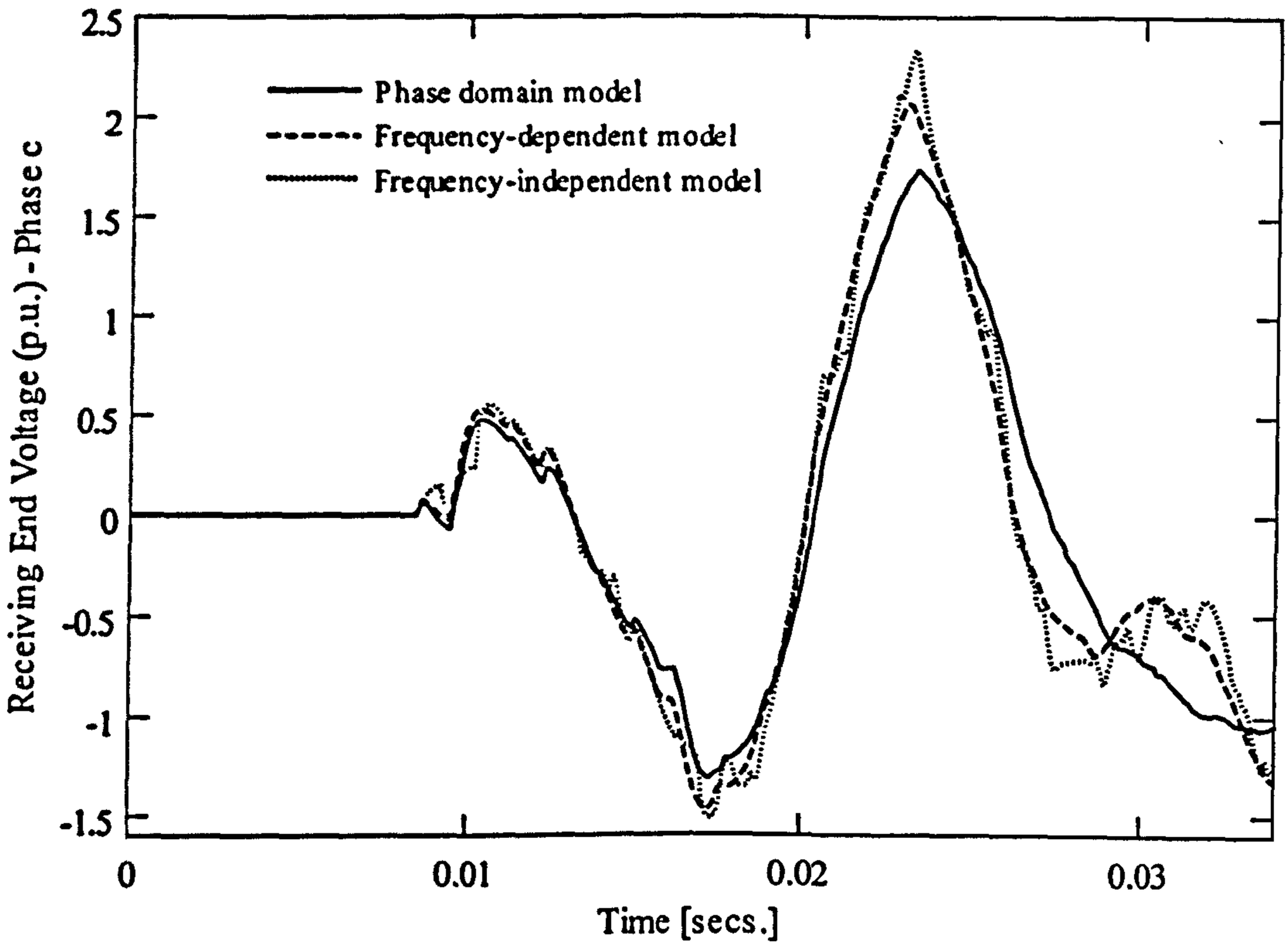

Figure 5.9. Receiving end voltage after simulated sequential energization - Phase c

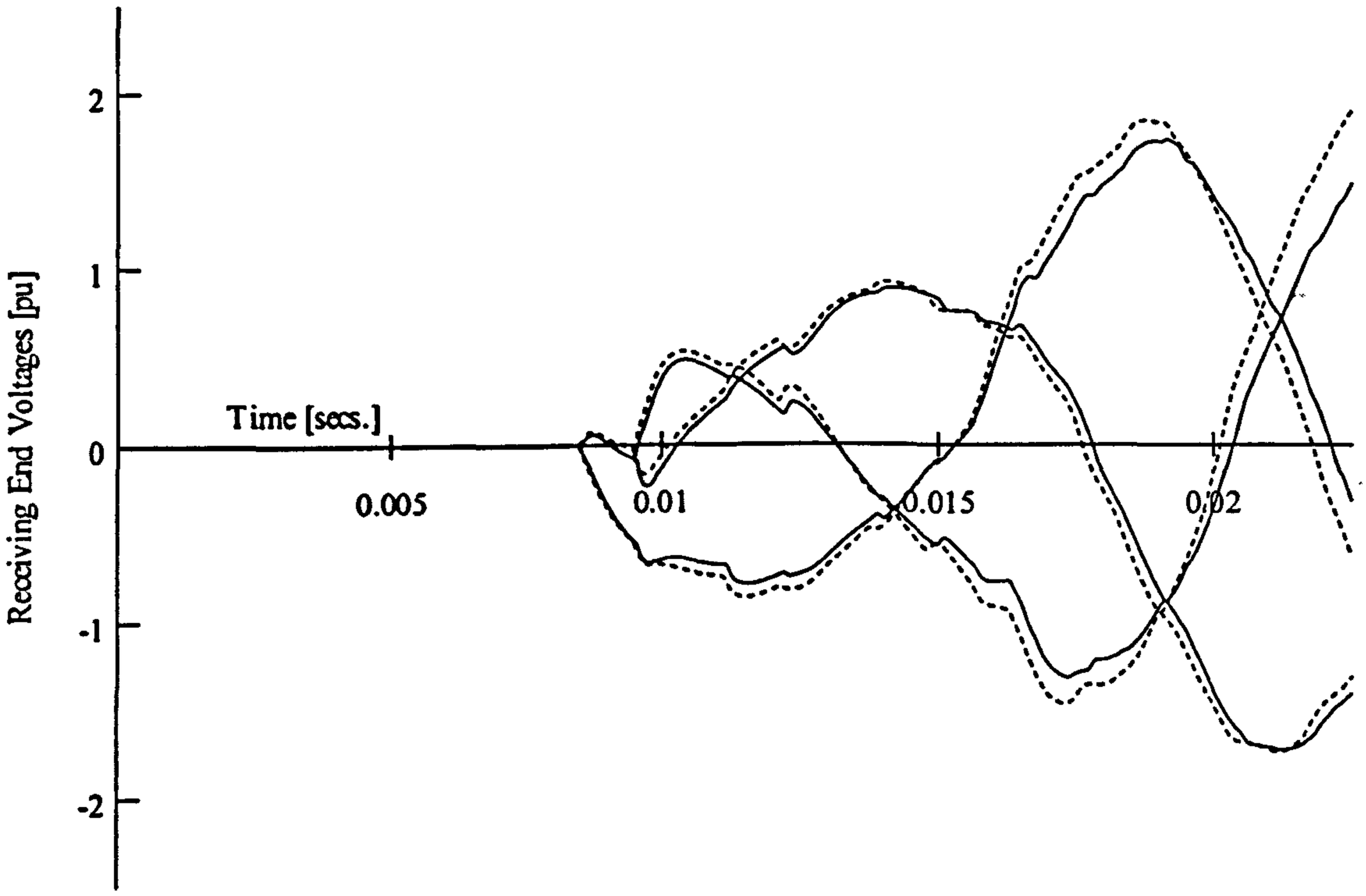

Figure 5.10 Receiving end voltages after simulated sequential energization for phase domain model (solid line) and frequency-dependent model (dashed line)

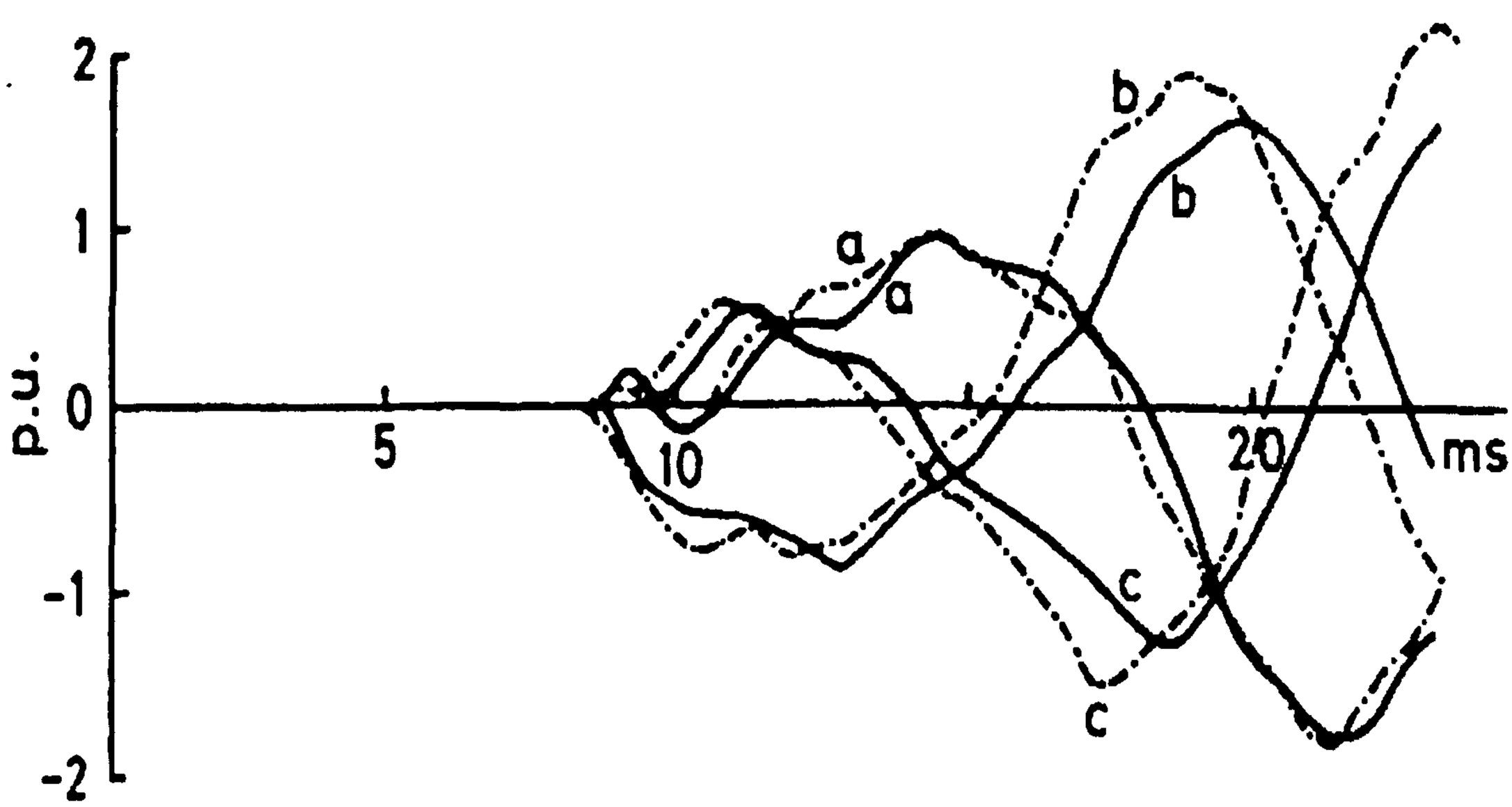

Figure 5.11 Receiving end voltages after sequential energization for field measurements (solid line) and electromagnetic transient program (dashed line)

a direct consequence of assuming the line is lossless and the parameters of the line constant, with respect to frequency [8,29]. However, as the waves travel along the line, they are subjected to both attenuation and distortion due to the presence of the resistive ground [7]. Neglecting this frequency-dependence can be seen to significantly effect the accuracy of the time domain solution.

For the phase a voltage, both the frequency-dependent and the phase domain transmission line models exhibit similar characteristics. After 20ms, a small delay is apparent in the transient voltage computed with the phase domain model when compared to that of the frequency-dependent method. For phase b and c this delay is more clearly visible, also the peak voltage magnitudes for both phase b and c are also reduced as compared to the frequency-dependent line. A summary of the peak voltage magnitudes for the phase domain, frequency-dependent and frequency-independent line models is provided in the following section.

5.3.5 Comparison with Field Measurements (Receiving End)

The accuracy of the newly developed phase domain transmission line model is assessed further by comparing the simulated phase voltages with the actual field recordings of the sequential energization of the Jaguara-Taquaril transmission system, as described in [8].

Figure 5.10 shows the computed transient voltages of the three phases at the receiving end of the line for the phase domain transmission line model (solid line), superimposed on those of the frequency-dependent model (dashed line). Figure 5.11 shows the corresponding transient voltages obtained from the available field measurements (solid line), superimposed on those from an electromagnetic transient program (dashed line) [29]. A summary of the peak voltage magnitude for each phase, within the time period of the available field measurements, is provided in Table 5.4 for the three line models and the field measurements.

Table 5.4. Peak voltage magnitude (receiving end)

Method	Peak voltage magnitude (p.u.)		
	Phase a	Phase b	Phase c
Field Measurements	1.88	1.6	1.35
Phase domain model	1.726	1.736	1.314
Frequency-dependent model	1.738	1.846	1.468
Frequency-independent model	2.01	1.82	1.501

Table 5.5. Error in peak voltage magnitude (receiving end)

Method	Error in peak voltage magnitude (%)		
	Phase a	Phase b	Phase c
Phase domain model	8.19	8.5	2.67
Frequency-dependent model	7.55	15.375	8.74

Table 5.6. Time of peak voltage magnitude (receiving end)

Method	Peak voltage magnitude (ms)		
	Phase a	Phase b	Phase c
Field Measurements	21.28	19.5	18.2
Phase domain model	21.25	19.142	17.34
Frequency-dependent model	21.18	18.768	17.27

From Table 5.4 it can be seen that the predicted peak voltage magnitudes using the phase domain model are, in general, in better agreement than those of the frequency-dependent line representation when compared against the available field measurements. The exception is with the phase a voltage, where the value predicted by the frequency-dependent model is in slightly better agreement with the actual field measurement (by 0.012pu). The increased magnitude of the peak voltages associated with the frequency-independent method is due to the assumption of constant line parameters and a lossless line, as discussed previously.

A summary of the error for each peak voltage when compared to the measured values, for the frequency-dependent and phase domain models is shown in Table 5.5. The maximum error in peak voltage for the phase domain model is 8.5%, while that of the frequency-dependent line is 15.375%.

The corresponding times at which the peak voltages occur are presented in Table 5.6. It can be seen that the timings of the peak voltages for the phase domain model are closer to those of the actual field recordings. Both the measured values and those predicted by the phase domain model are delayed with respect to the transient voltages calculated with the frequency-dependent transmission line model.

5.4 Discussion

The receiving end transient voltages computed using the phase domain transmission line model show a greater attenuation of the peak voltage magnitudes, in comparison to the frequency-dependent transmission line. In this respect there is a better agreement between the field measurements and the computed transient voltages using the phase domain model, with the exception of the phase a voltage. In this case, the value predicted by the frequency-dependent model is in slightly better agreement with that of the field measurement.

The measured peak voltages are delayed in all phases as compared to the predicted transient voltages using both the frequency-dependent and phase domain line representations. However, the timing of each peak voltage using the phase domain model is in better agreement with those of the actual field measurements.

The differences between the computed transient voltages using the frequency-dependent and phase domain transmission line models are likely to be due to the assumption of a perfectly transposed line, in the case of the former. Assuming the line to be transposed will not accurately represent the imbalances naturally present in the transmission line, e.g. due to unequal conductor spacings and configuration. As discussed in the introduction to this chapter, the transient overvoltages arising from a sequential energization can be affected by the mutual coupling effects between the phase conductors [1]. Thus, if this coupling is not accurately taken into account, inaccuracies will inevitably be introduced in the final solution. This can be overcome by including the frequency-dependent behaviour of the transformation matrices by including additional time domain convolutions. In this case, the accuracy of the modal domain approach will be comparable to that of the newly developed phase domain model, where any imbalances in the transmission line are intrinsically taken into account as the analysis is conducted entirely in the frame of reference of the phases.

While the results obtained with the new phase domain transmission line model, in general, agree well with those of the field measurements, some differences can still be observed when compared to the measured transients. These discrepancies may be attributed to a variety of sources, such as the assumption of a constant earth conductivity [1,8]. Non-linear effects such as the magnetizing impedance and saturation

of the transformers, and corona are not represented in the time domain simulations. All of these phenomena will cause extra losses in transmission system.

Further discrepancies could also have arisen, as a result of inaccuracies in the original field measurements [8].

5.5 Conclusions

The newly proposed phase domain transmission line model that has been developed over the previous two chapters is applied here to simulate the transient voltages arising from the sequential energization of a real-life transmission circuit. The 345kV single-circuit system has been used to illustrate the accuracy of the proposed phase domain methodology, since actual field measurements for the sequential energization test are available.

Since the analysis is conducted in phase co-ordinates, any imbalances in the transmission line will be inherently taken into account in the solution process. This can be important when simulating transient overvoltages arising from the sequential energization of an overhead line, since the mutual coupling that exists between phase conductors can impinge on the magnitude and wave-shape of the transients produced during such disturbances. In order to accurately simulate the system under study, it is therefore necessary to incorporate the line imbalances in the analysis.

The results obtained from the phase domain transmission line are shown to be in good agreement with the measured transient voltages. For the frequency-dependent line model, the effect of using a constant transformation matrix to exchange information between the modal and phase domains (and vice-versa) and the assumption that the line is transposed is seen to influence the accuracy of the computed waveforms. Both the phase domain model and the measured transient voltages are delayed with respect to the waveforms generated by the frequency-dependent line. The degree of delay is quite similar for the phase domain model and the measured field data. If the frequency-dependence of the transformation matrices in the modal method is included, a similar degree of accuracy to that of the phase domain model would be expected.

The field recordings and the phase domain model also show, in general, a similar degree of attenuation as compared to the frequency-dependent line model utilizing a constant transformation matrix. The maximum error in peak voltage for the phase domain transmission line as compared to the field recordings is 8.5% (for phase b), this compares to 15.375% for the frequency-dependent line model (also for phase b).

5.6 References

[1] Bickford, J. P., Mullineux, N. and Reed, J. R.: 'Computation of power-system transients', IEE Monograph Series 18, 1980, ISBN 0-906048-35-4.

[2] Dommel, H. W.: 'Electromagnetic Transients Program (EMTP) Rule Book', EPRI EL6421-1, Vol. 1, June 1989.

[3] Dommel, H. W.: 'Digital Computer Solution of Electromagnetic Transients in Single-and Multiphase Networks', IEEE Transactions on Power Apparatus and Systems, Vol. PAS-88, No. 4, April 1969, pp. 388-399.

[4] Brandão, J. A. and Borges da Silva, J. F.: 'Wave Propagation in Polyphase Transmission Lines a General Solution to Include Cases Where Ordinary Modal Theory Fails', IEEE Transactions on Power Delivery, Vol. PWRD-1, No. 2, April 1986, pp. 182-189.

[5] Brandão, J. A.: 'Overhead Three-Phase Transmission Lines – Non-Diagonalizable Situations', IEEE Transactions on Power Delivery, Vol. 3, No. 4, October 1988, pp. 1348-1355.

[6] Marti, J.: 'Accurate Modelling of Frequency-Dependent Transmission Lines in Electromagnetic Transient Simulations', IEEE Transactions on Power Apparatus and Systems, Vol. PAS-101, No. 1, January 1982, pp. 147-157.

[7] Marti, J.: 'The Problem of Frequency Dependence in Transmission Line Modelling', PhD Thesis, The University of British Columbia, Canada, April 1981.

[8] Dommel, H. W., Yan, A., Ortiz de Marcano, R. J. and Miliani, A. B.: 'Case Studies for Electromagnetic Transients', Internal Report, The Department of Electrical Engineering, The University of British Columbia, Canada, May 1983.

[9] Gustavsen, B. and Semlyen, A.: 'Combined Phase and Modal Calculation of Transmission Line Transients Based on Vector Fitting', IEEE Transactions on Power Delivery, Vol. 13, No. 2, April 1998, pp. 596-604.

[10] Gustavsen, B., Sletbak, J., and Henriksen, T.: 'Calculation of Electromagnetic Transients in Transmission Line Cables and Lines Taking Frequency Dependent Effects Accurately Into Account', IEEE Transactions on Power Delivery, Vol. 10, No. 2, April 1995, pp. 1076-1084.

[11] Nguyen, H. V., Dommel, H. W. and Marti, J. R.: 'Direct Phase Domain Modelling of Frequency-Dependent Overhead Transmission Lines', IEEE Transactions on Power Delivery, Vol. 12, No. 3, July 1997, pp. 1335-1342.

[12] Nguyen, H.: 'Simulation of Lightning Surges on Transmission Lines', PhD Thesis, The University of British Columbia, Canada, February 1996.

[13] Castellanos, F. and Marti, J. R.: 'Phase-Domain Multiphase Transmission Line Models', International Conference on Power System Transients, Lisbon, 3-7 September 1995.

[14] Castellanos, F., Marti, J. R. and Marcano, F.: 'Phase-Domain Multiphase Transmission Line Models', Electrical Power & Energy Systems, Vol. 19, No. 4, 1997, pp. 241-248.

[15] Noda, T., Nagaoka, N. and Ametani, A.: 'Phase Domain Modelling of Frequency-Dependent Transmission Lines by Means of an ARMA Model', IEEE Transactions on Power Delivery, Vol. 11, No. 1, January 1996, pp. 401-411.

[16] Noda, T., Nagaoka, N. and Ametani, A.: 'Further Improvements to a Phase-Domain ARMA Line Model in Terms of Convolution, Steady-State Initialization, and Stability', IEEE Transactions on Power Delivery, Vol. 12, No. 3, July 1997, pp. 1327-1334.

[17] Angelidis, G. and Semlyen, A.: 'Direct Phase-Domain Calculation of Transmission Line Transients Using Two-Sided Recursions', IEEE Transactions on Power Delivery, Vol. 10, No. 2, April 1995, pp. 941-949.

[18] Gustavsen, B: 'A Study of Overvoltages in High Voltage Cables With Emphasis on Sheath Overvoltages', Dr. Ing. Thesis, The Norwegian Institute of Technology, Trondheim, Norway, 1993.

[19] Morched, A., Gustavsen, B. and Tartibi, M.: 'A Universal Model for Accurate Calculation of Electromagnetic Transients on Overhead Lines and Underground

Cables', IEEE Transactions on Power Delivery, Vol. 14, No. 3, July 1999, pp. 1032-1038.

[20] Soysal, A. O. and Semlyen, A.: 'State Equation Approximation of Transfer Matrices and its Applications to the Phase Domain Calculation of Electromagnetic Transients', IEEE Transactions on Power Systems, Vol. 9, No. 1, February 1994, pp. 420-428.

[21] Castellanos, F. and Marti, J. R.: 'Full Frequency-Dependent Phase-Domain Transmission Line Model', IEEE Transactions on Power Systems, Vol. 12, No. 3, August 1997, pp. 1331-1339.

[22] Gustavsen, B. and Smelyen, A.: 'Rational Approximation of Frequency Domain Responses by Vector Fitting', IEEE Transactions on Power Delivery, Vol. 14, No. 3, July 1999, pp. 1052-1061.

[23] Wedepohl, L. M.: 'Application of Matrix Methods to the Solution of Travelling-Wave Phenomena in Polyphase Systems', Proceedings of the IEE, Vol. 100, No. 12, 1963, pp. 2200-2212.

[24] Hedman, D. E.: 'Propagation on Overhead Transmission Lines I-Theory of Modal Analysis', IEEE Transactions on Power Apparatus and Systems, Vol. PAS-84, March 1965, pp. 200-205.

[25] Carson, J. R.: 'Wave Propagation in Overhead Wires with Ground Return', Bell System Tech. J., Vol. 5, 1926, pp. 539-554.

[26] Deri, A., Tevan, G., Semlyen, A. and Castanheria, A.: 'The Complex Ground Return Plane, a Simplified Model for Homogeneous and Multi-Layer Earth Return', IEEE Transactions on Power Apparatus and Systems, Vol. 100, 1981, pp. 3686-3693.

[27] Lewis, V. A. and Tuttle, P. D.: 'The Resistance and Reactance of Aluminium Conductors Steel Reinforced', Transactions on AIEE PAS, Vol. 77, 1958, pp.1189-1215.

[28] Semlyen, A. and Deri, A.: 'Time Domain Modelling of Frequency Dependent Three Phase Transmission Line Impedance', IEEE Transactions on Power Apparatus and Systems, Vol. 104, 1985, pp. 1549-1555.

[29] Naidu, S. R. and de Lima, F.N.: 'A frequency-dependent transmission line model for electromagnetic transient studies', IEE Proceedings, Vol. 132, Pt. C, No. 6, November 1985.

CHAPTER 6

REAL-TIME DIGITAL POWER SYSTEM SIMULATION

This chapter describes the development of a real-time simulation environment for conducting electromagnetic transient simulations on a commercially available real-time digital simulator. The implementation of three different transmission line models, of varying degrees of sophistication, is described and their suitability for sustained real-time electromagnetic transient simulations assessed. The first transmission line model represents the line as a pure delay and a characteristic impedance. The model assumes that the parameters of the line are frequency-independent. The second model takes into account the frequency domain variation of the line responses by fitting them with rational functions using the method of Vector Fitting. The final model represents the transmission line directly in the phase domain, intrinsically taking into account any geometric imbalances and frequency-dependent effects of the line. By conducting the analysis directly in phase co-ordinates the use of transformation matrices to exchange information between the modal and phase domains, and vice-versa, at every time step in the simulation is completely avoided. This is the first time that such a line representation has been developed for real-time simulations. The real-time sequential energization of a real-life transmission network is performed and the results for the different line models presented. The actual frame times are recorded during this test simulation and the difference in computational efficiency between the three line representations is discussed. The accuracy of the real-time phase domain transmission line model is assessed by comparing the simulated results with available field measurements.

6.1 Introduction

Digital computer based simulation packages such as EMTP [1] and EMTDC [2] have been used extensively for analysing the transient phenomena that arise as a result of disturbances to the otherwise normal steady-state operation of power system networks. In principal, the results obtained from performing such analysis can be utilized to achieve effective system protection and insulation co-ordination. This is essential if the transient waveforms injected into the system are to be limited to safe levels to ensure that equipment failures and unnecessary transmission line outages are avoided during these conditions [3-6].

Since a transient disturbance in the power system may only last for a period of milliseconds [5,6], a principal drawback of these software based simulators concerns the computational efficiency with which they operate. In evaluating the response of the network to a switching transient, for example, the simulator may take many seconds or even minutes to perform the necessary computations and produce a solution for the disturbance [12,13]. This non-real-world time operation (i.e. the solution output is determined at either a faster or slower rate) precludes the interfacing of external equipment to the simulator.

Effective testing of physical control or protection equipment requires the simulated waveforms to be input into the device in real-time, since in most cases the control inputs required are dynamic in nature. Simulation packages such as EMTP [1] and EMTDC [2] are therefore of little use in these areas.

Physical control and protection testing has instead been undertaken using special playback devices, or analogue simulators [12,13,17,22,23]. A typical playback device feeds the results from an off-line simulation, or actual field data obtained from Digital Fault Recorders (DFRs), in real-time, to the device under test. However, since no dynamic interaction between the simulator and the external equipment can take place, these simulators are limited to open loop testing only [12]. Furthermore, storage requirements can limit the length of the simulation that can be played back for a particular test [17].

Analogue HVDC simulators and AC Transient Network Analyzers (TNAs) have been widely used throughout the power system industry for testing physical control and protection devices [12,13,17,22,23]. These simulators consist of scaled down power system components, with each component physically connected to the next in a similar manner to that of the real system. However, associated with analogue simulators are high capital and operating costs. Also, a single study may occupy the simulator for many weeks so that general accessibility is very low [12,13].

Since the beginning of the last decade, manufacturers, large utilities and research organizations have increasingly turned to a more cost effective and flexible alternative to the previous generation of analogue network analyzers - real-time digital power system simulators with hardware-in-the-loop (HIL) capabilities [7-16,18-26].

These simulators operate in real-world time so that actual physical hardware can be mixed with computer models to replicate the total power network under investigation, providing a very powerful tool for extensively evaluating and accurately test the performance of new and existing equipment under various operating conditions. This closed loop performance also permits the response of the power network, to the operation, or miss-operation of the actual device under test, to be thoroughly analysed. The ability to assess the interactions and effects of the various power system components on each other is increasingly important, particularly since the complexity of modern power systems is increasing. Real-time digital simulators provide a convenient tool to analyze such phenomena [12,13,23].

This chapter describes the development of a real-time environment for conducting electromagnetic transient simulations on a commercially available real-time digital simulator. The newly developed phase domain transmission line model is incorporated within this environment and the accuracy and computational efficiency of this model is assessed against conventional frequency-independent [28] and frequency-dependent [29] line models utilizing modal decomposition methods [30,31]. The development of this phase domain model, in the context of real-time simulations, represents the first time that such a methodology has been applied to perform electromagnetic transient studies.

The results of a real-time sequential energization of a real-life, single-circuit transmission system are presented and the actual frame times recorded for the three transmissions line models, with the computational efficiency of each line model subsequently assessed. The time domain simulations presented in this chapter are restricted to single-circuit systems, for practicality reasons. With the current hardware and software configuration of the Real-Time Station (RTS), it would be very difficult to simulate multi-circuit transmission line configurations. However, due to the open

architectural design of the simulator, it is envisaged that these restrictions could be relaxed in the near future with additional hardware installed and software upgraded.

The following section provides an overview of the real-time station and describes the current hardware and software configuration of the simulator.

6.2 Real-Time Station (RTS)

The Real Time Station (RTS) is a commercially available simulator, developed by Applied Dynamics International (ADI), and designed specifically for real-time, hardware-in-the-loop dynamic simulation. Unlike the majority of real-time digital simulators presented in the open literature in this research area, the RTS is not specifically designed for power system analysis. Indeed, the primary use of the simulator has been in the development of sophisticated control systems for the automotive and aerospace industries. There are a wide range of functional blocks (summers, dividers, wave generators, integrators, etc.), as well as extensive pre-defined components (pumps, gears, engines, etc.) and application libraries (aerospace vehicle, multiphase fluid, thermal hydraulic etc.) ideally suited for control system applications. However, the software is also very flexible in that user-defined source code can be imported directly into special FORTRAN components within the GUI, or dynamically linked during compilation. This enables a wide variety of dynamical systems to be analyzed in real-time, including power systems, with relative ease.

The Real-Time Station is a multiprocessor system, capable of parallel processing and I/O interactions in real-time. This is coupled with the host workstation (Sun SPARCstation 4) which serves as the driver for the GUI based simulation package in which the power system models are constructed. The real-time simulation is also initiated directly from the host workstation. The following sections provide a description of the current hardware and software setup of the RTS.

6.2.1 Real-Time Station Hardware

The Real-Time Station is an open architecture system, consisting of several types of processors coupled to a common VMEbus backplane. There are three different types of processor within the RTS, namely: Communication (COP), Simulation (SP) and Compute Engine (CE) processors, each designed for a specific task. The current configuration of the RTS is given in Figure 6.1.

6.2.1.1 Communication Processor (COP)

The Communication Processor (COP) is a Am2900 processor whose primary function is to direct all data traffic within the RTS and between the RTS and the host workstation. The COP is also responsible for synchronizing all the processors within the RTS to enable a regular frame time to be attained across all the processors.

6.2.1.2 Compute Engine (CE3/CE4)

The Compute Engine is used to perform the computations required to model the particular dynamic system under investigation. The current standard CE's include several versions of the Motorola PowerPC family of VMEbus-based single board computers. In its current configuration, the RTS has two such CE's - a 133MHz CE3 and the faster 333MHz CE4. The open architecture design of the RTS allows expansion of further CE's. Models can be distributed across multiple CE's through highly efficient shared memory exchanges using ADI's Integrated Development Environment (IDE).

For the work undertaken in this research project, the IDE software has not been available for use. However, at this time the software has been installed on the host

workstation and promises to provide a significant increase in the capabilities of the RTS in conducting real-time electromagnetic transient studies. The advantages of using the integrated development environment will be discussed later in this chapter.

6.2.1.3 Simulation Processor (SP)

The computational power of the SP is available for general interfacing activities such as filtering signals to remove unwanted high frequency components (signal conditioning), and synchronizing the signals on all channels.

The SP is contained within a Parallel Intelligent Resource (PIR). The PIR allows the I/O to be operated in parallel with model execution, to reduce VMEbus traffic. The PIR also comprises Analogue (AIM) and Digital (DIM) Interface Modules. These modules can be used to interface the power system components modelled on the RTS to external devices. Only fully refined data appears on the system bus instead of all the intermediate activity. This reduces the processing load on the compute engine(s). The simulation processor has a dual-ported memory, which allows the COP to efficiently accomplish all VMEbus transactions for the PIR.

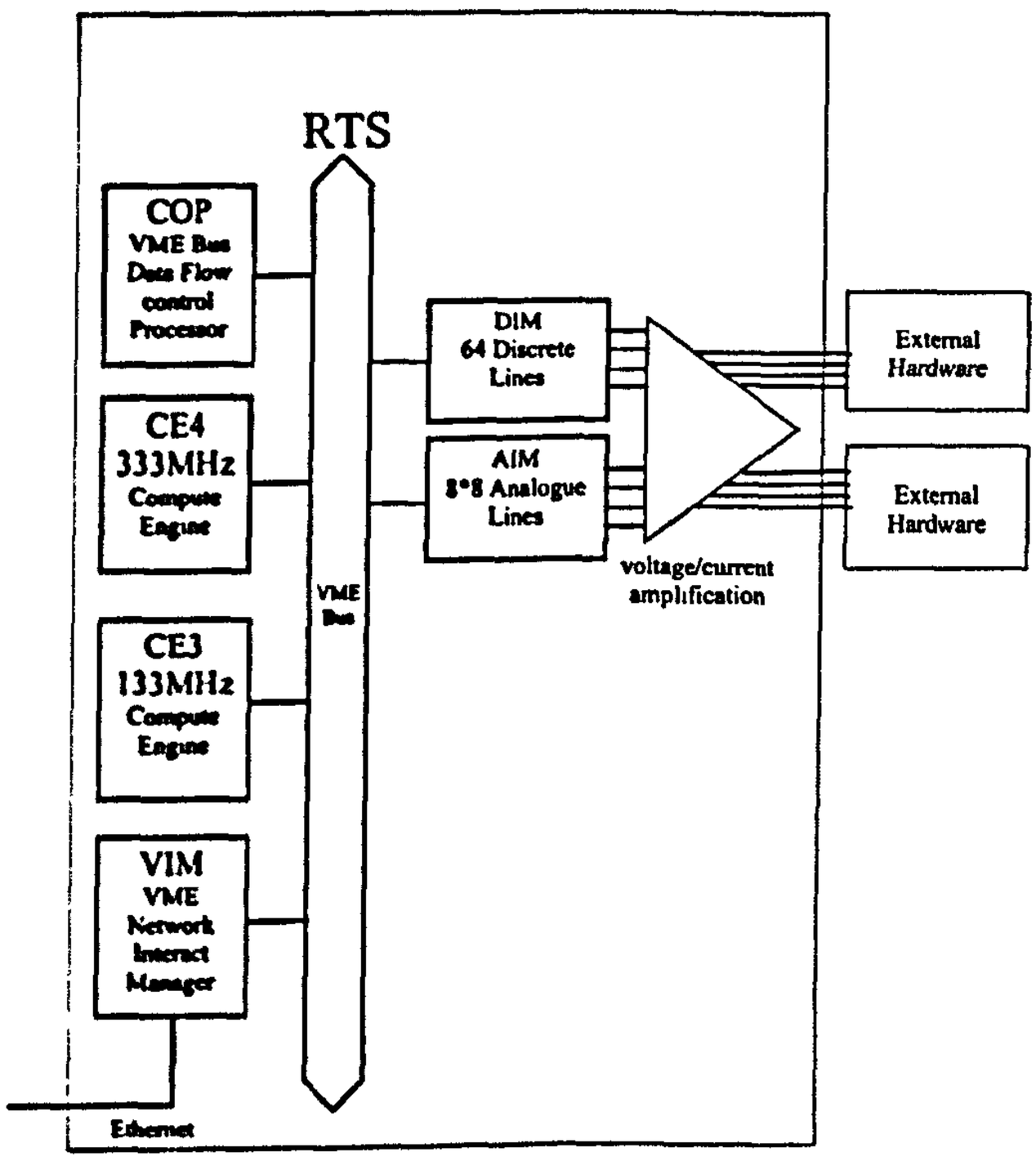

Figure 6.1 Real-Time Station (RTS) Configuration

6.2.1.4 Analogue Interface Module (AIM)

This module is used for conversion of the analogue signals (±10V peak) from external equipment into digital data for transmission to the RTS. The AIM is also responsible for conversion of the digital information generated by the RTS into analogue waveforms that will be applied to any device under test. The AIM converts the digital data into low level analogue signals (±10V peak) required for the main amplification units. Each AIM has 8 A/D and D/A converters with a 12-bit resolution for each channel. The sampling frequency of the converters is approximately 116kHz.

6.2.1.5 Digital Interface Module (DIM)

This module provides a 64-bit bi-directional interface for digital I/O.

The PIR may be expanded to include a combination of up to six AIMs and DIMs using the VME Subsystem Bus. This allows the processing power of a single SP to be applied to many interface tasks, without effecting the primary system bus.

6.2.1.6 Power Amplification Units

The output signals from the real-time station must be delivered to any external equipment under test at the appropriate in-service operating levels required by the device. Since the RTS can only output low-level analogue signals (±10V peak), in general, amplification units are required for this purpose.

At the present time, the hardware resources available in this respect are three single-phase voltage amplification units, designed by Techron (TEC3622). The output signals can be amplified to a maximum peak voltage of 305V. The actual level of amplification is determined by scaling the output signals from the RTS.

6.2.1.7 VMEbus Interact Manager (VIM)

Although the RTS is run as a stand-alone resource, it can be configured as a shared network resource, connecting to the Local Area Network (LAN) through the VMEbus Interact Manager (VIM). The VIM communicates with the host computer workstation (or workstations on the LAN, if the RTS is run as a network resource) for program loading and run-time interaction. The user retains the ability to communicate nonintrusively with the simulation during run-time to select variables for display, data logging, or parameter adjustment. The VIM does not actively take part in the power system solution but instead functions as an interface and simulation control device. This allows a high level of interactive control and display without interfering with real-time simulation.

6.2.2 Software

All the interaction between the user and the Real-Time Station is performed using a sophisticated, GUI-based software (EASY5) developed by BOEING Inc. The EASY5 software can be used to model, analyze and design dynamic systems containing hydraulic, pneumatic, mechanical, thermal and digital sub-systems. As discussed earlier, systems can be constructed using the large variety of functional blocks and pre-defined components – particularly suitable for control system studies. Alternatively, user defined code can be inputted directly into FORTRAN components within the EASY5 GUI. External FORTRAN and C source code can also be called from within a FORTRAN component. This flexibility makes it possible to simulate a large variety of dynamical systems, without restricting the analysis to control system based studies. It is by using these FORTRAN components that the power transmission line models have been implemented within EASY5, for real-time electromagnetic transient studies.

Models can be executed 'off-line' on the host workstation, or run in real-time on the RTS. This capability permits user models to be thoroughly analysed, verified and debugged off-line, avoiding such problems in the real-time execution. The appropriate mode (off-line/real-time) is selected within EASY5 before the model executable is built. If the model is to be run in real-time, then additional components are required, which represent the real-time hardware that is being used. These components include blocks for defining the analogue and digital I/O and compute engines in use. There are 8, scaleable I/O analogue channels (±10V). Each analogue I/O channel has a numbered address, which can be set in the Analogue I/O (AI/AO) blocks. A DC offset can also be applied to the I/O signals by adjusting the appropriate parameter in the AI/AO components. Figure 6.2 shows a typical schematic diagram of an EASY5 real-time model.

After all component parameters have been set, the EASY5 code-generator translates the interconnected blocks and components in the schematic model into either Fortran or C source code. The executable model is then executed from within EASY5 when an analysis is launched.

If a real-time simulation is selected, the model source code is automatically downloaded onto the real-time station and converted into real-time code, when the simulation is initiated from within EASY5. The source code is converted into COSIM – ADI's scheduling, synchronization, and communications-control software for the RTS. COSIM is a high-level coordination language used to manage data flow and to coordinate and synchronize the parallel processors in the RTS as they execute simulation and I/O-related tasks.

The integration between EASY5 and the real-time station is seamless – no extra work is required by the user to run the model in real-time, other than including the appropriate real-time icons in the schematic model.

Simulation results can be viewed at the end of the analysis using the plotting capabilities within EASY5. If required, the results can also be viewed in real-time using ADI's SIMplot as the simulation proceeds. The appropriate plot mode is set before entering the EASY5 environment.

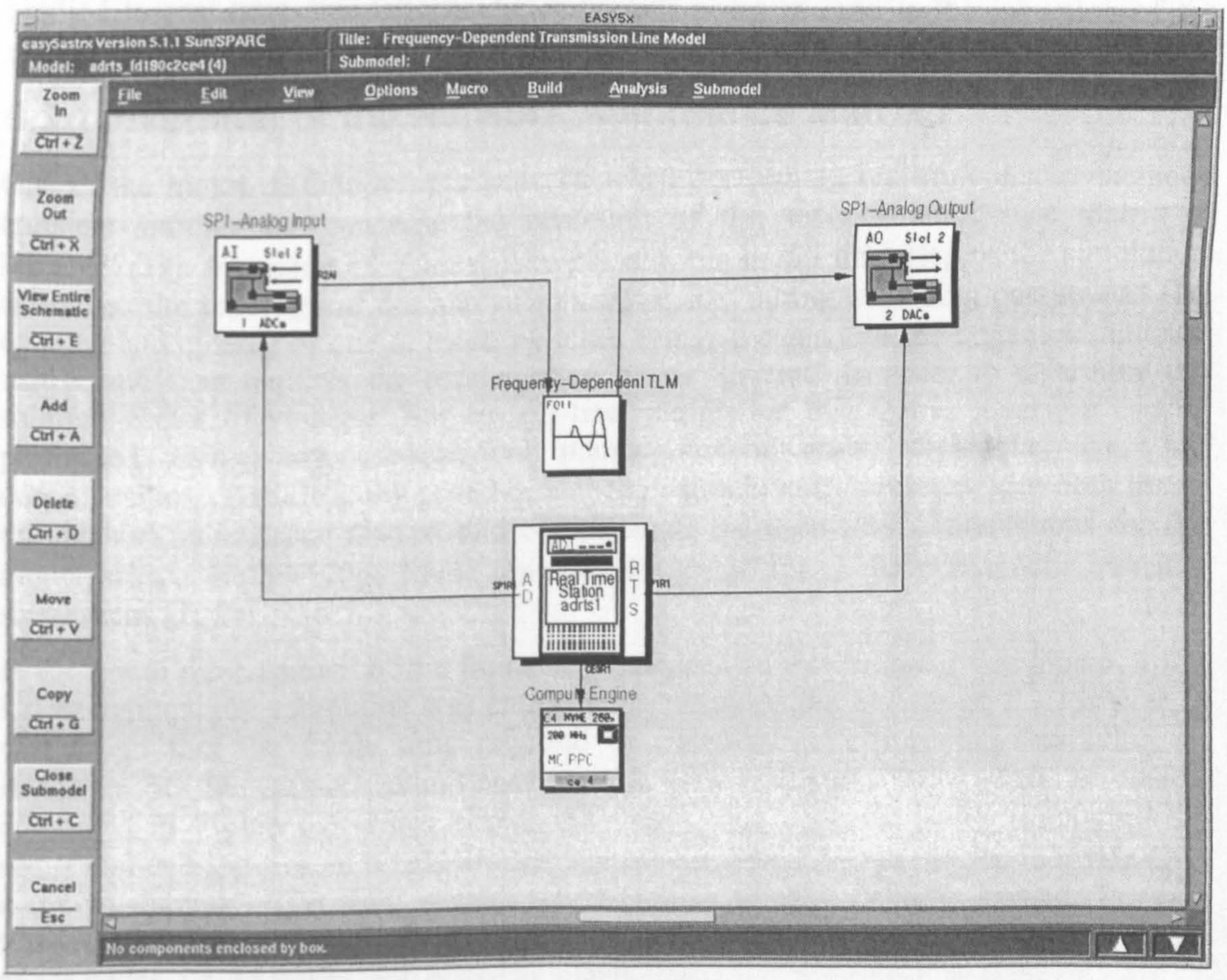

Figure 6.2 EASY5 Graphical User Interface (GUI)

Information regarding the actual time the simulator takes to compute each time-step in the analysis is available at the end of each simulation. The Actual Frame Time (AFT) can be plotted as a function of simulation time and from this plot it can be seen whether or not the AFT has exceeded the time-step chosen for the simulation. If this is the case,

then real-time operation has failed to be maintained. This problem can be resolved, albeit with a decrease in accuracy, by increasing the time available for the simulator to compute each time-step.

6.3 Real-Time Model Implementation

The three transmission line models described before in previous chapters, namely the frequency-independent [28], frequency-dependent [29] and phase domain line representations, were initially developed 'off-line' within the EASY5 simulation environment. The benefit of proceeding in this way is that almost all the testing and debugging of the models can be performed in a more efficient way, with real-time and non-real-time compilation and execution errors isolated.

Once confidence is gained in the fidelity of the model it is incorporated within EASY5 to operate in real-time. In order to do this, the four components necessary for real-time operation, as described in section 6.2.2, are combined with the existing model by connecting the appropriate I/O.

Due to the very stringent CPU requirements imposed by real-time electromagnetic transient analysis (a time step of 50-100μs is usually aimed for [10]) incorporation of these models into a real-time environment is not straightforward. Procedures which are regarded as standard in non-real-time studies may be completely unsuitable when applied to real-time simulations. An important point in case is the inversion of the network admittance matrix, which is discussed in more detail below.

6.3.1 Inversion of the Network Admittance Matrix

One of the major difficulties encountered when performing real-time electromagnetic transient simulations, concerns the inversion of the network admittance matrix **Y** [22,24,32,33]. Inversion of **Y** must take place at the initial time step of the simulation and when the topology of the network changes, e.g. during switching operations. The opening and closing of one or more switches brings a change in the system admittance matrix and thus requires the recalculation of its 'inverse' in order to determine the solution vector of voltages. For an 'off-line' simulation this matrix inversion can be performed using any conventional matrix decomposition technique, e.g. LU decomposition. The difficulty posed in real-time simulations, however, is to both invert the network admittance matrix, and complete all the necessary computations for the model, within the 50-100μs frame time usually aimed for in electromagnetic transient simulations [10].

In the initial development of the frequency-independent transmission line model, a full LU decomposition subroutine was employed to compute the inverse of **Y**. However, it was found that the frame time required to compute each time step involving an inversion of the network admittance matrix was extremely high. This is clearly illustrated in Figure 6.3 which shows the frame time obtained when simulating the sequential energization of a real-life transmission system [34], using the 133MHz CE3 compute engine. The test system corresponds to the 345kV Jaguara-Taquaril transmission system described in Appendix III. The network is comprised of 5 three-phase nodes, i.e. 15 nodes, and contains 6 switches.

Seven peaks in Actual Frame Time (AFT) are clearly visible, each one associated with a call to the LU decomposition subroutine. The largest peak has a maximum value of approximately 665μs. The magnitude of subsequent peaks in the AFT are seen to be progressively smaller, since the order of network admittance matrix is reduced with the closing of each switch. Real-time operation can only be maintained as long as the AFT is less than the selected time step for the simulation. Thus, if the frequency-independent

transmission line model is implemented in this way, using a full LU decomposition approach, it would not be possible to set a time step of less than 665μs for real-time operation to be sustained throughout the simulation. This is evidently much greater than the preferred time step usually considered (50-100μs) and subsequently the accuracy of the solution in this case would be severely reduced.

In order to rectify this problem, several alternative methods were investigated to efficiently invert the network admittance matrix and solve the nodal voltage equations in real-time. The first method attempted was to try and exploit the sparsity of the network admittance matrix in the solution process. However, the frame time obtained using this method was essentially the same as that obtained using the original LU decomposition method. It was concluded that for the practical power networks under consideration for real-time analysis, sparsity orientated solution techniques produce few advantages in terms of computational efficiency over the existing LU decomposition technique.

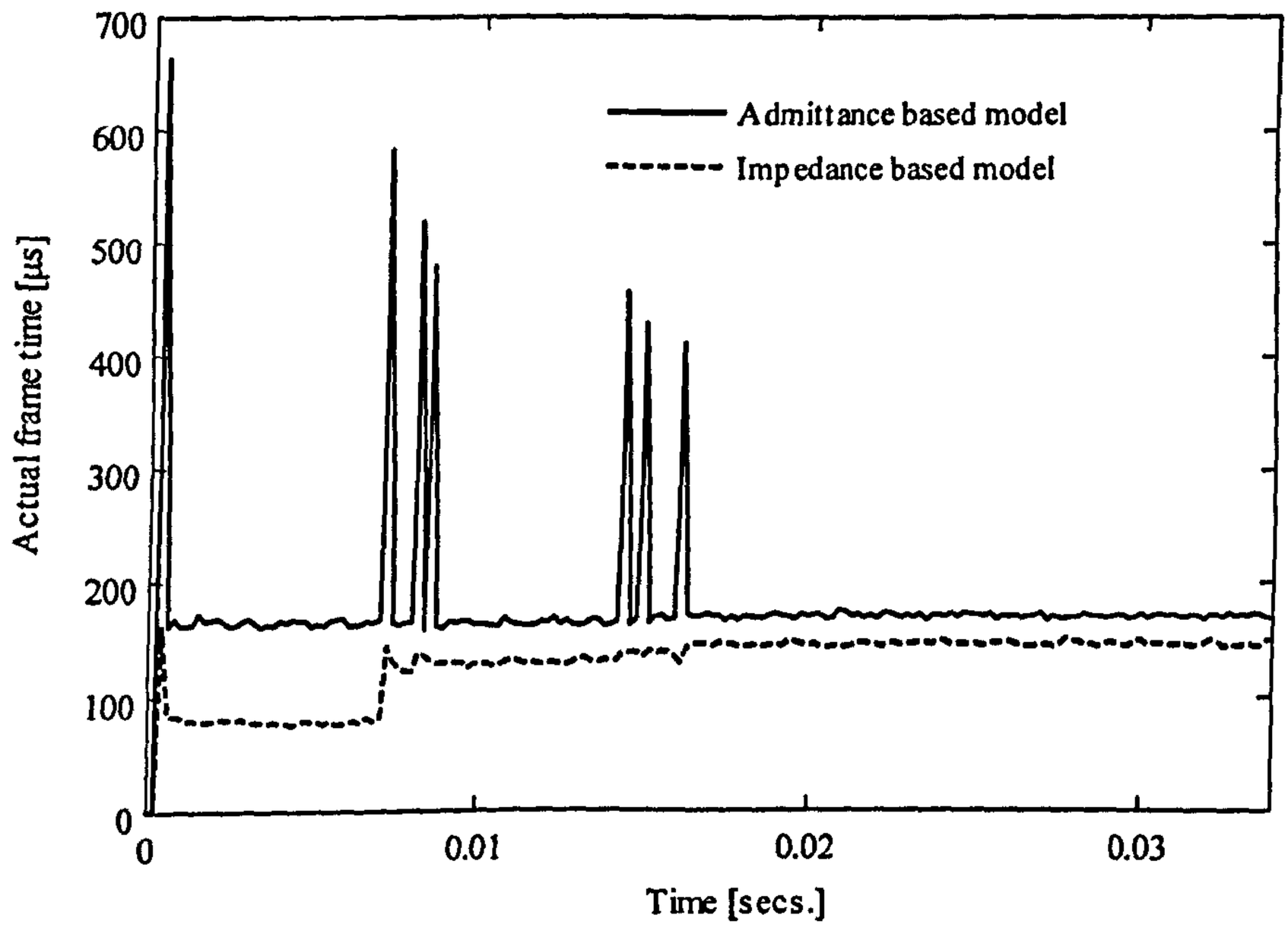

Figure 6.3. Comparison of the actual frame time obtained when using admittance and impedance based methods for the sequential energization of a real-life transmission circuit in real-time

A second method employed a Cholesky factorization on the network admittance matrix, assuming the network admittance matrix is symmetric positive definite [32]. However, as for the sparsity approach, the technique was found to provide little improvement in the AFT when compared with the original LU decomposition method.

A viable approach to this problem was obtained by pre-calculating the network impedance matrix, **Z**, before the real-time simulation was run [7,32,33]. The resulting impedance matrix data is stored within input arrays, defined in the FORTRAN component in EASY5, and in which the transmission line code is contained. The data is then read from the specified array when required during the real-time simulation. The solution vector of voltages is then obtained from efficient matrix-vector multiplications during the simulation.

Figure 6.3 also illustrates the frame times associated with this impedance matrix approach, again using the CE3 compute engine. It can be seen from Figure 6.3 that the reduction in the AFT at the initial time step, and during the sequential switching operations, is considerable. The maximum value in the AFT is now approximately

165μs. Since the time step chosen for both simulations was 190μs, only the impedance matrix based technique has managed to maintain real-time operation throughout the simulation. A summary of the frame times for each method is shown in Table 6.1, including an average value for the frame time over the whole simulation. The initial maximum peak in actual frame time and its implications in terms of conducting electromagnetic transient simulations is discussed in more detail in section 6.5.1.

Table 6.1. Summary of frame times for admittance and impedance matrix based methods using the CE3 compute engine

Method	AFT of initial time step (μs)	Switching Operation AFT (μs)						Average AFT (μs)
		1	2	3	4	5	6	
Admittance	665	582	518	479	456	428	410	178.7166
Impedance	165	145	139	133	139	135	130	127.66

All the transmission line models presented in the following sections have been implemented in real-time using this impedance matrix based approach.

6.4 Real-Time Simulations

In the following sections, an analysis of the accuracy and efficiency of the transmission line models described in this thesis, in the context of real-time simulation, is discussed. These transmission line models correspond to a frequency-independent [28], frequency-dependent [29] and phase domain representation of the line.

A test system corresponding to the 345kV Jaguara-Taquaril transmission system, described in Appendix III, is used for the real-time simulation tests. The transmission line is 398km in length [34]. The system is comprised of 15 nodes and 6 switches and represents a typical size of power network that can be analysed on the real-time simulator with its current hardware and software configuration. The configuration of the transmission system has been illustrated in the previous chapter, but is reproduced again here for convenience in Figure 6.4. Data pertaining to the closing of the circuit breakers can be found in Appendix III

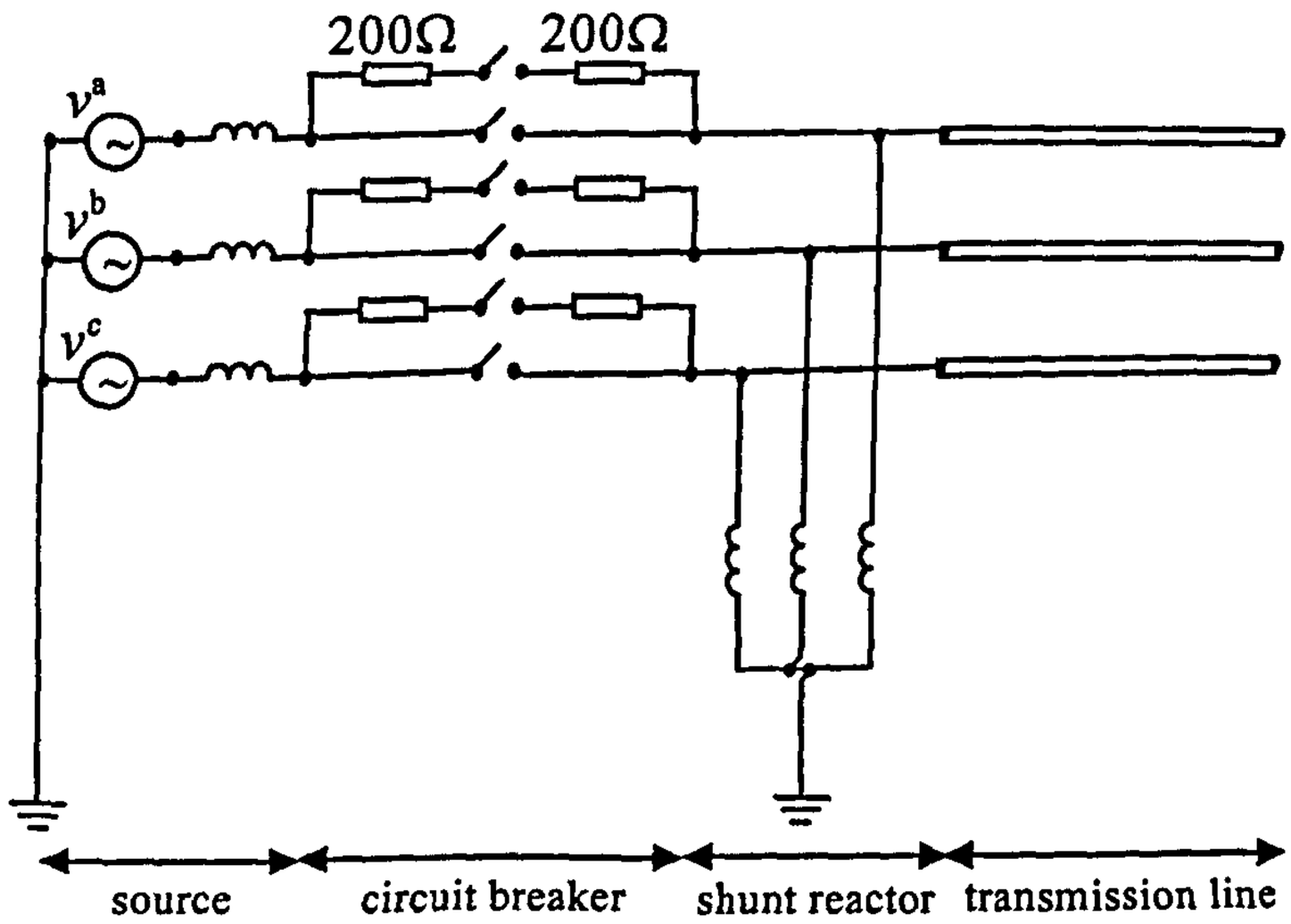

Figure 6.4. Jaguara-Taquaril 345kV transmission system

All the simulations performed in the following sections are undertaken using the latest 333MHz CE4 compute engine.

6.4.1 Modal Domain Transmission Line Models

The first two models to be implemented on the real-time station (RTS) were the frequency-independent and frequency-dependent transmission line models, as described previously in chapter two. The results of a validation test with EMTP [1] for both models were shown in section 2.8.2 and, in the case of the frequency-dependent model, against actual field measurements [34] in section 2.8.3 of chapter two.

Both models were implemented within EASY5 using the network impedance matrix based approach, as discussed earlier, in order to avoid directly inverting the network admittance matrix in real-time. The pre-calculated network impedance matrices are conveniently stored within arrays, defined in the single FORTRAN component that contains the main transient program. The frequency-independent transmission line model has 262 lines of code contained in the FORTRAN component, while the frequency-dependent model has 513. Both models also have seven supporting subroutines that are pre-compiled and linked with the real-time executable generated by EASY5.

For the frequency-dependent model, the real-time simulations were performed with different order approximations of the modal characteristic impedance, $Z_c(\omega)$, and shifted weighting function, $P(\omega)$. The elements of the weighting function, $A(\omega)$, are unwound as discussed in section 2.6.2 before the fitting process takes place so that the elements of $A(\omega)$ are found as smooth functions of frequency and amenable to low-order approximations [29]. The transmission line responses are approximated in the frequency domain with rational functions using the method of Vector Fitting [27], as described in section 2.5.1 of chapter two.

For real-time simulations, if the network solution is to be obtained in the given 50-100μs interval, the order of the approximating rational functions must be kept as low as possible, while still maintaining a high degree of accuracy [10]. A direct relationship exists between the order of rational function approximations and the minimum step size that can be selected for continuous real-time operation. As the number of poles contained in the rational functions is increased, (therefore improving the level of accuracy of the approximations), so does the time required to compute each time step of the simulation. A balance must therefore be sought between the accuracy of the rational function approximations, and the minimum time step that can be selected, for continuous real-time operation to be achieved [10].

Table 6.2. Summary of Approximation Orders for $Z_c(\omega)$ and $P(\omega)$

Fit	$Z_c(\omega)$ zero seq.	$Z_c(\omega)$ pos. seq.
Fit 1	12	12
Fit 2	8	2
	$P(\omega)$ zero seq.	$P(\omega)$ pos. seq.
Fit 1	12	12
Fit 2	6	6

The number of poles and residues used in the fitting of both $Z_c(\omega)$ and $P(\omega)$ are as described previously in Table 2.1 of chapter two, and repeated in Table 6.2 for convenience. The frequency responses are approximated in the interval 10^{-2}-10^{6}Hz.

6.4.2 Real-Time Sequential Energization Results

Figures 6.5-6.7 show the simulated phase voltages at the receiving end of the line after a sequential energization test for both the frequency-independent and frequency-

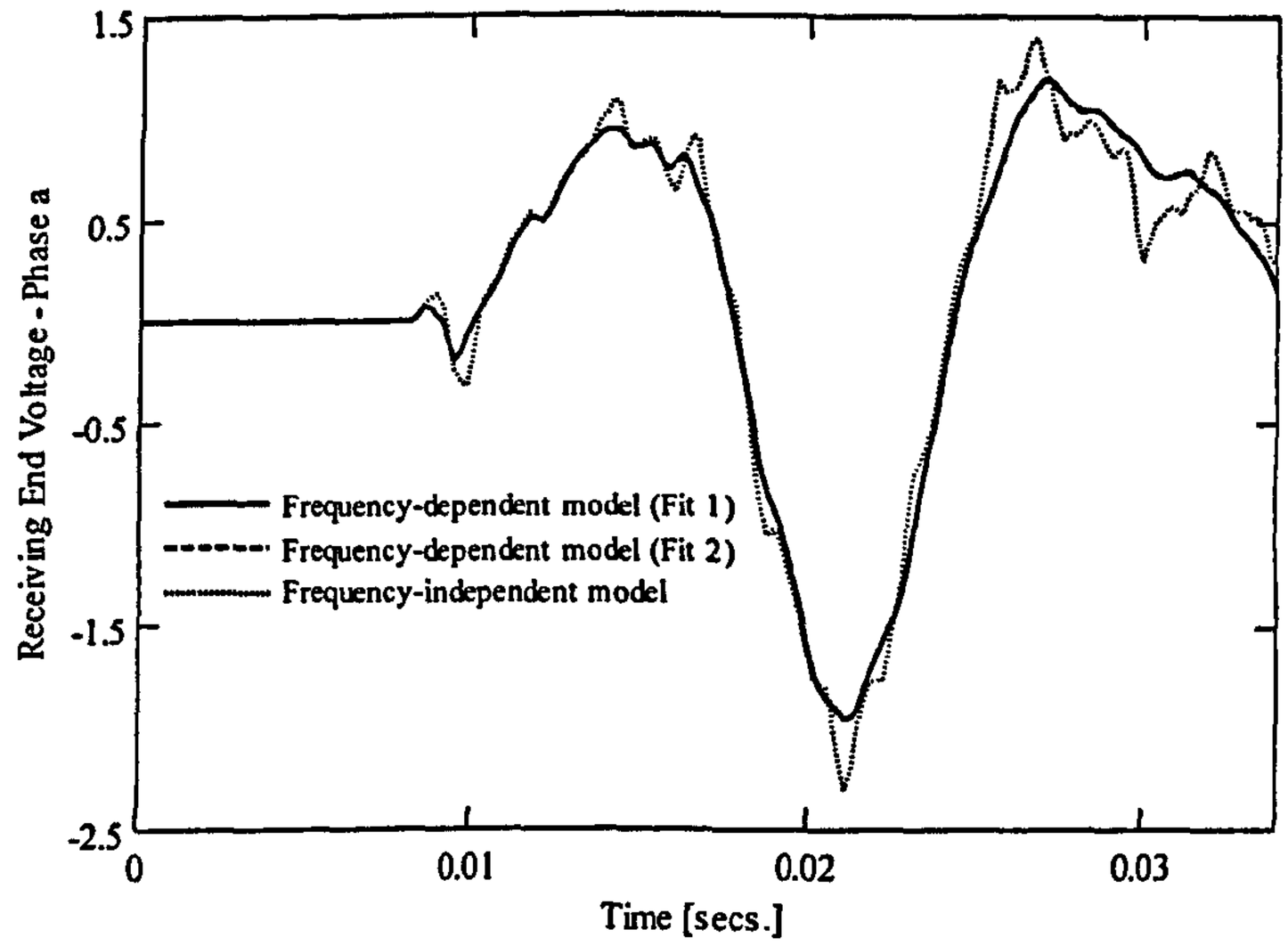

Figure 6.5. Receiving end voltage after simulated sequential energization - Phase a (Real-time frequency-independent and frequency-dependent models)

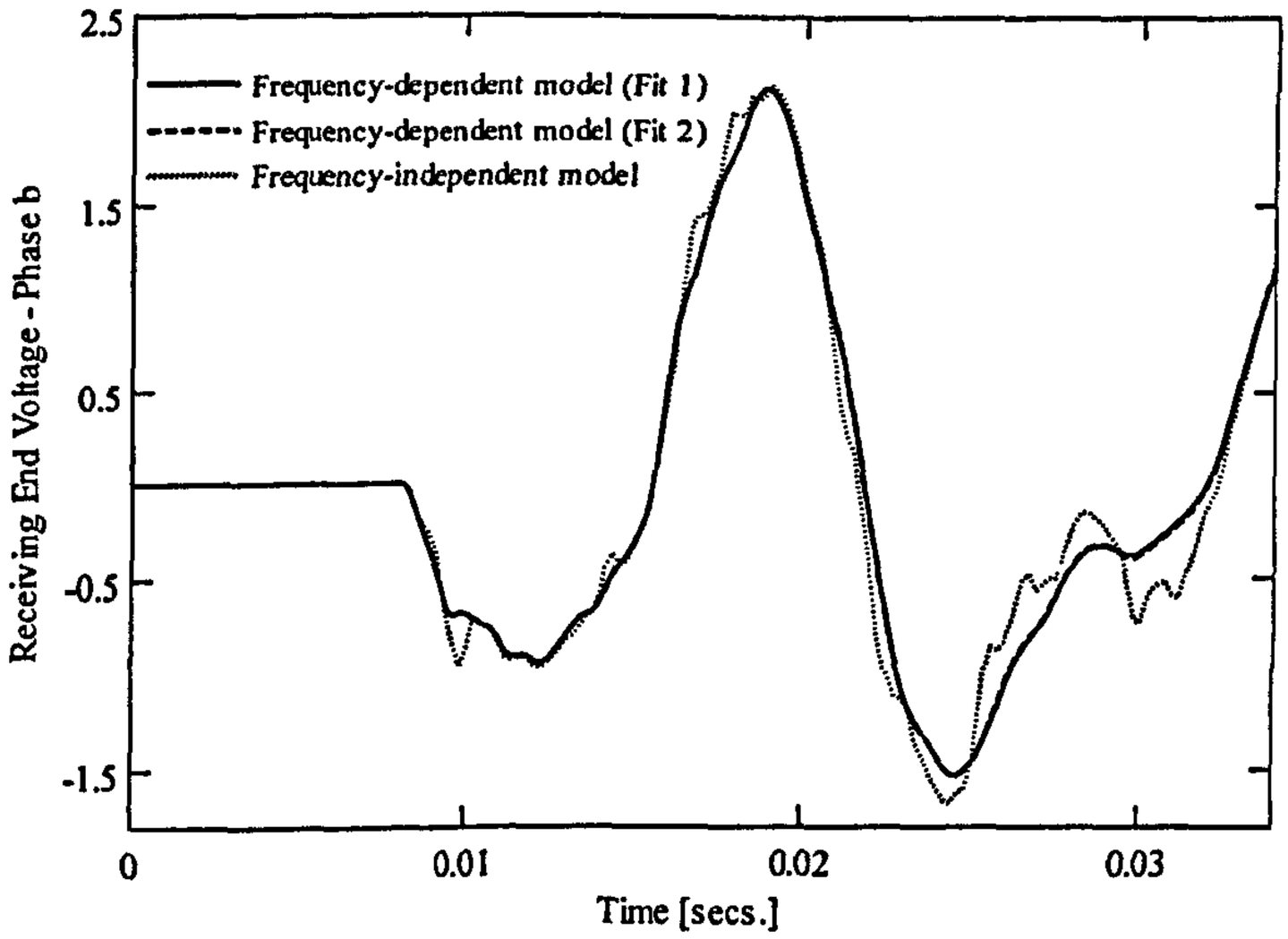

Figure 6.6. Receiving end voltage after simulated sequential energization - Phase b (Real-time frequency-independent and frequency-dependent models)

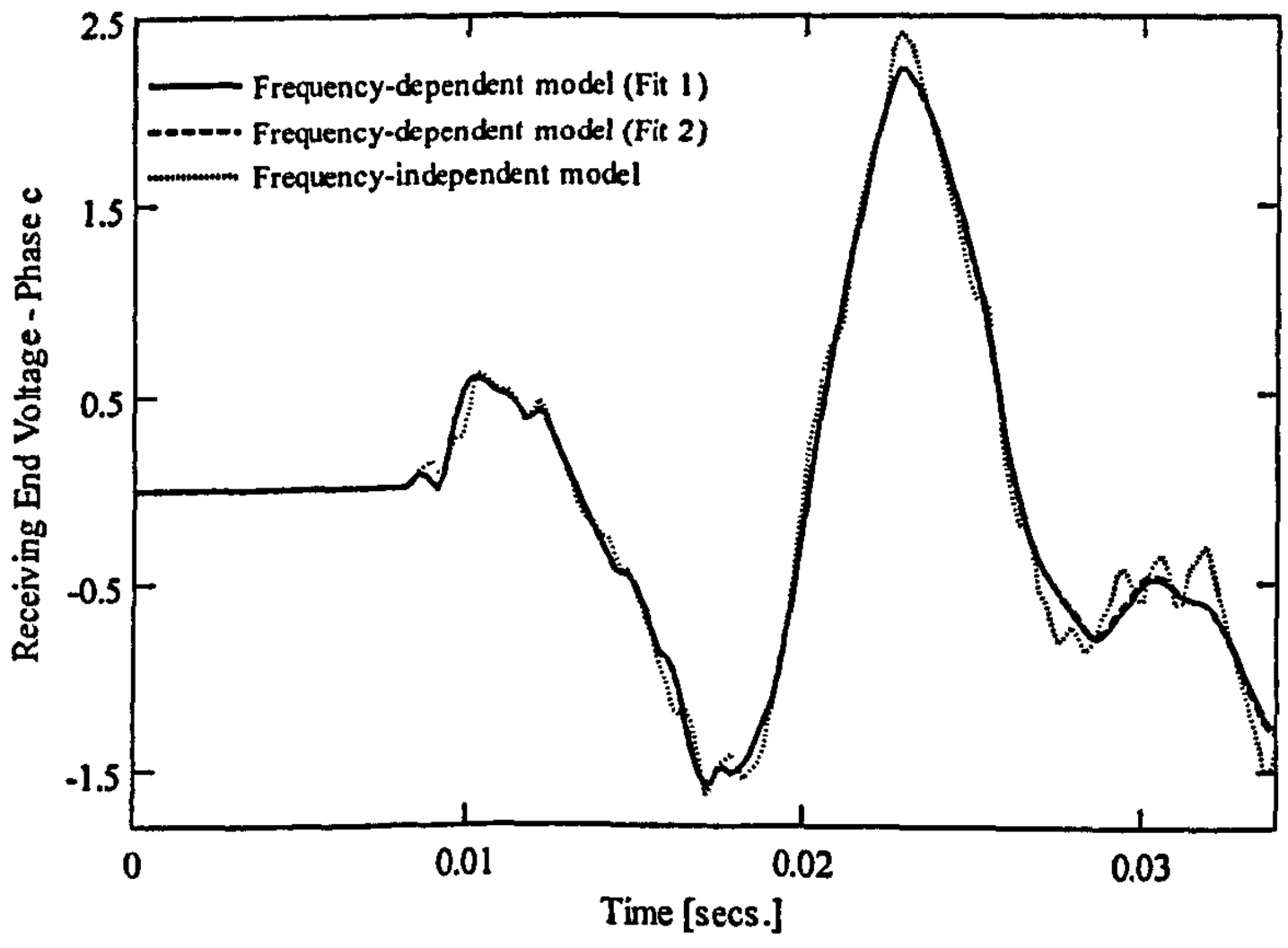

Figure 6.7. Receiving end voltage after simulated sequential energization - Phase c (Real-time frequency-independent and frequency-dependent models)

dependent line models. For the frequency-dependent line representation, the results corresponding to the two different sets of approximating functions, as described in Table 6.2, are presented. The time step chosen for both simulations is 190μs. In this simulation, the reactor at the sending end of the line, as illustrated in Figure 6.2, is not included. The transmission line in these cases is assumed to be perfectly transposed.

It can be seen from Figures 6.5-6.7 that there is little difference in the accuracy of the results for the frequency-dependent model using the two different sets of rational function approximations, despite the increased accuracy obtained with Fit 1. However, as expected, the results can be seen to be much more accurate than those obtained using the frequency-independent line model, which shows an increase in the peak magnitudes of the phase voltages as well as an amplification of the higher harmonics contained in the waveforms. This is a consequence of assuming the parameters of the transmission line are constant, evaluated at the power frequency, and neglecting the losses inherent in the system [35].

Figure 6.8 shows the actual frame time (AFT) associated with each time step of the sequential energization simulation for the three different cases, as a function of simulation time. As expected, the frequency-independent model, having the least amount of computations to perform (there are no convolution operations required in this case), requires the least time to compute each time step of the simulation. The average frame time for the whole simulation is approximately 52.6611μs. For the frequency-dependent line model using the low order approximation (Fit 2), there is an increase of approximately 4.1μs, with an additional 5.2μs on top of this for the higher order approximation (Fit 1).

The higher order set of approximations (Fit 1) can be seen to have a significant influence on the time required to compute each time step of the simulation. Indeed, the increase in frame time for the frequency-dependent model, using the two different sets of approximations, is greater than that between the frequency-dependent model using fit 2 and the frequency-independent line representation. This reaffirms the importance of seeking the lowest order possible for the approximating functions used in the frequency-dependent model when performing real-time electromagnetic transient simulations.

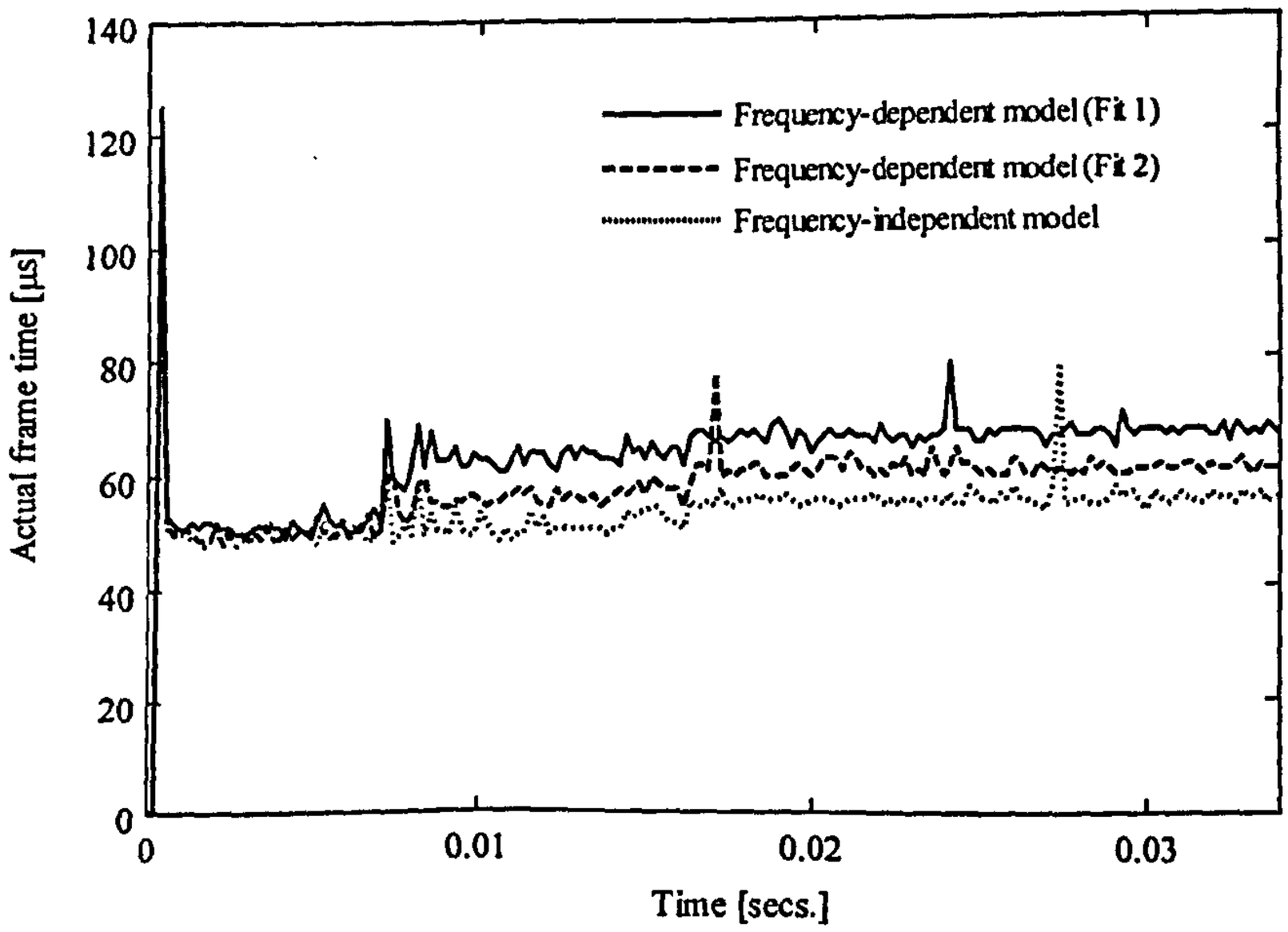

Figure 6.8. Actual frame time (AFT) when simulating a sequential energization of the Jaguara-Taquaril transmission using modal domain models

6.4.3 Phase Domain Transmission Line Model

The sequential energization test case described previously was repeated (including the reactor at the sending end of the line) using the phase domain transmission line model that has been developed over the previous three chapters. The transmission line in this case is intrinsically modelled as untransposed, accurately taking into account any geometric imbalances naturally present in the line. The frequency-dependent effects of the line are also taken into account by approximating the transmission line responses with rational functions in the frequency domain.

The elements of the characteristic admittance, $\mathbf{Y}_c(\omega)$, and shifted wave propagation matrices, $\mathbf{P}(\omega)$, are approximated using the method of Vector Fitting [27] directly in frame of reference of the phases. The elements of each column of $\mathbf{Y}_c(\omega)$ are approximated with the same set of poles, and similarly for $\mathbf{P}(\omega)$. Only the residues for each element of a given column differ from each other. This columnwise realization is expected to provide a 2-fold increase in the efficiency of the time domain simulation as compared to conventional element-by-element fitting [36].

As for the modal domain based transmission line models described earlier, the real-time application of this phase domain model is based on the network impedance based approach.

The code for the phase domain model is directly incorporated within a single FORTRAN component in EASY5, with 1486 lines of code in the main transient program. Seven supporting subroutines are also pre-compiled and linked with the real-time executable generated by EASY5. As with previous simulations, the step size in this case is selected at 190μs.

The real-time simulations were performed with different order approximations of the characteristic admittance matrix, $\mathbf{Y}_c(\omega)$, and shifted wave propagation matrix, $\mathbf{P}(\omega)$. The number of poles and residues used in the fitting of both $\mathbf{Y}_c(\omega)$ and $\mathbf{P}(\omega)$ are described in Table 6.3. The characteristic admittance was approximated in the interval 1-10^6Hz, while the shifted wave propagation matrix was fitted in the interval 1-10^5Hz.

The maximum frequency under consideration when fitting the shifted wave propagation matrix was selected at 10^5Hz in order to ensure a sufficiently reduced order rational function approximation for $\mathbf{P}(\omega)$ was obtained, suitable for real-time simulations.

Table 6.3. Summary of Approximation Orders for $\mathbf{Y}_c(\omega)$ and $\mathbf{P}(\omega)$

Fit	Number of poles	
	$\mathbf{Y}_c(\omega)$ (all columns)	$\mathbf{P}(\omega)$ (all columns)
Fit 1	10	10
Fit 2	8	10
Fit 3	5	10

As discussed earlier, the order of the approximating functions play a very important role in the selection of the integration time step for a given real-time simulation. The higher the order of the approximating functions, the less likely it is that real-time operation can be performed continuously using a time step in the desired range (50-100μs) [10]. Bearing this in mind, it was felt that real-time operation could only be performed with a sufficiently small time step if the frequency range considered for approximating the shifted wave propagation matrix was reduced to (1Hz-10^5Hz). By fitting the elements of $\mathbf{P}(\omega)$ in this frequency range, a very low-order rational function approximation could always be obtained.

In contrast, since the elements of the characteristic admittance matrix are smooth functions of frequency, it is not difficult to obtain an accurate, very low-order approximation for this function up to frequencies of 1MHz.

6.4.4 Real-Time Sequential Energization Results

Figures 6.9-6.11 show the simulated phase voltages at the receiving end of the line after a sequential energization, obtained using the phase domain transmission line model using the approximating functions obtained in fit 3, as described in Table 6.3. Only the results pertaining to fit 3 are shown in Figures 6.9-6.11 since the differences between the three fitting approximations are negligible. The results from fit 3 are superimposed on those obtained using the frequency-dependent model using the fit 2 data.

It can be seen from Figures 6.9-6.11 that there is little difference in the accuracy of the phase a and b voltages for both methods up to approximately 25ms, although both of these phase domain voltages are seen to slightly lag those of the frequency-dependent model. A significant difference can be observed in phase c however. A peak voltage of 1.963pu is obtained at a time t=22.8ms for the frequency-dependent method. For the phase domain model, the peak voltage has a magnitude of 1.598pu and is delayed by approximately 0.57ms.

6.4.5 Comparison with Field Measurements

A further analysis of both results can be obtained by comparing the results with actual field measurements [34].

Figure 6.12 shows the receiving end results for all three phases obtained using the phase domain transmission line model using the fit 3 data. Superimposed on these results are those of the frequency-dependent line model using the approximating functions obtained with fit 2, as described in Table 6.2. Figure 6.13 corresponds to the results obtained from the actual field measurements, superimposed with those calculated using an electromagnetic transients program [35].

Comparing the results of both line models with those of the field measurements it can be seen that in general the results corresponding to the phase domain transmission line compare better with those of the field recordings. The peak magnitude of the phase c voltage has a value of 1.287pu for the phase domain model compared with 1.498pu for the frequency-dependent line model. The corresponding value obtained from the field data is approximately 1.35pu. After 20ms, at the zero crossing of phase c, the field measurements are delayed by 0.9ms when compared to the frequency-dependent phase c voltage. In the case of the phase domain model, the phase c voltage lags that of the frequency-dependent line by approximately 0.2ms.

6.4.6 Actual Frame Times for Phase Domain Model

Figure 6.14 shows the values of the Actual Frame Time (AFT) obtained for the sequential energization test using the phase domain model with the three different fitting orders, as summarized in Table 6.3.

The influence of the fitting order can be seen to significantly effect the frame time over the time period of the simulation. There is an increase in frame time of approximately 15μs using the approximating functions of fit 1, as compared to the other two data sets of reduced order (fit 2 and fit 3). The initial peak values in AFT are approximately 228μs, 176μs and 173μs for fit 1, fit 2 and fit 3, respectively. The initial peak in frame time will be discussed in more detail in section 6.5.1.

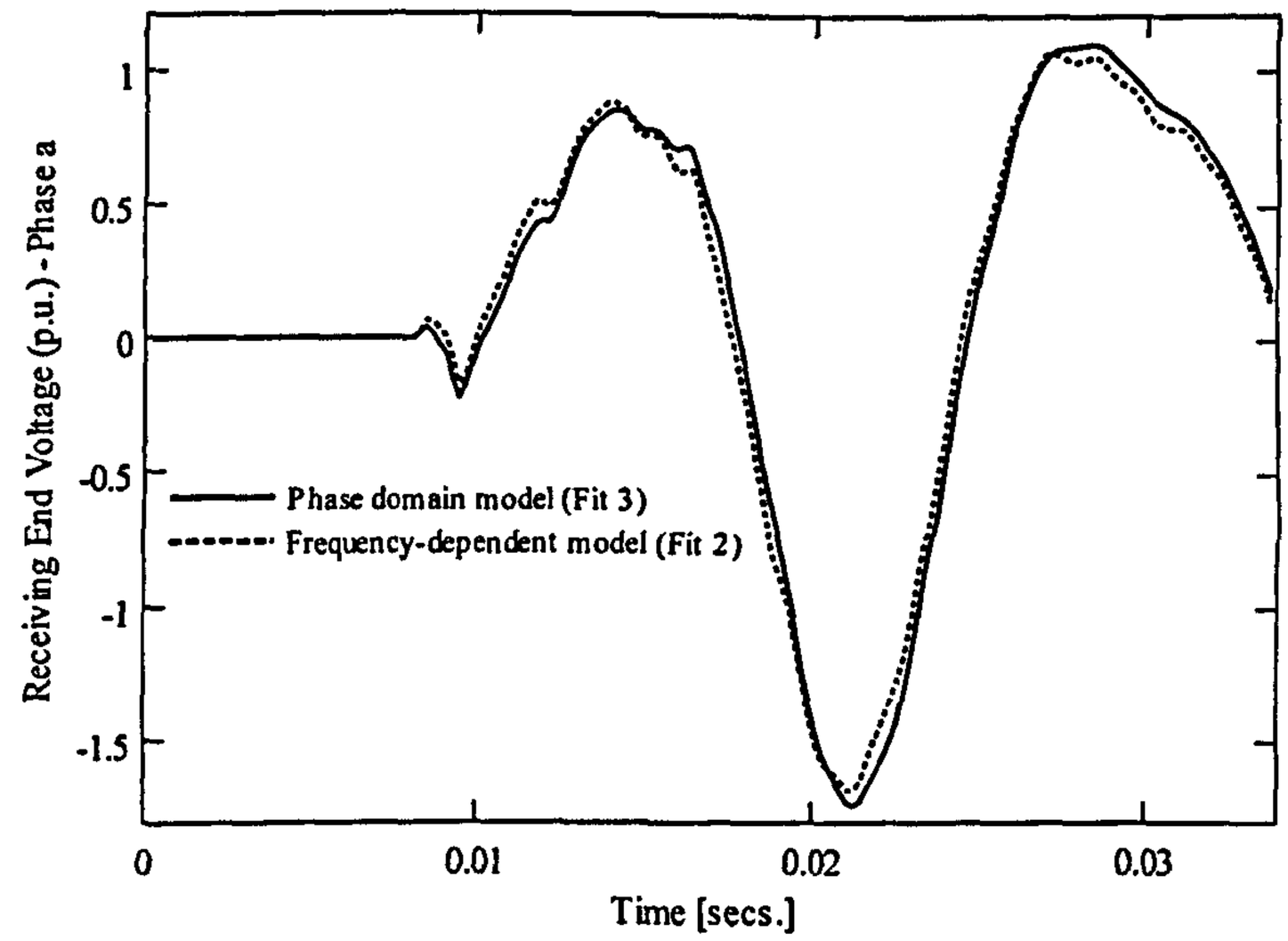

Figure 6.9. Receiving end voltage after simulated sequential energization - Phase a (Real-time frequency-dependent model and phase domain model)

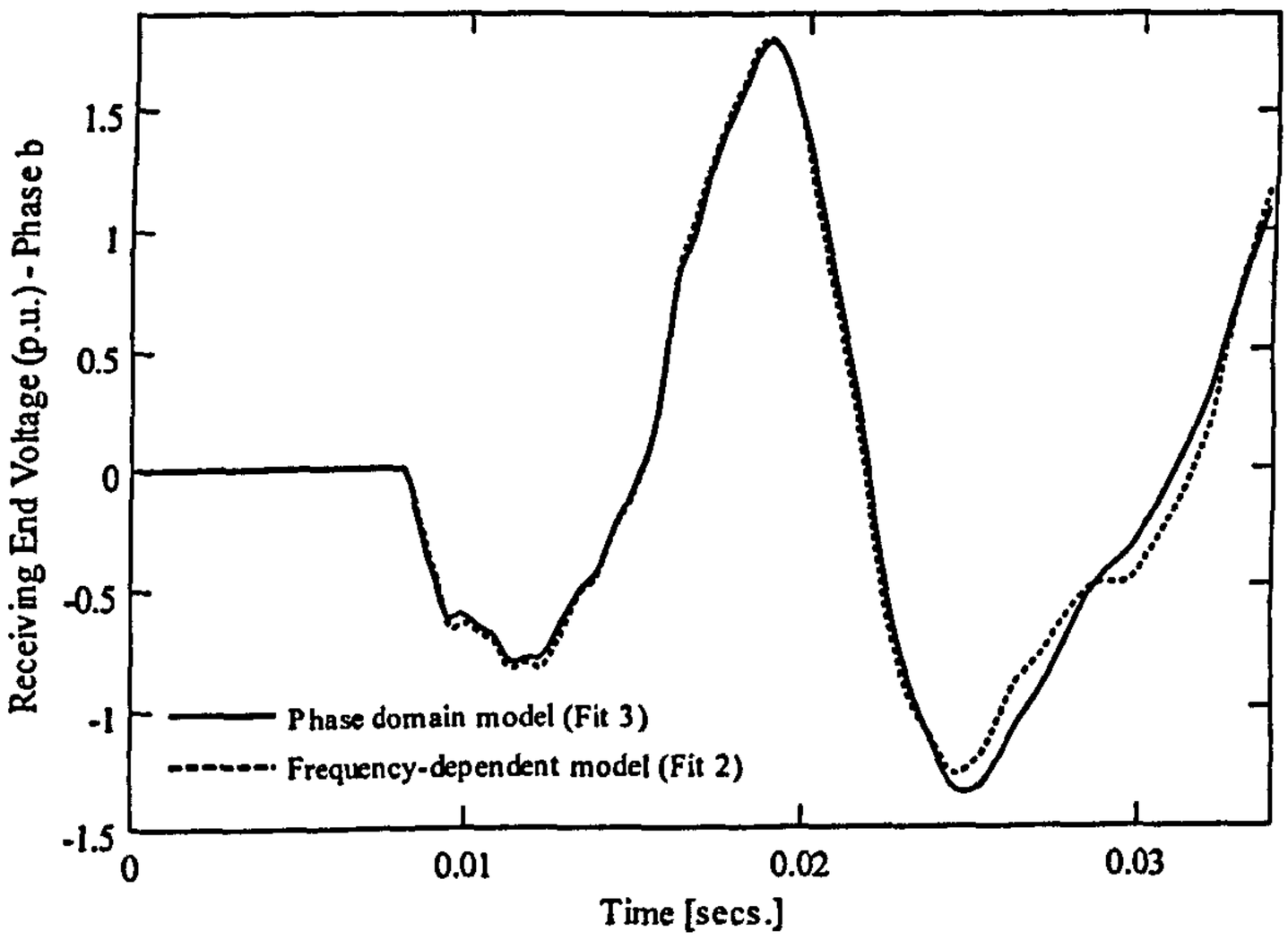

Figure 6.10. Receiving end voltage after simulated sequential energization - Phase b (Real-time frequency-dependent model and phase domain model)

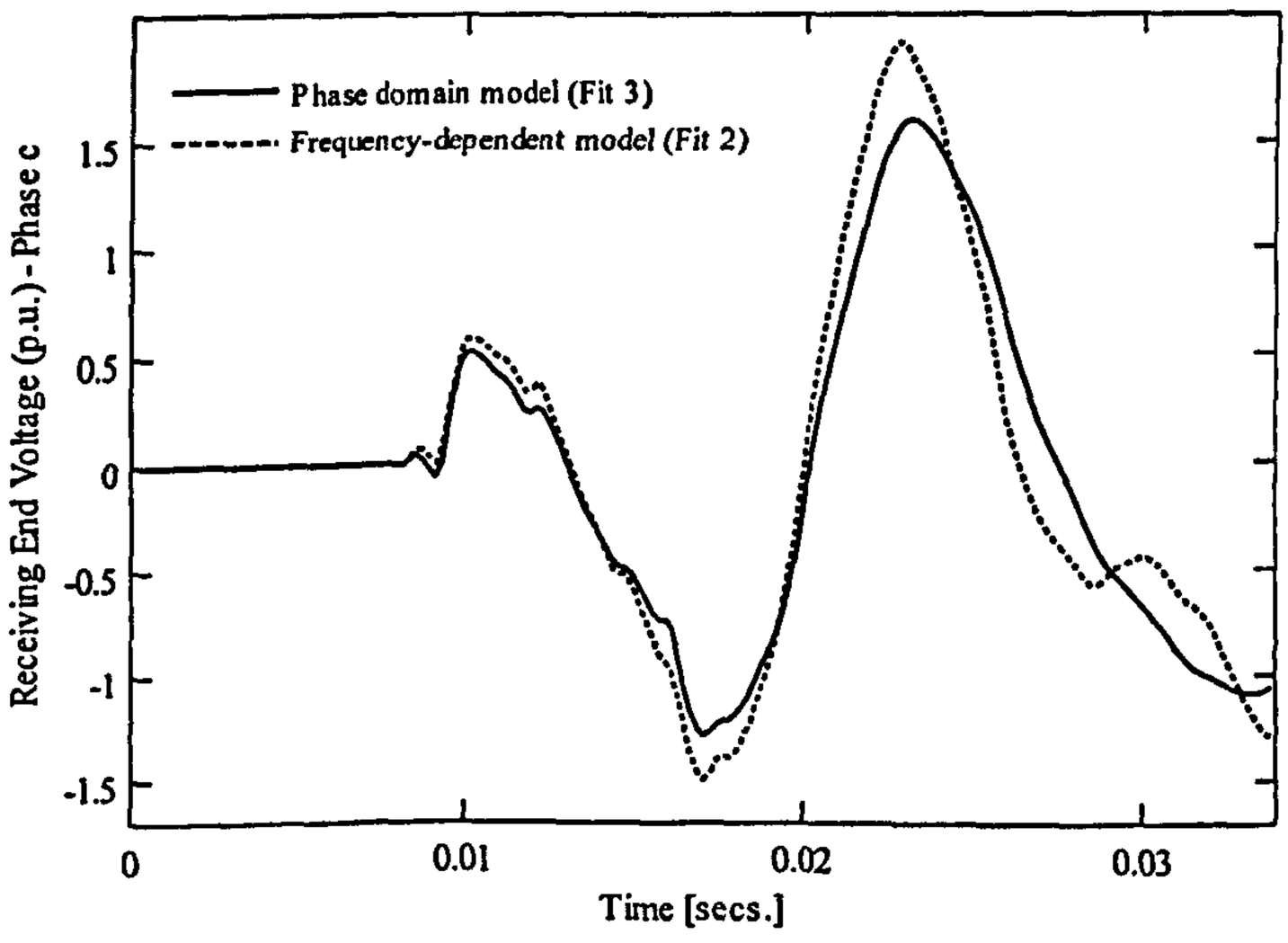

Figure 6.11. Receiving end voltage after simulated sequential energization - Phase c (Real-time frequency-dependent model and phase domain model)

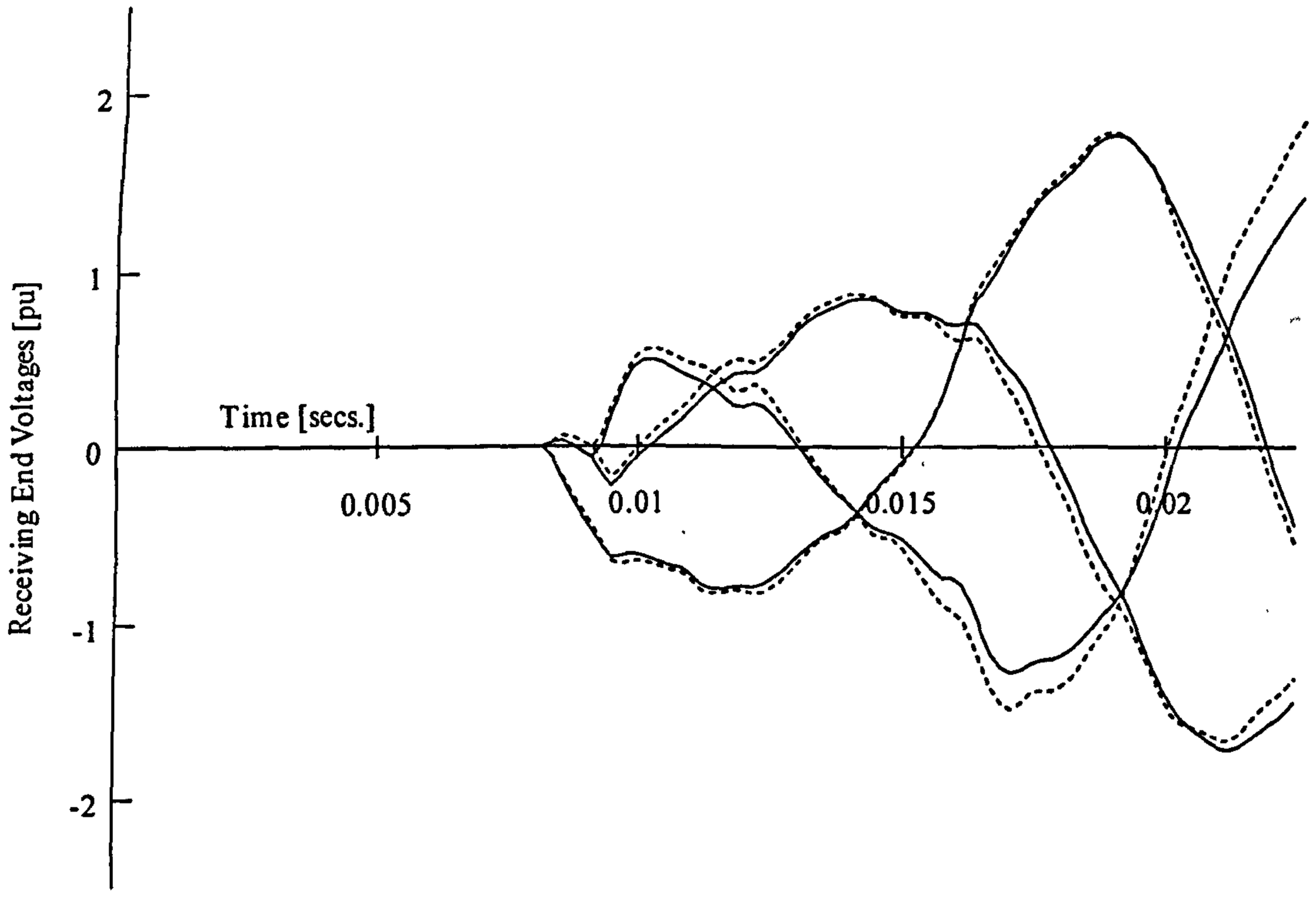

Figure 6.12 Simulated energization results for frequency-dependent (dashed line) and phase domain line model (solid line)

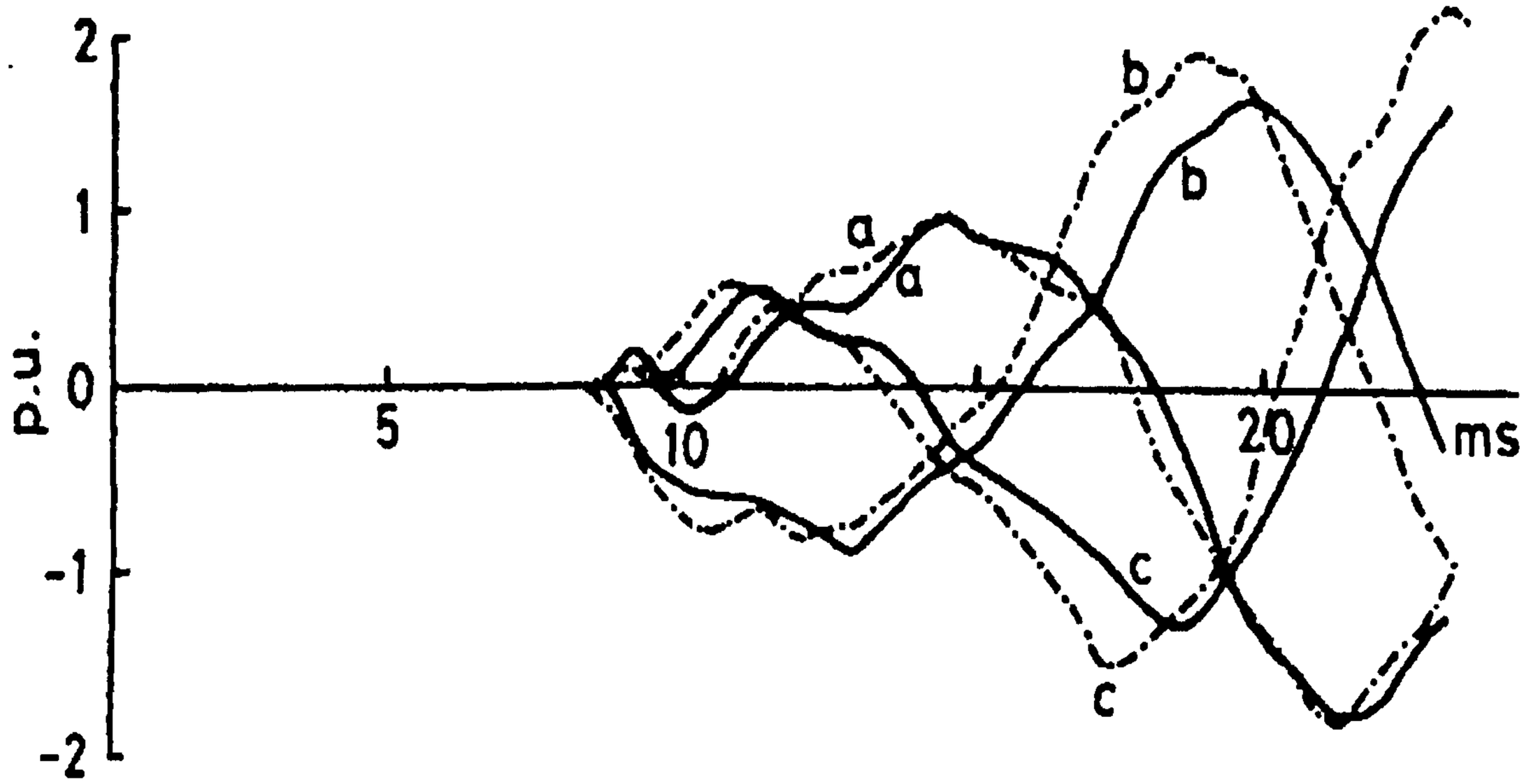

Figure 6.13 Energization results for actual field measurements (solid line) and electromagnetic transient program (dashed line)

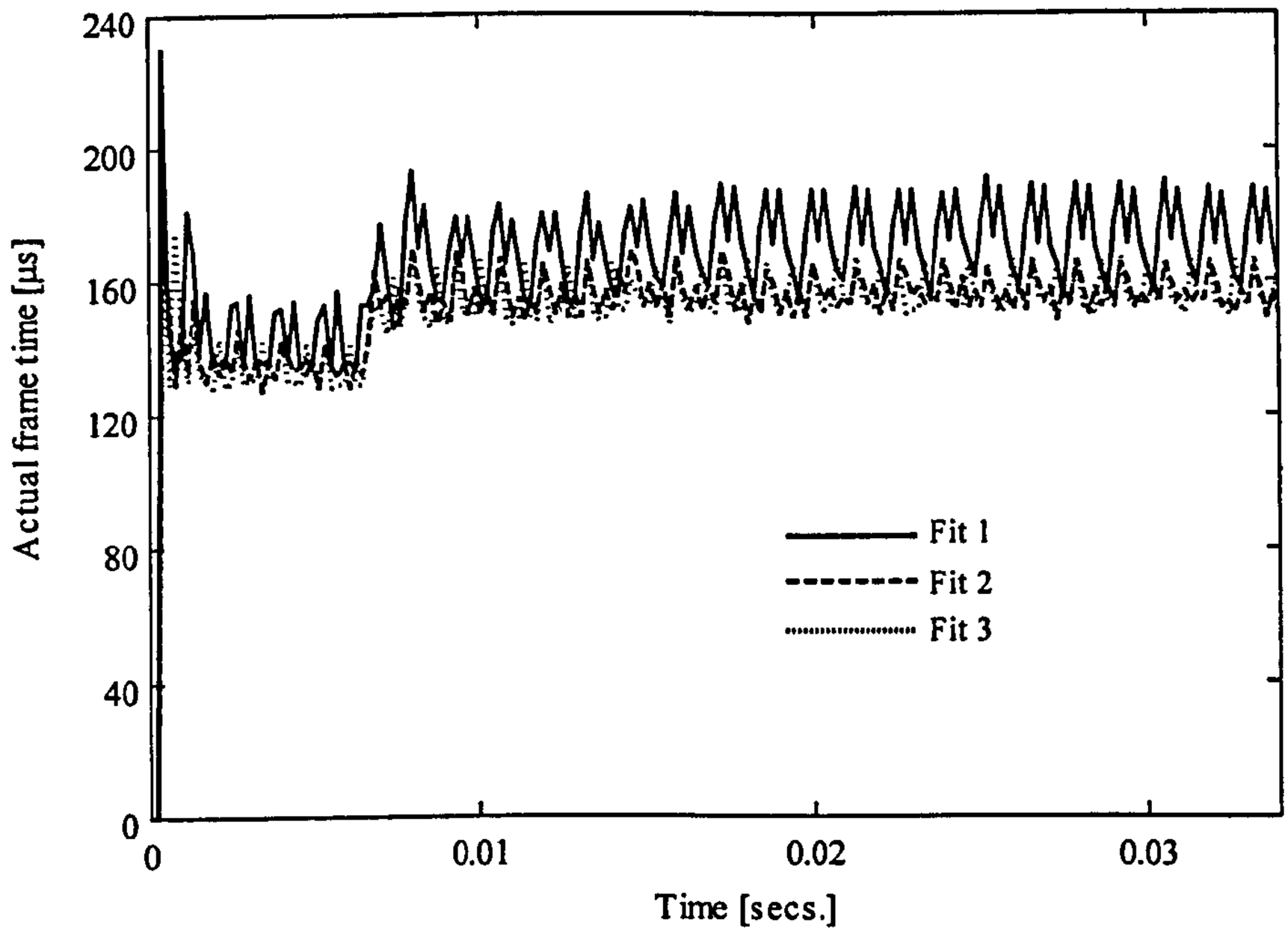

Figure 6.14 Actual frame time obtained for a sequential energization of a real-life transmission circuit using the phase domain transmission line model

6.5 Summary of AFT for Transmission Line Models

A summary of the Actual Frame Times (AFT) obtained for each model when using the CE3 and CE4 computes engines for the sequential energization simulation described in the previous sections, is provided in Tables 6.4-6.6. The AFT for each simulation case was obtained using a step size of 190µs. The phase domain transmission line model was only executed in real-time using the CE4 compute engine, hence there is no data referring to the CE3 compute engine given in *Table 6.6.*

The performance enhancement of the CE4 compute engine over the CE3 is quite clearly shown in Tables 6.4 and 6.5. For the frequency-dependent transmission line model, using the CE3 it was not possible to maintain real-time operation with the desired step size, despite the small number of poles used in the second fitting. For both cases, a single frame overrun occurred at the initial time step. However, when using the CE4 compute engine, no overruns were recorded, and the average value of the AFT for both fits was at least 120µs smaller than the actual step size used for the simulation. The initial peak in frame time does, however, preclude a reduction in step size to no less than approximately 140µs, taking into account any 'hidden' frame time.

For the frequency-independent transmission line model, continuous real-time operation was attained with both compute engines, with no frame overruns recorded. The step size of 190µs does however represent the lowest Δt possible to maintain real-time operation using the CE3 compute engine, again bearing in mind there may be some hidden frame time.

Table 6.4. Summary of AFT for frequency-independent transmission line model

CE3 (133MHz)			CE4 (333MHz)		
AFT for initial time step (µs)	Average AFT (µs)	Frame Overruns	AFT for initial time step (µs)	Average AFT (µs)	Frame Overruns
170	138	0	112	52.6611	0

Table 6.5. Summary of AFT for frequency-dependent transmission line model

No. of poles				CE3 (133MHz)			CE4 (333MHz)		
Zero seq.		Pos. seq.		AFT for initial time step (μs)	Average AFT (μs)	Frame Overruns	AFT for initial time step (μs)	Average AFT (μs)	Frame Overruns
Z_c	P	Z_c	P						
12	12	12	12	255	175	1	125	62.016	0
8	6	2	6	240	155	1	118	56.7944	0

Table 6.6. Summary of AFT for phase domain transmission line model

No. of poles (all columns)		CE4 (333MHz)		
$Y_c(\omega)$	$H(\omega)$	AFT for initial time step (μs)	Average AFT (μs)	Frame overruns
10	10	228	165.155	43
8	10	176	151.044	1
5	10	173	151.82	0

The computational efficiency of the newly developed phase domain transmission line can be assessed against the two conventional modal domain approaches from analysing Table 6.6. For the three test cases run, with varying order approximations of the transmission line responses, only the third case (with the lowest order approximation of the characteristic admittance) achieved continuous real-time operation. The initial peak in this case was recorded at 173μs, with the average AFT for the rest of the simulation at 151.82μs. This represents and increase of approximately 89-95μs as compared to the frequency-dependent transmission line, depending on the number of poles chosen in the fitting process. When compared to the frequency-independent line model, the phase domain method requires an extra 99μs to execute.

It should be noted however, that both the frequency-independent and frequency-dependent transmission line models assume that the transmission line is perfectly transposed, so that a constant transformation matrix can be used to exchange information between the phase and modal domains, and vice-versa [29]. This assumption considerably increases the efficiency of the time domain model, since the numerical burden in evaluating the time domain solution is reduced [29].

6.5.1 Initial Peak in AFT

In all of the real-time simulations presented, an initial peak in the actual frame time (AFT) has always occurred. For all these cases, this initial peak in AFT has been the limiting factor in determining the time step chosen for the real-time simulation. This is inevitably the case since continuous real-time operation can only be maintained as long as the frame time remains below that of the selected integration time step over the complete time period of the simulation. Thus, if the time step is chosen below the value of the peak AFT (which in this case arises at the initial tine step) then real-time operation has not been sustained.

The peak in AFT appears to be caused by a necessary initialization and synchronization phase for the processors in the RTS as the simulation is initially executed. Investigations have shown that as much as 120μs is generated at the initial time step as a result of these activities, in addition to the frame time required to compute the modelled system equations.

A possible way forward could arise by instructing the processors to delay the actual initiation of the transient simulation, until such time as the processors have settled to what could be regarded as a 'steady-state' operating condition. In doing so, the initial peak in frame time would be avoided and the time step for a simulation could be reduced significantly. However, it has not been possible to attempt to try this strategy at

the current time.

6.5.2 Integrated Development Environment

At the present time, it is not possible to combine the computational power of both compute engines (CE3 and CE4) during a simulation. The executable model must be built using either the 133MHz CE3 or 333MHz CE4 compute engines. However, in the near future it will be possible to incorporate both the compute engines currently available in the RTS (and any subsequent additional CEs) within a real-time model, by making use of ADI's newly developed Integrated Development Environment (IDE).

Using IDE, specific computations performed during the simulation can be executed on a specific processor, e.g. the initialization of model arrays at the initial time step could be split between the two processors. This is expected to reduce the AFT that occurs at the start of a simulation. The required I/O is then transferred at the appropriate time between compute engines.

This software enhancement is expected to significantly improve the overall performance of the real-time simulator. In particular, it is anticipated that the phase domain transmission line model could be successfully operated with a time step in the 50-100μs range, usually aimed for in electromagnetic transient simulations [10].

6.6 Future Real-Time Simulation Applications Overview

Real-time digital simulators have increasingly been adopted by manufacturers, large utilities and research organizations over the last decade since they provide a cost effective and flexible technology to replace the previous generation of analogue simulators. Real-time digital simulators are being used more and more in many areas of power systems analysis, such as for the closed-loop testing of control and protection equipment [13-18]; to perform analytic system studies [13]; and to educate operators, engineers and students.

With further development, and utilizing the real-time simulation environment that has been developed for conducting electromagnetic transients as a part of this research, the real-time station is expected to be applied to the following future activities.

6.6.1 Protection Equipment Testing

The electromagnetic transient simulation environment that has been developed within the real-time station (RTS), incorporating frequency-independent, frequency-dependent and phase domain representations of power transmission lines provides an accurate and flexible means to perform hardware-in-the-loop testing of protection and control systems.

However, in order to maintain a good degree of accuracy it will be necessary to model instrument transformers, such as the current transformer (CT) and Capacitive Voltage Transformer (CVT), since during transient conditions these devices may significantly effect the wave-shapes that are seen by the protective relay.

6.6.2 Harmonic Waveform and Power Quality Disturbance Generator

The study of power quality in power systems has become a very important area of power system engineering. Many industrial and commercial electric customers now require a high level of power quality due to the increasing sensitivity of sophisticated process controls and the growing reliance on computers. These new customers are very sensitive to electric disturbances, principally to voltage sags. Power Quality (PQ) is a

new area in electric power systems which has assumed considerable importance in the 1990's. The focus of PQ has been on subjects such as harmonics, sags, swells, overvoltages, interruptions, flickers, transients, noise, etc., in power systems.

The Real-time station (RTS) provides an excellent platform to investigate PQ issues in real-time. Waveforms with transient, dynamic and harmonic characteristics can be generated using the RTS and fed through amplifiers to the external equipment under test, e.g. energy meters, protection devices, sensitive loads etc., to ensure proper operation. Field data from Digital Fault Recorders (DFRs) could also be used directly by the simulator for open loop testing of equipment.

6.6.3 FACTS and Custom Power Applications

Flexible AC Transmission Systems (FACTS) utilize power electronics technology to allow a greater control of power flow and a secure loading of High Voltage transmission lines to levels nearer to their thermal limits. Custom Power devices are the low voltage equivalents of FACTS devices and are used to enhance the reliability and quality of power flow in distribution systems. The new generation of FACTS and Custom Power devices are centred on Voltage Source Inverter (VSI) based controllers.

The application of the real-time station in this area would be for the testing of scaled down, low power prototypes of the FACTS and Custom Power devices mentioned above. For example, with a practical power network modelled within the RTS the simulated network can be combined with the actual prototype for performing closed-loop testing of the physical control scheme under the normal and abnormal operating conditions of the power system.

6.7 Conclusions

This chapter has described the development of an environment for performing accurate and reliable real-time electromagnetic transient simulations of practical transmission systems using a commercially available real-time digital simulator. Three transmission line models corresponding to frequency-independent, frequency-dependent and phase domain representations have been incorporated within this environment.

One of the main difficulties that must be overcome when performing real-time electromagnetic transient simulations concerns the 'inversion' of the network admittance matrix. This must take place at the initial time step of the solution and subsequently when the topology of the network changes, e.g. during a scheduled switching operation. The frame time required to perform this operation in real-time is considerably higher than the time step usually selected for real-time EMTP-type simulations (50-100μs). This problem has been overcome by calculating the network impedance matrix 'off-line'. The data is then stored in arrays until such time as it is required during the analysis. This method considerably reduces the frame time for each time step in the simulation, allowing a smaller integration step-size (and hence more accurate solution) to be selected for a given simulation.

The results of a sequential energization of a real-life transmission circuit have been presented for all three models. The results obtained from the phase domain and frequency-dependent line models are compared to those obtained from actual field recordings. In general, the results of both line models agree well with the field measurements, however overall, the phase domain results show a better agreement.

In order to determine the computational efficiency of the newly proposed phase domain model the Actual Frame Time (AFT) for this test case has been compared against that of the frequency-independent and frequency-dependent line models. In the case of the

phase domain and frequency-dependent line models, the effect of the order of the approximating functions on the AFT is investigated by conducting the analysis using several different fitting accuracies.

The AFT for the phase domain model is increased by about 89-95μs as compared to the frequency-dependent line representation, depending on the order of the approximating functions in both cases. In the case of the frequency-independent representation, the phase domain model requires an extra 99μs to execute. It should be emphasized however, that the phase domain model *intrinsically* takes into account any geometric imbalances naturally present in the line, whereas the frequency-independent and frequency-dependent modal domain methods were assumed transposed. A constant transformation matrix was then used to exchange information between the modal and phase domains, and vice-versa, which provides a further increase in computational efficiency for these models.

Although the time step used for all the results presented in this chapter were outside the recommended range of 50-100 microseconds for EMTP-type studies, it is anticipated that this could be overcome with the introduction of the Integrated Development Environment (IDE).

6.8 References

[1] Dommel, H. W.: 'Electromagnetic Transients Program (EMTP) Rule Book', EPRI EL6421-1, Vol. 1, June 1989.

[2] Manitoba HVDC Research Centre: 'EMTDC Reference – Theory Manual', 1988.

[3] Bickford, J. P., Mullineux, N. and Reed, J. R.: 'Computation of power-system transients', IEE Monograph Series 18, 1980, ISBN 0-906048-35-4.

[4] Gönen, T.: 'Electric Power Transmission System Engineering: Analysis and Design', Wiley, 1988, ISBN 0-471-53313-0.

[5] Humpage, W. D.: 'Z-transform Electromagnetic Transient Analysis in High-Voltage Networks', IEE Power Engineering Series 3, 1982, ISBN 0-906048-79-6.

[6] Glover, J. D. and Sarma, M.: 'Power Systems Analysis and Design', PWS-Kent, 1989, ISBN 0-534-07860-5

[7] Mather, R. M. and Wang, X.: 'Real-Time Digital Simulator of the Electromagnetic Transients of Power Transmission Lines', IEEE Transactions on Power Delivery, Vol. 4, No. 2, April 1989, pp. 1275-1280.

[8] Wang, X. and Mather, R. M.: 'Real-Time Digital Simulator of the Electromagnetic Transients of Transmission Lines with Frequency Dependence', IEEE Transactions on Power Delivery, Vol. 4, No. 4, October 1989, pp. 2249-2255.

[9] Devaux, O., Levacher, L. and Huet, O.: 'An Advanced and Powerful Real-Time Digital Transient Network Analyser', IEEE Transactions on Power Delivery, Vol. 13, No. 2, April 1998, pp. 421-426.

[10] Dufour, C., Le-Huy, H., Soumagne, J. and El Hakimi, A.: 'Real-Time Simulation of Power Transmission Lines Using Marti Model with Optimal Fitting on Dual-DSP Card', IEEE Transactions on Power Delivery, Vol. 11, No. 1, January 1996, pp. 412-419.

[11] Wang, X., Woodford, D. A., Kuffel, R. and Wierckx, R.: 'A Real-Time Transmission Line Model for a Digital TNA', IEEE Transactions on Power Delivery, Vol. 11, No. 2, April 1996, pp. 1092-1097.

[12] Wierckx, R. P.: 'Fully Digital Real-Time Electromagnetic Transients Simulator', IERE International Electric Research Exchange, Workshop on New Issues in Power System Computation, Caen, France, March 1992.

[13] Kuffel, R., Giesbrecht, J., Maguire, T., Wierckx, R. P. and McLaren, P.: 'RTDS – A Fully Digital Power System Simulator Operating in Real Time', 1st International Conference on Digital Power System Simulators, ICDS '95, College Station, USA, April 1995.

[14] McLaren, P., Kuffel, R., Wierckx, R., Giesbrecht, J. and Arendt, L.: 'A Real-Time Digital Simulator for Testing Relays', IEEE Transactions on Power Delivery, Vol. 7, No. 1, January 1992, pp. 207-213.

[15] Kuffel, R., McLaren, P., Yalla, M. and Wang, X.: 'Testing of the Beckwith Electric M-0430 Multifunction Protection Relay Using a Real-Time Digital Simulator (RTDS), 1st International Conference on Digital Power System Simulators, ICDS '95, College Station, USA, April 1995.

[16] McLaren, P. C., Dirks, E. N., Jayasinghe, R. P., Swift, G. W. and Zhang, Z.: 'Using a Real-Time Digital Simulator to Develop an Accurate Model of a Digital Relay', 1st International Conference on Digital Power System Simulators, ICDS '95, College Station, USA, April 1995.

[17] Kezunović, M. *et al.*: 'Digital Simulator Performance Requirements for Relay Testing', IEEE Transactions on Power Delivery, Vol. 13, No. 1, January 1998, pp. 78-84.

[18] Lerch, E., Ruhle, O., Winter, W., Kulicke, B. and Pannhorst, H. –D.: 'Real-Time Simulator ARTEMAC for Enhanced Automated Interactive Testing of Digital Relays', International Conference on Power System Transients, IPST '99, Budapest, Hungary, June 1999.

[19] Kaiser, S., Lerch, E., Ruhle, O., Winter, W. and Kulicke, B.: 'New Approach for PC-Based Interactive Real-Time Testing of Digital Relays and Controller Structures', 3rd International Conference on Digital Power System Simulators, ICDS '99, Västerås, Sweden, May 1999.

[20] Wierckx, R. P., Giesbrecht, W. J., Kuffel, R., Wang, X., Mazur, G. B., Weekes, M. A. and Gole, A. M.: 'Validation of a Fully Digital Real-Time Electromagnetic Transient Simulator for HVDC System & Control Studies', Athens Power Tech., Athens, Greece, September 1993.

[21] Wang, X., Giesbrecht, J., Woodford, D., Arendt, L., Wierckx, R. and Kuffel, R.: 'Enhanced Performance of a Conventional HVDC Analogue Simulator with a Real-Time Digital Simulator', 11th Power Systems Computation Conference, PSCC '93, Avignon, France, August 1993.

[22] Duchen, H., Lagerkvist M., Kuffel, R. and Wierckx, R. P.: 'HVDC Simulation and Control System Testing Using a Real-Time Digital Simulator (RTDS)', 1st International Conference on Digital Power System Simulators, ICDS '95, College Station, USA, April 1995.

[23] Kuffel, R., Wierckx, R. P., Duchén, H., Lagerkvist, M. and Wang, X.: 'Expanding an Analogue HVDC Simulator's Modelling Capability Using a Real-Time Digital Simulator (RTDS), 1st International Conference on Digital Power System Simulators, ICDS '95, College Station, USA, April 1995.

[24] Do, Van-Qué, Soumagne, J. C., Sybille, G., Turmel, G., Giroux, P., Cloutier, G.

and Poulin, S.: 'Hypersim, an Integrated Real-Time Simulator for Power Networks and Control Systems', 3rd International Conference on Digital Power System Simulators, ICDS '99, Västerås, Sweden, May 1999.

[25] Fujimoto, Y., Bin, Y., Taoka, H., Tezuka, H., Sumimoto, S. and Ishikawa, Y.: 'Real-Time Power System Simulator on a PC Cluster', International Conference on Power Systems Transients, IPST '99, Budapest, Hungary, June 1999.

[26] Snider, L., Ggnon, C. and Cloutier, G.: 'Real-Time Power System Simulators: Contributing to the Successful Development of Complex Power Systems', 4th International Conference on Advances in Power System Control, Operation & Management, APSCOM'97, Hong Kong, Nov. 11-14 1997.

[27] Gustavsen, B. and Smelyen, A.: 'Rational Approximation of Frequency Domain Responses by Vector Fitting', IEEE Transactions on Power Delivery, Vol. 14, No. 3, July 1999, pp. 1052-1061.

[28] Dommel, H. W.: 'Digital Computer Solution of Electromagnetic Transients in Single-and Multiphase Networks', IEEE Transactions on Power Apparatus and Systems, Vol. PAS-88, No. 4, April 1969, pp. 388-399.

[29] Marti, J.: 'Accurate Modelling of Frequency-Dependent Transmission Lines in Electromagnetic Transient Simulations', IEEE Transactions on Power Apparatus and Systems, Vol. PAS-101, No. 1, January 1982, pp. 147-157.

[30] Wedepohl, L. M.: 'Application of Matrix Methods to the Solution of Travelling-Wave Phenomena in Polyphase Systems', Proceedings of the IEE, Vol. 100, No. 12, 1963, pp. 2200-2212.

[31] Hedman, D. E.: 'Propagation on Overhead Transmission Lines I-Theory of Modal Analysis', IEEE Transactions on Power Apparatus and Systems, Vol. PAS-84, March 1965, pp. 200-205.

[32] Maguire, T. and Giesbrecht, W. J.: 'The implementation of the Cholesky Factorization Routine in the Real Time Network Solution', 3rd International Conference on Digital Power System Simulators, ICDS '99, Västerås, Sweden, May 1999.

[33] Larose, C., Van-Que, D., Sybille, G., Guay, F. and Soumagne, J. -C.: 'A PWM GTO-Inverter Model for the Hypersim Digital Power System Simulator', 3rd International Conference on Digital Power System Simulators, ICDS '99, Västerås, Sweden, May 1999.

[34] Dommel, H. W., Yan, A., Ortiz de Marcano, R. J. and Miliani, A. B.: 'Case Studies for Electromagnetic Transients', Internal Report, The Department of Electrical Engineering, The University of British Columbia, Canada, May 1983.

[35] Naidu, S. R. and de Lima, F. N.: 'A frequency-dependent transmission line model for electromagnetic transient studies', IEE Proceedings, Vol. 132, Pt. C, No. 6, November 1985.

[36] Morched, A., Gustavsen, B. and Tartibi, M.: 'A Universal Model for Accurate Calculation of Electromagnetic Transients on Overhead Lines and Underground Cables', IEEE Transactions on Power Delivery, Vol. 14, No. 3, July 1999, pp. 1032-1038.

CHAPTER 7

CONCLUSIONS AND SUGGESTIONS FOR FUTURE RESEARCH WORK

7.1 General Conclusions

The research work presented in this thesis has been directly oriented to develop a fundamental methodology for modelling power transmission lines for electromagnetic transient studies directly in the phase domain. Additional work has been directed toward developing a simulation environment for conducting real-time, hardware-in-the-loop dynamic simulations, incorporating this newly developed phase domain methodology.

Two algorithms have been presented for evaluating the characteristic admittance and wave propagation functions. Both algorithms do not require calculation of eigenvalues or eigenvectors at any point in the solution process and as such can be regarded as truly evaluated in phase co-ordinates. In addition, both algorithms have a very simplistic form, making them very easy to program unlike the eigen-analysis routines used in current 'phase' domain models.

The algorithm for calculating the characteristic admittance matrix is derived by exploiting a relationship between the matrix sign function and the matrix square root. A Padé iteration scheme to evaluate the matrix sign function is used to formulate an algorithm for evaluating the characteristic admittance matrix, directly in phase co-ordinates, using this relationship. The algorithm is numerically stable, inheriting its stability from the sign function from which it is derived. So far, the algorithm has never failed to converge, for any approximation order, having been tested rigorously for a variety of practical transmission line configurations.

The algorithm proposed to evaluate the wave propagation matrix is based on a Padé approximation to the matrix exponential. It was found that the method is particularly sensitive to the characteristics of the eigenvalues and norm of the argument matrix, as functions of frequency. However, by making use of a 'scaling and squaring' technique, the problems associated with the eigenvalues of the propagation constant diverging with frequency (due to the skin effect in conductors and ground), and a large magnitude of the argument matrix norm are overcome. The algorithm is shown to provide a very robust, accurate and efficient method for evaluating the wave propagation matrix for any practical transmission line configuration. It should be noted that in the practical evaluation of $\mathbf{H}(\omega)$, the eigenvalues of the system are not required in the calculation. However, in terms of explaining the characteristics of the algorithm, as a function of frequency, it is convenient to make reference to the eigenvalues of the argument matrix.

One of the most challenging aspects of modelling multiconductor transmission lines in the phase domain concerns the unwinding of the wave propagation matrix. The elements of $\mathbf{H}(\omega)$ are obtained as oscillating functions of frequency due to the time delays of the line. Therefore, in order to obtain accurate, relatively low-order approximations of the elements of $\mathbf{H}(\omega)$, the function must be unwound to remove these oscillations. The elements are then obtained as smooth functions of frequency. In current phase domain line models, the modal travel times of the system are required for

this purpose. In this research, the problem has been solved directly in phase co-ordinates by evaluating a *matrix* phase shift function to remove the oscillations. By conducting the analysis directly in the phase domain, the time delays of the line are intrinsically taken into account. The coupled time delays are then approximated in the time domain with a series of scalar impulse functions. At this point in time, a disadvantage with this approach is the necessity of having to apply an inverse Fourier transform in order to establish the time domain form of the elements of matrix phase shift function.

The phase domain transmission line model can be interfaced with existing general time-based electromagnetic transient programs, such as EMTP. The line model is incorporated within this environment as with other line representations, as a time-dependent current source in parallel with a constant admittance, i.e. a Norton equivalent representation.

A particular application of the developed phase domain methodology is shown for the analysis of transmission line switching transients. The time domain sequential energization of a 345kV-transmission system is performed and the results are obtained when using conventional modal domain approaches and the new phase domain line model. A comparison of these results with available field measurements highlights the accuracy of the method.

An environment for conducting real-time electromagnetic transient simulations has been developed on a commercially available real-time digital simulator. Existing modal, frequency-independent and dependent transmission line models have been incorporated within this environment, as well as the newly developed phase domain model. The computational efficiency of each model is assessed by analysing the actual frame times obtained during transient simulations. While the phase domain transmission line model is shown to be 2-2.5 times slower, in terms of computational efficiency, than existing methods, the accuracy and generality afforded with this methodology surpass those of existing line representations currently available for real-time analysis.

7.2 Future Research Work

The work presented in this research provides a fundamental methodology for the phase domain representation of power transmission lines for electromagnetic transient studies with application to real-time digital simulation. Related research that could be developed further, concerning the modelling of additional power system components, is outlined below.

7.2.1 High-Voltage Underground Cable Modelling

The emphasis of this research has been on the modelling of overhead transmission lines with no reference to underground power cables. However, high-voltage underground cable circuits are used extensively as a means of conveying bulk electrical power into large centres of population for aesthetic, safety and economic reasons. The accurate modelling of high-voltage underground cables is therefore of increasing importance in the calculation of transient overvoltages. As was the case for overhead transmission lines, a complete phase domain underground cable model for electromagnetic transient analysis is still to be realized. However, the author feels that the methodology presented in this thesis for the modelling of overhead lines could be extended to high-voltage cables.

As is the case for overhead line modelling, the unwinding of the phase domain wave propagation matrix is likely to provide the greatest challenge. This particularly true for

cables since in this case the modal velocities will show a much greater variation between modes.

7.2.2 Transformer Modelling

The electromagnetic transient behaviour of power transformers is very difficult to model accurately since the current and voltage characteristics at the terminals are strongly frequency-dependent and usually involve nonlinear phenomena, such as those attributed to saturation effects and hysteresis. A recent model has been presented for both phase and modal domains using Vector Fitting to include these frequency responses. However, non-linearities were not taken into account. The phase domain modelling of transformers for performing real-time electromagnetic transient simulations, including any nonlinear effects, therefore provides an interesting background for future research.

7.2.3 Transient Modelling of Instrument Transformers

Testing of equipment, such as control and protection devices in real-time, hardware-in-the-loop simulations requires not only accurate network transients to be evaluated, for a given system disturbance, but also the appropriate instrument transformer transients which are 'seen' directly by the equipment under test. Accurate modelling of these instrument transformers, such as the current transformer (CT) and the capacitor coupling transformer (CCVT) under transient conditions is therefore essential for performing such tests.

APPENDIX I

PHASE DOMAIN RECURSIVE CONVOLUTION INTEGRAL FORMULATION

II.1 Characteristic Admittance Convolutions

If the elements of the characteristic admittance matrix, $\mathbf{Y}_c(\omega)$ are approximated using rational functions, then the numerical convolution of (4.9) has the following form,

$$\mathbf{y}_c(t) * \mathbf{v}(t) = \zeta(t) = \mathbf{y}_{eq}\mathbf{v}(t) + \mathbf{J}_a(t) \tag{I.1}$$

where $\mathbf{J}_a(t)$ is a history current vector evaluated from previous values of $\zeta(t-\Delta t)$ and $\mathbf{v}(t-\Delta t)$, and $\mathbf{y}_{eq}$ is a real, constant and symmetric matrix. With each element of $\mathbf{Y}_c(\omega)$ approximated by rational functions in the frequency domain, the corresponding the time domain form, $\mathbf{y}_c(t)$, can be written as,

$$y_{c_{ij}}(t) = d_{ij}\delta(t) + \sum_{k=1}^{N} c_{ij_k} e^{-a_{j_k} t} u(t) \tag{I.2}$$

For element $y_{c11}(t)$ and phase a of $\mathbf{v}(t)$, the convolution integral of (I.1) can be performed recursively as follows,

$$y_{c11}(t) * v^a(t) = \zeta_{11}(t) = d_{11}v^a(t) + \sum_{k=1}^{N} c_{11_k} e^{-a_{1_k} t} * v^a(t) \tag{I.3}$$

For each k in the summation of (I.3) the following convolution integral is obtained,

$$\zeta_{11k}(t) = c_{11_k} \int_0^\infty v^a(t-u) e^{-a_{1_k} u} du \tag{I.4}$$

From [MARTI], it is shown that (I.4) can be written in the following recursive form,

$$\zeta_{11}(t) = q_k \zeta_{11_k}(t-\Delta t) + p_k v^a(t) + r_k v^a(t-\Delta t) \tag{I.5}$$

where,

$$q_k = e^{-a_{1_k}\Delta t} \tag{I.6}$$

$$p_k = c_{11_k}\left[\frac{1}{a_{1_k}} - \frac{1}{\Delta t a_{1_k}^2}\left(1 - e^{-a_{1_k}\Delta t}\right)\right] \tag{I.7}$$

$$r_k = c_{11_k}\left[\frac{-1}{a_{1_k}} e^{-a_{1_k}\Delta t} + \frac{1}{\Delta t a_{1_k}^2}\left(1 - e^{-a_{1_k}\Delta t}\right)\right] \tag{I.8}$$

Therefore, (I.3) can be written as,

$$y_{c11}(t) * v^a(t) = \zeta_{11}(t) = z v^a(t) + J_{a_{11}}(t) \tag{I.9}$$

where,

$$z = d_{11} + \sum_{k=1}^{N} p_k \tag{I.10}$$

$$J_{a11}(t) = \sum_{k=1}^{N} q_k \zeta_{11_k}(t - \Delta t) + r_k v^a(t - \Delta t) \tag{I.11}$$

I.1 Wave Propagation Convolutions

After the elements of the matrix $\mathbf{P}(\omega)$ have been successfully synthesized with rational functions in the frequency domain, the approximated wave propagation matrix, $\mathbf{H}_f(\omega)$, can then be obtained as,

$$\mathbf{H}_f(\omega) = e^{-j\omega\tau}\mathbf{P}_f(\omega) = \Phi^{-}(\omega)\mathbf{P}_f(\omega) \tag{I.12}$$

This can be re-written in the following form, dropping the subscript f for convenience,

$$\mathbf{H}(\omega) = \begin{pmatrix} \Phi_{11}^{-}(\omega) & \Phi_{12}^{-}(\omega) & \Phi_{13}^{-}(\omega) \\ \Phi_{21}^{-}(\omega) & \Phi_{22}^{-}(\omega) & \Phi_{23}^{-}(\omega) \\ \Phi_{31}^{-}(\omega) & \Phi_{32}^{-}(\omega) & \Phi_{33}^{-}(\omega) \end{pmatrix} \begin{pmatrix} P_{11}(\omega) & P_{12}(\omega) & P_{13}(\omega) \\ P_{21}(\omega) & P_{22}(\omega) & P_{23}(\omega) \\ P_{31}(\omega) & P_{32}(\omega) & P_{33}(\omega) \end{pmatrix} \tag{I.13}$$

With each element of $\mathbf{P}(\omega)$ approximated with a sum of partial fractions, and each element of $\Phi^{-}(\omega)$ approximated with a sum of scalar phase shifts (in the frequency domain), then (II.2) can be written as in a more compact form as follows,

$$\mathbf{H}_{ij}(\omega) = \sum_{k=1}^{n}\sum_{l=1}^{n}\sum_{m=1}^{N} w_{ik_l} e^{-j\omega\tau_l}\left[\frac{c_{kj_m}}{s - a_{j_m}}\right] \tag{I.14}$$

In the time domain this can be written as,

$$\mathbf{h}_{ij}(t) = \sum_{k=1}^{n}\sum_{l=1}^{n}\sum_{m=1}^{N} w_{ik_l} c_{kj_m} e^{-a_{j_m}(t-\tau_l)} \tag{I.15}$$

Equation (I.15) can be written in a slightly expanded form as,

$$\mathbf{h}_{ij}(t) = \sum_{k=1}^{n}\sum_{m=1}^{N} w_{ik_1} c_{kj_m} e^{-a_{j_m}(t-\tau_1)} + \sum_{k=1}^{n}\sum_{m=1}^{N} w_{ik_2} c_{kj_m} e^{-a_{j_m}(t-\tau_2)} + \sum_{k=1}^{n}\sum_{m=1}^{N} w_{ik_3} c_{kj_m} e^{-a_{j_m}(t-\tau_3)} \tag{I.16}$$

Consider now the matrix-vector convolution involving the wave propagation matrix, $\mathbf{h}(t)$, and the forcing vector, $\mathbf{f}(t)$,

$$\mathbf{h}(t) * \mathbf{f}(t) = \xi(t) \tag{I.17}$$

The convolution in (I.17) is carried out as a normal matrix multiplication, but each multiplication involves scalar convolutions. For example, consider the convolution between the ij^{th} element of $\mathbf{h}(t)$, and the first element of the forcing function, $f^a(t)$, as follows,

$$h_{ij}(t) * f^a(t) = \xi_{ij}(t) = \sum_{k=1}^{n}\sum_{m=1}^{N} w_{ik_1} c_{kj_m} e^{-a j_m (t-\tau_1)} * f^a(t) + \sum_{k=1}^{n}\sum_{m=1}^{N} w_{ik_2} c_{kj_m} e^{-a j_m (t-\tau_2)} * f^a(t) + \sum_{k=1}^{n}\sum_{m=1}^{N} w_{ik_3} c_{kj_m} e^{-a j_m (t-\tau_3)} * f^a(t) \quad (I.18)$$

Each individual convolution element can be written as follows [1],

$$\xi(t) = \int_{\tau_k}^{\infty} f^a(t-u_k) e^{-a j_m (t-u_k)} du \quad (I.19)$$

This can be written in a recursive manner as *follows [1],*

$$\xi(t) = \alpha\xi(t-\Delta t) + \beta f^a(t-\tau_k) + \chi f^a(t-\tau_k-\Delta t) \quad (I.20)$$

where,

$$\alpha = e^{-a j_m \Delta t} \quad (I.21)$$

$$\beta = \left[\frac{1}{a_{j_m}} - \frac{1}{\Delta t a_{j_m}^2}\left(1 - e^{-a j_m \Delta t}\right)\right] \quad (I.22)$$

$$\chi = \left[-\frac{1}{a_{j_m}} e^{-a j_m \Delta t} + \frac{1}{\Delta t a_{j_m}^2}\left(1 - e^{-a j_m \Delta t}\right)\right] \quad (I.23)$$

Combining (I.20)-(I.23) in (I.18) gives rise to the following,

$$h_{ij}(t) * f^a(t) = \xi_{ij}(t) = \sum_{k=1}^{n}\sum_{m=1}^{N} w_{ik_1} c_{kj_m} \left[\alpha_m \xi_{ij_1}(t-\Delta t) + \beta_m f^a(t-\tau_1) + \gamma_m f^a(t-\tau_1-\Delta t)\right] + \sum_{k=1}^{n}\sum_{m=1}^{N} w_{ik_2} c_{kj_m} \left[\alpha_m \xi_{ij_2}(t-\Delta t) + \beta_m f^a(t-\tau_2) + \gamma_m f^a(t-\tau_2-\Delta t)\right] + \sum_{k=1}^{n}\sum_{m=1}^{N} w_{ik_3} c_{kj_m} \left[\alpha_m \xi_{ij_3}(t-\Delta t) + \beta_m f^a(t-\tau_3) + \gamma_m f^a(t-\tau_3-\Delta t)\right] \quad (I.24)$$

Finally, the recursive convolution of the ij^{th} element of $\mathbf{h}(t)$ and the first element of the forcing function, $\mathbf{f}(t)$, can be written in more compact form as,

$$\begin{aligned} h_{ij}(t) * f^a(t) &= \xi_{ij}(t) \\ &= \sum_{k=1}^{n}\sum_{m=1}^{N}\sum_{l=1}^{n} w_{ik_l} c_{kj_m} \left[\alpha_m \xi_{ij_l}(t-\Delta t) + \beta_m f^a(t-\tau_l) + \gamma_m f^a(t-\tau_l-\Delta t)\right] \quad (I.25) \\ &= J_{b_{ij}}(t) \end{aligned}$$

I.3 References

[1] Marti, J.: 'The Problem of Frequency Dependence in Transmission Line Modelling', PhD Thesis, The University of British Columbia, Canada, April 1981.

APPENDIX II

NEGATIVE PHASE SHIFT FUNCTION

II.1 Eigenvalue Description of Negative Phase Shift Function

In order to aid the discussion of section 4.6 concerning the time domain form of the negative phase shift function, the matrix is described below in terms of the eigenvalues of the phase domain travel time (PDTT) matrix, τ.

The negative phase shift function, $\Phi^{-}(\omega)$, can be expressed in terms of the eigenvalues of the PDTT function as outlined below. The case illustrated is for a 3-phase system, but the idea can be extended to any multi-phase system with ease.

The PDTT function is diagonalized as follows,

$$\mathbf{T}^{-1}\tau\mathbf{T} = \tau_D \tag{II.1}$$

where τ_D is a diagonal matrix. The elements of τ_D can be regarded as equivalent to the modal travel times of the system. The negative phase shift function can now be obtained as follows,

$$\Phi^{-}(\omega) = e^{-j\omega\tau} = \mathbf{T}\begin{pmatrix} e^{-j\omega\tau_{D_1}} & 0 & 0 \\ 0 & e^{-j\omega\tau_{D_2}} & 0 \\ 0 & 0 & e^{-j\omega\tau_{D_3}} \end{pmatrix}\mathbf{T}^{-1} \tag{II.2}$$

$$= \begin{pmatrix} T_{11} & T_{12} & T_{13} \\ T_{21} & T_{22} & T_{23} \\ T_{31} & T_{32} & T_{33} \end{pmatrix}\begin{pmatrix} e^{-j\omega\tau_{D_1}} & 0 & 0 \\ 0 & e^{-j\omega\tau_{D_2}} & 0 \\ 0 & 0 & e^{-j\omega\tau_{D_3}} \end{pmatrix}\begin{pmatrix} T^{I}_{11} & T^{I}_{12} & T^{I}_{13} \\ T^{I}_{21} & T^{I}_{22} & T^{I}_{23} \\ T^{I}_{31} & T^{I}_{32} & T^{I}_{33} \end{pmatrix} \tag{II.3}$$

Therefore, each element of $\Phi^{-}(\omega)$ can be written as follows,

$$\begin{aligned}
\Phi^{-}_{11}(\omega) &= T_{11}e^{-j\omega\tau_{D_1}}T^{I}_{11} + T_{12}e^{-j\omega\tau_{D_2}}T^{I}_{21} + T_{13}e^{-j\omega\tau_{D_3}}T^{I}_{31} \\
\Phi^{-}_{12}(\omega) &= T_{11}e^{-j\omega\tau_{D_1}}T^{I}_{12} + T_{12}e^{-j\omega\tau_{D_2}}T^{I}_{22} + T_{13}e^{-j\omega\tau_{D_3}}T^{I}_{32} \\
\Phi^{-}_{13}(\omega) &= T_{11}e^{-j\omega\tau_{D_1}}T^{I}_{13} + T_{12}e^{-j\omega\tau_{D_2}}T^{I}_{23} + T_{13}e^{-j\omega\tau_{D_3}}T^{I}_{33} \\
\Phi^{-}_{21}(\omega) &= T_{21}e^{-j\omega\tau_{D_1}}T^{I}_{11} + T_{22}e^{-j\omega\tau_{D_2}}T^{I}_{21} + T_{23}e^{-j\omega\tau_{D_3}}T^{I}_{31} \\
\Phi^{-}_{22}(\omega) &= T_{21}e^{-j\omega\tau_{D_1}}T^{I}_{12} + T_{22}e^{-j\omega\tau_{D_2}}T^{I}_{22} + T_{23}e^{-j\omega\tau_{D_3}}T^{I}_{32} \\
\Phi^{-}_{23}(\omega) &= T_{21}e^{-j\omega\tau_{D_1}}T^{I}_{13} + T_{22}e^{-j\omega\tau_{D_2}}T^{I}_{23} + T_{23}e^{-j\omega\tau_{D_3}}T^{I}_{33} \\
\Phi^{-}_{31}(\omega) &= T_{31}e^{-j\omega\tau_{D_1}}T^{I}_{11} + T_{32}e^{-j\omega\tau_{D_2}}T^{I}_{21} + T_{33}e^{-j\omega\tau_{D_3}}T^{I}_{31} \\
\Phi^{-}_{32}(\omega) &= T_{31}e^{-j\omega\tau_{D_1}}T^{I}_{12} + T_{32}e^{-j\omega\tau_{D_2}}T^{I}_{22} + T_{33}e^{-j\omega\tau_{D_3}}T^{I}_{32} \\
\Phi^{-}_{33}(\omega) &= T_{31}e^{-j\omega\tau_{D_1}}T^{I}_{13} + T_{32}e^{-j\omega\tau_{D_2}}T^{I}_{23} + T_{33}e^{-j\omega\tau_{D_3}}T^{I}_{33}
\end{aligned} \tag{II.4}$$

It follows that each element of $\Phi^{-}(\omega)$ can be written in the frequency domain in a more compact form as,

$$\Phi^{-}_{ij}(\omega) = \sum_{k=1}^{n} T_{ik}T^{I}_{kj}e^{-j\omega\tau_{D_k}} \tag{II.5}$$

Thus each element of $\Phi^{-}(\omega)$ is composed of n weighted scalar phase shifts (where n is the number of phase conductors in the system).

APPENDIX III

TRANSMISSION LINE DATA

III.1 Jaguara-Taquaril Transmission System

The following test system corresponding to the 398 km, 345kV Jaguara-Taquaril power transmission system in the State of Minas Gerais, Brazil that is used for time domain simulations. The system is illustrated in Figure III.1.

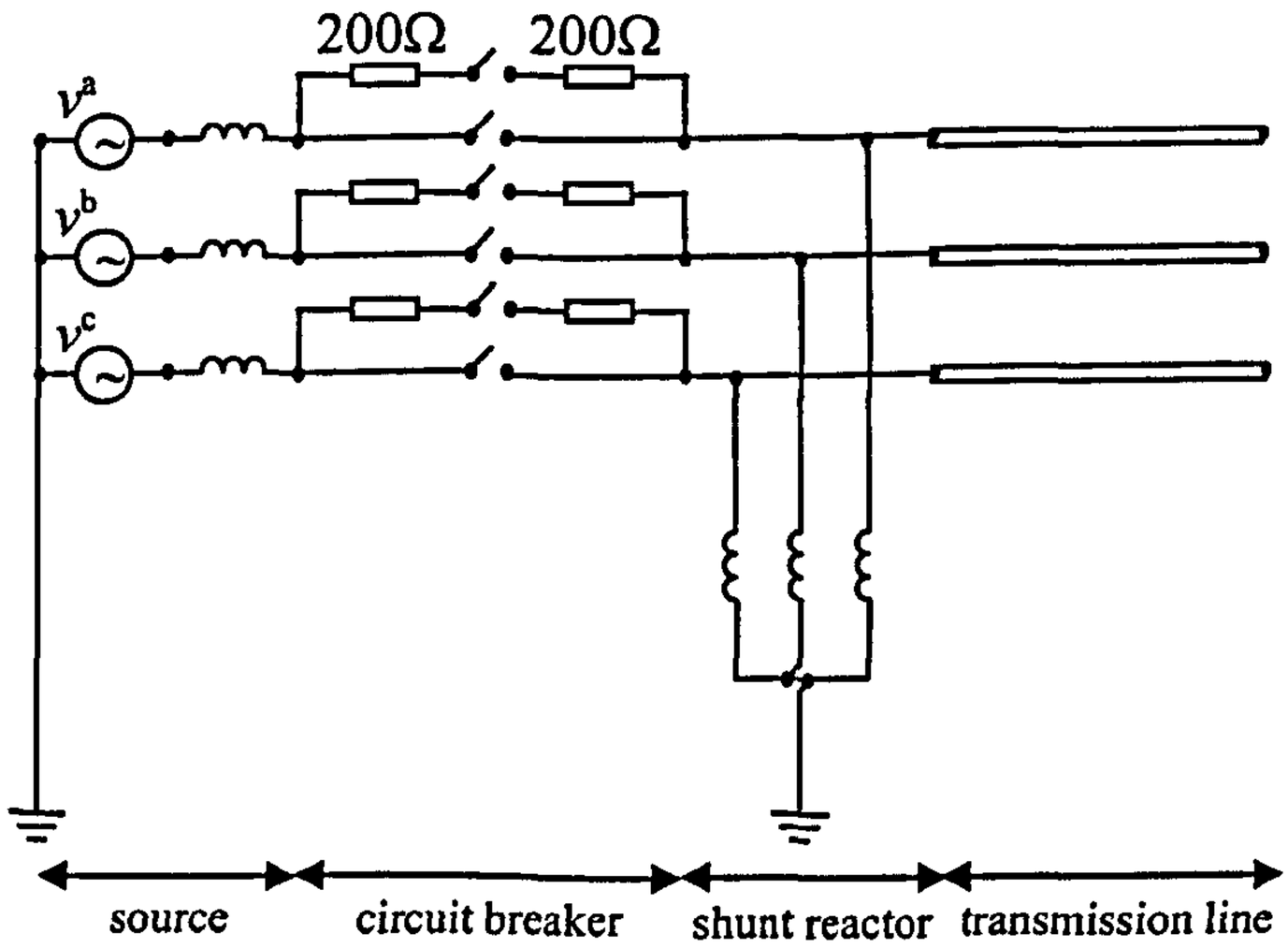

Figure III.1 Jaguara-Taquaril 345kV transmission system

The power plant is represented by a 3-phase voltage source behind a 3-phase coupled inductance having self-inductance L_s = 0.206H and mutual inductance L_m = -0.058H. The 3-phase shunt reactor is modelled by a coupled 3-phase inductor having self inductance L_s = 4.4192 H and mutual inductance L_m = -1.228H.

The line is energized by the following source voltage:

$$v^a(t) = 0.95\cos(\omega t + \frac{\pi}{2})$$

$$v^b(t) = 0.95\cos(\omega t - \frac{\pi}{6}) \qquad \text{(III.1)}$$

$$v^c(t) = 0.95\cos(\omega t + \frac{7\pi}{6})$$

For the time domain simulations, the contacts of the circuit breakers are closed according to the sequence given in Table (III.1).

Table III.1. Circuit breaker switching data

Phase	Aux. Contacts	Main Contacts
a	8.50 ms	15.98 ms
b	7.14 ms	14.28 ms
c	8.16 ms	14.96 ms

The line parameters for the system, evaluated at 60Hz, for the frequency-independent transmission line are given in Table (III.2).

Table III.2. Line parameters calculated at 60Hz.

Parameter	Zero Seq.	Pos. Seq.
R	0.32183 Ω/km	0.03419 Ω/km
X	1.26693 Ω/km	0.37478 Ω/km
C	0.008 μF/km	0.0118 μF/km

The single-circuit transmission line configuration is shown in Figure III.2.

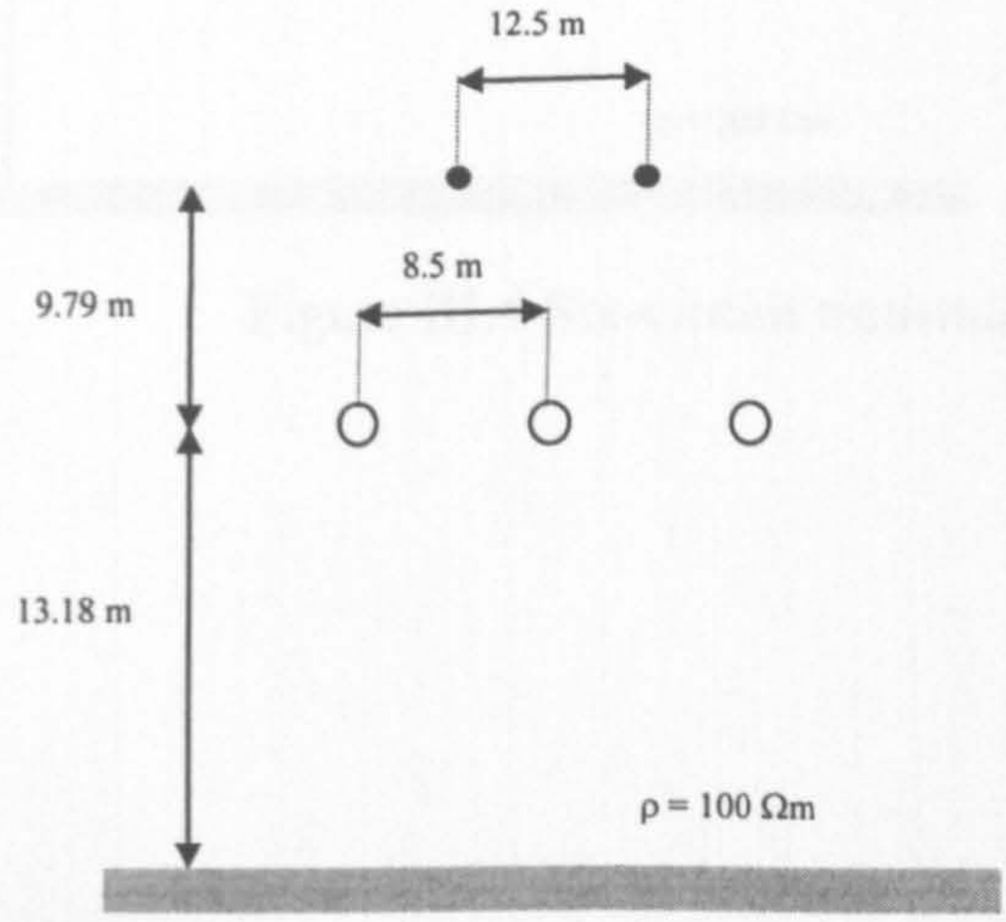

Ground wire $\begin{cases} r_{ext} = 0.4760\,\text{cm} \\ R_{dc} = 3.99\,\Omega/\text{km} \end{cases}$

Length = 398km

Phase Conductor:

$2\times\begin{cases} r_{ext} = 1.519\,\text{cm} \\ r_{int} = 0.5\,\text{cm} \\ R_{dc} = 0.06669379\,\Omega/\text{km} \end{cases}$ o—o

at 40cm spacing.

Figure III.2 Single-circuit transmission line configuration

III.2 Double-Circuit Transmission Line Configuration

Figure III.3 illustrates the 220kV double-circuit transmission line used. The line is taken to be 152.90km in length.

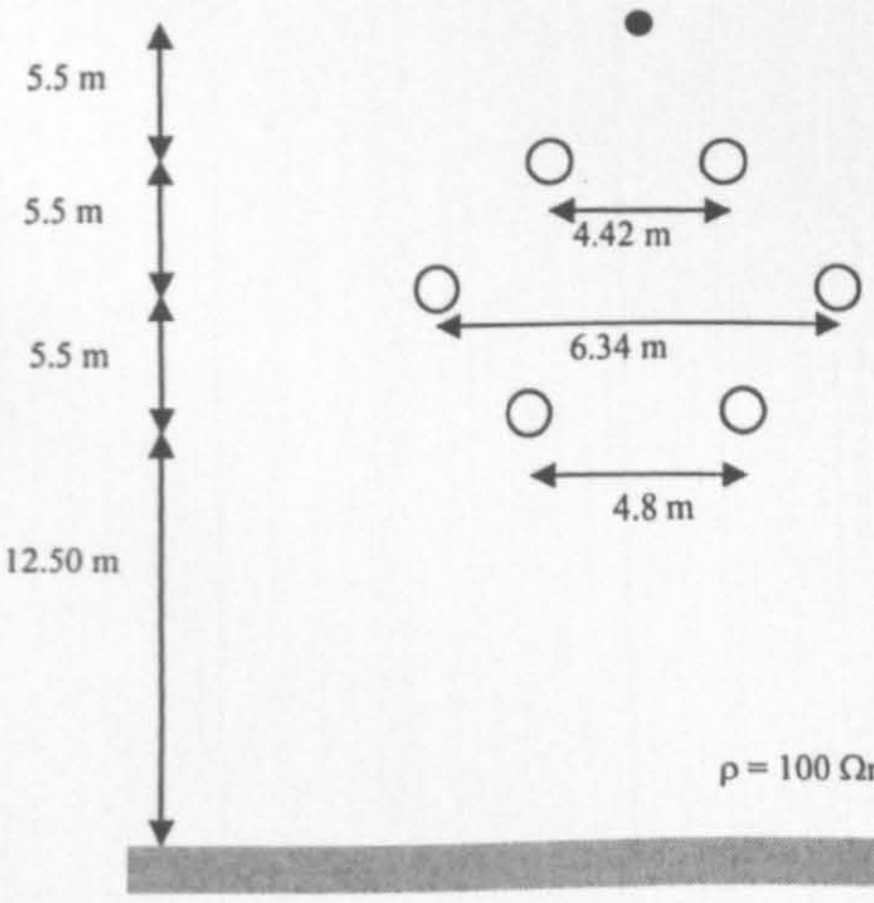

Ground wire $\begin{cases} r_{ext} = 0.4570\,\text{cm} \\ R_{dc} = 5.00\,\Omega/\text{km} \end{cases}$

Length = 152.90km

Phase Conductor:

$2\times\begin{cases} r_{ext} = 1.298\,\text{cm} \\ r_{int} = 0.5570\,\text{cm} \\ R_{dc} = 0.09013564\,\Omega/\text{km} \end{cases}$ o—o

at 46cm spacing.

Figure III.3 Double-circuit transmission line configuration

III.3 Six-Circuit Transmission Line Configuration

Figure III.4 illustrates the six-circuit 230kV transmission line used. The line is taken to be 100km in length.

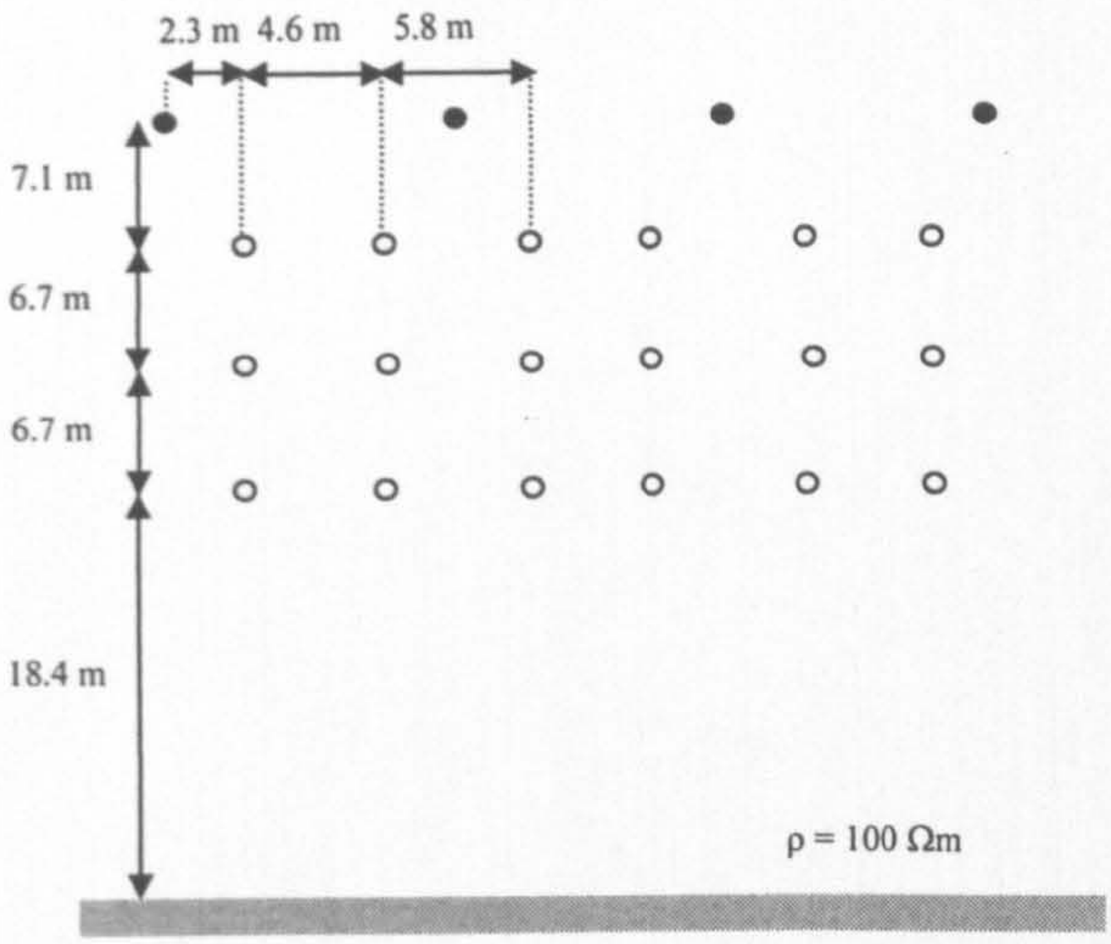

Ground wire $\begin{cases} r_{ext} = 0.4570\,\text{cm} \\ R_{dc} = 5.00\,\Omega/\text{km} \end{cases}$

Length = 100km

Phase Conductor:

$$2\times\begin{cases} r_{ext} = 1.298\,\text{cm} \\ r_{int} = 0.5570\,\text{cm} \\ R_{dc} = 0.09013564\,\Omega/\text{km} \end{cases}$$

at 46cm spacing.

Figure III.4 Six-circuit transmission line configuration